The measurement of rotary shaft seal film thickness.

Binnington, P G.

The Measurement of Rotary Shaft Seal Film Thickness

University of Durham
School of Engineering & Applied Science

P.G. Binnington

Declaration

No material in this thesis has been previously submitted for a degree at the University of Durham or any other University. Except where stated otherwise, the thesis reports individual research carried out by the author.

5th March 1991

Dedication

This work is dedicated to my grandfather Montague Edwards Douglas, who for want of more prosperous times would have been at university long before me.

Acknowledgements

It is not possible to acknowledge everyone who helped me to complete this thesis. Not all the help that I received was in the form of technical advice. What I found just as valuable, was the support of a more encouraging nature. I would especially like to say thank-you to my family, my girlfriend Liz Haynes and my supervisor Professor Harry Marsh.

I would also like to thank George Angus & Co, David James, Graeme Willis, Antonio Strozzi, Stan Davidson, Ken Southam, Bob Bond, Gerhard Poll, Ton Lubrecht, John Tripp, Stathis Ioannides, Antonio Gabelli and Ann Vollmer, to list but a few.

Summary

A powerful new film thickness measurement technique is developed that utilises a fluorescence imaging technique. This technique has been applied to study discreetly the lubricant film thickness of a rough tribological rotary lip shaft seal contact. Results are presented that show that the contact of a rotary lip shaft seal operates under conditions of mixed lubrication and that the performance of a rotary lip shaft seal is roughness governed. The film thickness is highly unstable. The nominal radial load of the seal is shared between the tips of flattened asperity summits in contact with the shaft, compressed lubricant trapped in the asperity valleys of the seal surface and micro asperity hydrodynamic action.

Nomenclature

a	Absorbtivity
a_i	Radius of summit contact
A	Real area of contact
A_i	Real area of contact of a summit
A_o	Apparent area of contact
c	Dye concentration
C	Constant
d	Mean plane separation of surfaces
D	Optical density
E	Exposure
E_1	Modulus of rubber
E_2	Modulus of quartz
E^*	Plain strain modulus
f	Focal length
f_r	Elastic force
H	Enthalpy
i	Image location
I	Unabsorbed light intensity
I_o	Incident light intensity
k	System optical constant
K_s	Peak summit curvature
$\overline{K}_s$	mean peak summit curvature
L	Length

m	Magnification
n	Number of summits in contact
N	Number of summits
N_l	Length of surface in contact
o	Object location
P	Pressure
$\overline{P}$	Average pressure
P_i	Force required to compress an asperity
S	Entropy
t	Film thickness
T	Transmittance
T^*	Temperature
U	Internal energy
V	Volume
W	Work
Z_s	Summit height
δ	Compliance
ν_1	poisons ratio of rubber
ν_2	poisons ratio of quartz
π	Pi
σ	Deviation of the surface heights
σ_s	Deviation of the summit heights
$\phi(Z_s)$	Distibution function of the summits
$\tan\delta$	Loss Tangent
∞	Infinity

$f(\delta_i)$	Shape compliance function for a single asperity
$f(\delta)$	Shape compliance function
$g(\delta_i)$	Load compliance function for a single asperity
$g(\delta)$	Load compliance function

Contents

Chapter Three

Chapter Four

Chapter Five

Chapter Six

Chapter Seven

Chapter Eight

8.1 Analysis of the Localised Seal Contact Experimental Results

8.1.1 Establishing that the ratio of the real to the apparent area of contact can reach or exceed 0.5
8.1.2 Why doesn't the real area of contact exceed 0.5 in the lubricated condition ?
8.1.3 The increase in film thickness with speed

Discussion

9.1 The Fluorescence Technique

9.1.1 The minimum resolvable film thickness
9.1.2 The range of film thickness that can be measured
9.1.3 The maximum spatial resolution

9.2 The Experimental Results

9.2.1 The effect of roughness on the ability of the surface to trap fluid
9.2.2 The effect of roughness on friction
9.2.3 The boundary contribution to friction
9.2.4 The lubricant shear contribution to friction
9.2.5 Roughness and wear
9.2.6 The film thickness dynamic instability

Conclusions

Experimental Technique

Experimental Results

Chapter One

1.1 Garter Spring Radial Lip Seals

Garter spring radial lip seals are used extensively in many varied rotating shaft applications. For the most part a garter spring radial lip seal provides a low cost, reliable solution to the problem of isolating one area from another. One of the reasons why it may be desirable to do this is to confine a substance to a particular area. Such materials are usually liquids such as grease, oil, kerosene or water. An alternative reason is to isolate an area from components that may be damaging to that area, such as dirt, grit, slurries or chemical corrosives. In certain circumstances applications arise where both confinement of a substance and isolation from a substance are required at the same time, such as the sealing of bearings where lubricant needs to be kept in and contamination needs to be kept out if the bearing is to function properly.

There are currently hundreds of patented designs for garter spring radial lip seals, but it would be fair to say that virtually all of them have three things in common. These are a flexible rubber lip, a garter spring and a reinforcing insert which is usually made from steel. The arrangement of the seal used in the experiments outlined in this thesis can be seen in

Fig 1.0.0. The co-ordinates of the seal were obtained by first mounting the seal on a dummy shaft and then casting a portion of the assembly in epoxy resin. The casting was then sectioned and the cordinates were measured optically.

The common prerequisites for garter spring radial lip seals are no or minimal fluid leakage, low frictional losses and long life. The factors governing these pertain to the operating conditions existing at the lip-shaft contact interface.

To optimise the operational characteristics of a garter spring radial lip seal, research is directed towards understanding the conditions prevailing within the contact zone and the governing parameters that give rise to these conditions. These include the existing lubrication conditions, the controlling lubrication mechanisms, the fluid pumping effects, the material properties and any changes in the material properties due to thermal or chemical degradation. This research was directed towards obtaining further information on the lubrication conditions existing within the contact region of a garter spring radial lip seal by the experimental determination of the fluid film thickness present at the lip-shaft interface. There follows in this section a brief outline of certain topics that are important with regard to the performance of garter spring radial lip seals.

1.2 Material Properties

The elastomeric compounds used in garter spring radial lip seals are materials that have a number of constituents. It is these constituents that determine the final properties of the sealing material under any specific set of operating conditions. The constituents of particular importance are the polymer type, the filler types and their loadings, the curative system and its loading, the plasticiser types, friction modifiers, and the conditions under which the material is processed. There follows a discussion of these constituents and a few of the effects they can have on the properties of lip seal elastomeric compounds

1.2.1 Polymer types

The use of the appropriate elastomeric polymer is of fundamental importance to the life of a seal operating under a specific set of imposed service conditions. The decision on which polymer to choose so that the seal can operate effectively under those conditions is usually decided by the compatibility of the polymer with the fluid it is intended to seal, and the upper temperature limit of the polymer which leads to a rapid deterioration of the polymer's physical properties. The lower temperature limit at which the polymer retains its elastic characteristics is usually of lesser importance because in most applications the low temperature performance of all the polymer types used in shaft seals is

normally adequate. In seals for high temperatures this is not so and polymer types vary greatly in their performance. In order of decreasing upper temperature performance, the polymers that are commonly employed in rotary shaft seal materials are fluorocarbon, silicone, polyacrylic and nitrile rubbers. The polymer which formed the base for the sealing material used in this particular study was of a fluorocarbon type (Viton, manufactured by Dupont de Nemoins).

1.2.2 Fillers

Fillers are materials that are incorporated into the rubber to modify existing physical properties or to impart physical properties and to reduce the cost of elastomeric compounds. In shaft sealing compounds, carbon blacks and talcs are virtually always used to fill fluorocarbon, polyacrylic and nitrile elastomers. With silicone elastomers, silicas and silicates are mostly employed. The proportion of the fillers by weight and the types, predominantly determine the wear characteristics and elastic modulus of the sealing material [1,2].

1.2.3 Curative systems

Because elastomers are in a sense viscous liquids, they flow. The long chain molecules that make up the polymer network slip past each other when subjected to a distorting force. To restrict the limit of this relative movement between polymer

chains, anchor points within the network are created by joining polymer chains together at discrete points. These joints are known as crosslinks. This anchoring process is known as curing or vulcanisation. The degree and type of crosslinking markedly affects the physical properties of the material. Important properties from a sealing point of view are permanent set (non-recoverable deformation) and cyclic fatigue. As the number of crosslink sites increase, the polymer's resistance to cyclic fatigue decreases which will lead to a reduction in the life of the seal. As the number of crosslinks increases and the length of the crosslinks decreases, the resistance to permanent set increases. Permanent set leads to a reduction in the radial load of the seal with time. The aim is to strike a balance between both permanent set and cyclic fatigue.

The type of curative system employed in a sealing material is dependent upon which base polymer is used. With nitrile rubbers, sulphur plus activators (stearic acid and zinc oxide) and an accelerator system such as MBTS (mercaptobenzothiazole disulfide), TMTD (tetramethylthiuram disulfide) are used. To a lesser extent, dicumyl peroxide or benzoyl peroxide curing systems are employed. Polyacrylic polymers have curing systems based on soap/amine activated thiol, soap/sulphur, lead/thiourea or diamine components. Silicone materials have peroxide curing systems: dicumyl peroxide or benzoyl peroxide.

Fluorocarbon materials have curing systems based on an acid acceptor such as magnesium oxide and something that removes hydrogen fluoride to generate a cure site that can react with, for example, bisphenol plus and accelerator such as a quaternary phosphonium salt.

1.2.4 Plasticisers

Plasticisers are not used in all shaft seal elastomeric compounds but are used in compounds based upon nitrile or polyacrylic polymers. Their primary function is to improve the processing characteristics of the material. To a lesser extent they are used to enhance the low temperature elasticity of the sealing material.

1.2.5 Friction modifiers

The addition of PTFE, molybdenum disulphide or paraffin wax can in certain circumstances reduce the frictional losses of shaft sealing materials and alter their wear characteristics.

1.3 The Origins of Rubber Elasticity

The elastic properties of rubbers over a wide range of strains owe their origin to the molecular structure of polymer chains. Polymer chains consist of many randomly coiled segmented units. These chains are in a constant state of motion, even at room temperature in the absence of a deforming force. The distance from one end of the chain to the other end of the chain is constantly changing as a consequence of this Brownian motion, but it can be shown that the chain end to end distance variation exhibits a Gaussian distribution [3]. If an external force is imposed upon the polymer network so that the network becomes extended and the chain end to end distances are increased, this reduces the randomness of the coiled segmented units between the ends of the chain, and the entropy of the polymer system is decreased. It is this reduction in entropy that results in a tension developing in the rubber [4]. The elastic behaviour of the test seal rubber used in this thesis over a large value of strains is shown in **Fig. 1.0.1** At low extensions the elastic response of the material is governed by the decreasing entropy of the polymer system. At higher extensions it can be seen that an upturn in the curve develops. This is attributed to the importance of the enthalpy of the polymer system beginning to outweigh the importance of the entropy of the system in governing the overall elastic response. The elastic response is markedly affected by

temperature. The relationship between entropy and enthalpy and the elastic restoring force of a rubber system can be shown in the following way. If the first and second laws of themodynamics are combined then for a reversible process

$$dU = T^{*}\, dS - dW \qquad (1.00)$$

dW refers to all the work performed by the system and in the case of gases it is simply **PdV** the pressure volume work. In the case of a rubber deformed in tension by an amount **dL**, and exerting a restoring force f_r, the mechanical work performed on the system to accomplish this work must also be included in **dW** therefore

$$dW = P\, dV - f_r\, dL \qquad (1.01)$$

and

$$dU = T^{*}\, dS - P\, dV + f_r\, dL \qquad (1.02)$$

if it is assumed that temperature and pressure remain constant then the enthalpy H is given by

$$H = U + PV \qquad (1.03)$$

differentiating at constant pressure results in

$$dH = dU + P\,dV \qquad (1.04)$$

substituting dU from eqn (1.02) then

$$dH = T^{*}\,dS + f_r dL \qquad (1.05)$$

Thus the restoring force f_r exerted by the rubber after it has undergone an extension dL is

$$f_r = (\delta H/\delta L)_{T^*,P} - T^{*}(\delta S/\delta L)_{T^*,P} \qquad (1.06)$$

1.4 The Causes and Character of Lip Seal Dry Friction

The kinetic friction of rubbers is generally thought to be composed of two components these are the adhesive friction component and the geometrical interactive component [5,6]. What follows is a brief discussion of these components.

1.4.1 Adhesive friction

The frictional force associated with rubber shaft sealing materials operating under unlubricated conditions and sliding against a theoretically smooth surface is generally thought to be governed by the molecular kinetics of the sliding system. The atoms within all materials exert forces of attraction on their neighbouring atoms throughout the bulk of the material. It is also possible for the atoms of one material to exert attractive forces on the atoms of other materials.

Throughout the bulk of any material these forces can be found in the form of primary covalent bonds. It is this force that is predominantly responsible for the strength of materials. Alternatively, short distance attractive forces can also be in operation throughout the bulk of a material in the form of secondary bond forces such as dipole-dipole interactions or van der Waal's forces. These forces are weaker than covalent bond forces and only operate when the atoms of materials are in very close proximity to each other in the order of a few angstroms. The attractive force decays very rapidly as the

separation distance between atoms increases. These secondary bond forces can operate between the atoms of different materials when they are placed in intimate contact with each other. It is these forces coupled with the cyclic stress strain characteristics of the materials forming the seal/shaft friction pair that are primarily responsible for the development of an adhesive frictional force.

The polymer molecules of the rubber sealing material are in a continual state of Brownian motion. At the surface of the seal in the lip-shaft contact region, segments of the rubber's polymer chains at the tips of flattened asperities in contact with the shaft jump randomly in any direction from one position on the shaft surface to another. The minimum energy of relative motion between the atoms of the rubber material and the shaft material necessary for an interaction between the atoms of both materials to proceed is termed the activation energy. It is the activation energy of the rubber/shaft interface that determines the magnitude and rate of the secondary bond formation process. The positions within the contact region where these secondary bond forces are in operation are termed adhesive junctions.

If a torque is imparted to the shaft so that it is made to rotate, then the force required to break the polymer/shaft adhesive junctions causes a deformation of the polymer

molecules in the bulk of the polymer in the direction of rotation of the shaft. As a consequence of the rubber material's viscoelastic nature, the energy of the deformation process is not fully recoverable and a portion is lost through hysteresis. It is this lost energy of deformation that manifests itself as kinetic friction.

1.4.2 Geometrical interactive friction

In reality, engineering surfaces are never smooth. The contact region of a rubber lip seal has a surface roughness typically of the order of 1 to 2 μm Ra. {The arithmetic average value of the departure of the surface profile from the centre line throughout the sampling length.} The surface of a shaft on which a lip seal slides is also rough. If the shaft is forced to rotate the asperities of the rubber will be deformed by the asperities of the shaft as they move over each other. As with adhesive friction, the energy required to deform the rubber asperities is not fully recoverable due to the hysteresis losses within the elastomeric material. This results in a kinetic friction force [7].

1.4.3 Effect of sliding speed

The variation of friction with velocity was examined in some detail by Grosh [8]. He found that the friction increased with increasing speed at low sliding velocities and decreased with increasing speed at higher velocities **Fig. 1.0.2** The increase

in friction at low speeds has been discussed by Bartenev [9]. The decrease in friction at higher velocities has been demonstrated experimentally and is thought to be due to a decrease in the real area of contact which leads to a reduction of the number of adhesive junctions and therefore less adhesive friction. This is caused by a stiffening of the rubber[10,11]. The stiffening effect is due to the dependence of the rubber modulus on the rate of strain.

1.4.4 Effect of temperature

The friction force of rubber has been shown to increase with increasing temperatures at low temperatures to a maximum then decrease as the temperature is increased further [12,13,14] **Fig. 1.0.3.** This is thought to be related to the mechanical losses of the system which exhibit a similar trend. The variation in the mechanical losses with temperature for the rubber material that formed the basis for this study can be seen in **Fig. 1.0.4**

1.5 Lubrication Conditions

There are three possible modes of lubrication under which a seal contact region could operate. These are the boundary lubrication mode, the mixed lubrication mode and the full elastohydrodynamic mode. The mode in operation at any time depends upon the normal contact pressure and the load-carrying capacity of the lubricant film which is governed by the lubrication mechanisms. These mechanisms will be discussed in the next section. A brief description of the modes of lubrication is given below.

1.5.1 Boundary lubrication

A sliding lip seal contact can be said to be operating under conditions of boundary lubrication when there are negligible or no hydrodynamic forces present in the contact region. All the nominal contact force at the contact interface is carried by the flattened asperity tips of the rubber surface lubricated by a thin molecular surface layer and an oxide between the asperity tips and shaft surface, **Fig. 1.0.5** Such lubrication exists under conditions of low sliding velocities or starved lubrication. The friction force in this type of lubrication is high.

1.5.2 Mixed lubrication

As the velocity of the rotating shaft increases, load-carrying capacity develops in the fluid film present within the contact region. The pressure within the fluid film is not capable of completely carrying the nominal contact load but will carry a portion of the load, **Fig. 1.0.6** This leads to a reduction of the load that has to be supported by boundary lubrication. The frictional losses within the system reduce as the seal contact region moves into this mode of lubrication because the viscous shear losses within the lubricant are lower than the friction losses of boundary lubrication.

1.5.3 Full elastohydrodynamic lubrication

As the velocity of the rotating shaft increases further the portion of the total contact load carried by the fluid film increases and the average fluid film thickness throughout the contact region increases. When the average fluid film thickness is comparable to the peak to valley height Rt of the combined roughness of the asperities on the shaft and rubber surfaces within the contact region, the seal lip leaves the surface of the shaft. All the shear induced into the contact region by the rotating shaft then takes place in the fluid film, **Fig. 1.0.7.** As the velocity of the shaft increases the viscous losses within the fluid film rise. This results in an

increase in the frictional losses within the system.

The three different lubrication modes of boundary, mixed and full, and their consequence on the frictional losses within the contact region can be shown by the generalised Striebeck curve **Fig. 1.0.8**

1.6 Lip Seal Lubrication Mechanisms

At a first glance the lubricated contact of a rotary lip seal running against a rotating shaft seems to be operating under conditions of parallel sliding. The existence of this situation contradicts classical lubrication theory which predicts that such a sliding system would not be able to sustain itself as no pressure variation and load-carrying capacity would develop within the lubricant film.

Several hypotheses have been presented that attempt to explain this anomalous situation. The proposed mechanisms of lubrication in apparently plane sliding surfaces are formed around a consideration of not the macro geometry but the micro geometry of the sliding system. Surface roughness and waviness are the categories of geometrical irregularity that constitute the micro geometry of the system. If these categories are considered then the surfaces of the sliding contact are, on average, parallel, but when viewed discreetly they consist of asperities that are both divergent and convergent.

It is easy to see how a positive pressure can develop within a fluid when it is flowing into a convergent geometry. It is also easy to see how a negative pressure can develop within a fluid film if it is flowing into a divergent geometry.

What is not so easy, though, is to see how fluid flowing alternately into the convergent then equally divergent geometries of asperities at the sliding contact surface can generate a positive pressure once the discrete positive and negative pressures have been added together. The following sections discuss some of the various hypotheses that have attempted to rectify this situation.

1.6.1 Micro-asperity lubrication

If a single asperity on the surface of the rubber is considered then it can be treated as a sliding bearing. In the direction of flow, with the direction of rotation of the shaft, the fluid flows into the converging geometry of the asperity, **Fig. 1.0.9** As a consequence, the pressure begins to rise. After passing through the minimum clearance between the asperity summit and the shaft surface, the pressure begins to decrease. It can be seen from **Fig. 1.09** that the pressures on the left and the right of the asperity are symmetrical, i.e., equal but of opposite sign." It must be stated that the diagram only illustrates a point and that in reality the surface of the slider deforms especially in the region of the outlet [15]." If these pressures are summed, then the average pressure in the fluid is zero and no net load capacity develops within the film. However, if it is assumed that fluids cannot withstand large, continuous, subambient pressures, then the fluid film ruptures or cavitates. This

results in a limiting value to the sub ambient pressure that can develop **Fig.1.1.0**. Various studies have been made covering this mechanism [16,17,18,19]. The pressures generated are assumed to be due solely to EHL. The mechanism was further refined [20,21,22] to take into account the squeeze film contribution to load support due to the normal approach of interacting asperities when the sliding contact is operating in the mixed lubrication regime.

1.6.2 Thermal wedge mechanism

If fluid is flowing between a parallel gap between a slider, then the volume flow rate will depend on the pressure gradient. With the thermal wedge mechanism it is thought that as the fluid flows through the gap, viscous losses in the fluid give rise to an increase in temperature. It is assumed that this increase in temperature is non-uniform along the length of the slider which results in a variation in the density of the fluid between the inlet and the outlet of the slider. Now the continuity equation demands that the mass flow rate of the system be constant, which means that the flow rate of the fluid with the medium density towards the outlet of the slider increases. This can only happen if the pressure gradient becomes more negative. If it is assumed that the pressure in the inlet and outlet regions is zero, then a positive pressure develops within the film and the parallel slider has load-carrying capacity.[23,24].

Chapter Two

2.1 Experimental Methods of Determining Film Thickness

A good experimentalist should attempt to understand the parameter that is to be measured before it is measured. When searching for a method to carry out the measurement, an attempt is made to isolate the parameter. If possible any system effect that is not understood should be minimised or eliminated. All of the experimental procedure should be reported, whether or not it is thought relevant at the time.

During the history of experimental tribology, there have been numerous studies directed towards the measurement or estimation of the film thickness present in lubricated contacts. This important tribological parameter has justifiably received much attention as it is primarily responsible for the continued functioning of most lubricated components.

There have been several investigations conducted into the determination of film thickness in elastomeric reciprocating seal contacts. Unfortunately the number of experimental investigations carried out to measure the film thickness

present in an elastomeric rotary lip seal contact have been somewhat more scarce. It would be fair to say that all the various experimental techniques employed could be broadly categorised into two groups: indirect methods and direct methods which may be defined in the following way.

Indirect methods involve deriving the film thickness numerically or analytically by making certain assumptions about the functioning and condition of the contact region. The verification of that calculation is normally carried out by comparison with measured data, of what are presumed to be one or more associated parameters.

Direct methods, as the term implies, involves a direct measurement of the film thickness by the determination of some unique quality possessed by the lubricant film only.

There follows in this chapter a discussion of first the indirect techniques, followed by the direct experimental techniques, employed to measure or estimate the lubricant film thickness in elastomeric sealing contacts.

2.2 Indirect Methods

Unfortunately, with indirect methods the final results are determined by the lubrication model itself. In this section the indirect approach of estimating the elastomeric seal film thickness by calculation and a measurement of the frictional losses will be discussed. The calculation methods that can be used, and the assumptions that are normally made about the contact condition and operating mechanisms will be described. The parameters that are usually measured, the experimental techniques used to perform the measurements will be stated.

2.2.1 The calculation of film thickness in sealing contacts

With reciprocating seals, the lift force that develops in the contact region can be attributed to the converging and diverging geometry of the reciprocating seal lip normal to the direction of sliding. The understanding of the sliding conditions of fully lubricated line contact converging diverging systems is fairly well developed and several techniques can be used to calculate film shape and thickness. One technique, the Dowson and Higginson [25] EHL solution is commonly employed. With hard sliding contacts the accuracy of the EHL solution can be further improved when it is used in conjunction with models that take into account deviations in

the lubricant flow through the contact caused by asperities in the contact region. One commonly employed method is the Patir and Cheng approach [26]

Unfortunately the accuracy of the Patir and Cheng average flow model decreases markedly when it is applied to contacts where the reciprocal of the contact RMS roughness multiplied by the contact nominal film thickness is below 3 (private verbal communication with H.S. Cheng). With seal contacts this is normally the case. Also, the Patir and Cheng approach assumes no deformation of the surface, i.e., it is a hydrodynamic model. In soft contacts, as with seals, deformations can be high even when pressures are low. The use of the model with seals is most definitely less justified.

In the case of reciprocating seals, the lift is assumed to be due to the macro geometry; in the case of face or lip seals the lift is assumed to be due to micro-roughness only, or the lift is just assumed and the running faces of the contact are said to be parallel.

2.2.2 The measured parameters

The parameters that are normally measured within rotary or reciprocating sealing systems are torque, sliding velocity and temperature. The parameters that are measured externally to the system are the elastic properties of the rubber material,

the lubricant viscosity and how the lubricant viscosity varies with temperature.

2.2.3 Experimental methods employed to measure friction in elastomeric seals

The experimental design of the rig is of critical importance and much thought must be given to what is to be measured and how it can be influenced by possible factors in the rig design. A few examples of rigs designed specifically to measure the friction of elastomeric seals will be mentioned.

Some investigators have attempted to measure the friction force generated at the sliding shaft-seal interface by monitoring the force generated within the whole system via strain gauges attached to the housing. [27,28,29,30,31,32,33]. others have attempted to measure the sliding shaft-seal friction force by measuring the whole force that develops in the system via strain gauges attached to the shaft,[34,35,36,37,38,39,40].

The differences between measuring the friction force via the shaft or via the housing depends upon which part of the system is static and which part is driven. There are three popular configurations.

With the first arrangement the housing is static, the shaft is

driven and the housing reaction force is measured. With this arrangement if two seals are tested then what is being measured is the averaged instroke outstroke reciprocating seal friction or averaged rotary seal friction plus the viscous losses of the lubricant in the housing [33,29,30]. When one seal is tested, leakage is prevented at the other end of the housing shaft interface by a clearance bush. With such an arrangement then both instroke and outstroke seal friction or rotary seal friction, plus the viscous losses of the lubricant in the housing is measured if the rig is run vertically and the housing is only half full [28]. If the rig is run full, then both the instroke and outstroke seal friction losses or rotary seal friction losses are measured together with the viscous losses of the lubricant in the housing and the clearance bush [27,32,31].

In the second arrangement the housing is static, the shaft is driven and the reaction force is measured at the shaft. Under these circumstances what is measured depends upon the position where the reaction force is measured. If the shaft is supported between the force measuring device and the seal then the frictional losses of the support bearings, the seal losses and the viscous losses in the lubricant housing are measured by the force measuring device, which is less satisfactory [38]. If the force measuring device is between the seals and the support bearings then only the viscous losses in the

housing and the seal losses are measured, which is better [40].If the force measuring device is between the seals, and the shaft is only supported at one end, then the viscous losses of the lubricant in the housing plus the instroke and the outstroke seal friction or rotary seal friction are measured, [34].

In the third arrangement the housing is driven the shaft is static and the reaction force is measured at the shaft. If the rig is run horizontally and one seal is tested, then leakage is prevented at the other end of the shaft by a clearance bush. The frictional losses of the seal plus the viscous losses from the lubricant in the housing and the clearance bush are measured [35]. If two seals are tested then the averaged instroke outstroke friction or rotary seal friction plus the viscous losses in the housing are measured [41,36].

2.2.4 The generally applied assumptions about elastomeric seal contacts

When a measurement of friction is used to estimate the film thickness in an elastomeric seal contact some or all of the following assumptions are normally made about the contact condition.

The contact is assumed to be operating under conditions of full lubrication !

It is far from satisfactory to assume without proof that most sealing contacts are operating under conditions of full lubrication. The seal contact may be operating in the mixed lubrication mode under conditions of low sliding velocity, [42,29,38], low lubricant viscosity, high lubricant pressure [30,28] or with reciprocating seals at the two extremes of the shaft stroke when the shaft reverses its sliding direction and is momentarily stationary and film collapse may occur [43]. It would therefore seem unreasonable to automatically assume full lubrication .

The contact condition is assumed to be isothermal !

No lift generating contact can ever be truly isothermal. However for the most part, variations in temperature and temperature rise in normal EHL converging diverging contacts operating in a correct manner are relatively small. Because of this, the effect of temperature variation on fluid density and viscosity is normally neglected. The case with elastomeric seals is different. The measured underlip temperature rise in reciprocating seals can be relatively high, in the order of 20 to 120 degrees centigrade [44]. The temperature effect

problem is made even worse by the fact that the rubber lip has a low thermal conductivity. The assumption that a seal contact is isothermal would therefore seem less reasonable.

The contact condition is assumed to be isoviscous !

A contact can be considered to be isothermal or isothermal and isoviscous but with normal lubricants it cannot be isoviscous alone.

The only reason that a normal isothermal EHL contact could not be considered as isoviscous would be if either the contact pressure or the shear rate were very high. In the case of high pressure this can result in a solidification of the oil. In the case of high shear rate, then a limiting lubricant shear stress may be reached. It would be most unlikely for such conditions to exist in the contact of a seal. However in the last paragraph it was concluded that it was not reasonable to assume that the contact of a seal was isothermal. Therefore it would seem incorrect to assume an isoviscous condition with normal lubricants.

The lubricant film is assumed to be axisymetric in the circumferential direction !

The lubricant film will only be axisymetric if the pressure distribution is axisymetric and the inlet-outlet conditions are equal. If there were any housing offset, shaft out of round or a lack of concentricity between the internal and external diameters of the seal, the assumption would cease to be valid. In reality all of these irregularities will always be present to some extent.

All frictional losses measured within the system are assumed to arise solely as a consequence of the viscous shear losses within the lubricant film present within the contact region !

It is very difficult to construct an apparatus to measure the frictional losses of the contact zone in isolation from the power losses of the rest of the measurement system.
Such system losses will occur in the lubricant filled shaft housing clearances and the system support bearings. Also depending upon the sliding speeds, secondary flows in the form of Taylor vortices can develop in the shaft-housing and lip angle-shaft clearances which will lead to increased power losses [45]. Although researched, the onset of these secondary flows and the resultant increase in power losses are difficult to quantify and predict.

2.3 Direct Methods

2.3.1 Interferometry

Numerous interferometric studies have been carried out on smooth lubricated contacts. However interferometry is not suitable for studies where the contact film thickness is smaller or of the same order of magnitude as the contact roughness [46]. This is the case with most sealing contacts and therefore interferometry will no longer be discussed.

2.3.2 Electrical methods

Resistance and capacitance methods have often been used to study the film thickness of metallic lubricated contacts, Leeuwen 1986. They are based upon the principle that the lubricant film is more electrically insulating than the two metallic bodies that it is sandwiched between. Measurements of the lubricant film thickness in sealing contacts has been performed using resistance and capacitance techniques. The use of both these methods in this context has been discussed in detail by Visscher [47]. With both these methods, the primary problem that is encountered when they are applied to the lubricated contact of a seal is that ordinarily rubber is nonconducting. The resistance of rubber can be decreased by the use of certain conducting carbon black fillers. However

even in this form, rubbers can still be regarded as insulators. The measurement of the resistance or capacitance of the contacting system is an average measurement over the area of rubber contact and the shaft probe. This means that the film thickness measurement is averaged, which is not very satisfactory. At very thin films the electric field can become very large and the film can be broken down, giving erroneous results.

The resistance method has been applied by Wernecke [48] to measure the lubricant film thickness of a reciprocating seal. An electrode with a diameter of 0.5mm was embedded into the surface of the reciprocating shaft. The specific resistance of the lubricant was measured externally. The relationship between the measured voltage, the applied voltage and the lubricant film thickness was calculated. The influence of the resistance of the seal and the capacitance of the lubricant film was neglected.

The capacitance method has been applied by Jagger [49] to measure the film thickness of a rubber rotary face seal. The capacitance of the system over the whole of the contact width and circumference was calculated from measurements of the applied and measured voltage in the system. This meant that the film thickness was averaged over all the contact area.

2.3.3 Fluorescence

A fluorescence method has been used to measure the film thickness of sliding contacts. Ting [50] utilised fluorescence to measure the film thickness between the walls of a sleeve and a piston ring. Kassfeldt [51] utilised fluorescence to measure the contact film thickness of a reciprocating seal. Both these methods used a photomultiplyer tube as the fluorescence detecting device. The fluorescence from the contact was collected with a lens and directed into the photomultiplier tube. This meant that an average film thickness was being measured over the area that the fluorescent light was being gathered.

In this thesis an attempt was made to develop a new more powerful technique that imaged the fluorescence from the contact zone and thus allowed non averaged discrete measurements of seal film thickness.

Chapter Three

3.1 Fluorescence

It is possible for molecules to absorb light which can then induce the atoms of that molecule to vibrate. This results because the molecule initially undergoes an electronic redistribution. The electronic transition rapidly builds up a charge density in new regions, this charge density exerts a force on the nuclei of the atoms. This new force can drive the atoms of the molecule into oscillation. An alternative fate for the excited electronic state of a molecule is that the molecule will discard its excitation energy before it has a chance to induce vibration between the nuclei of its atoms. It achieves this by emitting a photon. There are two known mechanisms by which this can occur, fluorescence and phosphorescence. With fluorescence the emitted radiation ceases about 10^{-8} sec. after the exciting light source is removed. Its reappearance is just as rapid if an exciting light source is re-established. With phosphorescence the time required to emit photons after the establishment of an exciting light source is just as rapid as with fluorescence however after removal of the light source photons may continue to be emitted for prolonged periods, even hours.

Two fundamental laws govern the passage of light through an absorbing medium, the Lambert law and the Beer law. The Lambert law states that the rate of decrease in intensity of the incident exciting light as it travels through an absorbing medium is proportional to the light intensity of the beam. If a certain thickness absorbs half the light then the thickness that follows the first and is equal to it will not absorb the entire second half, but only half of this half and will consequently reduce it to one quarter. Hence

$$- dI = k\, dt\, I$$

Where I equals the quantity of light remaining unabsorbed after passage through a thickness t. On integration and setting I equal to I_o the initial intensity of the beam when t equals 0,

$$I = I_o\, e^{-kt}$$

This is saying that the intensity of the unabsorbed light decreases exponentially as the thickness of the absorbing medium increases arithmetically. Beers law states that the intensity of a beam of light passing through an absorbing

medium decreases in a similar manner as the concentration of the light absorbing medium increases.

$$I=I_o\ e^{-kc}$$

Where c is the concentration. The two laws may be combined and written with a single constant to form the well known Beer Lambert law.

$$I=I_o\ e^{-atc}$$

The absorbtivity a is a constant for a particular material and depends upon the wavelength of the incident light and the nature of the absorbing medium.

If an absorption leads to fluorescence then the intensity of fluorescence will be dependent upon the number of fluorescent molecules that are capable of fluorescing in the solution and the thickness of the solution the exciting beam has to travel through. The total fluorescence intensity will be equal to the rate of light absorption multiplied by the efficiency of the molecule at producing fluorescence

$$\text{Fluorescence} \propto I_o(1-e^{-atc})$$

The fluorescent light is emitted in all directions. It is only

viewed from one direction and therefore it is necessary to include a constant for any particular viewing system into the above.

$$\text{Fluorescence} = K\ I_o(1-e^{-atc})$$

If the intensity of the incident light remains constant, and the concentration c of the fluorescing molecules is assumed to be homogeneous and constant throughout the film, then for a particular system K and a are constant. It is therefore possible to obtain the thickness of the film by measurement of the fluorescence intensity. This forms the basis of the experimental technique developed by the author.

3.2 Proving The Fluorescence Technique

Oils sealed by rotating lip seals are known to fluoresce when subjected to light produced by a mercury arc lamp. Mercury arc lamps produce long wave, middle wave and short wave ultraviolet light. In these spectral regions emission lines can be found at 312,334,365,405,435 and 546 nm. The relative intensities of these lines are not equal. The fluorescence induced by such lamps is not intense enough to be recorded photographically unless long exposure times are used typically several minutes. To reduce exposure times it is necessary to increase the intensity of fluorescence. One method of achieving this is by increasing the intensity of the incident light source. The wavelength of the incident light used must be in the region where the oil absorbs light. It was therefore necessary to determine the absorption spectrum of the oil that was to be excited. The intensity of fluorescence varies with thickness. How it appears to vary with thickness depends upon the physical circumstances under which the fluorescence is measured. Experiments were conducted to obtain further information on these subjects.

3.2.1 Determining the absorbtion spectrum of the oil

The absorption spectrum of the oil in the visible range was determined using an absorption spectrometer. A sample of the oil was placed into a quartz curvet. Light of different wavelengths was directed through the sample. The amount of light absorped at the different wavelengths was determined by comparing the beam that had passed through the sample with a reference beam. The shell 15W40 oil was seen to absorb strongly throughout all of the visible spectrum.

3.2.2 Oil fluorescence

An experimental model was constructed to see how fluorescence intensity varied with thickness. The model tried to represent the situation that would be present in a lip seal glass shaft system. The arrangement of the model experimental apparatus is represented schematically in **Fig 3.0.1** As can be seen from **Fig 3.0.1** a wedge shaped cavity was to be traversed through a beam of light. This light would induce fluoresence in an oil contained within the cavity. How the fluoresence intensity varied with film thickness could then be determined.

The machine used to measure the fluorescence intensity was called a fluorimeter. It was of the type known as a fluorescence spectrometer. The fluorescence was excited using

an argon ion laser producing light at a wavelength of 514nm. It was known that this wavelength would be absorped by the oil because of the experiment conducted in 3.2.1 Normally with this type of fluorimeter instrument the resultant fluorescence intensity is measured at 90 degrees to the incident laser beam by a photomultiplier tube. As can be seen from **Fig 3.0.1** the fluorescence is viewed along the same axis as the incident laser light beam. This was made possible by the use of an interference edge filter. The spectral performance curve of this filter can be seen in **Fig 4.0.7** and a more detailed description of these types of filters can be found in chapter four. This filter reflected laser light wavelengths but transmitted the fluorescence wavelengths.

The experimental apparatus consisted of the following.
A square quartz window made of spectrasil 200 measuring 25.4x25.4x2.0mm thick was mounted onto a blackened aluminium back plate and held at its periphery by a plastic retaining clamp. This clamp was fixed to a back plate by eight retaining screws **Fig 3.0.2.** The front face of the back plate had been hand lapped to ensure maximum flatness. Under one end of the glass window was placed a piece of steel shim 25.4 microns thick. The other end of the plate was clamped firmly to the back plate. The quartz window was sealed to the back plate along three of its edges. The fourth was left open to facilitate filling of the cavity with shell 15w/40 oil. The

result was a wedge shaped cavity that was 25.4 microns thick at one end and nominally zero at the other. The back plate was mounted on a small travelling table that could move along one axis. The movement of the table was controlled by an imperial micrometer with a 40 tpi thread. The edge filter was mounted on an extension arm. The axis of the filter was at 45 degress to the axis of the oil cavity. The laser beam, on striking the filter would be turned through 90 degrees, travel through the glass window and excite fluorescence in the oil film. Some of the fluorescence would travel back along the same axis as the incident beam until reached the cut off filter whereupon it would pass through because it was of a different wavelength. The fluorescence then passed on to the detector where its intensity and wavelength was to be determined. The travelling table allowed movement of the glass window along an axis of 45 degrees to the cut off filter. This allowed the laser beam to excite fluorescence at different thicknesses of the cavity. The window was scanned through the beam from left to right and the intensity of fluorescence was measured after every 0.075 inch of travel. The units of fluoresence intensity was measured in (counts per second) C.P.S this was the number of photons counted by the photomultiplier tube per second. These intensity measurements, together with the corresponding cavity oil thicknesses are shown in a graph of intensity vs. film thickness **Fig 3.0.3.** It is interesting to note the two dips in the curve which correspond to the positions of the

retaining screws holding the window in place.

3.2.3 Photographing Fluorescence

The experiment outlined in section 3.2.2 was repeated except this time the photomultiplier detector was replaced by a camera. The camera was a Canon AE1 Program that had a standard 35mm lens. Image magnification was achieved by use of a bellows arrangement The camera was loaded with a 36 exposure Ilford 35mm 400 ASA black and white film. The camera shutter speed was set at 125th/sec. 10 photographs were taken at 10 different fluorescent intensities produced by 10 known film thicknesses. This procedure was repeated a further two times at camera shutter speeds of 250th/sec. and $500^{th}/_{sec}$. The film was developed for five minutes in a $^{1}/_{30}$ dilution strength solution of Kodac HC-10 developer. The resultant negatives were underexposed and no information could be drawn from them.

3.2.4 Increasing Fluorescence Intensity

It was thought that if a substance which produced a greater fluorescence intensity for a given incident intensity than oil could be found then it may be possible to incorporate that substance into the oil. This would result in increased fluorescence intensity for a given film thickness. Several fluorescent dyes were investigated as possible substances. It proved difficult and in some cases impossible to dissolve the

dyes in Shell Super 15W40.

Because of this a viscous fluid was sought that would be compatible with fluoresent dyes. One fluid, glycerol, proved ideal; glycerol does not absorp light throughout most of the visible spectrum **Fig 3.0.4.** Rhodamine B was dissolved in glycerol giving a concentation of 8.36×10^{-5} gm/cm^3. The absorption spectrum of Rhodamine B was found by the method outlined in section 3.2.1 and is shown in **Fig 3.0.5.** It can be seen that it absorps strongly in the 400 to 600 nm region. It was ideally suited to excitation by an argon ion laser source which has wavelengths of 488 and 514nm. The experiment outlined in section 3.2.2 was repeated to find out how the intensity of fluorescence varied with film thickness when Rhodamine B was present in the glycerol. The intensity fluorescence and the calculated associate thicknesses are shown in **Fig 3.0.3** If this curve is compared to the shell 15w/40 curve it can be seen that incorporation of Rhodamine B into glycerol increased the rate at which fluorescence intensity increased with thickness. The experiment outlined in section 3.2.3 to see if it was possible to record photographically changes in fluorescence intensity with oil film thickness was repeated with Rhodamine B in glycerol. The results obtained showed exposure on all negatives.

Chapter Four

4.1 Proving the Fluorescence Technique with a Seal

Experiments described in chapter three suggested that fluorescence may be utilised to measure film thicknesses present in a sealing contact of a rotary shaft seal. Before a rig was built to attempt to measure those thicknesses, it was first decided to verify the fluorescence technique by applying it to a seal called the floating element seal. This particular seal was chosen only because a quartz glass window that allowed viewing of a sealing contact had already been manufactured for the project sponsoring company.

The oil film between the seal and the quartz window was to be induced to fluoresce by an exciting light source. The fluorescence was to be imaged at some point away from the contact. The image was to be recorded photographically by a high speed cine camera. The object of the exercise was to see if the resultant fluorescence would be of high enough intensity to expose the photographic film. What follows is a discussion of the photographic techniques required, the light sources, the optics, and the test rig.

4.2 Photography

4.2.1 Cameras

High speed photography is considered to begin at frame rates of 100 pictures per second. Cameras are available with framing rates as high as 600 million frames per second. There are various types of high speed camera that have different maximum framing rates. The camera used within this project was of a type known as a high speed rotating prism camera because it was the only one available. A brief description of various other types of camera plus the rotating prism camera follows.

Intermittent pin register cameras **Fig 4.0.0** work on the same principle as a conventional motion picture camera. They offer a maximum framing rate of 500 frames per second. The film is pulled down into a gate by a claw which fits into the perforations on the edge of the film. When the film is in position the claw retracts and register pins are inserted into the perforation to hold the film steady while the shutter opens and closes. This type of operation produces a very sharp image whose quality is unrivalled by any of the other cameras.

Streak cameras **Fig 4.0.1** These cameras are not framing cameras. This is because the streak camera does not record individual pictures of an event. Instead an uninterrupted slit image is swept across the film. They have the ability of providing very accurate velocity measurements of transient events. There are

two major groups of streak camera, moving film types, where the film is transferred from reel to reel, or alternatively held on a rotating drum, and rotating mirror types, which employ a length of film held stationary on the inside of a fixed track. They can operate in the region of 20,000 to 1,000,000 frames per second.

Image converter cameras **Fig 4.0.2** With this camera an image on a photo-cathode is electronically displayed on a larger phosphorescent screen. The amplified image is then photographed by a camera. Because this is an electronic device, the exposure can be controlled down to about 1 nano-second. These cameras make it possible to produce recording rates from 50,000 to 600,000,000 frames per second.

Rotating prism cameras **Fig 4.0.3** These cameras are capable of frame rates up to 25,000 frames per second. This is achieved by a system that keeps the film continually moving through the camera. A prism positioned between the lens and the film rotates continuously at high speed. As it does so, it alternately transmits and blocks the light passing though the lens. The speed of the prism and the camera are synchronised so relative movement between the film and prism is zero. A shutter between the prism plane is used to adjust the amount of light falling incident on the film allowing the exposure of the film to be varied. Rotating prism cameras offer short exposure

times and short time intervals between exposures, but their resolution is inferior to those of pin register cameras. The camera used in this project was a Hycam K20S4E capable of framing rates from 10 to 11,000 frames per second. It was possible to use it in conjunction with a 16 mm film the length of which could be anything from 50 to 400ft.

4.2.2 Films

Films are available in colour or black and white. For most studies black and white film is the obvious choice. Its exposure times are shorter, a wider range of film speeds are available and processing is usually more straight forward. Black and white films consist of a suspension of silver chloride or bromide in gelatine, coated onto a plastic substrate. The silver halide is the photo sensitive component, the gelatine serves as a binding matrix. Silver bromide is the more light sensitive of the two. Its sensitivity can be further enhanced by the addition of some iodide. The size of the silver halide crystals present in the gelatine can be varied during film manufacture. The concentration of the gelatine during manufacture determines the ultimate size and uniformity of the silver halide crystals or grains. Because silver halide is only sensitive to ultraviolet and blue light, dyes are added that are adsorbed at the grain surfaces. These absorb longer wavelength light and transfer this energy to the crystal, enhancing the sensitivity of the film in these regions. The

plastic substrate normally used is cellulose triacetate but also cellulose buterate and polyethylene teraphthalate (ESTAR) substrates are also used. The choice of one base over another is mainly influenced by their optical properties and physical strength. Most film bases have substances coated on their under-side that reduces reflectivity. These reduce halation. Halation occurs because after light incident upon the film has passed through the gelatine and plastic substrate, a certain portion is reflected back. This causes exposure of the emulsion areas outside the image area.

The photographic image formation takes place in two stages. The first is exposure of the silver halide crystals to light which causes changes in the electronic structure of the silver halide atoms. These electronically changed atoms act as nucleation sites that catalyse the conversion of the whole silver halide crystal to metallic silver during the second development stage. Very few charged silver halide atoms are required to achieve this. This results in a massive gain. The more coarse the grain structure, the greater the gain because more metallic silver is produced for a similar number of light energised silver halide atoms. This reaction is achieved by immersing the previously exposed film in an alkaline developer solution. A small number of un-exposed grains will be turned into metallic silver during this stage. The effect is known as fog. There are agents within the developer to minimise this problem, however it will always

be present. After development the silver halide to metallic silver reaction is stopped by immersing the film in a stop bath which is a weak acid, usually dilute acetic. This neutralises the alkaline developer solution. The remaining silver halide crystals are removed from the film emulsion by immersing the film substrate in a fixing bath, usually a sodium thiosulphate solution. This converts the silver halide crystals to soluble salts which are dissolved in the bath. Because a fixed number of grains on the film emulsion are made developable by each incident photon, the number of exposed grains and hence their density grows with exposure. A plot of density D verses exposure E gives a characteristic curve of slope.

$$\text{slope} = {}^{dD}/_{d\log H}$$

Photographic density is measured by a densitometer [52]. It is found by a measurement of the transmittance T of light through the film, ie the ratio of transmitted to incident light intensity on the film.

$$D = -\log_{10} T$$

The amount of light allowed to impinge on the film emulsion at the photographic stage is normally measured in terms of exposure, which is the time integral of illumination. The

response of the photographic emulsion after processing is usually presented in the form of a curve in which density is plotted as a function of exposure to a particular light source usually tungsten **Fig 4.0.4**

It is divided up into three sections the toe, linear and shoulder. The linear region has constant slope. If various levels of fluorescence intensity are to be measured with photography then the exposure levels on the film must fall between the toe and the shoulder of the curve. Maximum change in film density for a given increase in fluorescence intensity is clearly gained by using exposure levels in this region of the curve.

The sensitivity of the film emulsion varies with the wavelength it is exposed to. To evaluate the exposure required to achieve a particular fog density with a particular exposure spectrum, then a spectral sensitivity curve is needed. These curves are usually given in terms of the reciprocal of the exposure required at any given wavelength to produce unit density or some other convenient density level **Fig 4.0.5**

Because of the low intensity of fluorescence, films for high speed photography must be of maximum sensitivity to the fluorescence wavelengths. Several films were considered. Eastman 4-X negative, Kodak Pan 2484 Estar-AH,and Kodak RAR

2479. RAR 2479 was finally chosen because of its sensitivity in the 600 nm region. It is the performance curves for this film that are used as examples in **Figs 4.0.4** and **4.0.5** .

4.3 Light Sources

A light source suitable for inducing fluorescence must have a wavelength that is capable of exciting the fluorescent dye Rhodamine B. Because it is necessary to separate the fluorescence from the exciting light, the light source must have wavelengths that are sharply defined and ideally none of those wavelengths should occur in the spectral region of the induced fluorescence. Because the fluorescence intensity was to be measured photographically, the light source had to have a high intensity to produce a high level of fluorescence for the reasons outlined in chapter three. The light source had to be focused to a spot of uniform intensity across its diameters. This would allow it to induce equal fluorescence intensity levels over the area on which it impinged, if the thickness of the film it was inducing to fluoresce was of uniform thickness and homogeneous.

The experiments conducted with the argon ion laser light source discussed in chapter three satisfied all but one of the aforementioned criteria. It did not have a uniform intensity

distribution across its diameters. This was because it was operating in a lasing mode known as TEM 001. TEM 001 is a lasing mode that results in a Gaussian intensity distribution across the diameters of the emerging light beam. If different optics are employed in the optical head of the laser then it is possible to tune the laser to operate in a mode known as MTM. A laser operating in MTM (multi-transverse-mode) produces a light beam whose intensity is approximately uniform across its diameters **Fig 4.0.6.**

The laser discussed in chapter three produced light at only one wavelength 514 nm, and was capable of delivering 2 watts of power. Such lasers are expensive to purchase and because of financial constraints it was decided to purchase a multiline argon ion laser. Multiline lasers produce light at more than one wavelength simultaneously. They have the advantage of producing more overall power output than a similarly priced single wavelength laser. The multiline laser used in the project operated in MTM mode and had the ability to output a overall maximum of 100 mW of power consisting mostly of 41.4mW at 488nm and 41.4mW at 514nm. The rest of the power was at 501,496,476,465 and 457nm. It was manufactured by Ion Laser Technology and had the model number 450A. The plasma tube was air cooled by two high volume fans. The power supply was separate and incorporated a MOS FET switching bridge and a high frequency isolation transformer, which resulted in total mains isolation and a more stable laser power output.

4.4 Optics

To separate the fluorescence light from the laser light it was necessary to employ some form of filtering arrangement. In order to image the fluorescence from the lip seal contact it was necessary to use some form of lens.

4.4.1 Lenses

The design and type of lens used will determine the magnification of the contact object plus the intensity and sharpness of the resultant image. For a particular lens of a given focal length **f**, the relationship between the object and the image locations can be related by the lens formula.

$$\frac{1}{f} = \frac{1}{o} + \frac{1}{i}$$

Where **o** is the distance between the object and the first principal plane of the lens, and **i** is the distance between the image and the second principal plane of the lens. The magnification of an optical system is defined as.

$$m = \frac{-i}{o}$$

A negative result, ie both **o** and **i** positive, indicates a real inverted image The focal length of the lens determined how

close it was possible to get to the object and form a subsequent real inverted image. Had the distance from the object to the lens been shorter than the focal distance of the lens, then a virtual image would have been formed. With a virtual image, light emerges from the lens appearing to diverge from some imaginary point behind the lens. Virtual images cannot be projected onto a plane and therefore cannot be photographically recorded.

As discussed in chapter three, the fluorescing molecule emitted photons in all directions, ie the light was divergent. In order to form an image of the brightest intensity it was necessary to capture as much light as possible. The closer to the object a lens is, the more light it will capture. Therefore a lens with a small focal length was required. Also the larger the diameter of the lens, the more light that is captured at a particular distance from the object. Therefore a lens with a large diameter was required.

4.4.2 Lens Design

There are numerous types of lens design. The choice of one type of design over another in this particular optical application, was driven by a need to minimise any inherent aberrations which could arise from the design of the lens itself. The most commonly used lens is the symmetric biconvex lens. A biconvex lens offers good performance at low magnifications. It has the

best shape to minimise spherical aberration at magnifications of 1:1. Spherical aberration arises because any light from an object that passes through the various diameters of the lens is not re-imaged at a finite plane behind the lens. This happens because the lens surfaces are spherical. The ideal shape for a lens surface would be parabolic. It is difficult to manufacture parabolic surfaces accurately. Such lenses can be purchased and are known as aspheric lenses. The quality of this type of lens is usually poor unless a high price is paid. The spherical aberration of a lens can be reduced by making one of the surfaces plain. Such lenses are known as plano-convex lenses, and are reasonably priced. With this type of lens the convex surface is faced toward the object. It was decided to use a plano-convex lens design with a focal length of 25 mm, a diameter of 30 mm and a centre thickness of 12.1 mm.

In addition to deciding upon the specifications for the lens diameter, its focal length and design, two other factors had to be considered with this particular application. One of these was the lens material the other was the possibility of reflections.

4.4.3 Lens Materials

Different lens materials have different transmission characteristics at different wavelengths. Lenses made from fused silica quartz have extremely good spectral transmission

in the ranges of 200-2000 nm. The fluorescence produced by rhodamine B had its maximum intensity at 600nm. The laser wavelengths produced by the multiline argon ion laser ranged from 457 to 514nm. It was therefore decided to use fused quartz lenses in the rig optical design.

As light passes through a lens system there is a certain amount of the light reflected at each surface. The degree of light reflected at a lens surface depends upon the angle of the incident light. Minimum reflection occurs when the incident light is at 90 degrees to the surface. When this condition is present about 4% of the total light intensity impinging upon the surface is reflected back. Because the final optical design involved six surfaces being used, approximately 22 milliwatts of the original 100 milliwatts would have been lost due to reflection. The scattered light from these back reflections and subsequent internal reflections would have dispersed light over a larger area than the diameter of the beam. This would have resulted in fluorescence being excited where it was not wanted.

It is possible to obtain lenses that have a deposit of a substance over their surface to help reduce reflection. The type of substance used and the thickness of the coating determines the light wavelengths over which the coating is effective in reducing reflection. One coating, magnesium fluoride, can reduce back reflection from 4 to 2% over the

wavelength regions of 400 to 700nm. It was to minimise unwanted reflection that lenses used in the rig optics were coated with magnesium fluoride.

4.4.4 Filters and reflectors

Interference filters operate through a complex process of constructive and destructive interference to precisely select a very narrow range of light wavelengths with maximum transmission efficiency. There are two types, bandpass filters and edge filters. Edge filters transmit only above or below a certain light wavelength. The wavelengths above and below this wavelength are either reflected or transmitted. The ability to reflect a particular percentage of a particular impinging wavelength is dependent upon the angle of incidence of the impinging light ray and the type and thickness of the coating employed at the filter surface. Maximum reflectivity of the filter to a particular light wavelength is usually achieved when the filter surface is at 45 degrees to the incident light ray

4.4.5 The filter and lens axis configuration

It was necessary to position the incoming laser beam on an axis at 90 degrees to the surfaces of the lenses and the quartz glass running face of the floating element seal for two reasons. The first was to reduce any reflection of the exciting

laser light source off the surfaces of the optics. The second was to prevent a form of aberration called comma. Comma is when the image of a point source appears to be spread out into a comet shaped flare. It arises when an optical system is designed off axis. The possibility that this form of aberration could arise was therefore taken into account when the geometrical design configuration of the apparatus was considered.

From the experiments discussed in chapter three it can be seen that an interference edge filter can be used to accomplish these ends. The problem encountered with the filter used in chapter three was that it only reflected 85% of the laser light incident upon it. The remaining 15% travelled through the filter then toward the camera lens. It was thought at the time that this light could be prevented from going into the camera lens by inserting a colour glass filter that would absorb the laser light but transmit the fluorescent light emitted from the contact zone. However what transpired was that the laser light was of high enough intensity to induce the dye in the coloured glass filter to fluoresce. Because the fluorescence from the glass and the fluorescence from the contact were of similar wavelengths they could not be distinguished which meant that there was no way of telling what the true intensity of the fluorescence from the contact actually was. Because of this, a different interference filter was acquired which had the

ability to reflect 99.98% of the laser light falling incident upon it. Its spectral response can be seen in **Fig 4.0.7** The schematic representation of how the lenses and filters axes were positioned can be seen in **Fig 4.0.8**

4.4.6 The filter and lens spatial configuration

Apart from the good reasoning behind the axial arrangement of the lenses and filter shown in **Fig 4.0.8**, the reasoning behind why two lenses were used, and why the lenses and filter were positioned in the way they were, will now be discussed.

The incoming laser light to the contact and the induced fluorescent light from the contact had to travel along the same axis but in opposite directions until they could be separated by the interference filter.

The lens had to be at as short a distance as possible to the contact zone in order to image as much fluorescent light as possible from the contact zone. To position the filter in front of the lens would not have been logical as it would have increased this distance. This meant that both the laser light to the contact and the fluorescence from the contact had to pass through the same lens before they could be separated by the interference filter. Now, as already stated, the function of this lens was to capture as much light as possible and image it at some plane behind the interference filter.

The distance of the image plane and the magnification of the contact image was governed by the distance of the lens from the contact zone. It was desirable to make the contact magnification variable. However it was crucial that the laser light intensity across the diameter of the laser spot falling incident upon the contact region be maintained constant. Although the laser light leaving the laser was parallel, after it had passed through the imaging lens it would become focused. This would mean that the intensity of the spot at the contact would vary depending on how far the contact was from the imaging lens, which would be dependent upon what magnification was required. This was extremely undesirable as the fluorescent intensity depended directly upon the incident laser intensity. To rectify this position a means was devised that ensured that the light leaving the imaging lens was parallel and therefore the intensity of the laser light spot falling incident upon the seal contact zone was independent of the distance of the imaging lens from the contact zone. This consisted of passing the laser light through a primary lens before it reached the imaging lens. The distance of the laser light path between the lenses was set at the combined focal distances of both lenses. The primary lens focused the incoming parallel laser light down to a plane at its focal length. The imaging lens then saw the light emanating from a plane that was at its own focal plane. Because of this the light leaving the imaging lens was always parallel.

4.5 The Optical Component Mounting

The optical arrangement that is depicted schematically in Fig. 4.0.8 required mounting in some manner. In this section a description of the method of mounting and the philosophy behind its design are discussed.

4.5.1 Mounting Philosophy

The primary function of the method of mounting was to ensure several desirable characteristics within the optics system. These were, a high mechanical and thermal stability. High resolution with rapid coarse adjustment and enough fine spatial movement to allow the two lenses, the filter, the laser light source and the seal contact region to be accurately aligned with the minimum amount of effort. Thought was given to how this position could best be attained.

The required structural flexibility throughout the system could be seen to be composed of three main sub-structures. The first was considered to be the relative spatial positions between the optics, that included the lenses and the filter. The second was considered to be the relative spatial position between the laser light source and the optics. The third was seen to be the relative spatial positions between the laser, the optics and the seal contact region.

After thought it was decided to allow relative movement between the lenses and the filter and to fix the relative spatial positions of each optic to a common position. It was then decided to allow relative movement between the laser and the optics and again to fix the relative spatial positions of each to another common position. This mutually common position was then to be moved in space relative to the seal contact zone. The various components involved that made this possible will now be discussed.

4.5.2 Lenses and filter mounts

The lenses and filter were mounted separately on three gimbal assemblies, **Fig. 4.0.9**, each gimbal assembly allowed the x,y,z pitch and the z height of each optic to be altered separately by turning in a clockwise or anti-clockwise direction three gimbal pitch adjusting bolts by different amounts. The stiffness of each gimbal stage was maintained at all times by a compression spring positioned underneath the base housing of each assembly **Fig 4.1.0.** The spring was slotted over a centralising spigot whose function was to allow a common point around which the stage could pivot and also to limit the extent of lateral movement of the spring. The centralising spigot had a head at one end of its length and was threaded at the other. The shank of the spigot slotted through a larger diameter clearance hole in the gimbal stage. The centre of this clearance hole was positioned at the centre of gravity of the

triangular plane prescribed between the longitudinal centre axes of the three pitch adjusting bolts **Fig.4.0.9.** The spigot shank length protruding from the bottom face of the gimbal stage slotted through a clearance hole drilled into the top face of the gimbal base. This clearance hole in the gimbal base ran into a larger clearance hole. Both the holes were concentric with each other. A compression spring slotted over the protruding spigot shank visible in the larger diameter clearance hole. A retaining nut and washer screwed onto the end of the spigot shank, maintaining the spring under permanent compression. The compression of the spring ensured that the bases of the three gimbal pitch adjusting bolts remained in contact with the top surface of the gimbal base. The bases of the three pitch adjusting bolts were hemispherical. These bases seated into three larger radius concave dimples machined into the top face of the gimbal base. This arrangement prevented the table twisting when the gimbal pitch adjusting bolts were screwed in or out **Fig. 4.1.0.**

The lenses and filter were held at their outer diameters by three bracket mounts, **Fig. 4.0.9.** The bracket mounts were designed so that the centre of each different diameter optic was positioned at the same vertical height distance from the top surface of the gimbal stage. Each bracket mount sat on the gimbal stage and was held in position by two Allen bolts that ran in slots machined into the flange base of each mount. The

reason for the slots was to allow a small amount of movement of each bracket mount along the secondary Y axis of each optic. The three gimbal assembles were mounted onto a 2 mm thick mounting plate **Fig. 4.0.9.** The lenses gimbal mounts were positioned on the mounting plate so that the primary X axes of both lenses were at 90° to each other. The filter gimbal mount was positioned so that the filter secondary axes was at 45° to both the primary axes of the lens mounts. Also the central axis at the top plane of the filter was positioned at the intersection of both the primary axes of the imaging and primary lenses.

The three gimbals were allowed to move on the mounting plate in different ways for the following reasons. It was intended that everything should be set from the spatial position of the first lens. The reason for this is that it was intended to fix the first lens to the position of the laser. The second lens gimbal and the filter gimbal were allowed to move relative to the first lens but about different axes. The filter gimbal was allowed angular movement about the top plane central axis of the filter in the x-y plane. This was done as follows.

A third hole was drilled into the bottom face of the filter gimbal base. A clearance hole was drilled into the base plate and a location peg seated into this hole. A radiused clearance channel was machined into the base. The threshold spigot was

placed into the base plate at this position and the clearance channel filter mount fitted over this threaded spigot. A nut screwed into the spigot thread allowing the whole filter gimbal assembly to be locked into any angular position prescribed by the clearance channel. The gimbal onto which the imaging lens was mounted was allowed to move along an axis normal to the axis of the primary lens. This was achieved as follows. A grub screw was screwed through an angled bracket which in turn was screwed to the top surface of the gimbal table. The bracket was positioned normal to the end face of the lens mounting flange, the grub screw passed through the angular bracket against the end surface of the end flange. At the opposite end of the end flange a second angular bracket was screwed onto the top face of the gimbal table. A compression spring was fitted into a pocket drilled into the end face of the mount. The movement of the grub screw against the face of the lens mount moved the whole lens mount along an axis normal to the axis of the primary lens.

4.6 The Floating Element Seal

The floating element seal was a development of the company George Angus and Co. It was designed for sealing the hubs and axles of heavy goods vehicles **Fig. 4.1.2.** Unlike most other lip seals it has two lips. These seal lips run on the inside of two steel casings and not on the shaft. The inner casing is an interference fit on the shaft that is to be sealed and thus rotates with the shaft during operation. The outer casing is an interference fit in the seal housing and is therefore static during operation. Because one lip of the V shaped sealing element seals on the stationary outer casing and the other lip seals on the rotating inner casing the V shaped element rotates at approximately half the shaft speed during operation. This reduces friction and thus heat build up and increases sealing life. In the floating element seal used in this project the outer sealing case was made from quartz glass to allow viewing of one of the lip contacts during running.

4.6.1 The floating element seal test rig

The floating element seal rig **Fig. 4.1.3** consisted of a housing cavity which contained the oil that was to be sealed and a shaft on which to drive the seal. The housing was a steel tube that had an outer diameter of 215mm an inner diameter of 205mm and was 103mm in length. To one end of the housing was bolted an annular plate, the internal diameter housed a plain lip

shaft

seal the other end of the housing had a 40 TPI thread cut into its inner diameter. Into this threaded portion screwed an annular ring that housed the stationary quartz glass sealing face of the floating element seal. The threaded annular ring allowed axial movement of the static glass sealing face relative to the inner rotating steel sealing face. This facilitated variation in the loading of the V shaped sealing element lips against the sealing surfaces, and hence variable contact load.

The shaft was supported at one end behind the housing by a roller bearing. The shaft was driven via a rubber drive dog by a 5 hp three phase electric motor with a mechanical gearbox that allowed the speed to be varied between 480 and 4320 r.p.m.

The lens filter combination and the argon ion laser were mounted on a flat X-Y table in front of the floating element seal as shown in **Fig. 4.1.3** . The centre height of the laser optical head and the centre height of the lenses and filter were positioned at the centre height of the floating element seal. After passage through the first lens the laser beam was turned through 90 degrees by the interference filter. The beam then passed through the second lens which directed it through the quartz glass outer case of the floating element seal and onto the contact where it induced fluorescence in the lubricant film. The resultant fluorescence travelled back through the

quartz glass outer casing to be collected by the lens. The lens then imaged the fluorescence at some point away from the contact.

4.6.2 Experiments with the floating element seal

It was first decided to see if the contact of the floating element seal could be photographed using a 35mm SLR camera before work was carried out using the high speed rotating prism camera.

A saturated solution of rhodamine B in shell 20w/50 was made by first dissolving Rhodamine B, 0.1672g in ethanol 10cm^3. This was then added to 4 litres of Shell 20w/50. The solution was stirred for five minutes to facilitate dispersion of the dye in the oil. The oil was then poured into the housing cavity of the floating element seal rig. The cavity was filled up to depth of half the shaft height. The shaft was rotated at 1041rpm. The laser was scanned radially across the contact. The position of minimum fluorescence intensity and hence the position of min film thickness at the contact was found by projecting an image onto a piece of white card **Fig. 4.1.4.** The fluorescence was imaged by the plano-convex lens. The position of the image plane behind the lens was determined by moving a piece of white card closer to and further away from the lens until the position of sharpest image was found at 104cm. A Cannon 35mm Program camera with its lens removed was mounted on a tripod.

The camera centre was positioned along the centre axis of the lens with its film plane at a distance of 104 cm from the lens **Fig. 4.1.5** The camera was loaded with Ilford 400 ASA black and white film. The shaft of the rig was rotated at 1041 r.p.m.. The seal was allowed to run at this speed for 15 minutes to allow the sealing condition to stabilise. After this period 9 photographs were randomly taken at an exposure of 1/125 sec. This was repeated at exposure levels of 1/250 1/500 sec. Each set of 9 photographs being taken immediately after the other. The exposed photographic film was developed for 5 minutes in a 1/30 dilution strength solution of Kodak HC-10 developer, then fixed for 10 minutes in a 1/4 dilution strength solution of Kodak Unifix. The resultant film was found to be under exposed at all exposure levels. The oil was drained the rig dismantled and cleaned free of the remaining oil with a rag soaked in acetone. The sealing element was also treated in this manner . After cleaning the element was allowed to dry overnight so that any acetone that had been absorbed by the element could evaporate off.

Rhodamin B, 3.6267g, was dissolved in $10cm^3$ of ethanol. This was then added to 4 litres of ethylene glycol. The rig was reassembled and the ethylene glycol rhodamine B solution was poured into the housing cavity up to a depth of half the shaft height. The experiment was repeated as before and the exposed film developed in the same manner. The film showed exposure at

all levels. No attempt was made to analyse the degree of film fog because a microdensitometer (chapter seven) was not available at the time and because a means of calibrating this rig had not been devised. The experiment was repeated again except this time the rotating prism camera replaced the Canon SLR. The films were all underexposed. The result had showed that that it was possible to record photographically laser induced fluorescence emanating from a sealing contact using the Canon SLR camera.

Chapter Five

5.1 Design of the Rotary Shaft Lip Seal Rig

In service and under testing conditions most lip seals are usually employed on horizontal shafts. With rigs designed to assess the performance of lip seals, the oil depth in the static rig assembly normally comes up to half shaft height. In order to avoid any variation in pressure head or possible non uniformity in the circumferential inlet conditions on the oil side of the lip contact region, it was decided to run the seal with a vertical shaft.

The shaft had to be connected to a driving unit and supported in some manner. Misalignment of the drive, shaft or supporting bearings could have resulted in complex signals that would have been transmitted to the seal via the shaft. This would have affected the seal's displacement characteristics during operation and hence influence the thickness of the oil film in the contact region. The design of the shaft bearings and drive unit strove toward minimising these input signals.

5.2 Design of the Shaft

In most rotating shaft applications, ball, roller or lubricated journal bearings provide a means of satisfactory support. However when it is desirable to minimise friction and reduce the possibility of oil fouling, air bearings are usually chosen because of their superiority over the others in this respect. An externally pressurised air bearing can typically hold a shaft centre axis of rotation ten times better than the out of round of the shaft and bearing surfaces. It was for these reasons that air bearings were selected as a means of supporting the shaft. What follows is a discussion of the various elements involved and the reasons behind the design.

5.2.1 Shaft material

The choice of shaft material was governed not only by the needs of the fluoresence viewing technique ie transparency to light, but also by the operational conditions the shaft had to encounter and the function it had to perform. The material had to be dimensionally stable and exhibit a high degree of rigidity to prevent flexure during operation which would have been transmitted to the seal. It was expected that the temperature of the seal contact area would rise very rapidly during shaft start up. Therefore the shaft material had to be able to withstand thermal shock. The lip seal elastomeric

material is very abrasive. A lip seal is capable of scoring deep grooves and scratches in a steel shaft within minutes of initial shaft start up. If this were to happen to the shaft that was to be used in the rig it would destroy the optical quality of the shaft surface which would then scatter fluorescent light from the contact area and deteriorate the subsequent fluorescent image. The shaft material had to have high transmission characteristics over the range of laser and fluorescent wavelengths. One material, silica quartz, fulfilled all the aforementioned criteria. This material is very rigid, a typical value for its flexural modulus is 31.4E+06 kN/m2. Its Young's modulus is approximately 72.6E+06 kN/m2. It has excellent resistance to thermal shock and can typically withstand a plunge into cold water from a temperature of 800 degrees Celsius. It is very hard and extremely resistant to scratches, having a value of 8 on the MHOS scale (Diamond being 15). Its spectral transmission is typically 96% over the wavelength range 180-2000 nm **Fig 5.1.3.** It was for these reasons that silica quartz was chosen as the shaft material. A particular grade of quartz, spectrasil (manufactured by Thermal Syndicate Ltd., Tyne and Wear), was used because of its high optical quality. There are no bubbles or imperfections in it.

5.2.2 Shaft Geometry

The shaft geometry shown in **Fig 5.0.3** was produced as follows.

The internal 15 mm bore was diamond drilled and then honed to size. The external diameters were ground between fixed centres from a solid quartz billet. The last 15mm along the axial length of the 25.4 mm diameter on which the test seal was to run and its associated 15 mm internal diameter were optically polished to allow viewing of the contact region. The surface finish of the 25.4 mm polished running surface was checked using a Talysurf 6 instrument and values for its various surface texture parameters are given in Table 5.0.0. Radial shaft movement was restricted by two air bearings that extended over 60mm of the axial length of the inner 15 mm diameter bore **Fig 5.0.3** (assembly drawing **5.0.0** detail number 7). Shaft axial float was restricted by two air bearings either side of the 60mm diameter 10mm thick flange on one end of the shaft **Fig 5.0.3** (assembly drawing 5.0.0 detail numbers 12 and 14). In order to keep dynamic shaft eccentricity to a minimum during the shafts manufacture, a 5 micron tolerance of concentricity was imposed between the outer 25.4 mm shaft diameter and the inner 15 mm bearing running surface diameter. Talyrond traces of the finished shaft showed that the degree of concentricity between these diameters was 3.5 microns. It was important that the 10mm thick flange bearing surfaces exhibited a high degree of parallelism and that the internal bore of the shaft and both the shaft flange bearing surfaces exhibited a high degree of squareness (flange runout over the whole bearing surface) to minimise shaft tilt and

overstressing of the shaft during rotation. A 5 micron manufacturing tolerance was imposed on both these dimensions. Tallyrond measurements of the finished shaft showed that the degree of parallelism between the shaft flange bearing surfaces was better than 0.5 microns and that the degree of squareness between the shaft inner 15 mm shaft bearing surface diameter and the shaft flange bearing surfaces, indicated by the total flange runout, was better than 2.0 microns. The degree of squareness between the flange surfaces and the 25.4 mm seal running surface was seen to be better than 0.5 microns. The out of round of the outer 25.4 mm shaft diameter was measured at better than 0.5 microns on the last 15 mm of polished seal running surface. No multilobing of the shaft was evident. The out of round of the inner 15 mm shaft diameter bearing surface was measured at better than 3.5 microns which meant that on a perfect bearing shaft the quartz shaft would hold a centre of rotation of approximately 0.35 microns about the centre of axis of the inner 15 mm bore (ten times better than the bore out of round).

5.3 Air Bearing Design

5.3.1 The shafts radial bearings

The bearings restricting radial movement of the quartz shaft **Fig 5.0.4** (assembly drawing 5.0.0 detail number 7) consisted of two 14.975 mm diameter bearings. Both bearings had a length/diameter ratio of 2 and each bearing had two rows of six equispaced plain jets placed at quarter stations. The jets were jewellers bushes with an internal diameter of 0.1 mm. The twenty four jets were press fitted into four rows of six equispaced air feed galleries drilled normal to the bearing surfaces at quarter stations in the bearing lengths. The galleries were fed with air from a main gallery that extended down the central axis of the main shaft. The bearings were operated with a diametral clearance of 25.4 microns between the shaft and bearing surfaces. They were designed for maximum stiffness and to operate at a line pressure of 5 bar. Air was vented from the bottom circumferential edge of the bottom bearing to atmosphere via the open bore of the quartz shaft. Air was vented from the top circumferential edge of the bottom bearing and the bottom circumferential edge of the top bearing into an annular cavity that separated both bearing surfaces. Air was vented to atmosphere from this cavity via hole positioned under the surface of the bottom bearing that connected with the open bore of the quartz shaft. Air was vented from the top circumferential edge of the top bearing

into an annular cavity. Air was vented from this annular cavity to atmosphere via a channel milled into the surface along the length of the bearing shaft location shank.

5.3.2 The shafts axial bearings

Axial movement of the quartz shaft was restricted by two thrust bearings acting upon opposite sides of the 10 mm thick flange of the quartz shaft. The bottom thrust bearing **Fig 5.0.9** had 20 equispaced jewellers bushes with an internal diameter of 0.45 mm acting as jets. The bushes were press fitted into twenty equispaced clearance holes. Air was fed to the jets via the clearance holes from an annular cavity machined into the top surface of the oil chamber housing **Fig 5.0.7.** Air was prevented from leaking from the annular cavity by two o-rings positoned in grooves machined into the top surface of the oil chamber housing at the inner and outer diameters of the annular air cavity. Air was fed to the annular cavity through a hole drilled under the top surface of the oil chamber housing. The hole extended radially outward to the external diameter of the oil chamber housing where it was plugged with a solid brass insert to make it air tight. Air was fed to this hole through an intersecting hole at 90 degrees drilled through the bottom thrust plate. Air was prevented from leaking from the hole across the surfaces of the bottom surface of the bottom thrust plate and the top surface of the oil chamber housing by an o-ring situated in a

groove machined in the bottom face of the bottom thrust plate.

The bottom thrust plate and the oil chamber housing were clamped together by eight Allen bolts. The bolt shanks ran through clearance holes drilled through the top of the oil chamber housing and then screwed into blind tapped holes drilled into the bottom of the bottom thrust plate. On tightening, the Allen bolts pulled the bottom surface of the bottom thrust plate onto the top surface of the oil chamber housing compressing the o-rings and affecting an air tight seal.

The inner diameter of the bottom thrust bearing was vented through a 3.6 mm diameteral clearance between the quartz shaft and inner diameter of the bottom thrust plate to an annular cavity in the oil chamber housing **Fig 5.0.7.** This cavity was vented to atmosphere via a hole drilled through the external wall of the housing. The outer diameter of the bottom thrust bearing was vented to a cavity in the top thrust plate **Fig 5.1.1** that housed the drive belt pulley and bearing, and then to atmosphere through the drive belt access and exit slots cut through the walls of the top thrust plate.

The top thrust plate had 13 equispaced jewellers bushes with an internal diameter of 0.4 mm acting as jets. The bushes were press fitted into thirteen equispaced holes drilled into the

thrust plate disc. Air was fed to the jets from an annular cavity cut into the top surface. Air was prevented from leaking to atmosphere from the inner diameter of the cavity along the shank of the bearing shaft by an o-ring postioned in a groove machined into the top surface. Air was fed to the annular cavity from a radially intersecting main feed channel machined into the top surface. Air was prevented from leaking to atmosphere from the main feed channel and the outer diameter of the cavity by an o-ring positioned in a groove machined into the top surface close to the external diameter of the top thrust plate.

Both the top thrust bearing and the bottom thrust bearing were designed for maximum stiffness to operate with a clearance of 25. 4 microns between the bearing surfaces and the quartz shaft flange surfaces. An annular spacing ring **Fig 5.1.0**, separated the top and bottom thrust plate surfaces. A clearance hole was drilled through the central diameter of the ring . This hole aligned with the clearance holes drilled in the top thrust plate and the bottom thrust plate that fed air to the bottom thrust plate jets. Air was prevented from leaking across the two mating surfaces by two o-rings housed in two grooves machined into the top and bottom surfaces of the spacing ring outside the circumference of the hole.

5.4 Design of the Drive Mechanism

Because quartz is so brittle it is difficult to machine complex geometries without the material incurring fracture. Indeed it took two attempts to manufacture the relatively simple shaft geometry shown in figure 5.0.3. The first attempt resulted in failure when the shaft shattered into several pieces during one of the grinding operations. This problem was anticipated during the design stage, and for this reason it was thought impractical to attempt to machine any gear teeth onto the shaft which would have allowed it to be driven in some manner. The possibility of bonding a metal gear ring onto the flange outer diameter of the quartz shaft was considered but then rejected because of the following reasons. It would have been impossible to produce a non flexible bond between quartz and steel because of the difference in the coefficients of expansion between these materials. It would have been difficult but not impossible to produce a flexible bond. However it would not have been easy to position accurately the quartz and steel components to be bonded nor would it have been easy to apply an even distribution of adhesive over the bonding area. As an adhesive polymerises and acquires its strength, it undergoes shrinkage. If the distribution of adhesive had been non-uniform then non-uniform dimensional shrinkage would have resulted and the relative positions of the bonded components could have been altered or the

components could have become distorted. Driving the quartz shaft using a flat rubber drive belt running on the outer diameter of the flange on the quartz shaft was considered but rejected because the tension that would have been needed in the belt to produce the required friction for driving would have imposed a sizeable out of balance radial load onto the shaft, imposing a different and an uneven circumferential loading on both the bearings that restricted radial movement of the shaft. The final design arrived at utilised a rubber drive dog and brass coupling. The drive dog was produced by compression moulding. The type of rubber used was neoprene. The dog had eight castlelations on its top surface **Fig 5.0.2.** The internal diameter of the drive dog was bonded to the outer diameter of the quartz shaft. The brass coupling was mounted onto a pulley. Part of the outer diameter of the pulley was press fitted and fixed with Loktite into the internal diameter of a ball bearing race **Fig 5.0.1.** The outer diameter of the race was press fitted into the bottom of the outer diameter of the annular cavity in the top thrust plate. On assembly the bottom face of the top thrust plate seated onto the top face of the spacing ring. The castlelations in the top of the drive dog mated with the female mirror cut into the surface of the brass coupling. The peaks of the castlelations on the brass coupling and the valleys of the castlelations on the drive dog were not in contact, being separated by a distance of 1 mm. This ensured that no load was placed upon the bottom thrust

bearing, and that the only force imparted to the shaft upon rotation of the brass coupling was torque. The pulley rotating the coupling was driven by a toothed drive belt. The belt entered and exited the annular cavity that housed the bearing coupling and dog via two slots machined into the cavity wall of the top thrust bearing. Power was transmitted to the belt from an identical pulley mounted on a shaft that was directly driven by an electric motor mounted vertically on a steel plate positioned at the side of the shaft bearings and drive mechanism assembly **Fig 5.1.2.** The 1.5 horse power motor had a variable speed controller that allowed the motor to rotate at speeds from 0 to 2000 rpm.

5.5 Shaft Bearings and Drive Mechanism Assembly

The rig assembly procedure was as follows. The bottom surface of the oil chamber housing **Fig 5.07** was placed onto a bench and centralised over a conveniently found hole in the bench top. **A location ring was seated into the location groove cut into the top surface of the oil chamber housing.** The groove and the ring were a tight fit. Two o-rings were dropped into two o-ring grooves that encompassed the inner and outer diameters of the annular cavity cut into the top surface of the oil chamber housing. The top face of the bottom thrust plate **Fig 5.09** was placed onto the bench next to the oil chamber housing. An o-ring was placed into the groove machined

into the bottom surface of the bottom thrust plate that encompassed the air gallery hole. An application of silicone grease to the o-ring ensured that it would not drop out of the groove when the bottom thrust plate was inverted. The air gallery hole in the bottom thrust plate was then aligned with the air gallery hole in the top of the oil chamber housing both these holes allowed air to be fed to the bottom thrust jets. The bottom surface of the bottom thrust plate was then seated onto the top surface of the oil chamber housing. **The location ring in the top surface of the oil chamber housing also fitted into a location groove cut into the bottom surface of the bottom thrust plate.** This ensured that the central axis of the bottom thrust plate and the central axis of the oil chamber housing were in alignment. This was important for reasons discussed later. A location ring was seated into the location groove machined into the top surface of the bottom thrust plate. The top surface of the spacing ring **Fig 5.10** was placed onto the bench next to the assembly. Silicone grease was applied to an o-ring that was then placed into the groove machined into the bottom surface of the spacing ring. The spacing ring was then inverted. The clearance hole in the spacing ring was aligned with the air feed hole drilled through the bottom thrust plate. The spacing ring was then seated onto the top surface of the bottom thrust plate. **The location ring in the top of the bottom thrust plate also fitted into the location groove cut into the bottom face**

of the spacing ring. This ensured that the central axis of the spacing ring was in alignment with the central axis of the oil chamber housing. The quartz shaft **Fig 5.03** was then slid into position through the clearance holes in the bottom thrust plate and the oil chamber housing until the bottom flange surface of the quartz shaft contacted the top surface of the bottom thrust plate. In this position the bottom polished seal running section of the shaft extended further than the bottom face of the oil chamber housing. This was why it was necessary to assemble the mechanism over a hole in the bench top. A location ring was seated into the location ring groove machined into the top surface of the spacing ring. A small o-ring was placed into the groove machined into the top surface of the spacing ring. The top surface of the top thrust plate **Fig 5.1.1** was placed onto the bench next to the assembly. The rubber drive belt was meshed with the drive pulley **Fig 5.0.1** sunk into the annular cavity machined into the bottom of the top thrust plate. The belt was also fed through the inlet and exit slots machined into the walls of the top thrust plate. The belt was held in position over the pulley and through the thrust plate walls by hand. The top thrust plate was then inverted. The peaks of the castlelations on the brass drive coupling and the valleys of the castlelations on the rubber drive dog bonded to the quartz shaft were then aligned by eye. The bottom surface of the top thrust plate was then lowered towards the top surface of the

spacing ring until the rubber drive dog and the brass coupling just meshed. The air gallery hole drilled through the top thrust plate was then aligned with the air gallery hole drilled through the spacing ring. The bottom surface of the top thrust plate was then seated onto the top surface of the spacing ring so fully meshing the drive dog and coupling. **The location ring in the top surface of the spacing ring also fitted into a location groove machined into the bottom surface of the top thrust plate.** This ensured that the central axis of the top thrust plate and the central axis of the oil chamber housing were in alignment. At this point the whole assembly was inverted. The bearing shaft **Fig 5.0.4** was pushed down the bore of the quartz shaft top end first. The shaft location shank was located into the reamed clearance hole that ran through the central axis of the top thrust plate. The shoulder of the shank was seated into the groove machined into the bottom surface of the top thrust plate. **At this point the central axis of the bearing shaft was in alignment with the central axis of the oil chamber housing because of the series of location rings running throughout the whole assembly.** Eight Allen bolts were pushed through the eight equispaced aligned holes drilled through the oil chamber housing, the bottom thrust plate,the spacing ring, and the top thrust plate. The assembly was then inverted. An o-ring was placed into the o-ring groove machined into the top surface of the top thrust plate. The whole assembly was then removed from the bench and

fixed to the mounting plate, by screwing the eight Allen bolts into eight blind tapped holes drilled into the bottom surface of the mounting plate. On tightening the Allen bolts, all the o-rings throughout the assembly were compressed so effecting an air tight seal. The air supply couplings were then screwed onto the threads cut into the top end of the bearing shaft until the shaft location shank was put under tension. The oil chamber seal housing **Fig 5.0.8** was fitted with its seal which had its lip lubricated with glycerol. The oil chamber seal housing was then pushed into the internal diameter oil chamber housing and at the same time the seal lip was stretched over the outer diameter of the quartz shaft. The oil chamber seal housing was held in position by eight Allen bolts that ran through clearance holes drilled through the oil chamber housing and then screwed into blind holes drilled into the bottom surface of the bottom thrust plate. The test seal **Fig 5.0.5.** was press fitted into the test seal housing **Fig 5.0.6.** using an arbor press. The arbor press pushed down onto the back of a plate which was in uniform contact with the back of the steel insert moulded into the seal body. This ensured a uniformly distributed load through the top of the insert. This prevented buckling of the insert and hence buckling of the seal during fitting. After the seal was bedded in an o-ring was coated with glycerol and placed into the groove machined into the bottom face of the oil chamber housing. The top face of the test seal housing was then seated onto the bottom face

of the oil chamber housing. **A location shoulder machined into the top face of the test seal housing and a location recess cut into the bottom face of the oil chamber housing ensured that the central axis of the test seal housing and the central axis of the oil chamber housing were in alignment.** The test seal housing was fixed to the oil chamber housing by eight Allen bolts that ran through eight equispaced clearance holes in the test seal housing and screwed into blind tapped holes drilled into the bottom face of the oil chamber housing. **The central axis of the test seal and the central axis of the bearing shaft were also in alignment because of the alignment of the test seal housing and the oil chamber housing.** This meant that the central axis of the test seal and the central axis of the quartz shaft would be in alignment when the air bearings were in operation. This was one of the main purposes for the incorporation of location rings throughout the assembly. The fully assembled main body of the mechanism was complete and can be seen in **Fig 5.0.0.**

5.6 Rig Assembly

The laser beam had to fall upon the lip seal contact region to subsequently induce fluorescence in the oil film that would be present there. To enable the laser beam to be directed onto the contact region it was necessary to have some form of relative movement between the contact region and the

laser-optics assembly. With this rig as with the floating element seal rig section 4.6.1 it was decided to fix the position of the contact region and hence the shaft bearings and drive mechanism assembly described in section 5.5.0, and move the optics assembly and laser light source. This movement was achieved by using a modified vertical milling machine with the cutting head removed.

The assembled shaft bearings and drive unit mechanism **Fig 5.0.0** was bolted to an angled plate. This angled plate was then fixed to the slide of a modified vertical milling machine **Fig 5.1.2.** Air feed to the rig bearings was filtered through charcoal filters. The optical assembly decribed in section 4.5.2 and shown in **Fig 4.0.9** was fixed to the to x,y,z, T slotted bed plate of the milling machine. How this was done and the various alignment procedures that were carried out will be discussed in the next chapter.

Chapter Six

6.1 Optical Alignment Procedure

Before Experiments began the optical system had to be assembled and aligned to allow the laser beam to be directed onto the seal contact region. The procedure for doing this was as follows.

6.1.1 Laser beam axis-bed plate axis alignment

The laser was fixed to the T slotted bed plate by two steel open ended box section brackets. Four bolts held the laser unit to the brackets **Fig 6.0.0.** These bolts screwed into the base plate of the laser unit. By screwing the bolts connecting the laser base plate to the front bracket and the bolts connecting the laser base plate to the rear bracket to different degrees it was possible to alter the Z pitch of the laser.

The laser was positioned centrally at one end of the bed plate. The laser was switched on and the lasing power reduced to a minimum. The emerging light beam was viewed along the Y-axis of the bed plate. The two adjusting bolts connecting the laser base plate to the rear bracket were screwed in or out, to position the emerging laser beam so that it was seen

to be parallel to the X-axis of the bed plate when viewed along the Y-axis of the bed plate.

Both mounting brackets were slotted along part of one of their faces **Fig 6.0.1.** The brackets were both clamped to the bed plate on the slotted faces by two bolts which ran in those slots. This allowed y-directional movement of the whole laser assembly across part of the width of the bed plate. The bolt holding the front bracket to the bed plate was lightly tightened. The emerging light beam was viewed from above down the Z-axis of the bed plate. The laser was then pivoted about the front bolt until the emerging light beam was seen to be parallel to the X-axis of the bed plate. When the laser was in this new position the rear bracket bolt was tightened and the front bolt was fully tightened. The emerging laser beam was now parallel to the X-axis of the bed plate.

6.1.2 First lens centre-laser beam axis alignment

The optical assembly mounting plate **Fig 4.0.9** was fixed to a 90 degree angled bracket by a bolt that ran through a slot cut into the bracket along its height. The base of the bracket also had a slot cut into it. The base of the bracket was clamped to the bed plate by a single bolt **Fig 6.0.2.** For simplicity the argon ion reflector the second imaging lens and their associated gimbal mounts are not shown.

The laser was switched on and its power reduced to a minimum. The laser attenuator cap was then placed on the laser head extinguishing the beam. The argon ion reflector was then removed from its gimbal housing. The attenuator cap was then removed restoring the beam. The laser light beam now passed through the first lens along the length of the slotted bed plate. The emerging laser beam was viewed along the z-axis of the bed plate. The optical assembly was then moved in the y-direction of the bed plate until the laser beam appeared to be parallel to the bed plate X-axis and appeared to be passing through the centre of the first lens. The bracket bed plate bolt was tightened in this position.

The bolt holding the optical assembly mounting plate to the 90 degree angled bracket was slackened so that it could be raised or lowered in the slot cut into the bracket **Fig 6.0.3.** The assembly was viewed along the Y-axis of the bed plate. The optical assembly was either moved up or down the Z-axis of the bed plate until the laser beam emerging from the lens appeared to be parallel to the X-axis of the bed plate.

The beam emerging from the first lens was now parallel to the X-axis of the bed plate. The light beam was also being directed roughly through the centre of the first lens.

6.1.3 First lens primary axis-laser beam axis alignment

To reduce back reflection of the laser beam off the centre surfaces of the first lens the laser beam had to fall incident onto the lens surface normal to the lens Y and Z axis's and parallel to the lens primary X axis. This meant that the X, Y and Z planes of the lens had to be aligned with the X, Y and Z planes of the laser beam. From the alignment carried out in the previous section only the centre of the lens was now in alignment with the X-axis of the beam. How the rest of the lens was aligned was carried out in the following manner.

The laser attenuator cap was removed and a piece of white square card with a hole cut in its centre was taped to the laser head **Fig 6.0.4.** The hole in the card was positioned over the area where the laser beam emerged from the lasing head at the centre axis of the lasing head. The laser was switched on and the lasing power was reduced to a minimum. The laser beam fell incident onto the lens surface and part of it was reflected back onto the surface of the white card. The gimbal bolts on the lens gimbal mount were adjusted by screwing them in or out to different degrees until the reflected beam formed a circular illumination upon the white card whose centre axis was in the same position as the centre axis of the laser head. The axis of the laser beam and the axis of the lens were now in alignment and the laser was switched off.

6.1.4 Argon Ion reflector alignment

The white card was removed from the laser head and the attenuator cap was replaced. The laser was switched on. The argon ion reflector was replaced in its gimbal mount. The second imaging lens was removed from its mount and the bed plate was moved to its maximum X travel position using the X-directional adjustment crank handle **Fig 5.1.2.** In this figure the bed plate is depicted in its normal rig operating position and not in its position of maximum travel in the X-direction. The bed plate was moved to this position for safety reasons to prevent the beam reflecting unpredictably at a surface on the rest of the rig bulk positioned above the optical assembly.

The attenuator cap was removed and the laser beam passed through the first lens and impinged upon the argon ion reflector **Fig. 6.0.5.** For simplicity the final imaging lens gimbal mount is not shown in figure **6.0.5.** The system was then viewed along the Y-axis of the bed plate. The argon ion reflector pivot bolt was slackened and the argon ion reflector gimbal mount was pivoted about its base plate mounting bolt until the reflected beam appeared to be parallel to the Z-axis of the bed plate.

The system was viewed along the X-axis of the bed plate **Fig 6.0.6.** The beam was directed upward by the argon ion reflector and onto the roof of the laboratory where the rig was

situated. The three gimbal adjusting bolts were screwed in or screwed out to different degrees until the beam was seen to be parallel to the Z axis of the bed plate when viewed along the X-axis of the bed plate. When the reflector was in this position, the pivot bolt was fully tightened.

The X, Y and Z axes of the laser beam were now aligned with the X, Y and Z axes of the bed plate.

6.1.5 Second lens centre-laser beam axis alignment

The attenuator cap was refitted to the laser head. The white card was retaped onto the laser head. A mirror was placed above the second imaging lens gimbal mount with its mirrored surface facing the incoming direction of the beam ie approximately normal to the beam **Fig 6.0.7.** The laser was switched on and the attenuator cap removed. The mirror reflected the beam back through the optical arrangement until it impinged upon the white card taped to the optical head. The mirror position was adjusted until the reflected beam impinging upon the white card produced a bright circle whose centre was in the same position as the centre axis of the emerging laser beam. The laser attenuator cap was replaced and the surface of the mirror was covered with a black plastic covering cap.

The second imaging lens was replaced in its gimbal mount. The

attenuator cap was removed. The laser beam passed through the centre of the first lens along the X-axis of the bed plate and was reflected through 90 degrees by the argon ion reflector along the Z-axis of the bed plate to impinge upon and then pass through the second imaging lens. The system was viewed along the X-axis of the bed plate **Fig 6.0.8.** The gimbal adjusting screws on the second imaging lens gimbal mount were screwed in or out to the same degree until the light emerging from the second lens was seen to be parallel to the Z-axis of the bed plate.

The system was then viewed along the Y-axis of the bed plate, **Fig 6.0.9.** The lens gimbal mount adjusting screws were screwed in or out untill the beam emerging from the imaging lens appeared to be parallel to the Z-axis of the bed plate. When the lens was in this position the laser beam axis was now passing through the centre of the first lens.

6.1.6 Second lens primary axis-laser beam axis alignment

The plastic covering cap was removed from the mirror surface. The laser attenuator cap was removed from the laser head the beam passed through the optical system and was reflected off the mirrored surface back through the optical system and onto the optical head **Fig 6.1.0.** The gimbal adjusting bolts on the second imaging lens gimbal mount were screwed in or out to

different degrees until the reflected beam entered into the optical head. When this position was reached the laser made a distinct noise and the centre axis of the reflected beam was in the same position as the centre axis of the emerging laser light beam. **The axis of the second imaging lens was now aligned with the X,Y and Z axes of the laser beam and the X , Y and Z axes of the bed plate.**

6.1.7 Shaft Axis-Laser beam axis alignment The rig assembly was stripped down and then reassembled in the manner described in Chapter 5 **Fig 5.0.0** with the test seal. The quartz shaft was replaced with a steel replica shaft. The glycerol solution (500 cm^3) from a Winchester bottle was poured into the oil chamber housing via the filling funnel.

The laser was switched on. The laser bed plate was moved to its position of maximum travel in the Y-direction. The attenuator cap was removed. The system was then viewed along the Y-axis of the bed plate **Fig 6.1.1**. The bed plate was moved in the X-direction until a position was reached where the laser beam was seen to emerge from the second imaging lens along the Z-axis of the shaft bearings and drive unit assembly.

The system was then viewed along the X-axis of the bed plate **Fig 6.1.2**. The bed plate was moved in the Y-direction until it

was in a position where the laser beam was seen to emerge from the second imaging lens along the Z-axis of the shaft bearings and drive unit assembly. The emerging laser beam was now aligned along the Z-axis of the shaft. The laser attenuator cap was replaced on the laser head extinguishing the beam. The optical alignment of the optical assembly was complete.

Chapter Seven

7.1 Experimental Procedure

7.1.1 Ethylene glycol lubricant preparation

A solution of rhodamine B (3.6267g) was dissolved in ethanol (10 cm^3) in a test tube. This was added to ethylene glycol (200 cm^3) that had been placed in a mortar. The ethylene glycol and the ethanol-rhodamine solution were then thoroughly mixed together in the mortar using a pestle. The new solution was then poured from the mortar into a large Winchester bottle containing ethylene glycol (4 litres). The contents of the bottle were then mixed by vigorous shaking. The residue of the original solution remaining in the mortar was rinsed out with some of the solution from the Winchester which was then returned to the Winchester. The Winchester was shaken once more and the preparation of the lubricant test fluid was complete.

7.1.2 Seal bedding-in

The quartz shaft was optically polished on the section of the shaft on which the seal was to run. Its surface finish was very high Table 5.0.0. It was thought that the seal would be unable to bed in on such a highly finished surface. If the

seal were not to bed in, then the sort of surface topography on the seal surface necessary to sustain a lubricant film at the sealing contact would not be formed. For these reasons it was decided to first bed in the test seal on a ground steel shaft to generate the required surface topography.

The shaft bearings and drive unit were assembled in the manner described in chapter five except that the glass shaft was replaced with a steel replica. Glycerol solution (50 cm^3) from the Winchester bottle was poured into the oil chamber housing, **Fig. 5.0.0**, via the filling funnel **Fig. 5.1.2.** The air pressure line valve was opened so providing air to the system floating the steel shaft on its air bearings. The motor speed controller was switched on and the motor speed was raised from 0 to 1500 r.p.m. over a period of 5 seconds raising the shaft speed from 0 to 1500 r.p.m. in the same period. The shaft was left to run at this speed for a period of 60 minutes. No screeching of the seal or visible leakage was detected during this running period. The test seal was now considered to be bedded in.

The motor was switched off and the glycerol solution was to be drained from the oil chamber housing. Before this was done plastic sheeting was placed over optical mounting plate. This was done to prevent accidental spillage of the glycerol solution onto the optical surfaces of the optical system. The glycerol solution was drained from the oil chamber housing by

twisting the funnel pipe at its threaded connection to the oil chamber housing into a position where the funnel end pointed downward. The glycerol in the oil chamber housing then drained off into a beaker under the action of gravity.

A large plastic bowl was placed under the shaft bearings and drive unit assembly. The 8 Allen bolts securing the test seal housing to the bottom of the oil chamber housing were then slackened off. The remaining glycerol solution in the bottom of the oil chamber housing drained into the plastic bowl. The Allen bolts were then fully removed. The test seal housing and the test seal which seated into it were then removed and placed on a bench.

The remaining glycerol solution on the surfaces of the test seal and the test seal housing was removed with a cleaning tissue. This was to remove any glycerol residue that may have contained any seal contact wear debris that would have been generated during the bedding in procedure. The oil chamber housing cavity was also cleaned in the same manner for the same reason.

7.2 Localised Seal Contact Experiments

It was intended to conduct experiments to measure the variation in film thickness at one point of the seal contact in the axial direction. This was to be accomplished by concentrating the laser light onto one part of the circumference of the contact and then record the levels of fluorescence. The procedure as to how this was achieved was as follows.

7.2.1 Laser beam-localised seal contact alignment

A plane circular mirror mounted on the threaded aluminium mount **Fig 7.0.0** was screwed into the threaded portion on the end of the bearing shaft. The surface of the mirror was inclined at 45 degrees to the Z-axis of the shaft.

The air pressure line valve was opened so providing air to the system floating the quartz shaft on its air bearings. The motor speed controller was switched on and the motor speed was raised until a shaft speed of 200 r.p.m. was reached. The shaft was left to run at this speed for a period of 20 minutes to allow the seal and the seal contact region to attain its normal operating condition. The laser was switched on and the lasing power set at its maximum value. The attenuator cap on the laser was removed. The laser beam passed through the

optical system, emerging from the final imaging lens along the Z-axis of the shaft. The beam was then reflected through 90 degrees by the plane mirror through the wall of the glass shaft **Fig 7.0.1.** The laser light excited fluorescence in the glycerol solution surrounding the outer wall of the shaft. The fluorescence travelled back through the wall of the quartz glass shaft and was turned through 90 degrees by the plain mirror inclined at 45 degrees on the end of the bearing shaft. The second imaging lens collected the fluorescence and directed it through the argon ion reflector. It was then turned through 90 degrees by a second plain mirror and projected down the X axis of the bed plate.

A piece of white card was placed in the path of the fluorescence light **Fig 7.0.2** in the position on the X axis where the camera film plane was to be located. A white disc of light was seen to be projected onto the card by the imaging lens. The imaging lens was moved closer to or further away from the fluorescing seal contact by moving the bed plate in the Z-direction until the sharpest image was projected onto the white card.

The mirror mount was moved in the Z-direction by screwing it in or out of the bearing shaft until a darker bar appeared across the centre of the circular disc image **Fig 7.0.3.**

When the mirror was in this position the laser beam was being directed onto the contact region. The darker bar was the reduced fluorescence emanating from the contact region. The attenuator cap was placed onto the laser head extinguishing the beam. The white card was removed from the bed plate and replaced with the camera. The position of the camera film plane was in the same position as the front face of the white card. The position at which the fluorescence was now imaged was at the camera film plane. The optical alignment of the whole system was now complete and the laser was switched off, the shaft rotation was stopped and the air supply to the system closed off.

7.2.2 Localised seal contact calibration procedure

A plastic sheet was placed over the optical assembly. The glycerol solution was drained from the oil chamber housing. The bolts clamping the test seal housing to the bottom of the oil chamber housing were unscrewed and the test seal housing and test seal were removed from the bottom of the oil chamber housing.

The calibration ring was seated into the calibration ring housing. The calibration ring housing was seated onto the bottom of the oil chamber housing and the internal diameter of the calibration ring was slid over the outer diameter of the quartz shaft. The calibration ring housing was clamped into

position on the bottom of the oil chamber housing by the mounting bolts. During this procedure care was taken not to touch the optical assembly in case its position were altered.

The optical system had been set into a position that directed the laser beam onto the seal contact region and induced fluorescence in the glycerol film present there. This fluorescence was subsequently imaged at the camera film plane by the second imaging lens. If the optical system was set in a particular position and film thickness/fluorescent intensity calibration data was obtained in that position, then the relationship obtained from that data between film thickness and intensity was only valid when the system was in that position.

A small amount of the glycerol solution containing the rhodamine B was slowly poured into the oil chamber housing via the filling funnel until glycerol solution was seen to leak from the clearance between the quartz shaft and the calibration ring. The laser was switched on and the lasing power set to its maximum. The laser was left for 30 minutes to allow the lasing power to stabilise. A 36 exposure Ilford black and white film cartridge was loaded into the camera. This film cartridge was one of two previously produced film cartridges that had been made by cutting one long film strip into two halves. This was done to avoid any variation in the

film substrate.

The attenuator cap on the laser was removed. All the bolts on the calibration ring housing were screwed out. The first bolt on the calibration ring was screwed in. This had the effect of compressing the internal diameter of the ring against the outer diameter of the shaft reducing the glycerol film at that point nominally to zero. The laser light travelled through the optical system, passed through the quartz shaft and entered into this region. Although the ring was pressed against the shaft at this point glycerol was still present, as it was impossible to obtain a film with an absolute thickness of zero. Because of this fluorescence was still emitted from the system.

The camera shutter was opened for 1/1000 th of a second using a cable release and a photograph was taken recording the fluorescence level at the position of zero film thickness. The film thickness at the position where the laser beam passed through the shaft was then changed by screwing out the first bolt on the calibration ring housing and then screwing in the second bolt. This increased the film thickness **Fig 7.0.5.** A second picture was taken recording the fluorescence intensity at this film thickness. This was repeated 4 more times compressing the ring against the shaft at 4 more positions. The film thickness that was observed was thus varied

sinusoidally from 0 to 8 micron and back down to 0 again. The calibration procedure was now complete.

7.2.3 Localised seal contact experimental procedure

The optics were cased with plastic film and the calibration ring housing and calibration ring were removed from the bottom of the oil chamber housing. The test seal housing into which the bedded-in seal was seated was screwed onto the bottom of the oil chamber housing and the seal was thus positioned onto the end of the quartz shaft. Fresh glycerol solution, 40 cm^3, was poured into the oil chamber housing via the filling funnel. The air supply valve on the air feed line was opened thus floating the shaft on its air bearings. The electric motor speed controller was adjusted until the speed of the quartz shaft reached a speed of 106 r.p.m.. As indicated by an optical speed measurement device. The shaft was allowed to run at this speed for 5 minutes to allow the lubrication conditions at the seal to stabilise.

Nine photographs were then taken in rapid sequence. Approximately 3 seconds elapsed between the taking of each photograph. The speed of the shaft was then increased to 205 r.p.m.. again the shaft was allowed to run at this speed for 5 minutes then 9 photographs were taken. Finally the shaft speed was increased to 505 r.p.m. 5 minutes later 9 more photographs

were taken.

The film was immediately removed from the camera and the second specially prepared film cartridge was loaded. The speed of the shaft was raised to 1015 r.p.m., 9 photographs were taken after 5 minutes. This was repeated at speeds of 1507 r.p.m. and 2000 r.p.m.. The shaft was then stopped, one more photograph was taken and the laser was switched off. The glycerol solution was immediately drained from the oil chamber housing.

The temperature of the glycerol leaving the oil chamber housing at the outlet of the funnel was measured with a mercury thermometer and found to be 25.5 degrees C. The film was removed from the camera and was developed in the manner described in chapter 4 together with the first film in the same developing flask to eliminate any possible differences in film developer strengths or development times.

7.2.4 Localised seal contact photographic film analysis

The developed films were cut into strips containing five frames. Care was taken not to touch the film surfaces, by handling film at the edges to reduce smears that would have affected the results of the analysis. The amount of film fog was determined using a laser densitometer.

A film section was placed upon the densitometer illuminator plate **Fig. 7.0.6.** The illuminator plate was constructed from frosted glass. A light underneath the illuminator plate allowed the film negative to be viewed more clearly and also allowed the film to be positioned manually relative to the x and y co-ordinates of the illuminator plate. Once the film had been aligned on the illuminator plate parallel to the plate y co-ordinates, the illuminator plate light was switched off.

The densitometer operated by directing a laser beam through the film strip, the difference between the original intensity of the laser, and the final intensity of the laser light beam that had passed through the film sample gave a measure of the absorbance of the film.

The absorbance of the film was determined by how much the film had been exposed to fluorescent light and was therefore an indirect measurement of the glycerol solution film thickness. The greater the measured absorbance the more crystals in the film substrate that had been converted to metallic silver during the film development. The greater the amount of silver the higher the fluorescent light intensity that had fallen incident on the film during exposure. The higher the intensity the greater the lubricant film thickness.

The film samples were scanned in sequence and plots of

absorbance against film distance were obtained for each photograph of the imaged contact

The absorbance plots were digitised using a digitising tablet and fed into a computer. The calibration film thickness vs absorbance plot was also digitised and fed into the computer **Fig 7.0.7.** The scanned absorbance plots vs axial distance of the seal contact operating at different speeds were then converted to film thickness vs seal contact width by the computer by comparison with the calibration curve. The results were output into graphs of film thickness vs contact width **Figs 7.0.8** to **7.6.2**

7.3 Entire Seal Contact Experiments

As can be seen from figures **7.0.8** to **7.6.1** the film thickness is very unstable at constant speed. It was intended to measure the whole film thickness in both the axial and circumferential directions simultaneously to see if any waveforms could be detected in the film thickness. This was attempted was as follows.

7.3.1 Laser beam-entire seal contact alignment

The plane circular mirror and its mount was screwed out of its threaded connection at the end of the bearing shaft. The

mirror and mount were then withdrawn from the end of the bore of the quartz shaft. A 45 degree diamond turned mirrored cone **Fig 7.7.0** was inserted up the bore of the quartz shaft and screwed fully home into the threaded end of the bearing shaft. The air pressure line valve was opened so providing air to the system floating the quartz shaft on its air bearings. The motor speed controller was switched on and the motor speed was raised until a shaft speed of 200 r.p.m. was reached. The shaft was left to run at this speed for a period of 20 minutes to allow the seal and the seal contact region to attain its normal operating condition. As before a piece of white card was placed over the aperture of the camera. The laser was switched on and the lasing power set at its maximum value. The attenuator cap on the laser was removed. The laser beam passed through the optical system emerging from the final imaging lens along the Z-axis of the shaft. The beam was then reflected through 90 degrees by the mirrored cone through the wall of the glass shaft **Fig 7.7.1.** The laser light excited fluorescence in the glycerol solution surrounding the outer wall of the shaft. The fluorescence travelled back through the wall of the quartz glass shaft and was turned through 90 degrees by the mirror cone on the end of the bearing shaft. The second imaging lens collected the fluorescence and directed it through the argon ion reflector. It was then turned through 90 degrees by a plain mirror and projected onto the white card. The bed plate was moved in the X and Y

directions until an annular fluorescent image appeared on the white card, that's internal diameters and external diameters appearing concentric with each other. In this position the laser light beam was striking the tip of the mirrored cone along the axis of the cone then being turned through 90 degrees and directed radially outward through the wall of the quartz shaft to excite fluorescence in the glycerol solution surrounding the outer diameters of the quartz shaft. The attenuator cap was screwed onto the end of the lasing head extinguishing the beam. The shaft speed was reduced to zero but air was still fed to the bearings allowing the shaft to float. A tool was inserted up the bore of the quartz shaft and the z height of the mirrored cone was reduced by screwing the mirrored cone out of its threaded connection with the bearing shaft by two full turns of the thread. The tool was removed and the attenuator cap on the laser head removed restoring the beam. The projected fluorescent imaged on the white card was observed. This process was repeated several times moving the mirrored cone progressively down in the Z-direction until a darker annulus appeared in the centre of the original annulus **Fig 7.7.2.** When the cone was in this position the laser beam was being directed onto the whole 360 degree contact region. The darker annulus was the reduced fluorescence emanating from the contact region. The optical alignment of the system was now complete and the laser was switched off, and the air supply to the system closed off.

7.3.2 Entire seal contact calibration procedure

Plastic sheet was placed over the optical assembly. The glycerol solution was drained from the oil chamber housing. The bolts clamping the test seal housing to the bottom of the oil chamber housing were unscrewed and the test seal housing and test seal were removed from the bottom of the oil chamber housing. The calibration ring housing was mounted onto the end of the oil chamber housing and the calibration ring was slid over the end of the quartz shaft in the same manner as described earlier in section 7.2.2. A small amount of the glycerol solution containing the rhodamine B was slowly poured into the oil chamber housing via the filling funnel until glycerol solution was seen to leak from the clearance between the quartz shaft and the calibration ring. The laser was switched on and the lasing power set to its maximum. The laser was left for 30 minutes to allow the lasing power to stabilise. A 36 exposure Ilford black and white film was loaded into the camera. The attenuator cap on the laser was removed. All the bolts on the calibration ring housing were screwed out. The first bolt on the calibration ring was screwed in. This had the effect of compressing the internal diameter of the ring against the outer diameter of the shaft. The film thickness between the outer diameter of the shaft and the internal diameter of the calibration ring varied from nominally zero at the point where the shaft was compressed onto the shaft and 8 microns directly opposite where the ring

was compressed against the shaft. The laser beam travelled through the optical system, passed through the quartz shaft and entered into the varying film thickness region. The camera shutter was opened for 1/1000 th of a second using a cable release and a photograph was taken recording the varying fluorescence levels around the shaft. The film thickness variation around the shaft was then changed by screwing out the first bolt on the calibration ring housing and then screwing in the second bolt. This moved the position of maximum film thickness and minimum film thickness to new positions. It was intended to calibrate the fluorescence produced by each part of laser beam entering the shaft-calibration ring oil filled cavity. This was done in-case there was any variation in the laser beam intensity around the shaft. A picture was taken recording the fluorescence intensity at this film thickness. As in section 7.2.2 this was repeated 4 more times compressing the ring against the shaft at 4 more positions. The film thickness that was observed on each picture varied sinusoidally from 0 to 8 microns but on each picture that variation was in a different position. The calibration procedure was now complete.

7.3.3 Entire seal contact film thickness experimental procedure

The experimental procedure followed in section 7.2.3 was repeated in exactly the same manner, except that this time

nine photographs were each taken at shaft speeds of 108 215 500 1022 1496 2051 r.p.m.. The temperature of the glycerol leaving the oil chamber housing at the outlet of the funnel was measured with a mercury thermometer and found to be 26.0 degrees C. The film was removed from the camera and was developed with the calibration film in the same developing flask in the same manner as in section 7.2.3. The films showed little trace of exposure. The intensity of the laser beam inducing fluorescence around the 360 degrees of the contact region was far less than the intensity of the laser beam that had induced florescence at one point in the contact region. This was because the beam had been dispersed by the mirrored cone as it was directed radially outward. The experiment was repeated again but this time the shutter speed on the camera was reduced to 1/500 th of a second the result was once again the same. Shutter speeds as low as 1/25 th of a second were eventually tried with no success. The measurement of the film around the whole 360 degrees of the contact region was then abandoned at this stage.

7.4.0 Determining the radial load, width and roughness of the seal contact

The test rig was dismantled and the test seal was removed from the test seal housing. The radial load of the seal was measured using an Angus radial load tester and found to be 10.8 N. The seal was then mounted on a 25.4 mm diameter hollow

perspex shaft and the contact width was measured opticaly and found to be 0.2 mm. The seal was mounted on a hollow steel shaft with an external diameter of 25.4 mm. A portion of the seal and the shaft were cast in epoxy resin. A radial section of the seal cast was taken. The coordinates of the seal geometry were measured optically **Fig 1.0.0.** A portion of the uncast circumference of the seal lip was removed using a scalpel blade. This portion was cemented to a flat plate. The roughness of the seal lip contact was then determined using a Talysurf stylus instrument. The stylus was moved in the circumferential direction of the seal contact. The results can be seen in **Fig 7.7.3.**

Chapter Eight

8.1 Analysis of the localised seal contact experimental results

The minimum film thickness of the seal contact at each speed was obtained from all the figures 7.0.8 to 7.6.2. and the results are shown in Table **8.0.0**. These are then shown graphically in a plot of the various minimum film thicknesses at each speed, **Fig 8.0.0.**

The average value of the various minimum film thickness's for each speed were calculated and are shown in Table **8.0.1.** The results are shown plotted in **Fig 8.0.1.** It can be seen that the measured average seal film thickness is not zero when the shaft is static. The reason for this is because fluid remains trapped in the valleys of asperities present within the seal contact region.

The contribution to film thickness caused by fluid present in the roughness valleys of the asperities on the shaft can be neglected because the shaft was optically polished therefore very smooth. Because of this the majority of trapping can be attributed to fluid trapped in the valleys of the rubber asperities on the seal surface.

To further establish this trapped fluid hypothesis it is necessary to proceed through a number of steps. The first step is to estimate the ratio of the real to the apparent area of contact in order to find out if it could equal or exceed a value of 0.5 under unlubricated dry conditions. Why this is necessary will become evident later.

8.1.1 Establishing that the ratio of the real to the apparent area of contact can reach or exceed 0.5

How to calculate the real area of contact under dry conditions has been shown by Johnson [53], who followed the analysis of Greenwood and Williamson [54]. However before this method is followed it is correct to state the limitations of the analysis. The results obtained by using the Greenwood Williamson approach are only reasonably accurate when the ratio of the real area to the apparent area of contact remains below 0.25. If this level is exceeded then the effect of neighbouring asperities hindering each others compression starts to become important and this is not taken into account within this analysis. However the objective of carrying out the procedure in this case is only to give a qualitative assessment of the contact condition. The reason why it is necessary to get an indication of the contact condition is to support the following hypothesis.

If no lubricant is present then the nominal radial load of

the seal is more than sufficient to compress the asperities on the rubber sealing contact and induce the real area of contact to exceed a value ~0.5. However because lubricant is present the real area of contact cannot increase beyond this value even though the dry contact analysis says it should.

If one considers the portion of the Talysurf profile of the test seal surface shown in **Fig 8.0.2** which is a part of the whole Tallysurf profile shown in **Fig 7.7.3**, then the most important aspect of the sealing surface when considering the contact condition are the tops of the asperities peaks. The tops of the peaks are normally called summits. The height of a particular summit is denoted Z_s. The mean height of all the summits is denoted $\overline{Z}_s$. The probability of finding a particular summit height Z_s in the interval between Z_s to $Z_s + dZ_s$ is called the distribution function of the summits and is denoted $\Phi(Z_s)$.

If one assumes the surface is Gaussian and that there are **N** summits in the total seal contact band area A_o then the number of summits in contact **n** at a particular seal shaft separation **d** is given by

$$n=N \int_d^\infty \phi(Z_s)dZ_s \qquad (8.00)$$

To allow one to calculate a value for **n** without resorting to numerical analysis it is necessary to assume an exponential

distribution function. The amplitude distribution of the summit heights is σ_s. The expression for the distribution function now becomes

$$\phi(Zs)=(C/\sigma s)\ \exp(-Z_s/\sigma s) \qquad (8.01)$$

If this expression is now substituted into (8.00) then the value of the number of asperities on the rubber sealing surface in contact with the shaft **n** is now equal to

$$n=(CN/\sigma s)\int_d^\infty \exp(-Z_s/\sigma_s)\ dZs$$

$$=CN\ \exp(-d/\sigma_s) \qquad (8.02)$$

To further simplify the calculation it is necessary to assume that all the asperity summits are spherical or elliptical and have a constant curvature K_s at their peaks. It is only necessary to consider the asperities on the surface of the rubber, the asperities on the surface of the shaft can be

neglected because the shaft was optically polished and could therefore be considered smooth, Table 5.0.0. If the height of any particular summit is larger than the distance between the seal surface and the shaft d, Fig 8.0.3 then it will be compressed by an amount $\delta = Zs-d$ and be forced into contact with the shaft. The point of contact between the asperity and the shaft will be a circle of radius a. The i^{th} summit therefore has a contact area which is equal to

$$A_i=\pi\ ai^2 =f(\delta_i) \qquad (8.03)$$

The force that was required to compress the rubber asperity by this amount is equal to

$$P_i=g(\delta i) \qquad (8.04)$$

for both cases in equations (8.03) and (8.04) the values of $g(\delta)$ and $f(\delta)$ depend upon the properties of the material in contact. Because in this application of the analysis the asperities are rubber then the deformation could reasonably be assumed to be elastic and so from Hertz it can then be shown that

$$f(\delta)=\pi\ \delta/K_s \qquad (8.05)$$

and

$$g(\delta)=(4/3)E^*\ K_s^{-1/2}\ \delta^{3/2} \qquad (8.06)$$

Where E^* is equal to

$$E^* \equiv \left(\frac{1-\upsilon_1^2}{E_1} + \frac{1-\upsilon_2^2}{E_2}\right)^{-1}$$

in this case the modulus of the quartz shaft E_2 is very high compared to the modulus of the rubber E_1 therefore it would be reasonable to neglect the shaft term and

$$E^* = \frac{E1_2}{1-\upsilon_1^2}$$

The total real area of contact **A** within the seal contact zone and the total nominal pressure $\bar{P}(=P/A_o)$ can be found by summing all the values of **Pi** and **Ai** for all the asperities thus

$$A=N \int_d^\infty f(Z_s-d)\phi(Z_s)dZ_s \qquad (8.07)$$

The exponential distribution function $\phi(Zs)$ given in (8.01)

can be substituted into (8.07) and now

$$A = (CN/\sigma_s) \int_0^\infty f(\delta) \exp(-Zs/\sigma_s)\, dZ_s$$

$$= CN \exp(-d/\sigma_s) \int_0^\infty f(\delta/\sigma_s) \exp(-\delta/\sigma_s)\, d(\delta/\sigma_s)$$

$$\equiv nI_f \qquad (8.08)$$

and

$$\overline{P}\, A_o \equiv P = \int_d^\infty g(Z_s - d)\, \phi(Zs)\, dZ_s \qquad (8.09)$$

again substituting $\phi(Z_s)$ into (8.09) from (8.01)

$$P = CN \exp(-d/\sigma_s) \int_0^\infty g(\delta/\sigma_s) \exp(-\delta/\sigma_s)\, d(\delta/\sigma_s)$$

$$\equiv nI_g \qquad (8.10)$$

Because the deformations of the asperities are elastic then it is possible to substitute the expressions for $f(\delta/\sigma_s)$ from equation (8.05) into equation (8.08) and the expression for $g(\delta/\sigma_s)$ from equation (8.06) into equation (8.10) and now

$$I_f = \pi \sigma_s / K_s \tag{8.11}$$

and

$$I_g = \pi^{1/2} E^* \sigma_s^{3/2} K_s^{-1/2} \tag{8.12}$$

The ratio of the real to the apparent area of contact within the seal contact region is given by

$$A/A_o = I_f/I_g \bar{P} = \pi^{1/2} (\sigma_s K_s)^{-1/2} (\bar{p}/E^*) \tag{8.13}$$

If one considers the portion of the profilometer trace of the seal contact used in the experiments presented in this thesis, **Fig 8.0.2**, then it is possible to measure all the heights of all the roughness peaks relative to the mean line These measured heights are shown in Table **8.0.2**. It is then possible to obtain the mean summit height and the standard deviation of the summit heights σ_s. It can be seen that for this seal contact $\sigma_s = 1.22 \times 10^{-3}$ **mm**.

It is possible to calculate an estimate of the peak summit curvature K_s for each peak on the profilometer trace by measuring the width of each peak at its base **w** and the height of each peak from its base **h** and assuming that the peaks are parabolas

$$Ks=(2xh)/(w/2)^2$$

The values of the heights, widths and calculated summit curvatures for each peak in the profile can be seen in Table **8.0.3**. The mean value $\bar{K}_s$ calculated from table 8.0.3 is found to equal **3.501 mm^{-1}**

The radial load of this seal was measured and found to be **10.79 N**. The apparent contact width of the seal was measured when it was mounted on a 25.4 mm diameter hollow perspex shaft and found to be **0.2 mm** .

The average contact pressure $\overline{P}$ then equals

$$\overline{P} = 10.79/\pi x25.4x0.2$$

$$= 0.678 \text{ N mm}^{-2}$$

The initial modulus of the seal E_1 obtained from uniaxial traction measurement equals 12.9 MPa. The Poisons ratio is assumed to equal 0.5. The calculated value of $E^* = 17.2$ N mm^{-2}

It now possible to calculate I_g using equation (8.10) and I_f from equation (8.08) by inputting the appropriate values that have been given. If this is done it is found that

$$I_f = 1.0985E^{-3}$$

and

$$I_g = 6.944E^{-4}$$

From equation (8.13) A/Ao the real area of contact, equals

$$A/A_o = I_f/I_g \overline{P}$$

$$\simeq 1.0$$

As can be seen the calculation very strongly suggests that the nominal load acting upon the contact is great enough to totally flatten the asperities on the surface of the seal. It would therefore seem reasonable to assume that even if the contact condition was calculated more accurately, that in the dry condition the real area of contact would at least achieve a value of 0.5 and probably more than exceed this value.

8.1.2 Why doesn't the real area of contact exceed 0.5 in the lubricated condition ?

If the distance between two theoretically flat two dimensional bodies of length L, separated by a fluid is continually reduced, then the fluid between them will be gradually squeezed out, **Fig 8.0.4.** Eventually the approaching bodies will contact and then there will be no fluid present at all.

If one of the bodies is now considered to have two dimensional roughness and the distance between them is reduced, then as before fluid will be initially squeezed out. However at some point during the process the highest summit peak on the rough body will contact the flat plane. As the distance between the bodies continues to decrease, the length of the rough body in contact with the flat plane N_1 will increase. Also the number of individual peaks on the

rough body contacting the flat plane will increase. As this process proceeds the number of routes the fluid has to escape out of the contact region will be reduced, and as a consequence the fluid will start to become trapped in the valleys between the portions of the asperities in contact with the plane. Any further reduction in the distance between the bodies after this time will cause the trapped fluid to become compressed, **Fig 8.0.5**. The case of fluid trapping due to two dimensional roughness has been evaluated by Kuznetsov [55] for two bodies steel and polystyrene separated by two fluids water and glycerin. Kuznetsov found that when a value of $N_1/L \sim 0.08$ is reached, then compression of the fluid starts to become significant. This has the effect of hindering the further increase in N_1/L as the load increases further. Finally N_1/L is prevented from increasing at all beyond a value of **0.15**

If one now considers the case of a fluid sandwiched between a body with three dimensional roughness that is gradually approaching a three dimensional flat plane, **Fig 8.0.6** then it will be seen that this case is somewhat different from the previous two dimensional case. This time when the ratio of the contacting area **A** to the non contacting area A_o reaches the same ratio of N_1/L that was required to trap the fluid in the two dimensional case, then with the three dimensional case the fluid still has a chance to escape. It can do this

by flowing around the areas in contact with the flat plane **A**, **Fig 8.0.7.** One might be tempted to think that the only way to prevent fluid from escaping from a contact under such circumstances would be if all the gaps between the contacting areas of the asperities were totally filled, and then **A=Ao**. If this were to happen then there would be no fluid left in the contact, as the rough surface would be completely flattened.

However this is not the case. The condition of a three dimensional rough surface contacting a three dimensional flat plane has been studied by Tripp [56], who used percolation theory to calculate the fraction of a surface that must be occupied by circular contacting areas to produce a network of interconnecting pathways. Tripp reported that such a network remains open until the ratio of **A/Ao** reaches ~ **0.5, Fig 8.0.7.** After this value has been exceeded the fluid can no longer escape from the contact region and as with the two dimensional case studied by Kuznetsov the fluid will also become compressed and prevent **A** from growing beyond **0.5.**

To estimate the average film thickness in the sealing contact when the shaft is static, one first needs to estimate the unit volume of fluid trapped in the valleys of asperities when the real area of contact reaches **0.5** that produces the hermetic sealing condition. After this has been done the

average film thickness is simply the volume of fluid trapped divided by the contact area **Ao**

If one considers the contact profilometer trace shown in **Fig 8.0.2**, then the volume of the solid rubber portions above the mean line are equal to the volume of the empty regions of the valleys below the mean line. The average height of the departures of both the rubber peaks above the mean line and the empty valleys below the mean line is termed the R_a value. If it is assumed that the surface is Gaussian then if one were to cut the profile along the mean line then one would cut through the same distance of empty valleys as solid rubber peaks. The ratio of solid rubber to empty valleys would equal **0.5**. at this point the average height of the fluid trapped in the valley portions below the mean line is equal to the **Ra** value. From the profilometer read-out, **Fig 7.7.3**, it can be seen that the **Ra** value equals **1.245** microns. The rubber occupies half the available length of the sampling length. If the trapped fluid were allowed to spread out over the full distance of the sampling length then the average height of the fluid would equal **Ra/2** which is equal to **0.622** microns.

If the film thickness vs fluoresence intensity calibration curve shown in figure 7.0.7 is extrapolated back to the Y axis, it can be seen that the intercept does not go through

the origin, but instead registers a negative film thickness of ≃ 0.2 microns. This is because the contibution to film thickness caused by fluid trapped in the surface roughness of the calibration ring was not taken into account when constucting the curve. However if this offset value is now taken into account and added to the measured average height of the lubricant trapped in the valleys of the sealing surface then the new average height would equal 0.822 microns. This is what you would expect the measured average height of the trapped fluid film to be in the seal if the fluid were trapped at **A/Ao=0.5**. It can be seen from **Fig 8.0.1**, that this corresponds remarkably well with the static measured height of the film thickness which equals 0.89 microns.

8.1.3 The increase in film thickness with speed

The values of the film thickness vs speed shown in table **8.0.1** were plotted in **Fig 8.0.8**. Also on the same graph are plotted the values of a constant multiplied by the square root of the speed vs the corresponding speeds. It can be seen that the increase in film thickness is reasonably proportional to the square root of the speed. This strongly suggests that there is hydrodynamic action present within the contact region.

Discussion

9.1 The Fluorescence Technique

9.1.1 The minimum resolvable film thickness

Both the minimum film thickness and the minimum variation in film thickness that the fluorescence method could ideally be expected to resolve should be in the order of the physical size of a dye molecule, which is Angstroms.

In reality it would not be possible to obtain such resolutions, because of the detection and analysis methods. As should now be clear, the experimental technique that has been developed is an imaging technique and as a consequence the resolution is at the mercy of the sensitivity of the imaging device, which in the case of the work presented in this thesis was a film substrate. The detector could just as easily have been a CCD camera. Both these detectors have sensitivities that are not capable of registering the low fluorescence intensity levels that would be emitted from a monolayer of dye molecules.

What was very encouraging about the sensitivity achieved with the experimental apparatus that was used, can be appreciated if one looks at the calibration curve shown in Fig 7.0.7. If

the fluoresence intensity, which is shown by the absorbency in this figure, is extrapolated, then it can be seen that it does not go through the origin, but instead registers a negative film thickness of between ~0.1 to 0.2 μm. This intensity level is of the order of what would be expected from fluorescent fluid trapped in the roughness valleys of the calibration ring. The Ra roughness of the ring is about 0.1.

9.1.2 The range of film thickness that can be measured

The range of film thickness that can be measured is limited by the fluorescent molecules, the detector system and the method of analysis.

In **Fig 7.0.7** it can be seen that at high film thicknesses the intensity no longer continues to increase with film thickness at the same rate. This is due to a combination of decreasing photographic film sensitivity and reabsorbance of the fluorescence light by the fluorescent molecules themselves. If it had been desirable to measure larger film thicknesses, then to counter the reabsorbtion effect, the concentration of the dye in the fluid would have simply been reduced. However this would also have reduced the intensity of the fluorescence and limited the measurement of thinner films because the detector would not have been capable of registering the low light levels. The useful working range of

the film substrate used in this work, can be seen from the film exposure curves to lie within the linear part of the curve **Fig 4.0.4.**

The densitometer instrument had a finite range of intensity measurement. If the detector had been a CCD camera and the images had been analysed by an image processing technique, then the measurement range would have been dictated by the sensitivity range of the camera and the number of assignable grey levels of the image processing software.

9.1.3 The maximum spatial resolution

For a diffraction limited optical system the spatial resolution can be expressed by the Rayleigh criterion to be

$$\lambda/1.22\ F$$

where F=f/aperture size. Therefore the best spatial resolution that could ultimately be achieved would depend on the wavelength of the fluorescent light that was being imaged and the **F** number of the optical system. In this case the optics were imaging light between 520 and 650 nm. Using an optical system having say an F number of 2.8 would mean that the smallest spatial distance that could be resolved would lie between 1.52 and 1.9 microns.

In reality it is not possible to obtain perfect optics that can image all wavelengths at the same image plane and are free of aberrations. But some lenses are better than others and are corrected for colour and aberrations. An extremely good lens could reasonably be expected to resolve a spatial distance slightly worse than the diffraction limited system. The optics used in this rig were not the best available, and if more money could have been spent to purchase better optics then no doubt the spatial resolution of the system would have been improved.

9.2 The Experimental Results

The results presented in this thesis show that the contact of a rotary lip shaft seal operates under conditions of mixed lubrication and that the film thickness is highly unstable. The seal and shaft surfaces are not fully separated. The nominal radial load of the seal is shared between the tips of flattened asperity summits in contact with the shaft, compressed lubricant trapped in the asperity valleys of the seal surface and micro asperity hydrodynamic action.

The performance of all lubricated contacts is governed by the lubrication conditions. With seals the lubrication conditions are governed by the surface roughness. Therefore it could be

concluded that the performance of a rotary lip shaft seal is in fact roughness governed.

This conclusion would correspond well with the empirical observations made by the sealing industry, where it has been known for years that seals must bed in and become rough to function correctly.

What follows is a discussion about what effect roughness may play in determining the operational characteristics of rotary lip shaft seals.

9.2.1 The effect of roughness on the ability of the surface to trap fluid

In the event of the contact collapsing then the ability of the lubricant fluid to carry the nominal radial load of the seal depends in part upon the ability of the seal surface to trap fluid.

The surface with the highest trapping ability is one that is uniformly random. Any surface that develops non random features such as axial grooves will have reduced trapping ability by providing flow channels for the lubricant to escape out of the contact region.

9.2.2 The effect of roughness on friction

The radial load acting upon the seal contact region results in the generation of a friction force. This friction force will be composed of two parts. The first part is the friction force generated at the boundary between the summits of flattened asperities in contact with the shaft. The second part will be the friction force generated by the shearing of lubricant in the valleys of asperities.

9.2.3 The boundary contribution to friction

The magnitude of the boundary contribution to friction in seals is dependent upon two things. The first is the size of the boundary areas which is the real area of contact. The second is the conditions within the boundary region.

With dry or boundary lubricated contacts the friction force is independent of the apparent area of contact. This is because the real area of contact where boundary friction arises increases in proportion to the load.

With seals however the friction force generated at the boundary is not independent of the apparent area of contact. This is because the real area of contact or boundary area is prevented from increasing beyond half the apparent area due to fluid trapping. And thus for the real area to increase the apparent area must also increase. The apparent area of

contact is governed by the radial load and the seal geometry ie the contact angles.

This conclusion corresponds well with the empirical observations made by the sealing industry, where it is known that the seal contact angles are extremely important in determining seal performance.

The conditions within the boundary regions are significantly modified by the presence of lubricant. The lubricant reduces the frictional force generated within the boundary. The lubricant can enter the boundary regions by absorbing itself onto the surface of the moving shaft or alternatively by micro EHD. The local contact stresses acting upon the rubber in the boundary regions will be dependent upon the shape of the asperities. If two contacts surfaces had equal values of A/A_o but one of the surfaces was positively skewed and the other was negatively skewed then the surface with the positive skew would have the highest localised contact pressures.

9.2.4 The lubricant shear contribution to friction

The contribution to friction caused by shear of the lubricant in the valleys of asperities will be dependent upon the depth of the valleys. The shallower the valleys the higher the shear stresses for a given speed. Thus seals with a smoother

contact surface will have a larger lubricant shear friction force than seals with a rough surface. Also the less lubricant there is in the valleys, the less lubricant there is to feed the boundary regions.

Higher friction forces will cause greater heat generation and degrade the properties of the rubber resulting in a reduction in the life of the seal.

9.2.5 Roughness and wear

It is usual when considering the terms roughness and wear to suppose that wear governs roughness. But with sealing contacts it may be that roughness governs wear.

When a new seal is run on a shaft for the first time, the wear rate is initially very high. The radial load will be carried in part by the tips of flattened asperities and in part by micro asperity hydrodynamic action. If the contact load is greater than the supporting ability of these two effects, then compression of trapped fluid in the valleys of asperities will ultimately prevent the contact from collapsing below $A/A_o = 0.5$. In this condition if the part load on the tips of flattened asperities is higher than the strength of the material, then heavy wear will take place. As this happens the contact width will increase. Two things will follow, the first is that hydrodynamic action will increase.

The second is that localised contact stresses on individual asperities will reduce. Eventually a point will be reached when the portion of the load that must be carried by the asperities is equal to the strength of the material. At this point the wear rate will slow down but not stop, because the rubber asperities will be subject to constant cyclic deformations as the shaft moves beneath them. Cyclic deformation has the effect of fatiguing the rubber and results in wear.

As this fatigue process proceeds, the wear contact band width will increase. The load carried by each individual asperity will reduce and as it does so the real area of contact will also decrease. Once the real area of contact drops below 0.5 then the contact can no-longer trap fluid and the possibility for compressed fluid support is removed. If hydrodynamic action fails in this condition then the tips of the asperities will have to carry all the load and the highest peaks will therefore be placed under increased contact stress. The tips of the asperities will wear flat and at the same time the depth of the asperity valleys will decrease. As a result, the shear in the remaining fluid will increase. This will generate more heat and accelerate wear by degrading the physical properties of the rubber this process will continue, continually increasing in speed until the seal eventually burns up.

9.2.6 The film thickness dynamic instability

The change in the magnitude of the film thickness variation at 1000 r.p.m. could be related to the frequency response of the material itself. If a sinusoidal stress is applied to the material then the amount by which the resultant strain lags behind the stress is given by $\tan\delta = E''/E'$, where E'is the modulus derived from the stress in phase with the strain, and E" is the modulus derived from the stress 90^{o} out of phase with the strain. The value of tanδ is related to the hysteresis losses because in phase stress and strain results in elastically stored energy which is completely recoverable, whereas out of phase stress and strain results in the dissipation of energy. The values of E" and E' for this material were measured with a dynamic response apparatus. At 1.5 Hz E' was found to equal 15.7 MN/m^2 and E" was found to equal 2.4 MN/m^2. At 15 Hz, E' was found to equal 19.0 MN/m^2 and E" was found to equal 5.99 MN/m^2. It can be seen that the material has more damping at low frequencies than at high frequencies. This could account for the increase in the variation of film thickness with speed. It would be interesting to evaluate the dynamic response of the sealing material in between these frequencies to see if the transition in hysterisis loss is sharp or gradual.

Conclusions

Experimental Technique

The measurement of film thickness developed in this thesis utilising a fluorescence imaging technique is a powerful new method that can be applied to study discreetly the lubricant film thickness of rough tribological contacts operating in the mixed lubrication regime.

As interferometry was to the development of the understanding of smooth rolling or sliding EHL contacts, it is hoped that the fluorescence imaging technique will allow more progress to be made towards the understanding of the tribological condition of mixed lubrication with rough contacts.

Experimental Results

The film thickness is highly unstable and varies considerably at constant speed. The magnitude of the film thickness variation at different speeds is not constant and appears to undergo a transition at around 1000 r.p.m. **Fig 8.0.1.**

The increase in average film thickness with speed from the starting initial film thickness is reasonably proportional to the square root of the speed **Fig 8.0.8.** This would suggest

that hydrodynamic lift is present and does contribute to film thickness.

The film thickness is not zero when the shaft is static because of trapped lubricant in the valleys of asperities. The magnitude of the minimum film thickness that can exsist in the contact is governed by the depths of asperity valleys when the real area of contact equals 0.5

References

[1] GUTH, E., Theory of filler reinforcement, Journal of Applied Physics, 16, (1945) p.20

[2] SMALLWOOD, H.M., Limiting law of the reinforcement of rubber Journal of Applied Physics, 15, (1944), p.758

[3] KUHN, W., Kolloid-Z , 76, (1936) p.256

[4] TRELOAR, L.R.G. Physics of Rubber Elasticity, Oxford Uni Press, London, (1958), chap.3.

[5] ROBERTS,A.D. Theories of Dry Rubber Friction, Tribology international, April (1976) pp75-81.

[6] BOWDEN,F.P., TABOR,D. Friction and lubrication of solids, Clarendon Press , Oxford. part 1 (1950), part 2 (1964).

[7] GREENWOOD,J.A., TABOR,D., The friction of hard sliders on lubricated rubber, the importance of deformation losses, Proc.Phys.Soc., 71, (1958), pp989-1001.

[8] GROSH, K.A., Relationship between the frictional and viscoelastic properties of rubber, Nature, 197, (1963), pp858-859.

[9] BARTENEV, G.M., LAVRENTEV, V.V., Friction and wear of polymers, Elsevier, (1981), pp.116-117.

[10] MOORE, D.F., GEYER, J., A review of hyseresis theories for elastomers, Wear, 30 (1974), pp.1-34.

[11] HALAUNBRENWER, J., KUBIZ, A., Paper No. 67-LUB-25, ASLE-ASME Lubrication Conference, Chicago, October 1967.

[12] SCHALLAMACH, A., The velocity and temperature dependance of rubber friction, Proc. Phys. Soc., B66 (1953), p.386.

[13] BULGIN, D., Polymers and friction, Publ. Plast. Weekly, 143 (No.16) 1962, p.636.

[14] BOGGS, F. and RIEMEN, Friction of rubber on rough surfaces, J. Rubber Age, 81 (No.4) 1957.

[15] DOWSON,D., HIGGINSON,G.R., A numerical solution to the elastohydrodynamic problem, J.Mech.Eng. Sci.,1, (1959),no6

[16] DOBRY, A., The transitions between boundary, mixed and hydrodynamic lubrication", Wear, 7, (1964), pp.290-297.

[17] ORCUTT, F.K., BELL, J.C., GLOESER, W.A., ALLEN, C.M., Summary report on the dynamic behaviour of high speed liquid lubricated face seals to the Rotary Shaft Seal Research Group, Battell Memorial Institute, Columbus, Ohio, January 24, (1965).

[18] HAMILTON, D.B., Final summary report on the dynamic behaviour of lubricated face seals to the Rotary Shaft Seal Research Group, Battelle Memorial Institute, Columbus, Ohio, February 22, (1965).

[19] ANNO, J.N., WALOWIT, J.A., ALLEN, C.M., Microasperity lubrication, Third International Conference on Fluid Sealing, Cambridge, UK, BHRA, Paper E.2, April (1967).

[20] RISTLER, A.L., CHENG, H.S., NIVAT, K., OZOKOT, I., Cavitation phenomina in face seals, Dept. Mechanical and Nuclear Engineers, Northwestern University, Evanston, Illinois, USA. Prepared under ONR Contract No. N00014-79-C-0007, (1981).

[21] FOWLES, P.E., The application of elastohydrodynamic theory to individual asperity-asperity collisions, J. of Lubr. Technology, ASME Trans., 93, (1971), pp.383-397.

[22] FOWLES, P.E., A thermal elastohydrodynamic theory for individual asperity-asperity collisions, J. of Lubr. Technology, ASME Trans., 93, (1971).

[23] OSTERLE, F., CHARNES, A., SAIBEL, E., On the solution of the Reynold's equation for slider-bearing lubrication - VI: The parallel surface slider bearing without side leakage", Trans. ASME, August (1953), pp.1133-1136.

[24] HALLING, J., Principles of Tribology, MacMillan Press, London.

[25] DOWSON, D., HIGGINSON, G.R. A numerical solution to the elastohydrodynamic problem", J. Mech. Eng, 1, (1959), pp 6-15.

[26] PATIR, N., CHENG, H.S., An average flow model for determining effects of three-dimensional roughness on partial hydrodynamic lubrication, ASME JOT, 100 (1978), pp12-17.

[27] FIELD G.J., NAU B.S., An experimental study of reciprocating rubber seals. , Pro. Symp on EHD Lubr Leeds Univ, (1972).

[28] KAWAHARA, Y., OHTAKE, Y., HIRABAYASHI, H., Oil film formation of oil seals for reciprocating motion. , 9th BHRA conference on fluid sealing (1981).

[29] WHITE, C.M., DENNY, D.F., The sealing mechanism of flexible packings. Ministry of supply Sci and Tech., Memo no 3/47, (1947), republished by BHRA (1972).

[30] NAU B.S., Friction of Oil Lubricated sliding rubber seals. BHRA Fluid sealing conferance, (1971).

[31] AUSTIN, R.M. , FLITNEY, R.K. , NAU, B.S., Contact stress friction and the lubricant film of hydraulic cylinder seals. BHRA fluid sealing conferance, (1978).

[32] LAWRIE, J.M. , O'DONOGHUE, J.P. , The mechanism of lubrication in a reciprocating seal. BHRA fluid sealing conferance, (1964).

[33] LINGREN, H., Scraper ring properties and behavior in hydraulic cylinders. M. Sc Thesis, Chalmers Univ. Tech, Sweden, (1986).

[34] GAWRYS, E. , KOLLEK, W. , The effect of the operating conditions on the design of seals for reciprocating motion., BHRA fluid sealing conferance (1984).

[35] KANTERS, A.F.C. , On the calculation of leakage and friction of reciprocating elastomeric seals., Phd thesis, Univ of Eindhoven, Netherlands, (1990).

[36] JOHANNESSON, H., On the optimisation of hydraulic cylinder seals., Phd Thesis, Machine elements division, University of Lulea, Sweden, (1980).

[37] HIRABAYASHI, H., KAWAHARA, Y. ,MUTO, Y., LIDA, S. , A study of lubrication characteristics on valve stem seals for automobile engines. SAE, congress and exposition Detroit, (1979).

[38] MULLER, H.K., Leakage and friction of flexible packings at reciprocating motion with special consideration of hydrodynamic film formation. BHRA COnferance on fluid sealing, (1964).

[39] KAWAHARA, Y., ISHIWATA, H., ICHIKAWA, Y., An experimental investigation of dynamical characteristics of U-seal in reciprocating motion., BHRA fluid sealing conferance, (1973).

[40] SICK, H.H. , Measurement and reduction of friction of reciprocating piston seals for hydraulic and pneumatic application. BHRA fluid sealing conferance, (1975).

[41] HIRANO, F., KANETA, M., Experimental investigation of friction and sealing characteristics of flexible seals for reciprocating motion. BHRA conferance on fluid sealing (1971).

[42] LANG, C.M., Oring friction and leakage in hydraulic systems. BHRA report T 974 november (1968).

[43] FIELD, G.J., The elastohydrodynamic lubrication of rectangular section rubber seals under conditions of reciprocating motion. Ph. D. Thesis, City Univ. London (1973).

[44] WERNECKE, P.W., Analysis of the reciprocating sealing process. BHRA sealing conf, (1987).

[45] VOHR, J.H., An Experimental Study of Taylor Vortices and Turbulence in Flow Between Eccentric Rotating Cylinders. Transactions of the ASME Journal of Lubrication Technology, Jan (1968), pp 285-296.

[46] OLGER, A.C., TAVALLAEY, S.S. , Elastohydrodynamisk Smorjning, Experimentella undersokningar for att visa inverkan av ytojamnheter pa oljefilsuppbyggnaden. Chalmers tekniska hogskola, Sweden (1987).

[47] VISSCHER, M., Analysis of electrical methods for measurement of leakage and lubricant film thickness of elastomeric seals. Eindhoven Univ of Tech, report no IAT/89.185, (1989).

[48] WERNECKE, P.W. , Untersuchung der physikalischen Vorgaenge in Spalten von Hydraulikdichtungen. Phd Thesis, Aachen Univ. of Tech, (1983).

[49] JAGGER, E.T. Study of the lubrication of synthetic rubber rotary shaft seals. Pro conf lubr and wear, (1957), pp409-415.

[50] TING, L.L., Development of a laser fluoresence technique for measuring piston ring oil film thickness, J Lubr. Techn. 102, (1980).

[51] KASSFELDT, E., Analysis and design of hydraulic cylinder seals. Phd Thesis, Univ. Lulea, Sweden, (1987).

[52] WEAVER, K.S., Measurement of photographic transmission density. J. Optical Soc AM 40 , (1950) pp524-536.

[53] JOHNSON, K.L., Contact Mechanics, Cambridge University press, London, (1987).

[54] GREENWOOD, J.A., WILLIAMSON, J.B.P., Contact of nominally flat surfaces.,Proceedings Royal Society, A295, 300, (1966).

[55] KUZNETSOV, A., Effect of fluid lubricant on the contact characteristics of rough elastic bodies in compression. Wear, 102, (1985) pp177-194.

[56] TRIPP, J.H., GARTE, S.M., The gas tightness of separable base metal contacts. IEEE trans on components hybrids and manufacturing tech, Vol CHMT-4, No 1 March (1981).

Seal R Value, Lip Angles and Spring Height

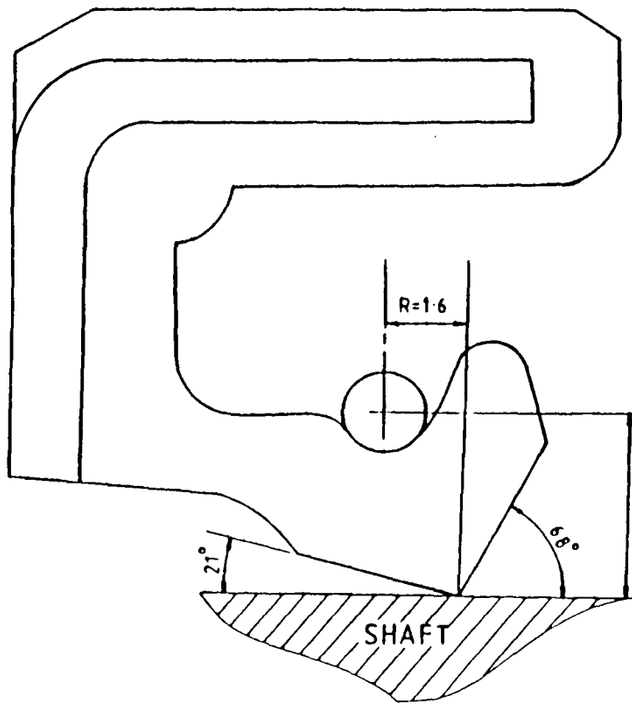

Fig 1.0.0 Test seal mounted on shaft

Seal Geometry (X,Y) Coordinate Values in mm

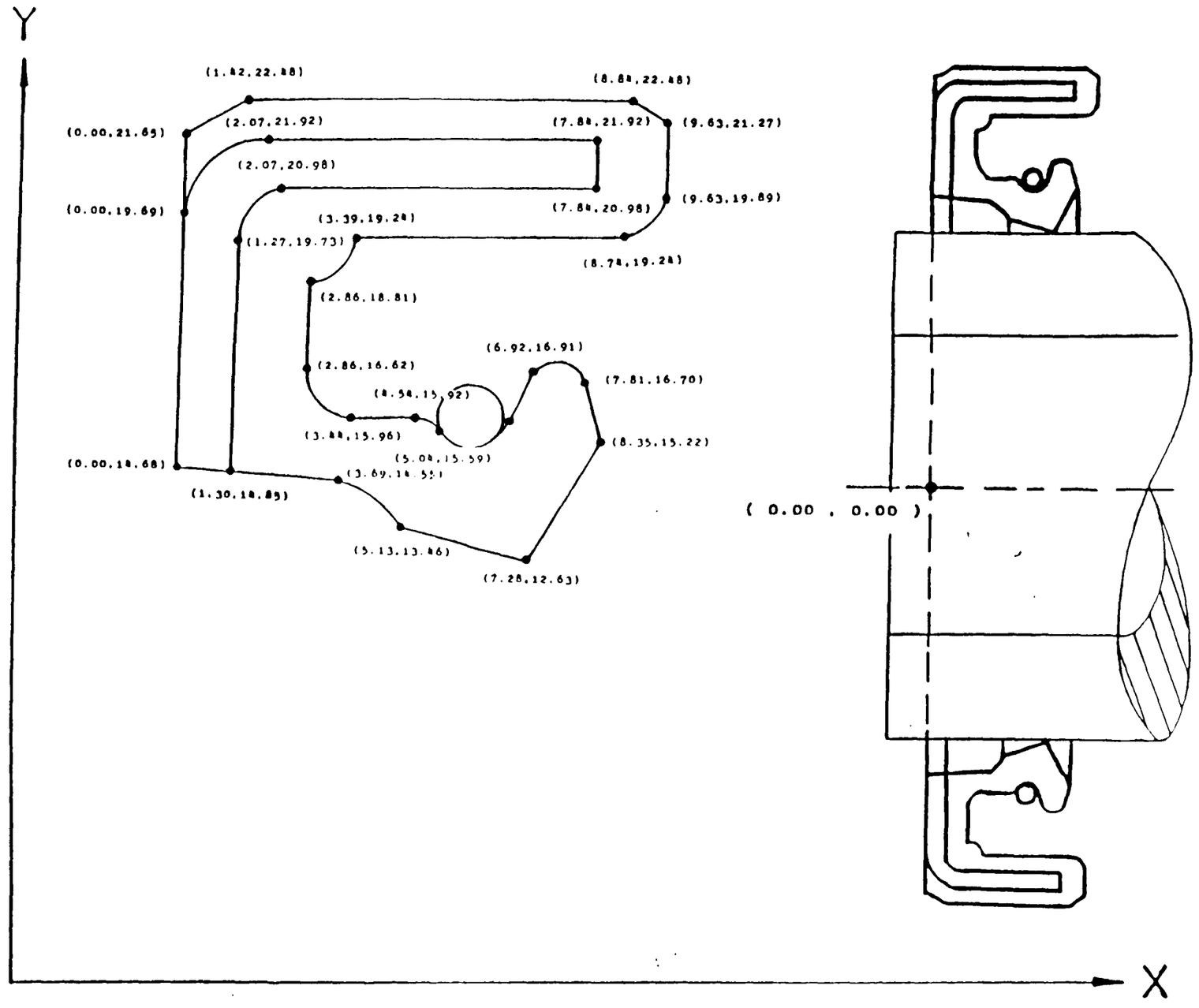

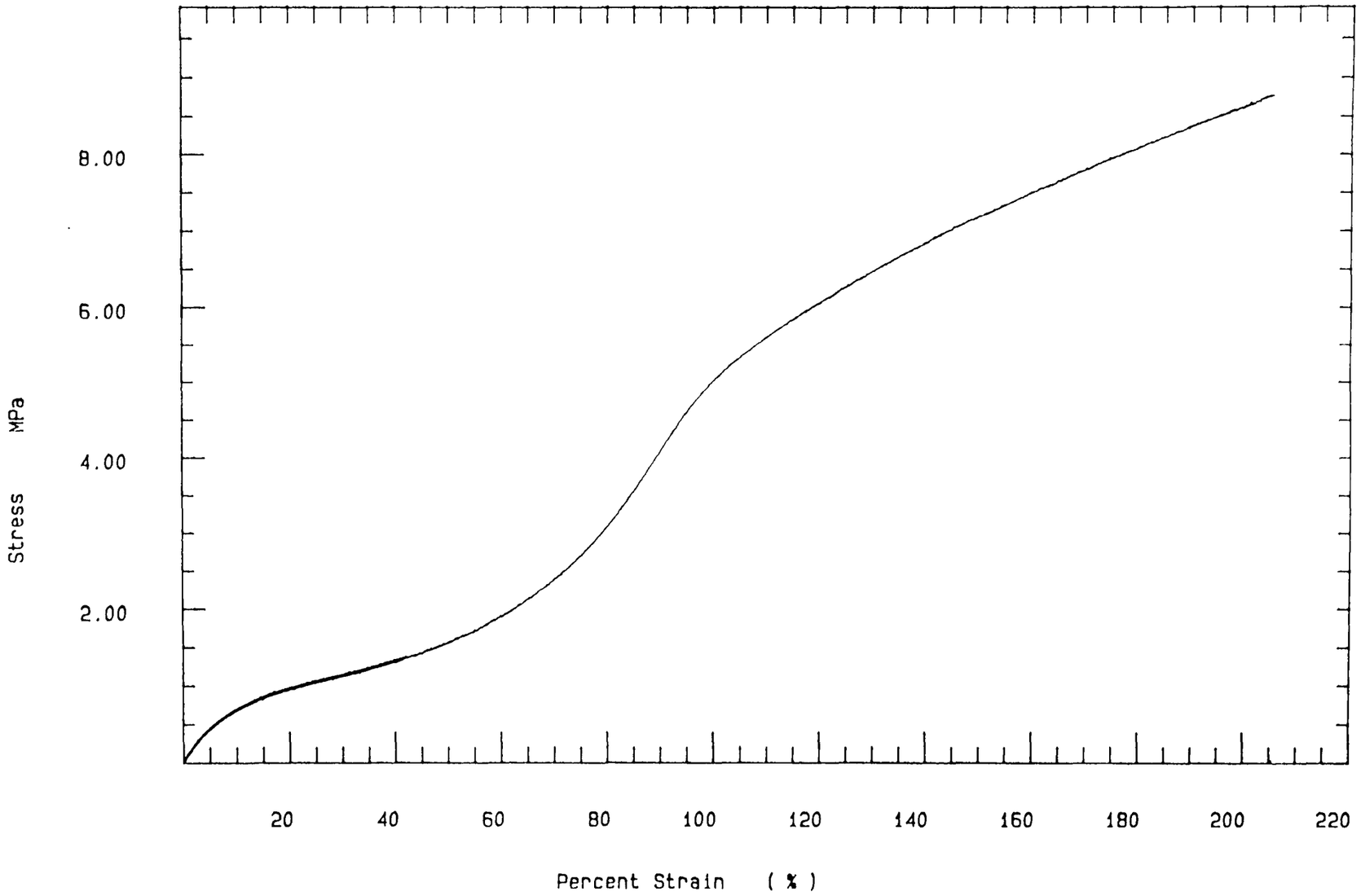

Fig 1.0.1 Elastic response of test seal rubber material

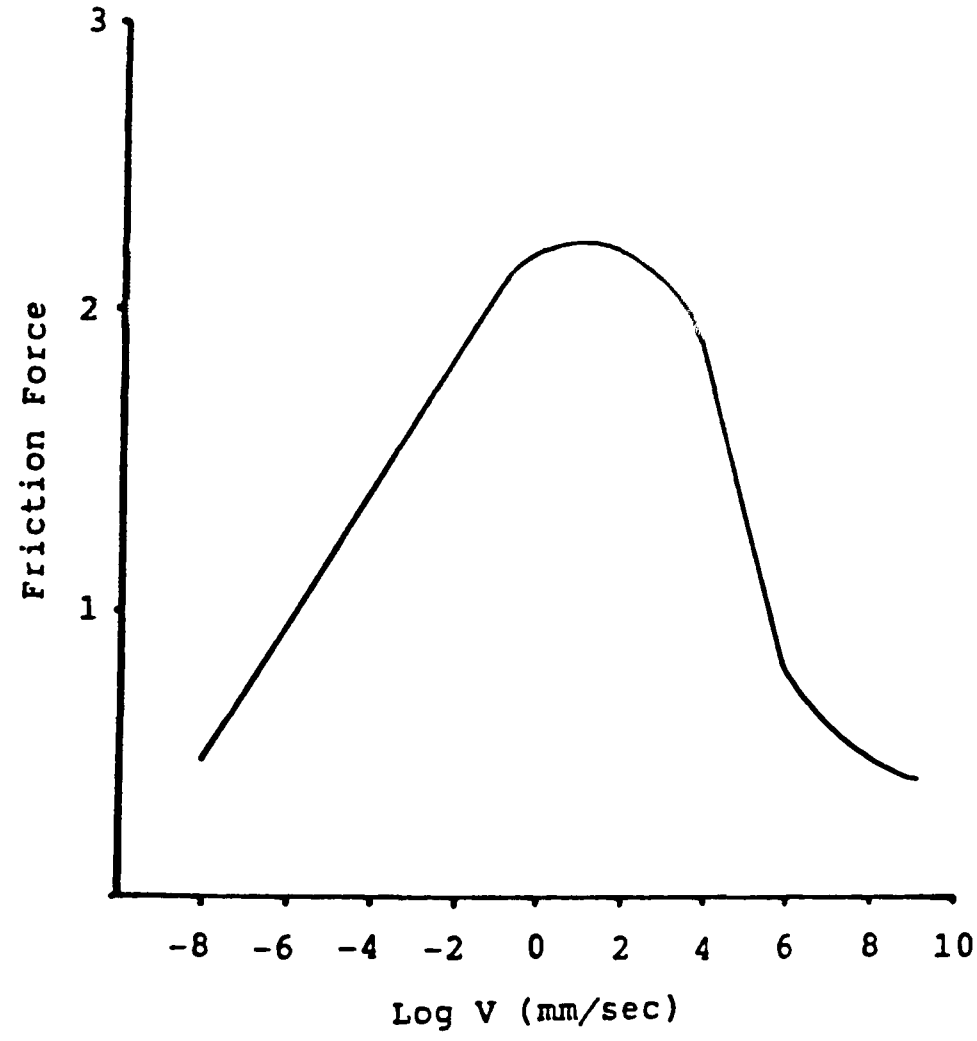

Fig 1.02 Typical curve showing the variation in rubber friction with sliding speed at constant temperature

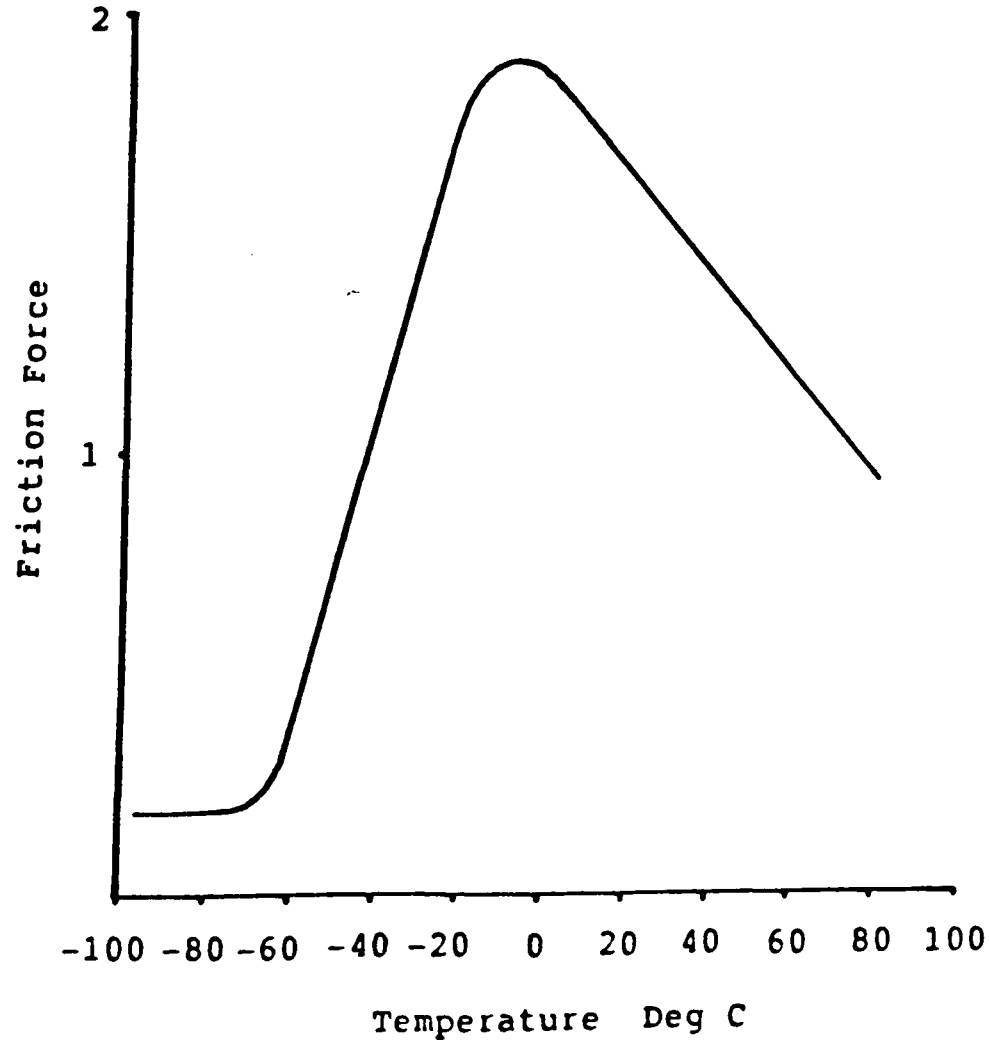

Fig 1.03 Typical curve showing the variation in rubber friction with temperature at constant sliding speed

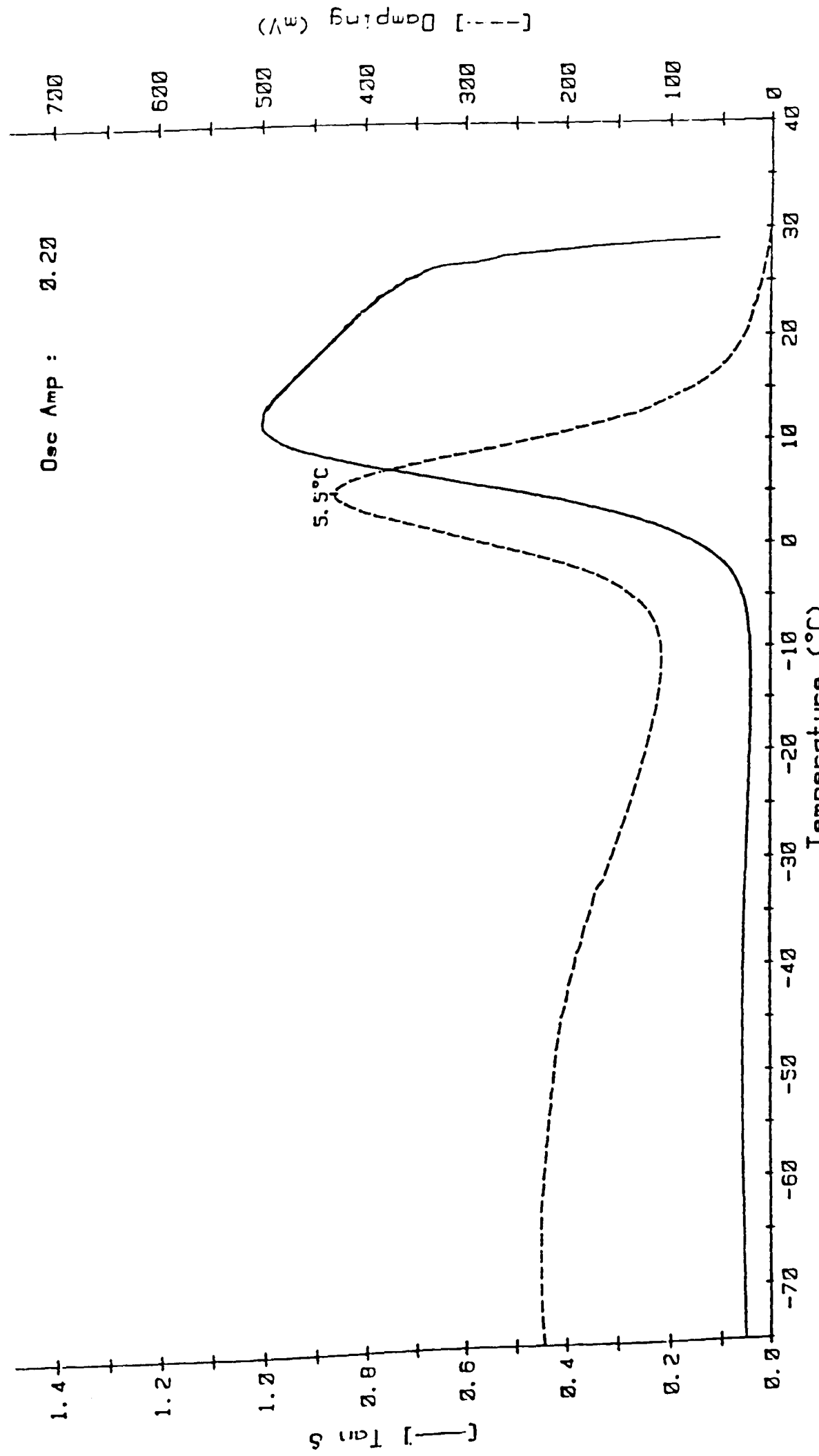

Fig 1.04 The Variation of the Mechanical Losses with Temperature for the Experimental Viton Material

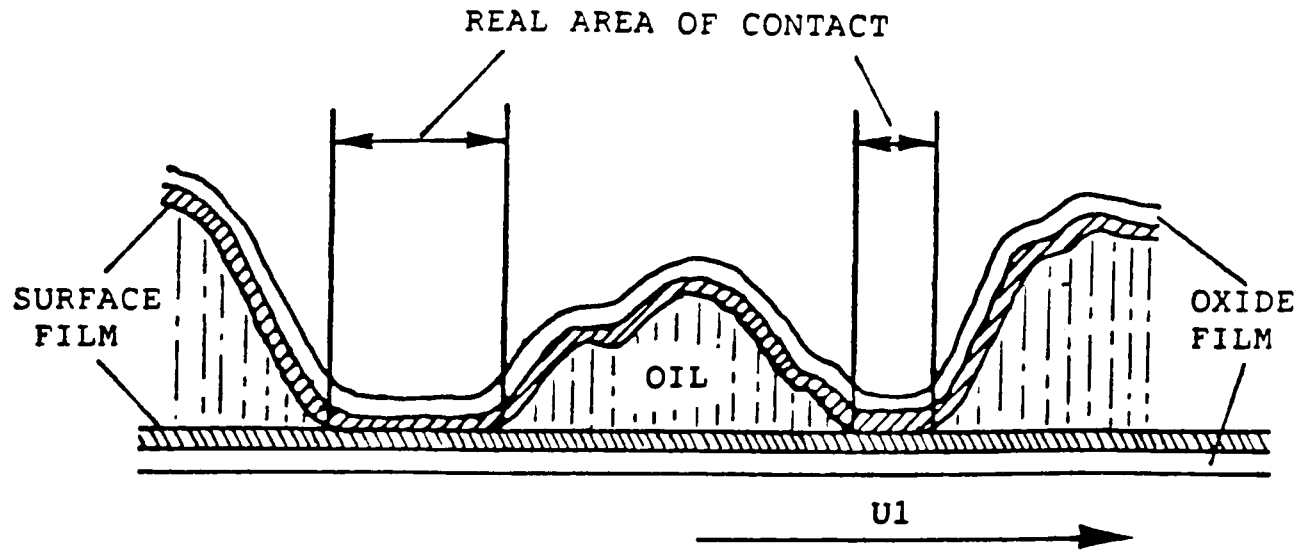

Fig 1.05 Boundary Lubrication Mode

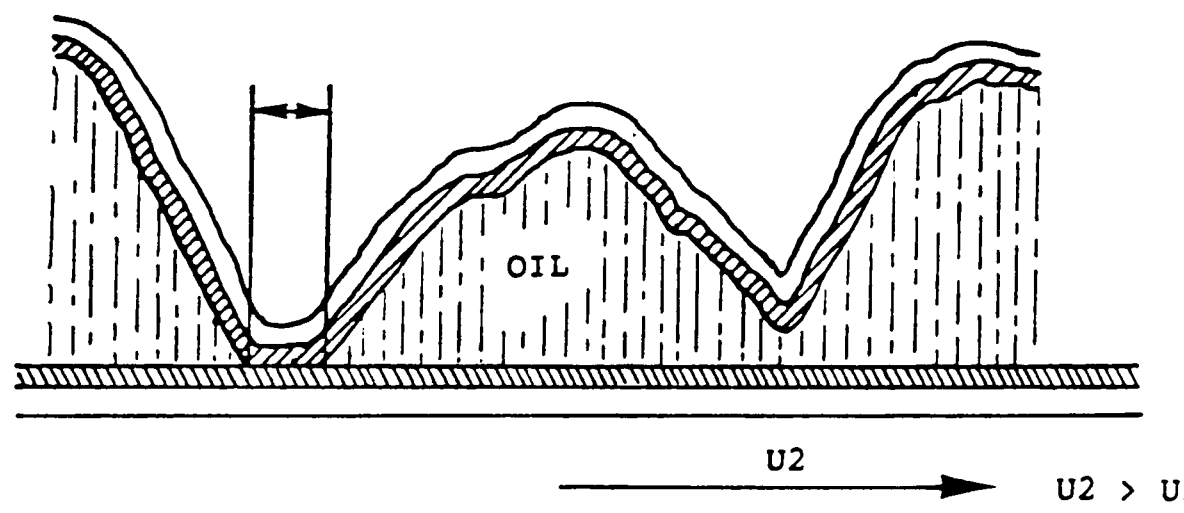

Fig 1.06 Mixed Lubrication Mode

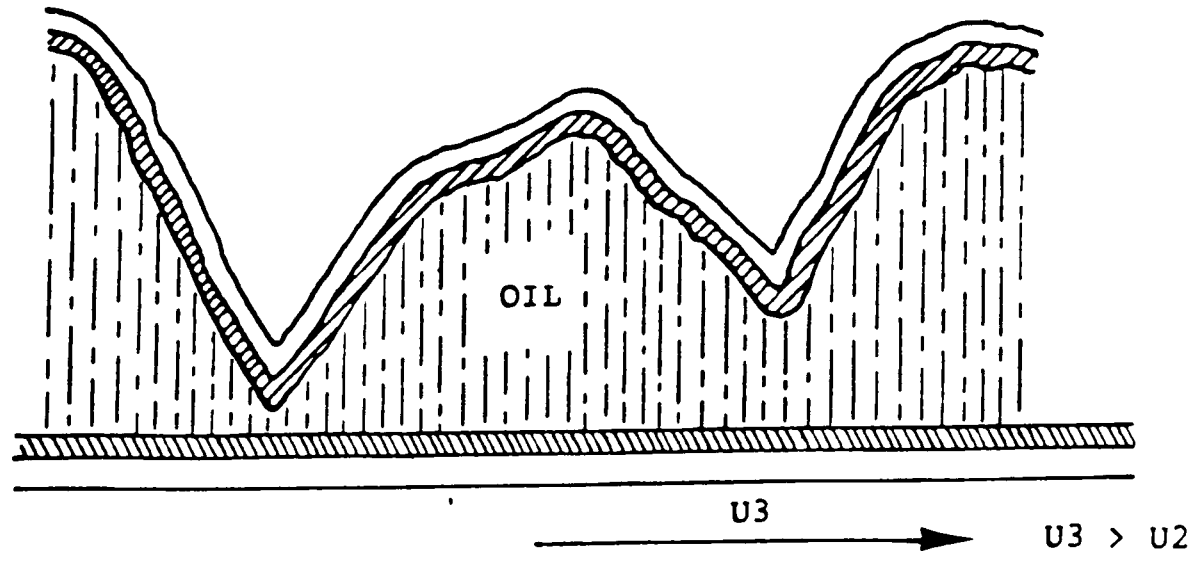

Fig 1.07 Full elastohydrodynamic Lubrication Mode

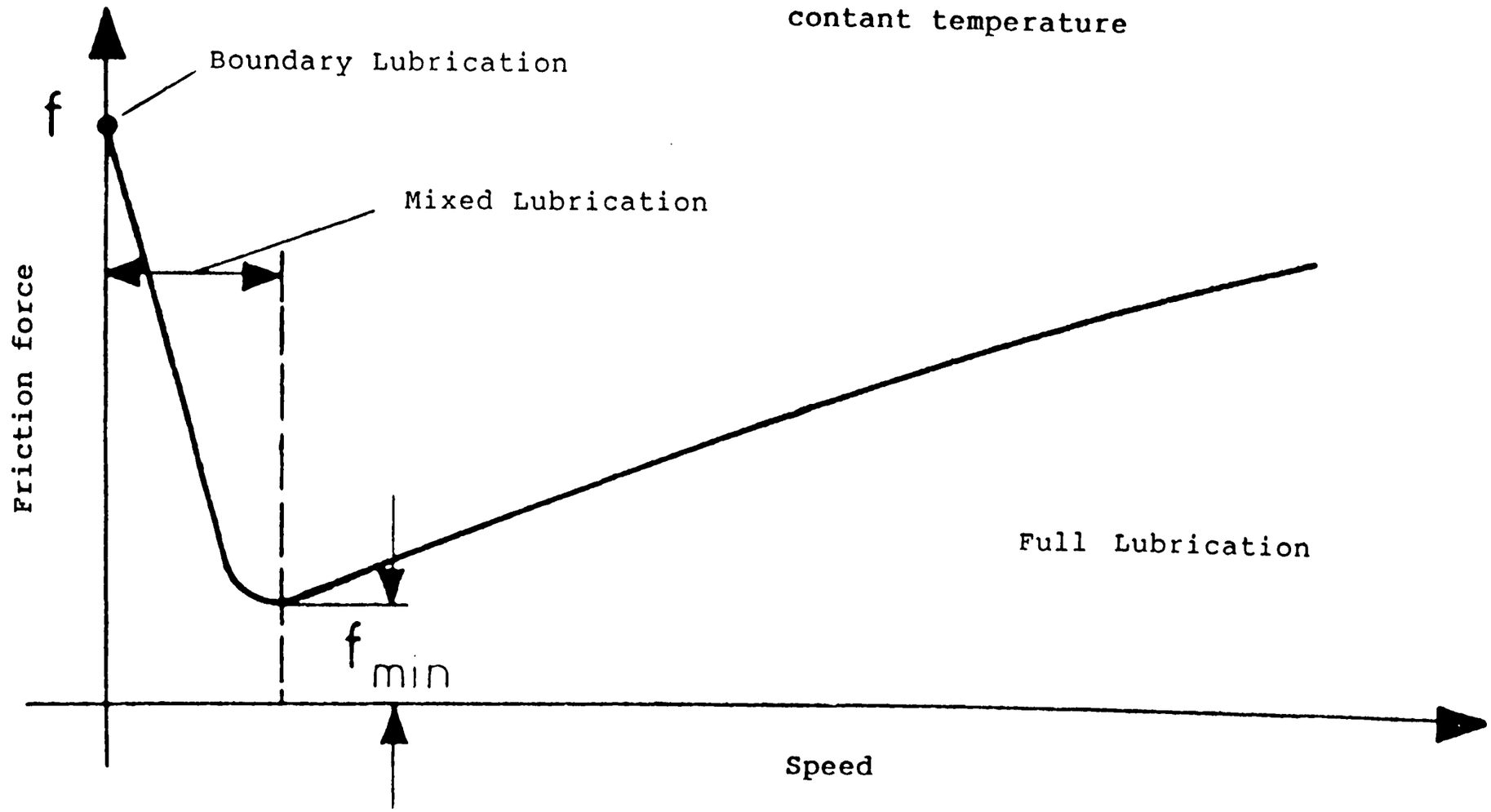

Fig 1.0.8 Generalised Striebeck curve

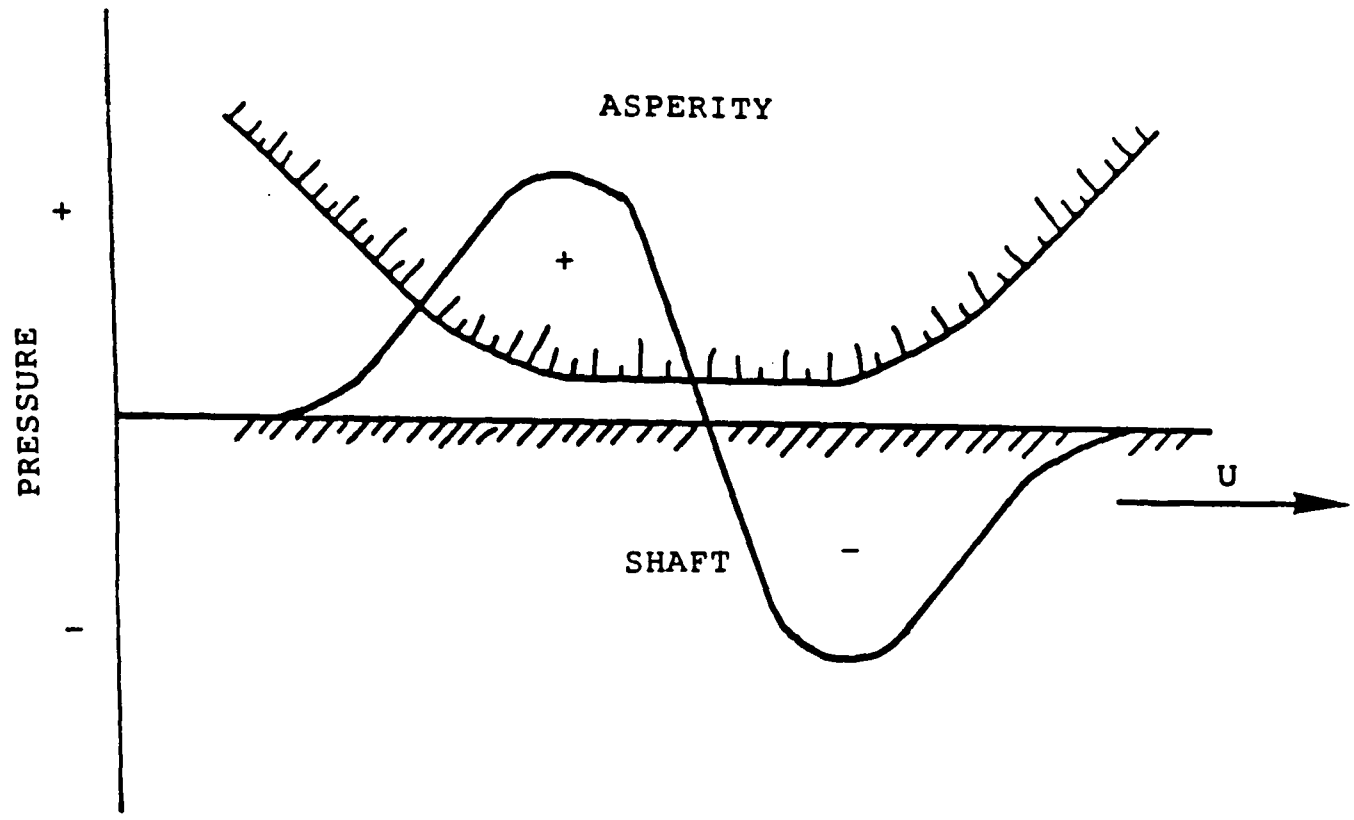

Fig 1.09 Pressure developed throughout a fluid film assuming that cavitation does not occur

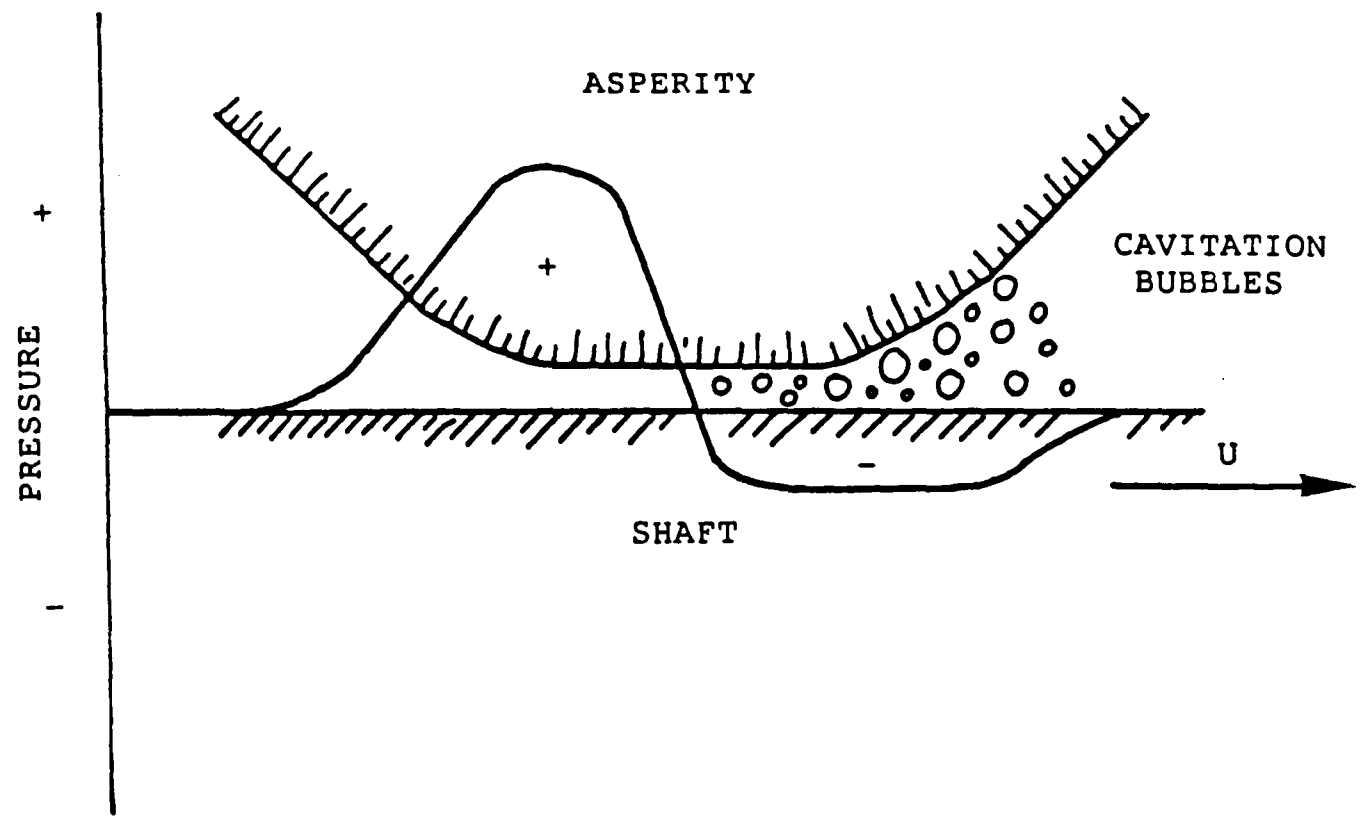

Fig 1.10 Pressure developed throughout a fluid film if cavitation is assumed to occur

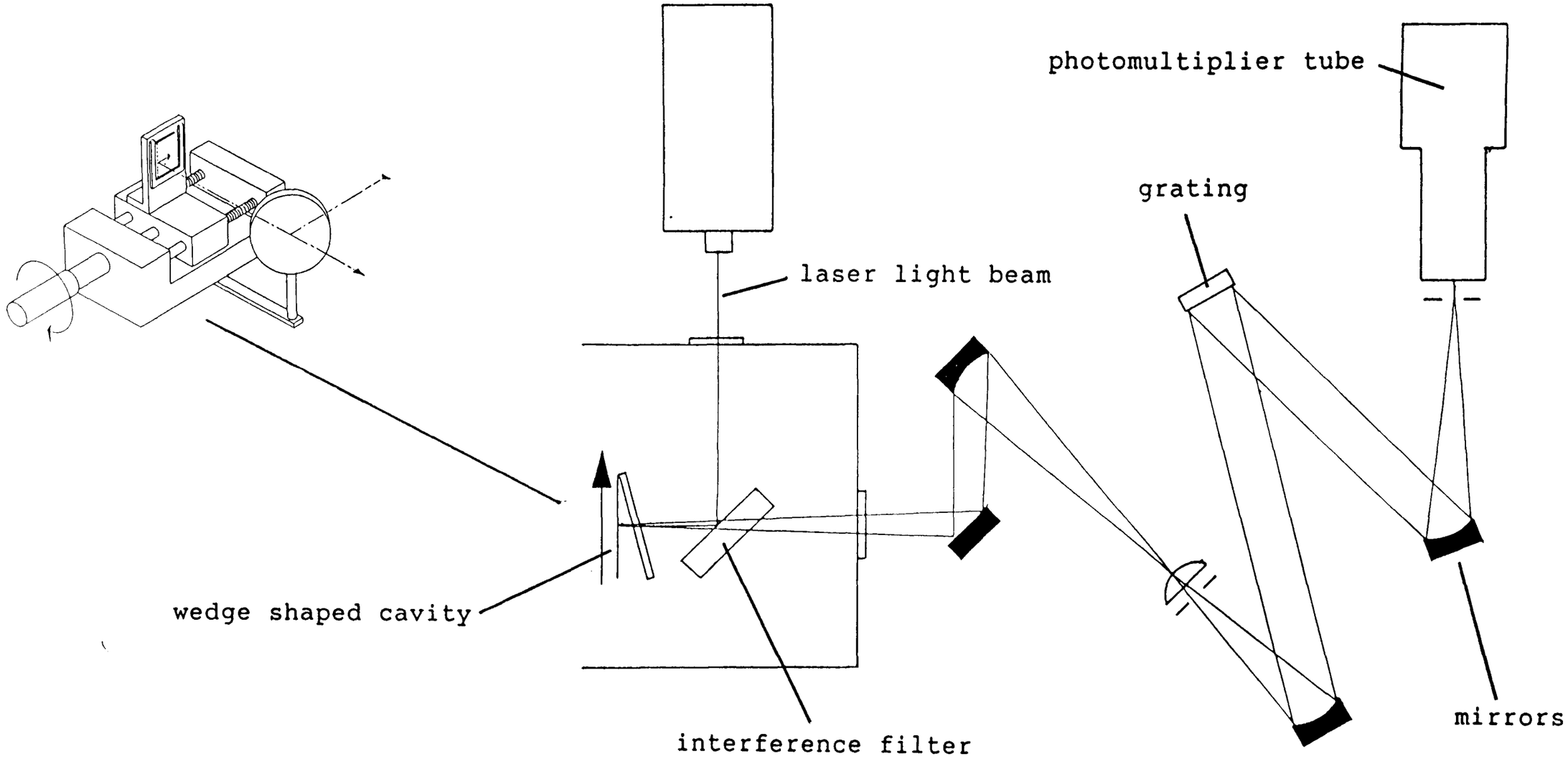

Fig 3.0.1 Fluorescence spectrometer

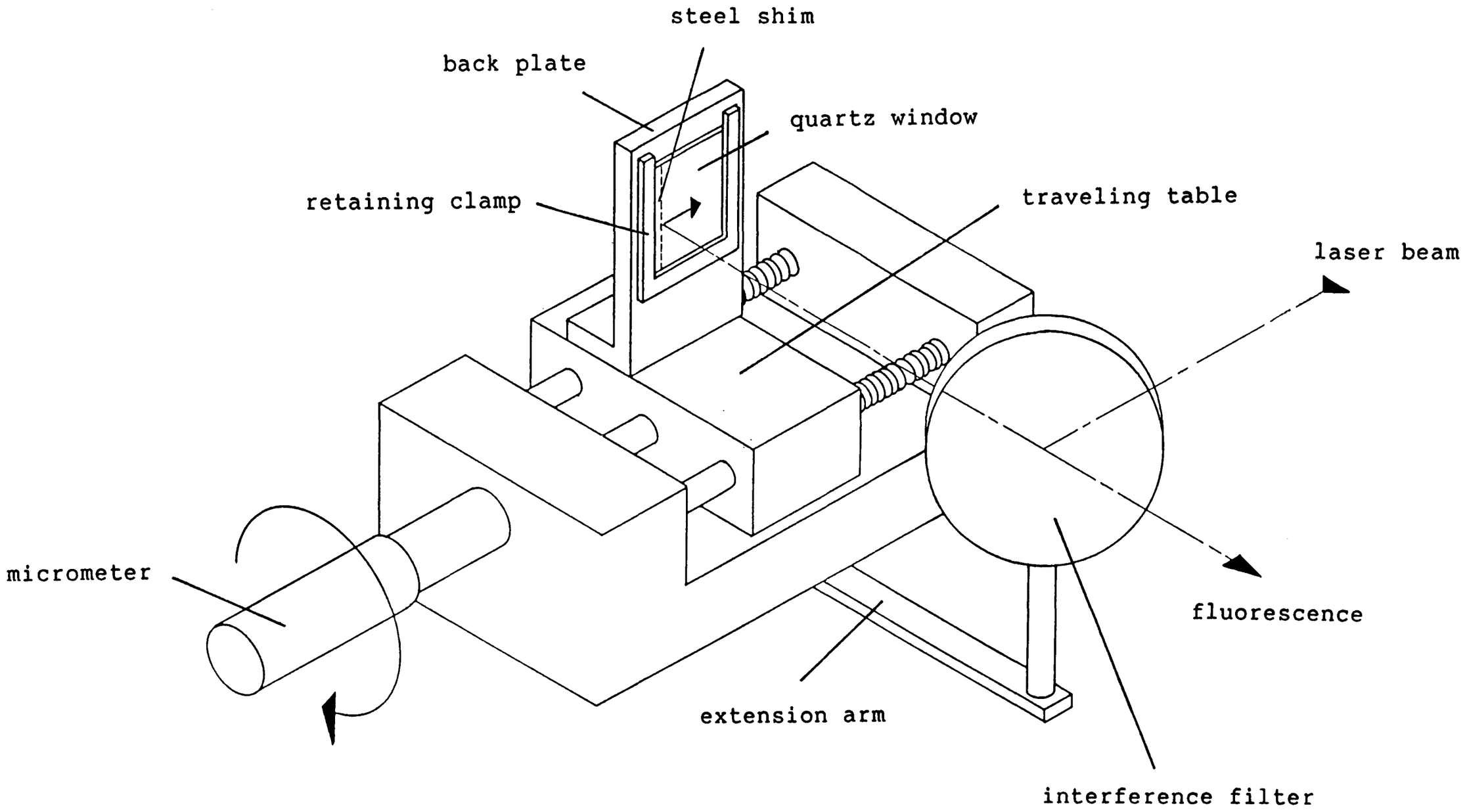

Fig 3.0.2 Model experimental apparatus

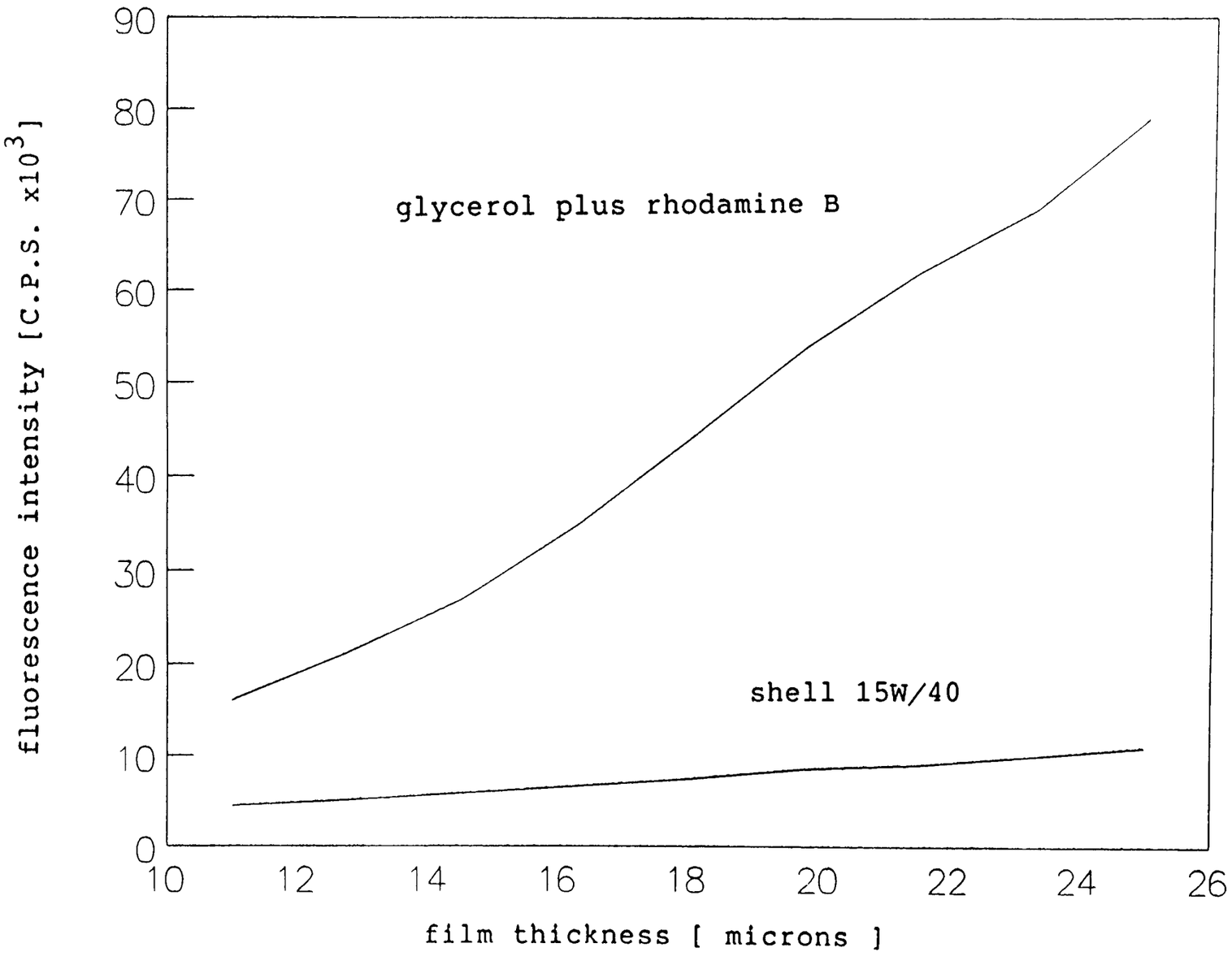

Fig 3.0.3 Film thickness Vs fluoresence intensity

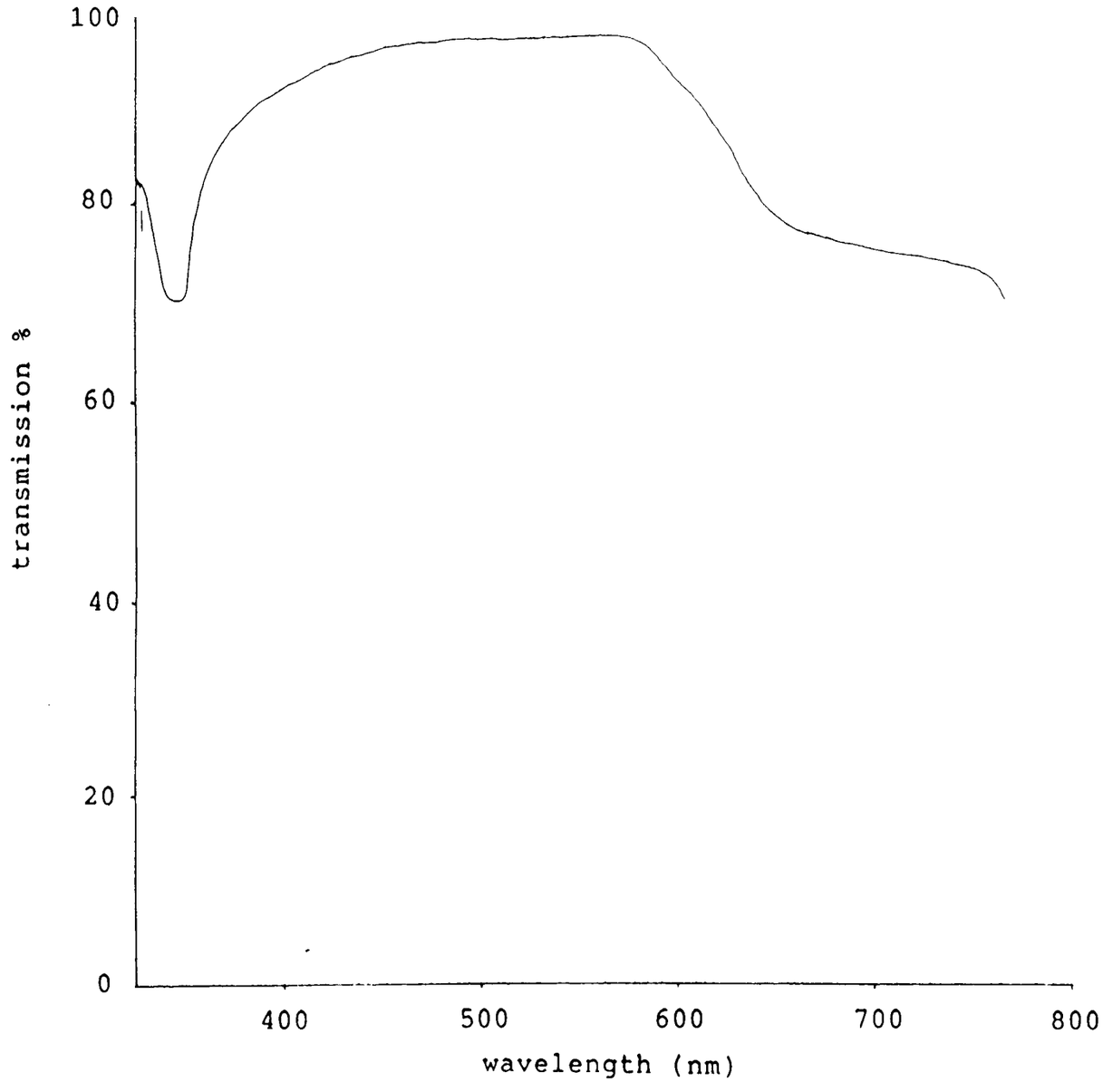

Fig 3.0.4 The visible absorbtion spectrum of Glycerol

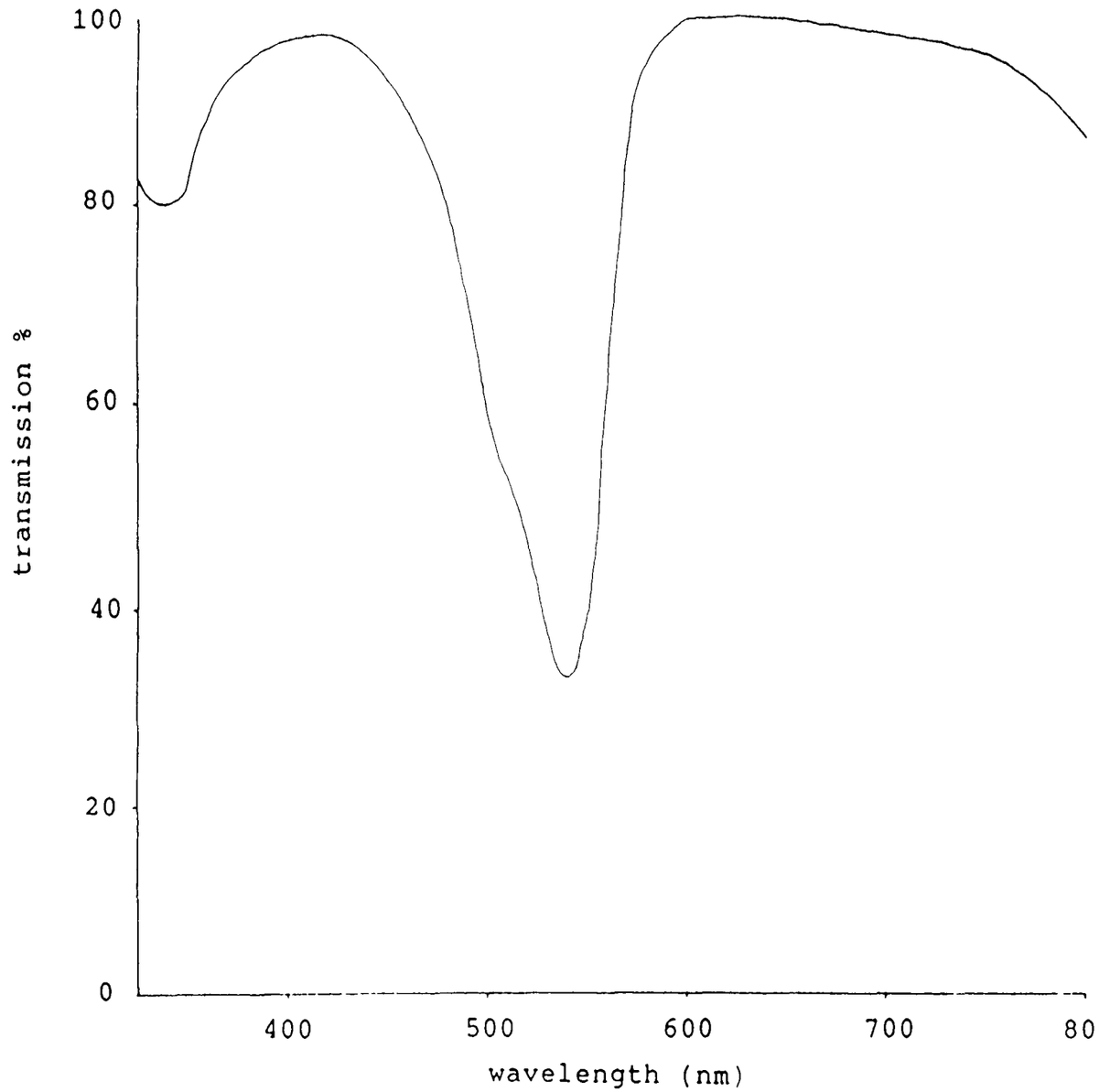

Fig 3.0.5 The visible absorbtion spectrum of Rhodamine B

Fig 4.0.0 Intermittent pin register camera

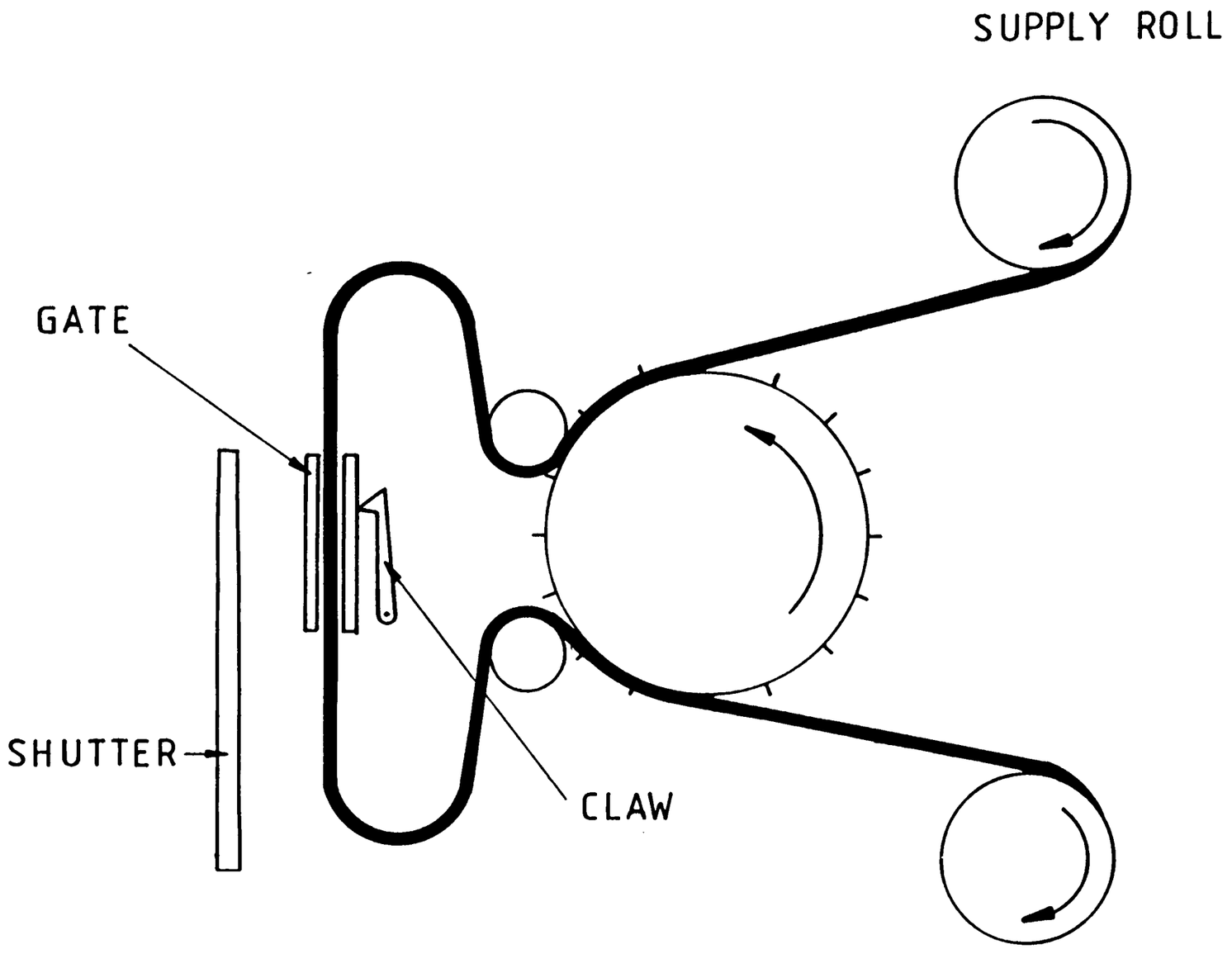

drum type

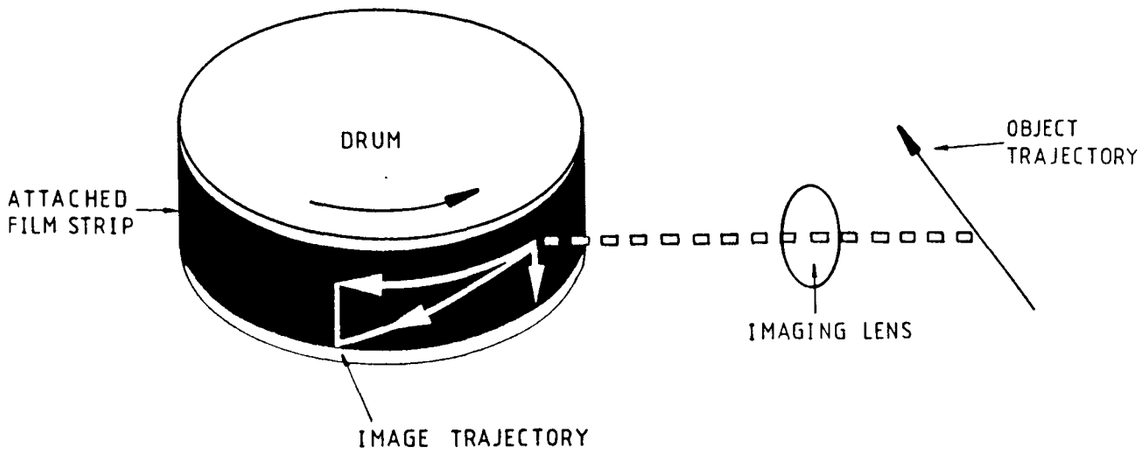

fixed film type

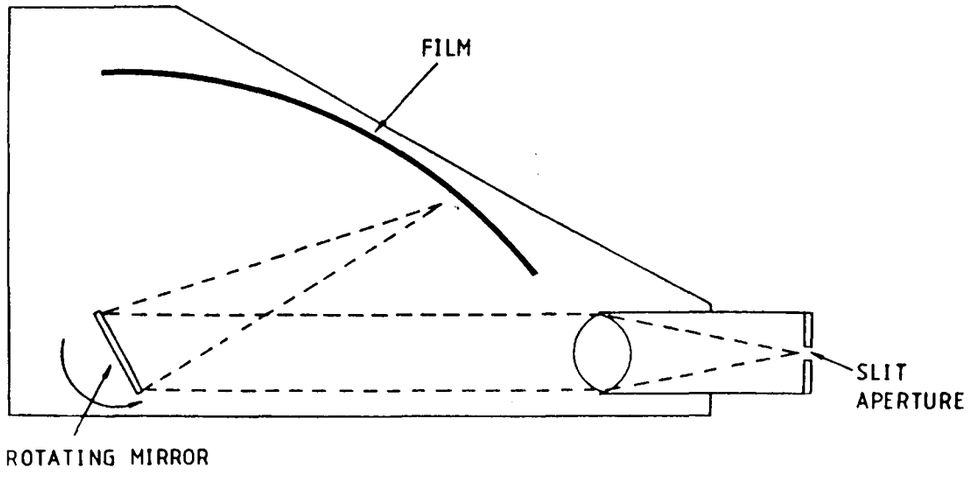

Fig 4.0.1 Streak Camera

Fig 4.0.2 Image converter camera

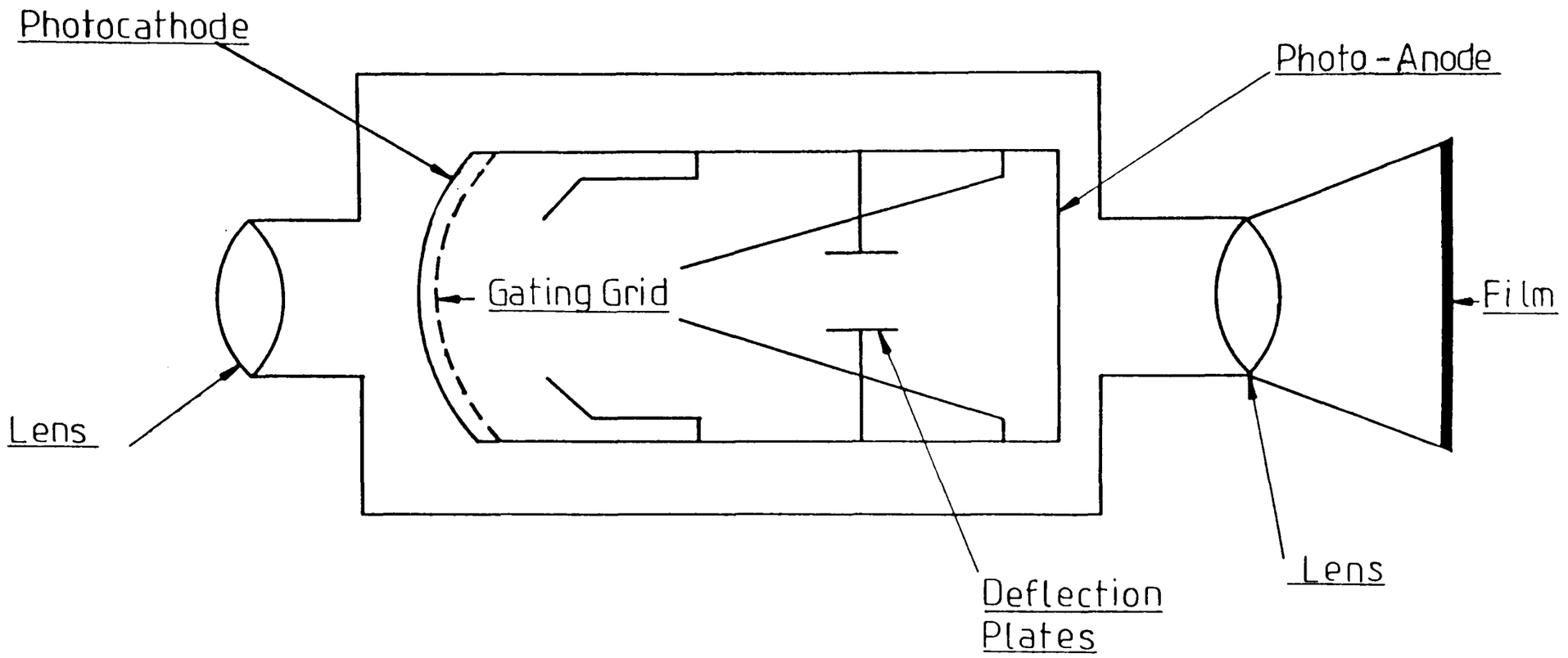

Fig 4.0.3 Rotating prism camera

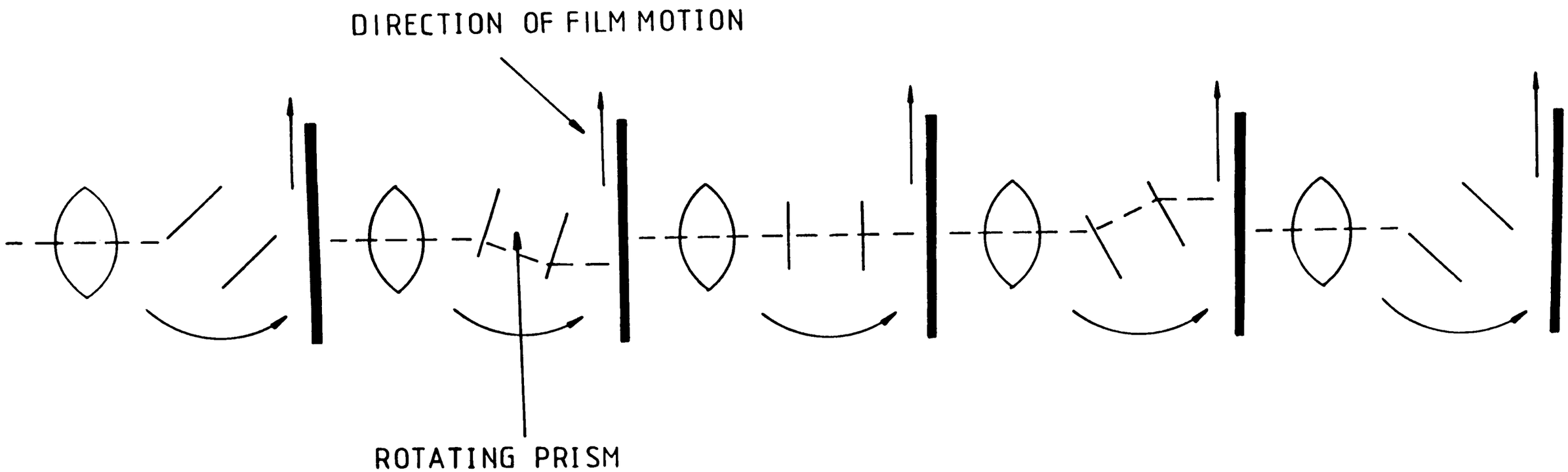

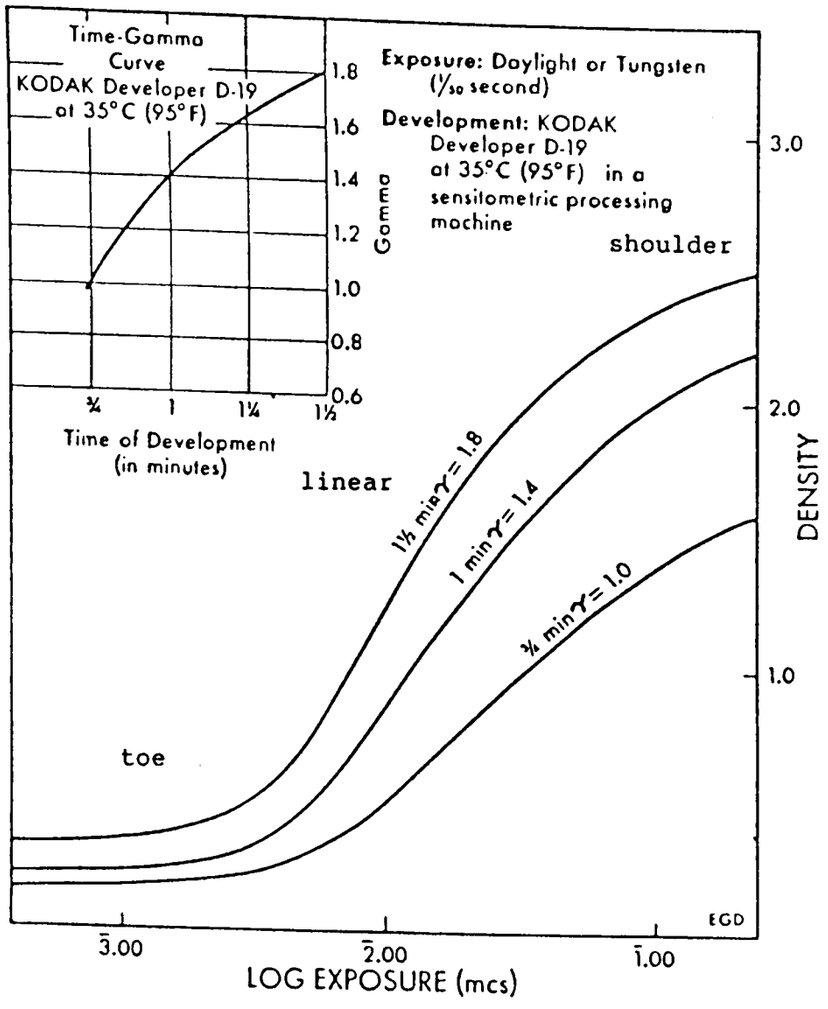

Fig 4.0.4 Film response curve

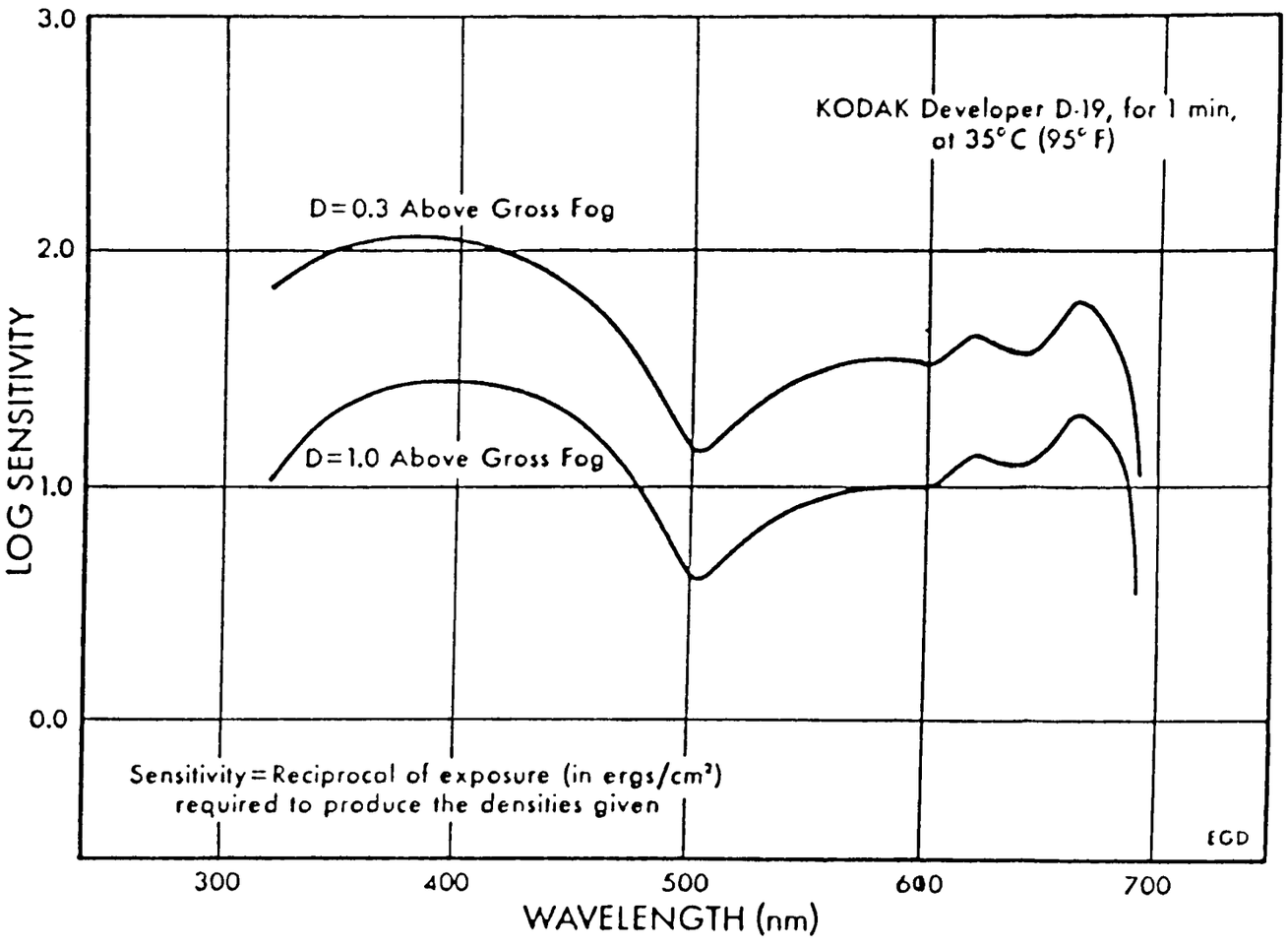

Fig 4.0.5 Spectral sensitivity curve

Both curves reproduced from Kodak pamphlet No. P-72

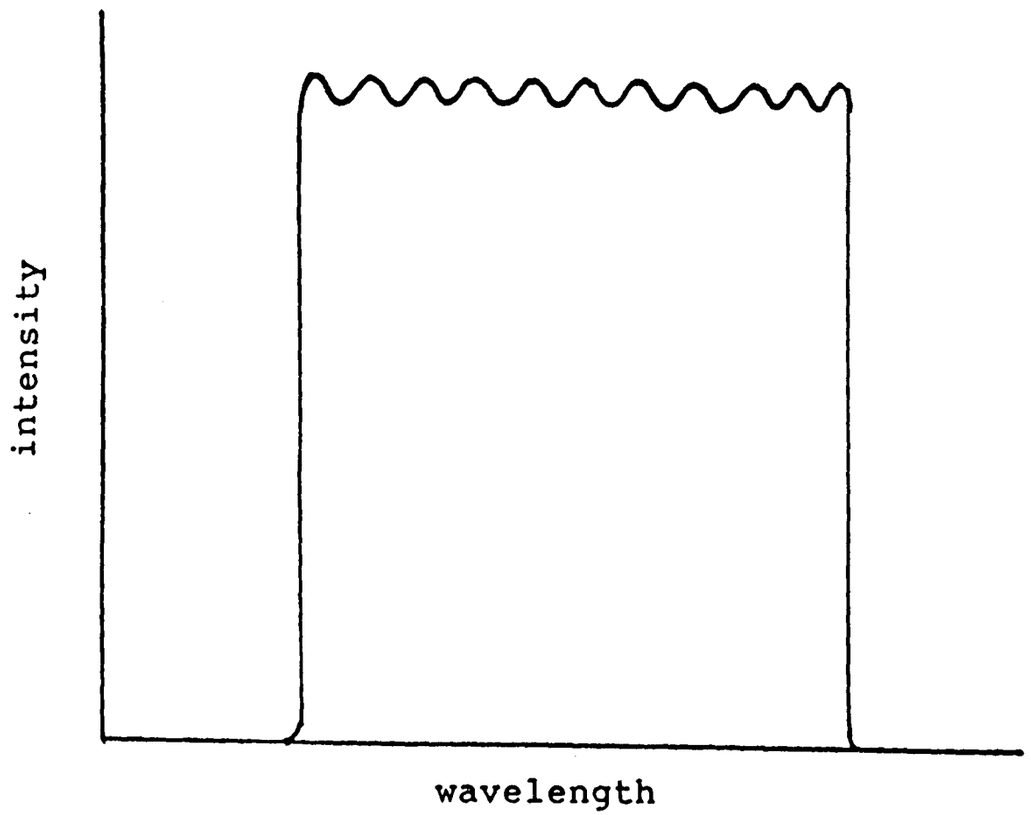

Fig 4.0.6 MTM laser intensity distribution

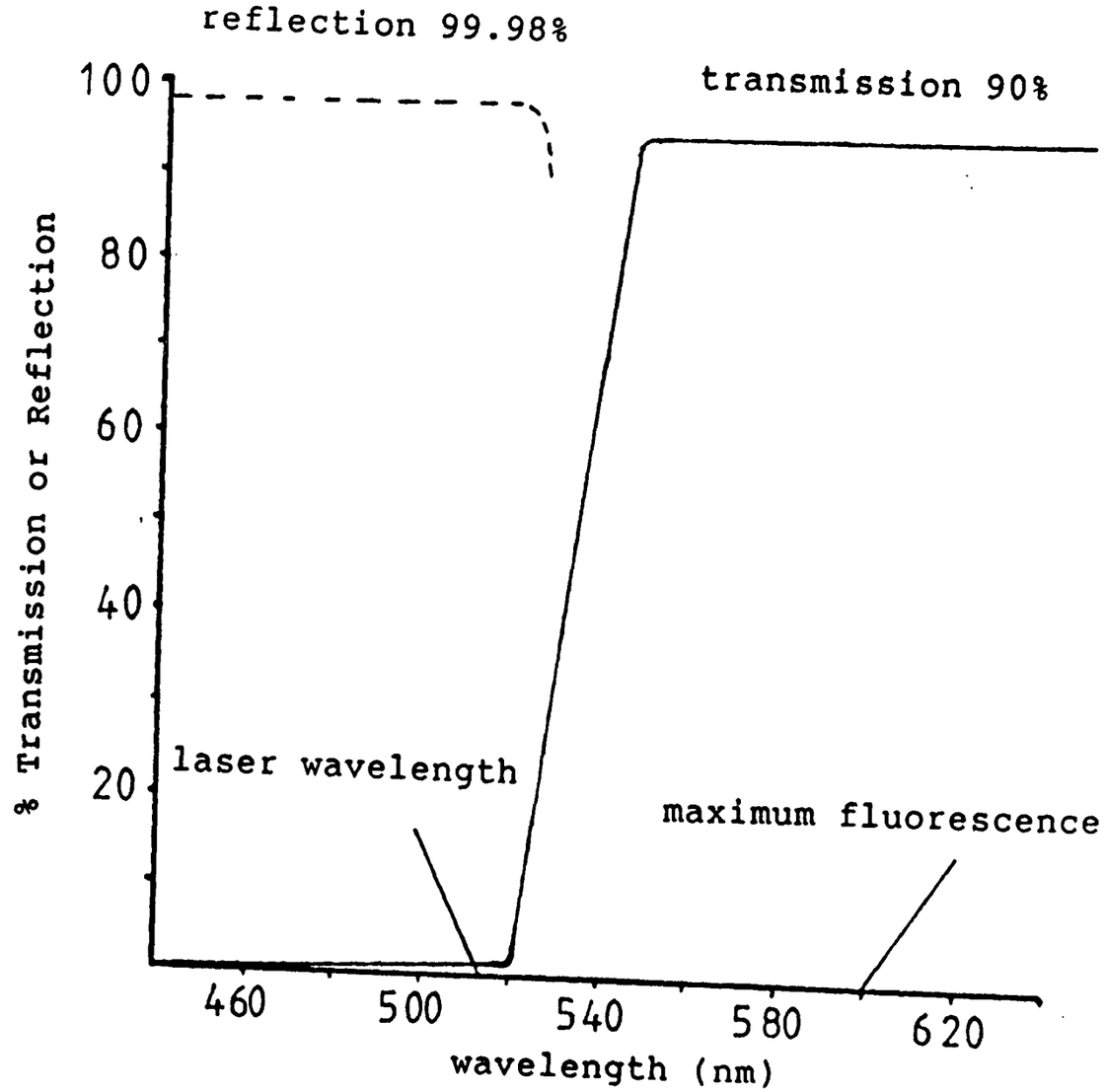

Fig 4.0.7 Interference filter performance curve

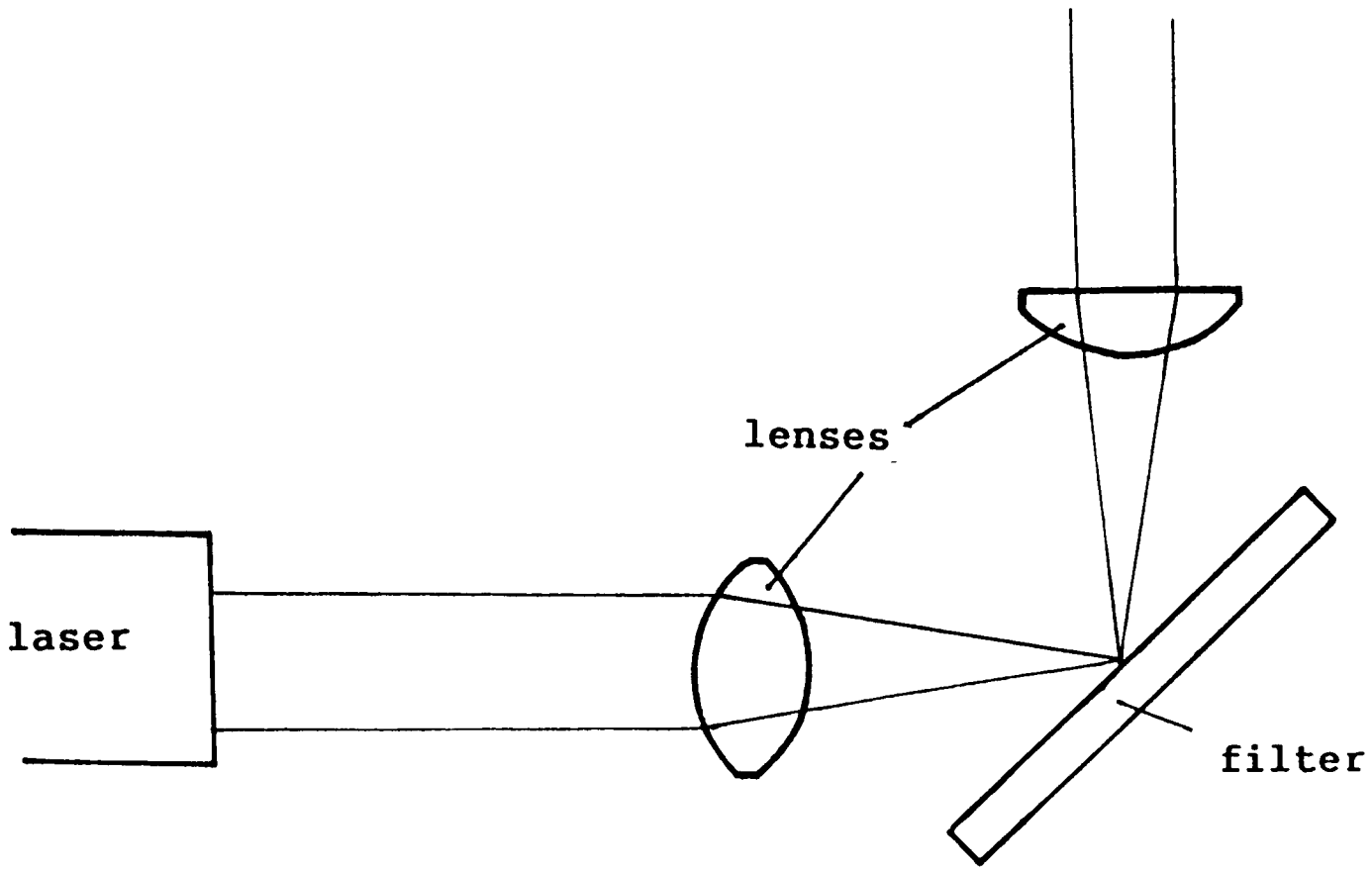

Fig 4.0.8 Position of the lenses and filter

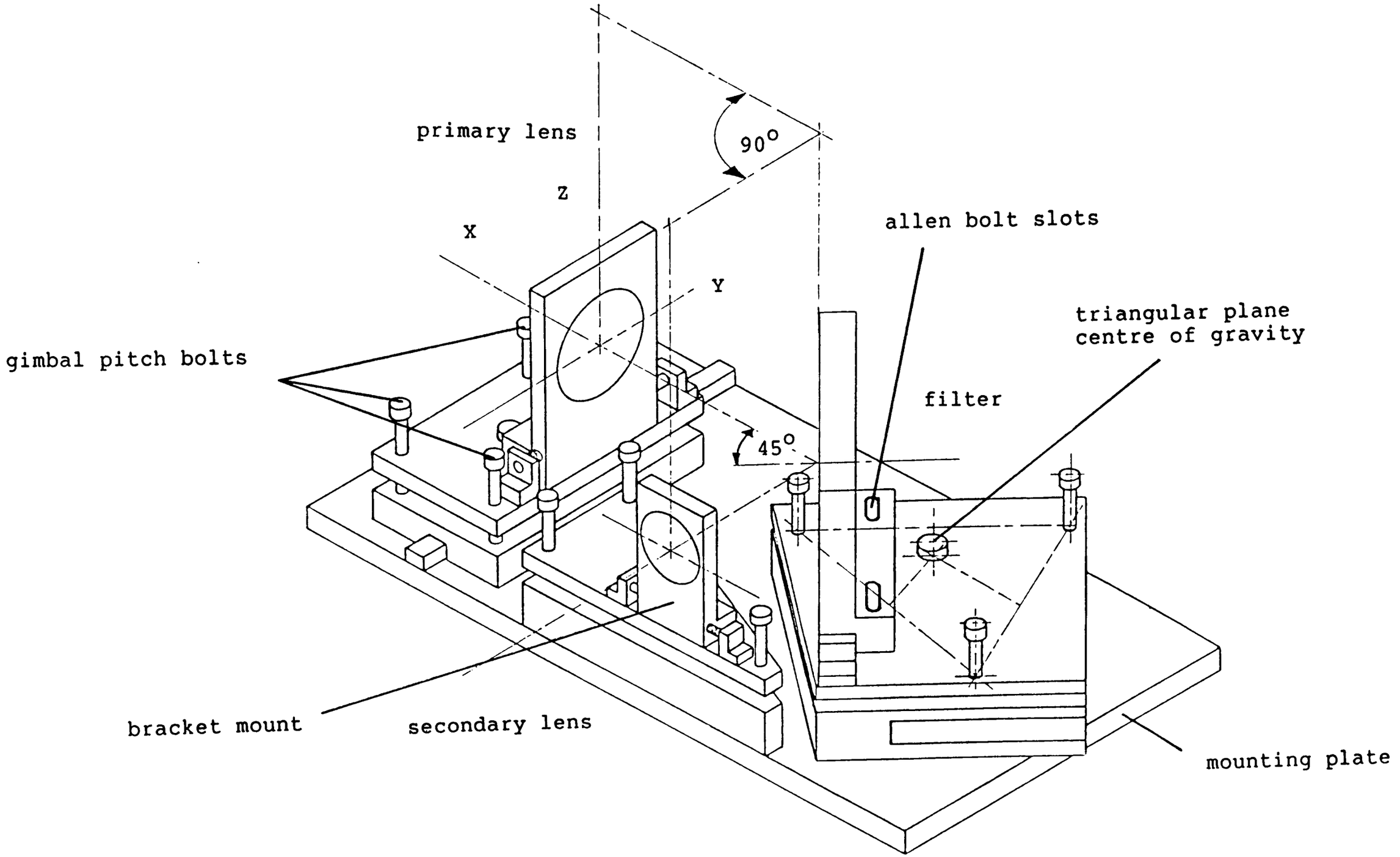

Fig 4.0.9 Lenses and filter gimbal mounts

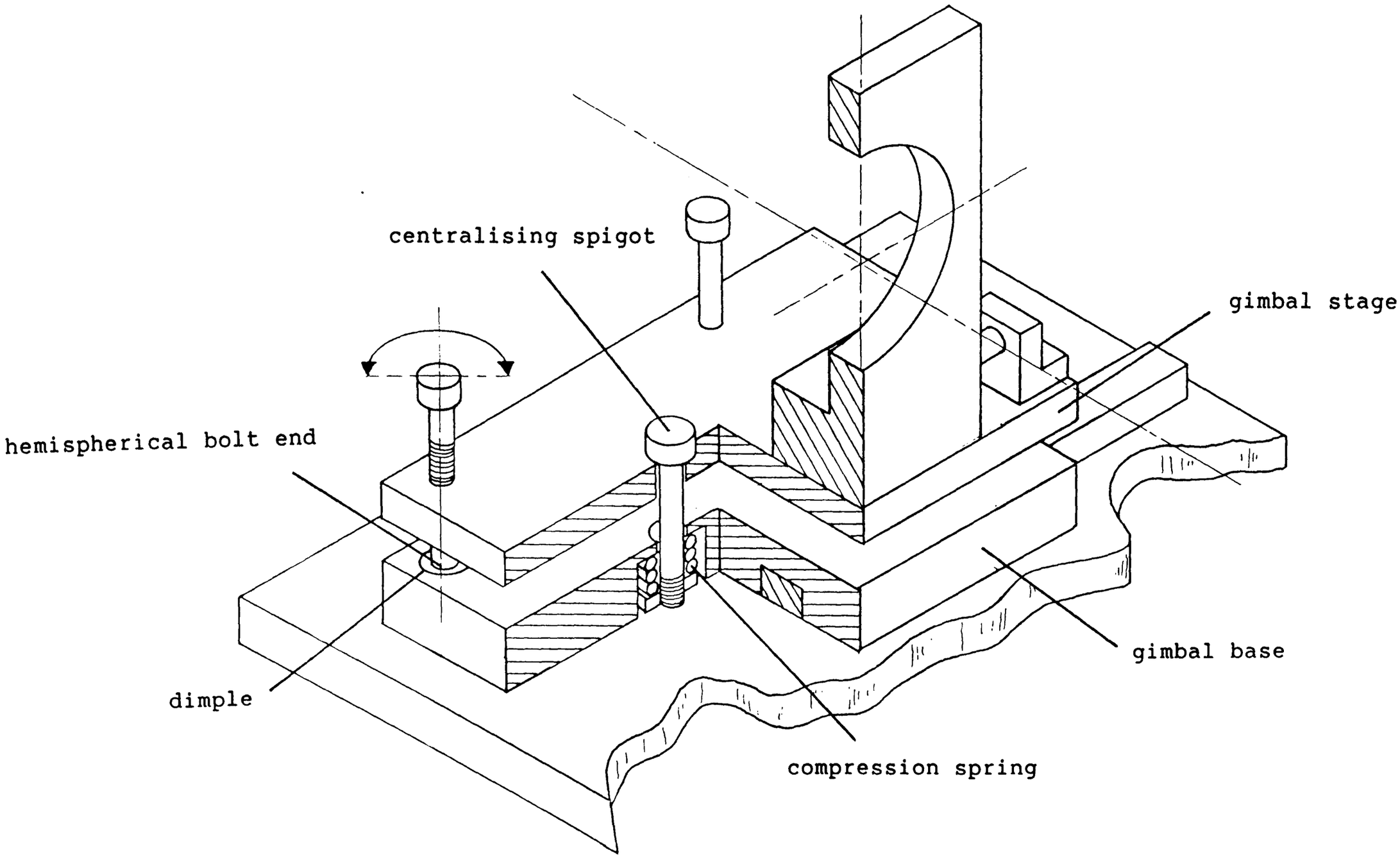

Fig 4.1.0 Gimbal

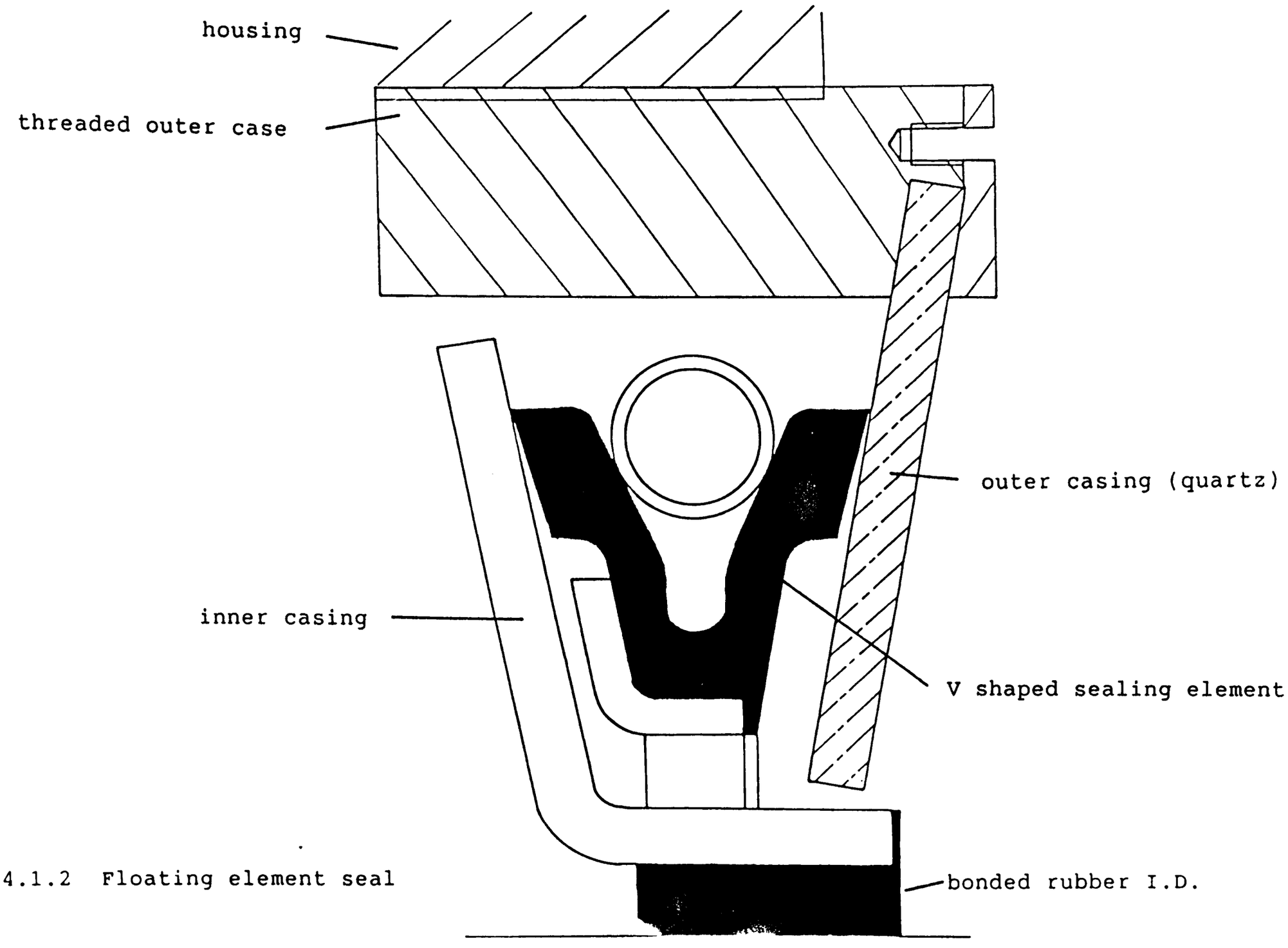

Fig 4.1.2 Floating element seal

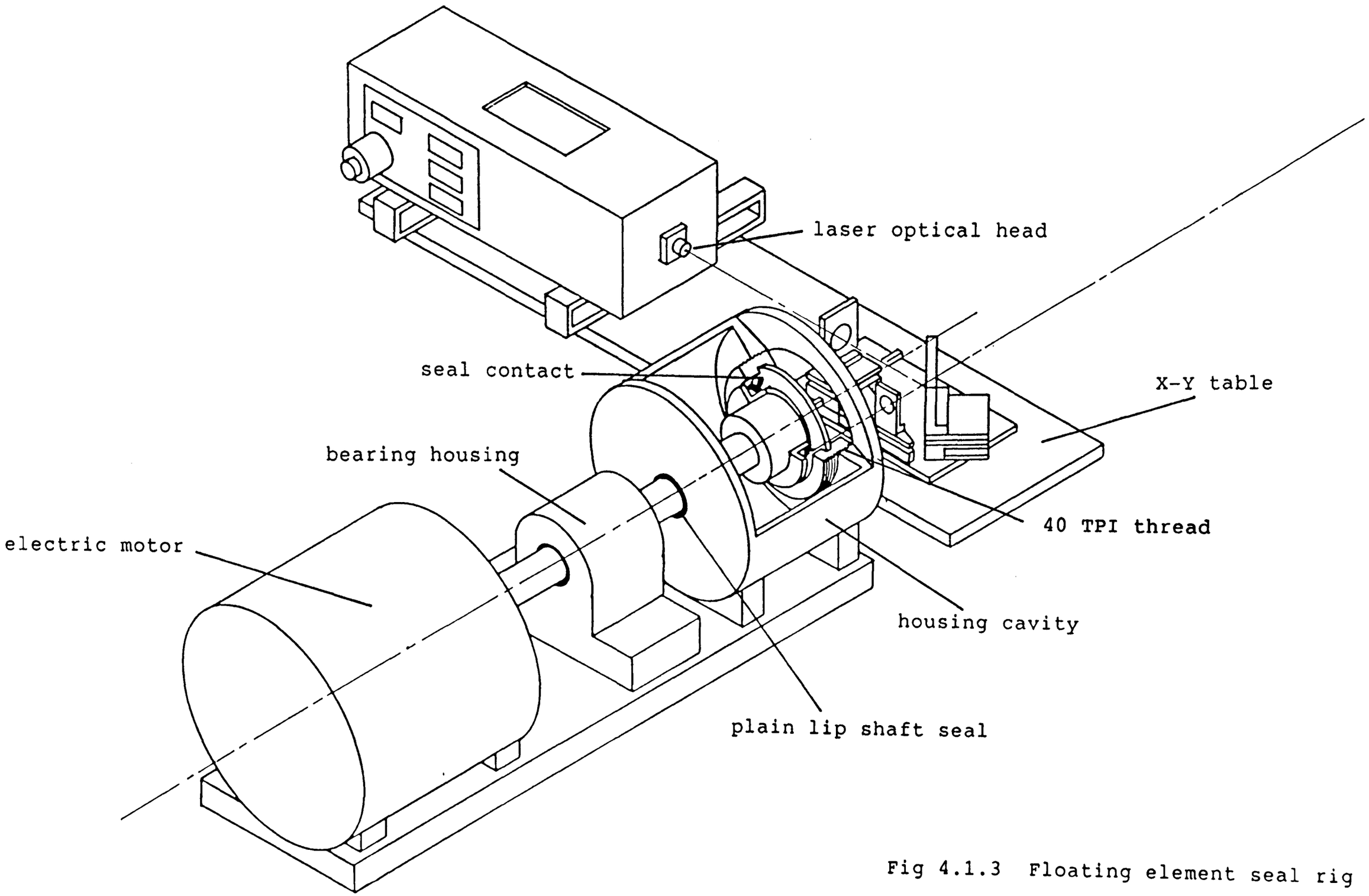

Fig 4.1.3 Floating element seal rig

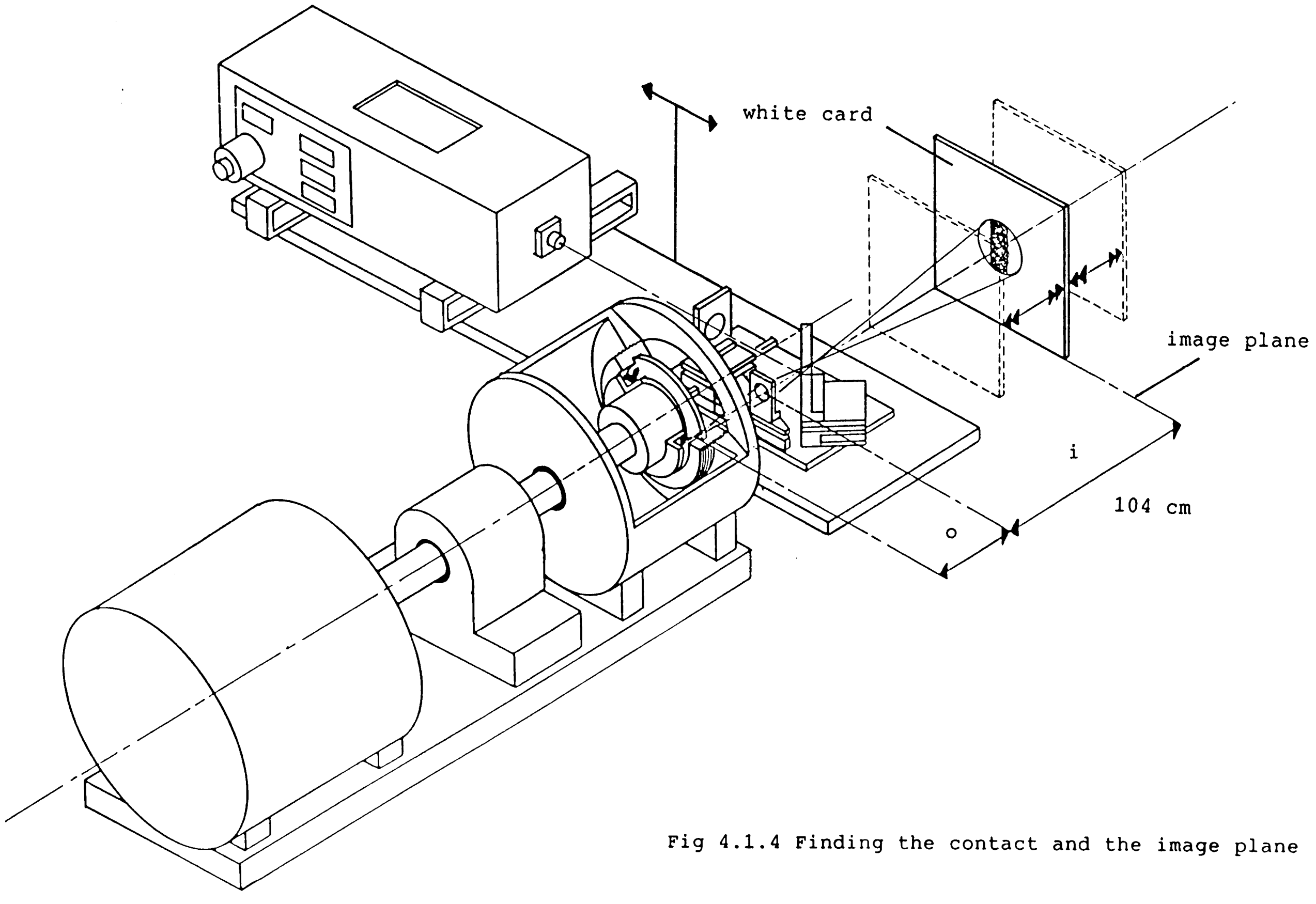

Fig 4.1.4 Finding the contact and the image plane

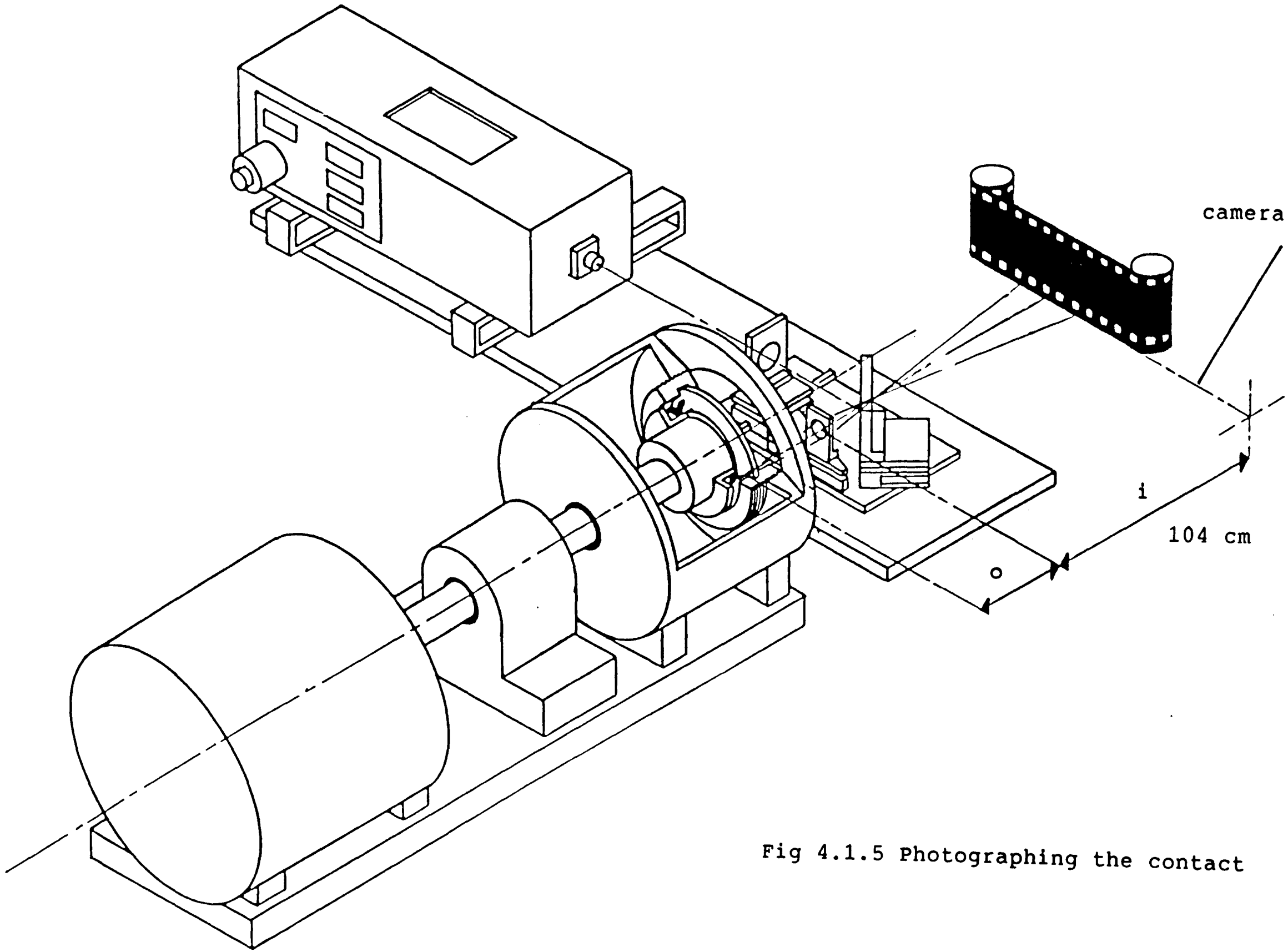

Fig 4.1.5 Photographing the contact

Table 5.00

Surface Texture Parameter	Parameter Values in microns unless otherwise stated
Rt1	0.011
Rt2	0.012
Rt3	0.011
Rt4	0.042
Ra	0.002
Rq	0.003
Ry	0.042
Rtm	0.019
Rv	0.046
Rp	0.002
Sm	9.0
LAM Q	41
DEL Q	0.0 Degrees
Rsk	-2.5 Dimensionless
Rku	28.6 Dimensionless
S	15.0
R3z	0.008
Rpm	-0.002
R3y	0.009

Fig 5.0.0 Shaft bearings & drive mechanism

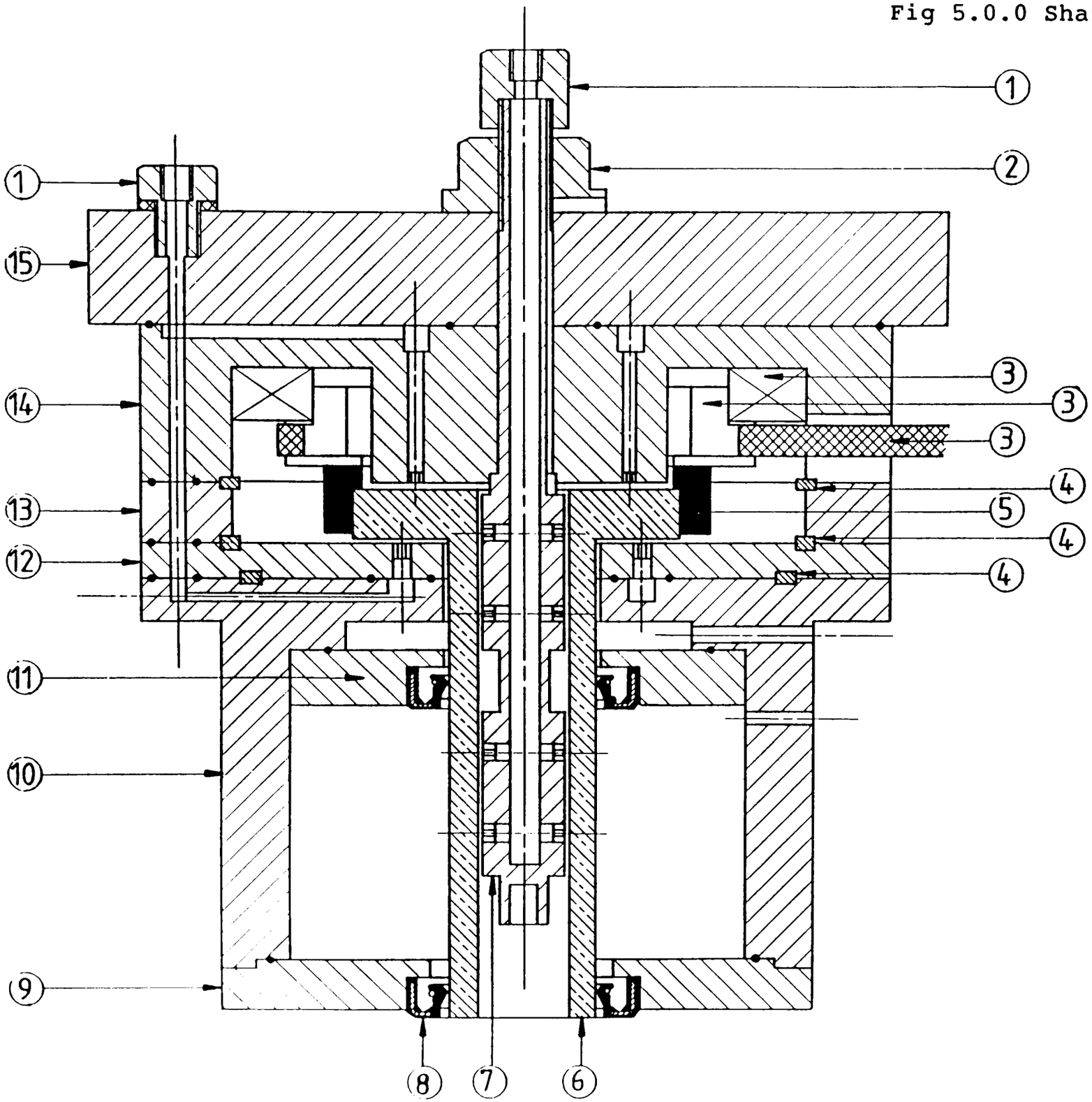

NUMBER	DRAWING DETAIL	FIGURE NUMBER
1	AIR SUPPLY COUPLINGS	
2	BEARING SHAFT TENSION NUT	
3	DRIVE BELT, PULLEY & BEARING	5.0.1
4	LOCATION RINGS	
5	RUBBER DRIVE DOG	5.0.2
6	QUARTZ SHAFT	5.0.3
7	BEARING SHAFT	5.0.4
8	TEST SEAL	5.0.5
9	TEST SEAL HOUSING	5.0.6
10	OIL CHAMBER HOUSING	5.0.7
11	OIL CHAMBER SEAL HOUSING	5.0.8
12	BOTTER THRUST PLATE	5.0.9
13	SPACING RING	5.1.0
14	TOP THRUST PLATE	5.1.1
15	MOUNTING PLATE	

Fig 5.0.1 Drive belt, pulley & bearing

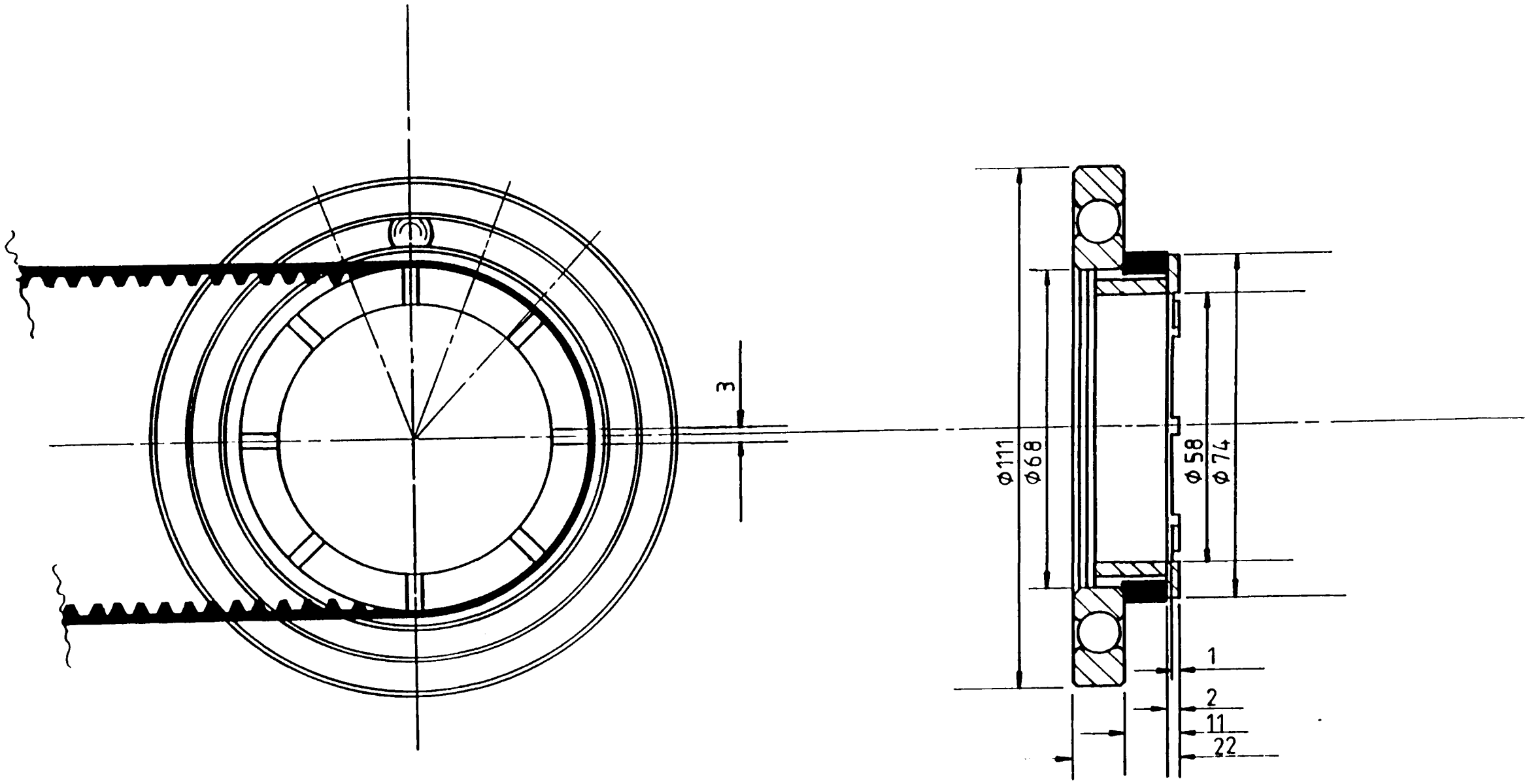

ALL DIMENSIONS IN mm
GEN· TOL:±0·0125 UNLESS
OTHERWISE STATED

Fig 5.0.2 Rubber drive dog

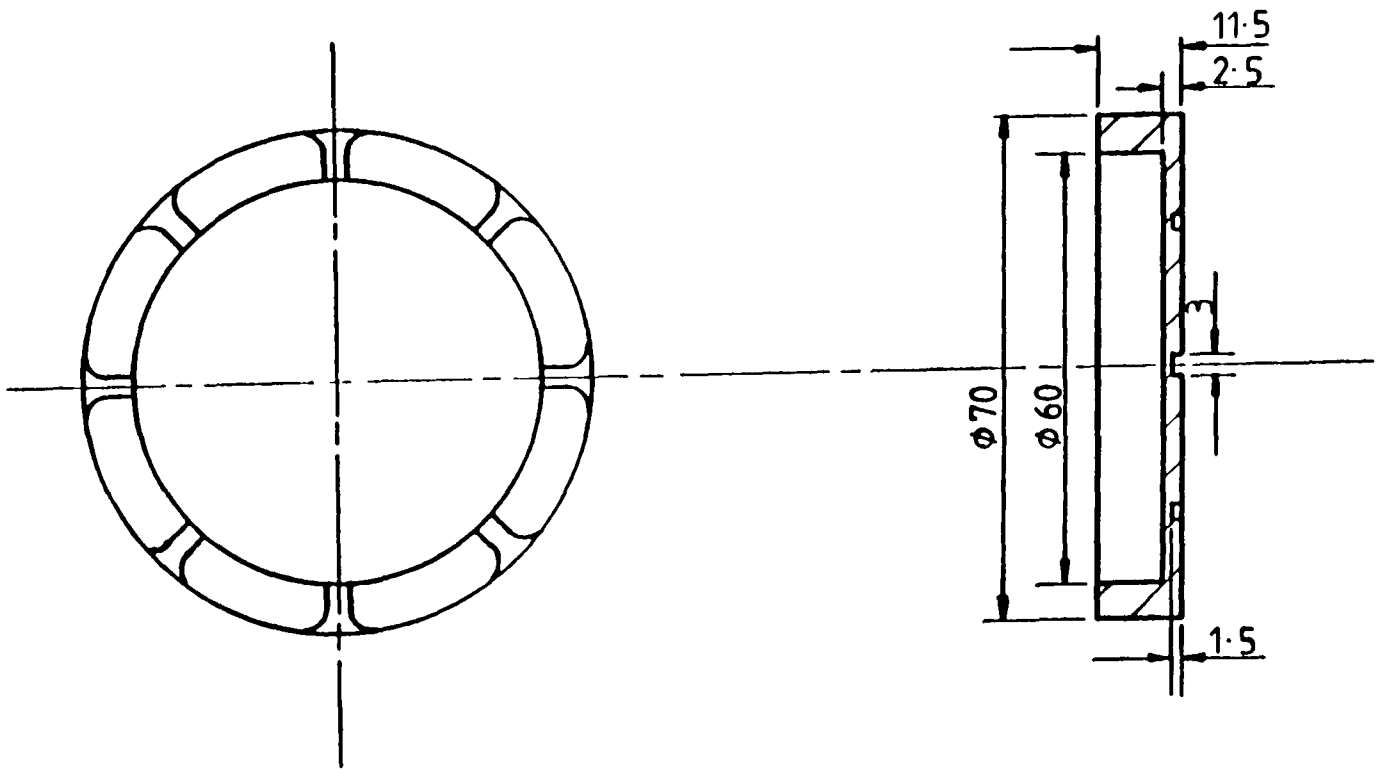

ALL DIMENSIONS IN mm
GEN· TOL :-± 0·1 UNLESS
OTHERWISE STATED

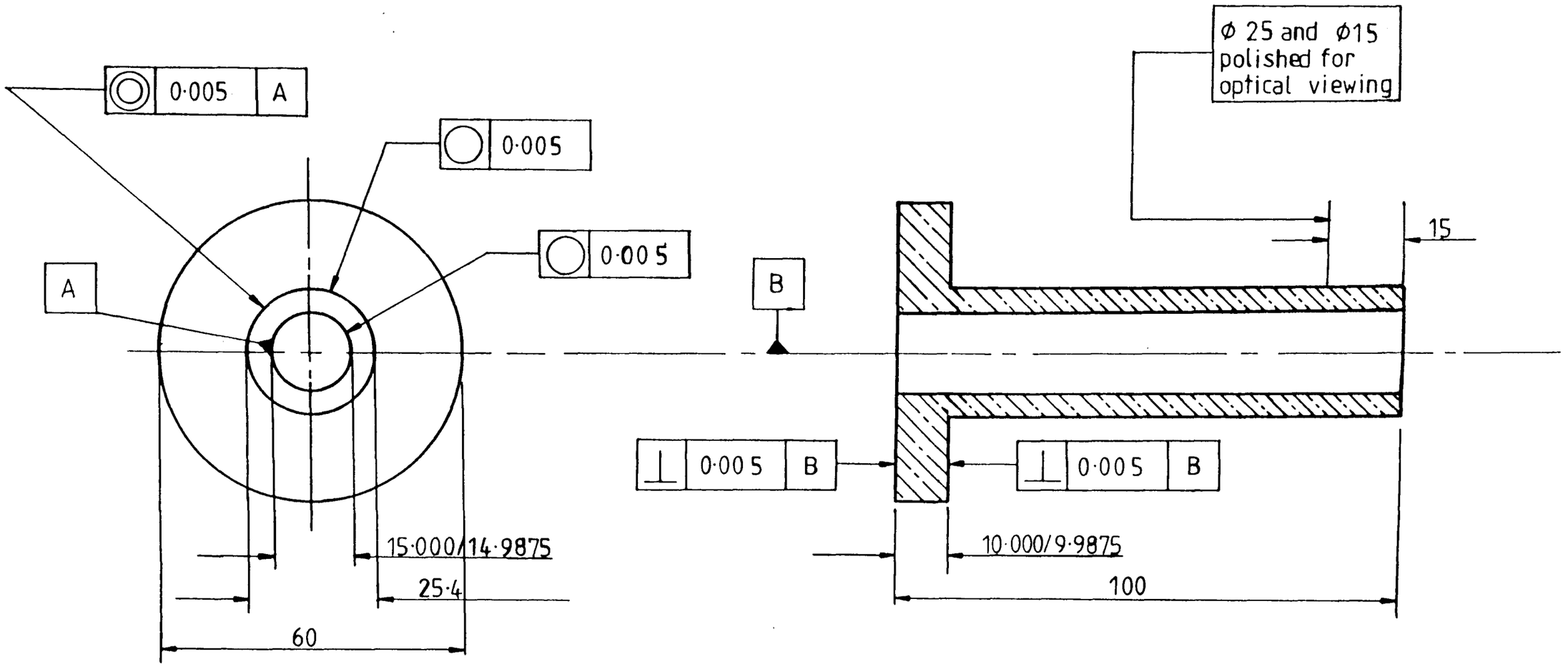

ALL DIMENSIONS IN mm
GEN· TOL : ± 0·1 UNLESS
OTHERWISE STATED

Fig 5.0.3 Quartz shaft

Fig 5.0.4 Bearing shaft

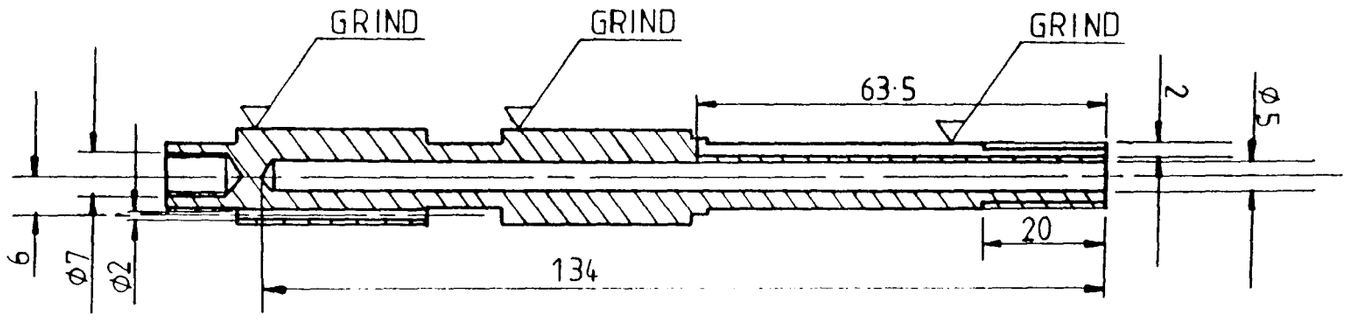

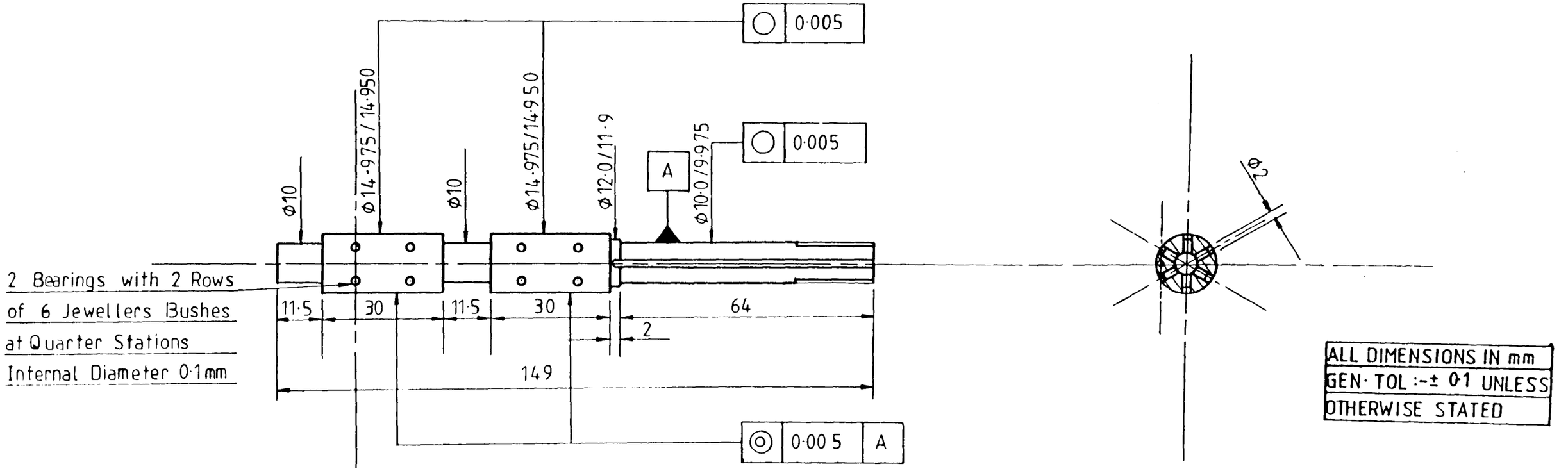

Fig 5.0.5 Test seal (Before Mounting on Shaft)

Seal R Value, Lip Angles and Spring Height

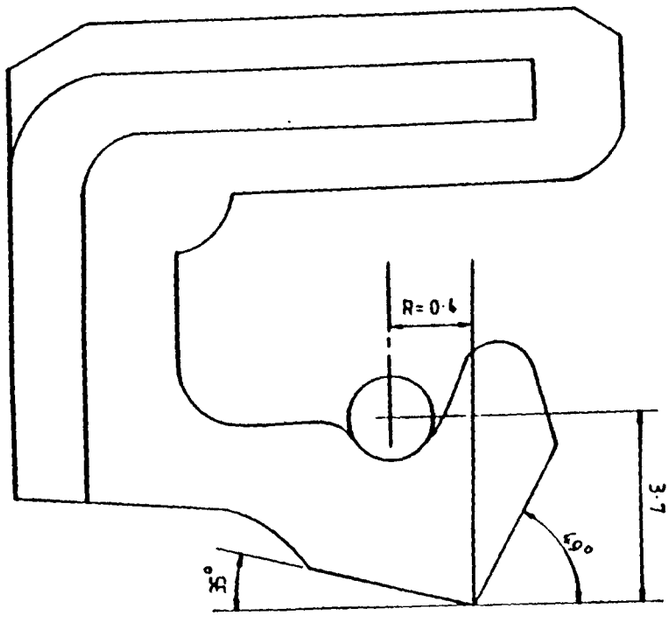

Seal Geometry (X,Y) Coordinate Values in mm

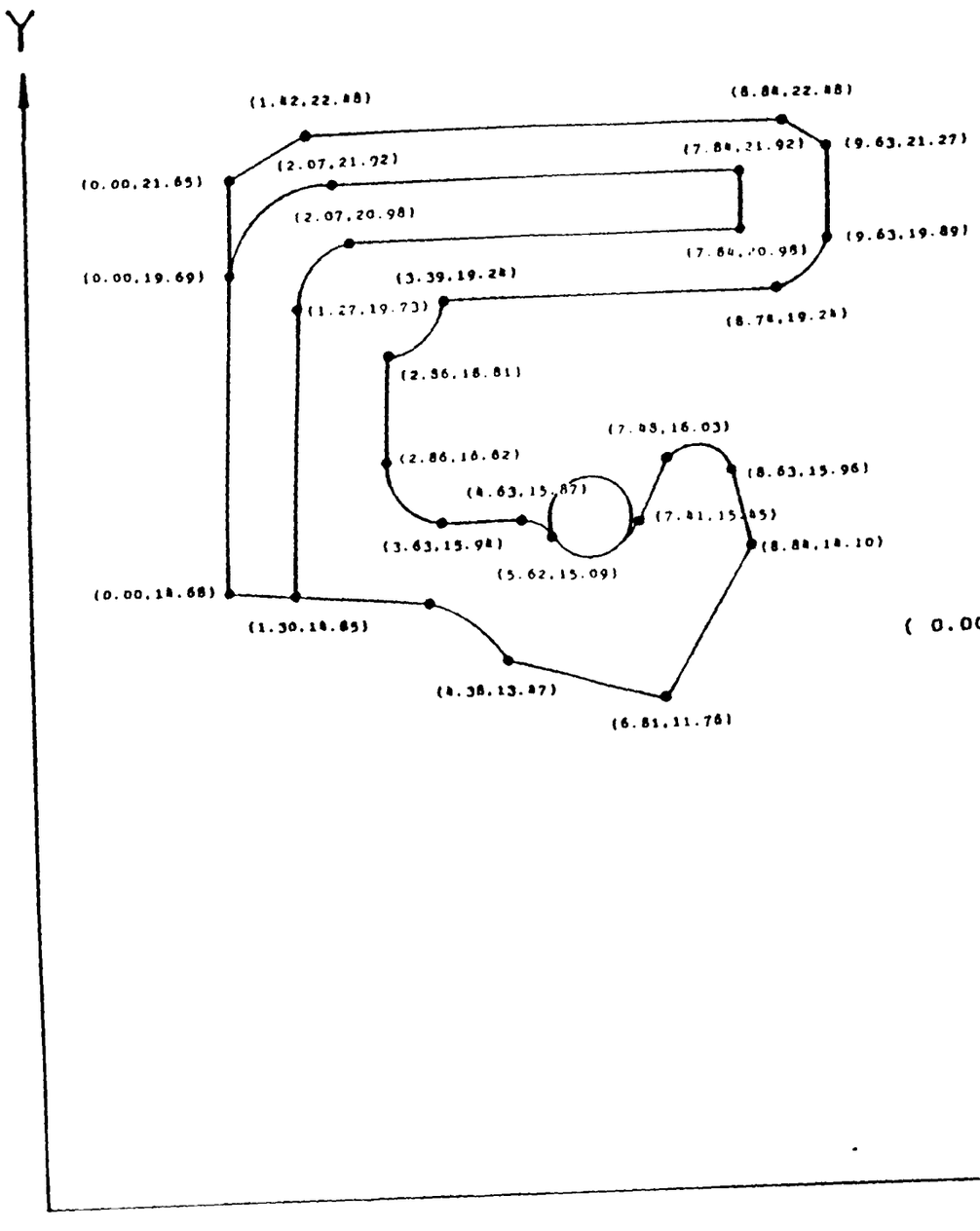

Fig 5.0.6 Test seal housing

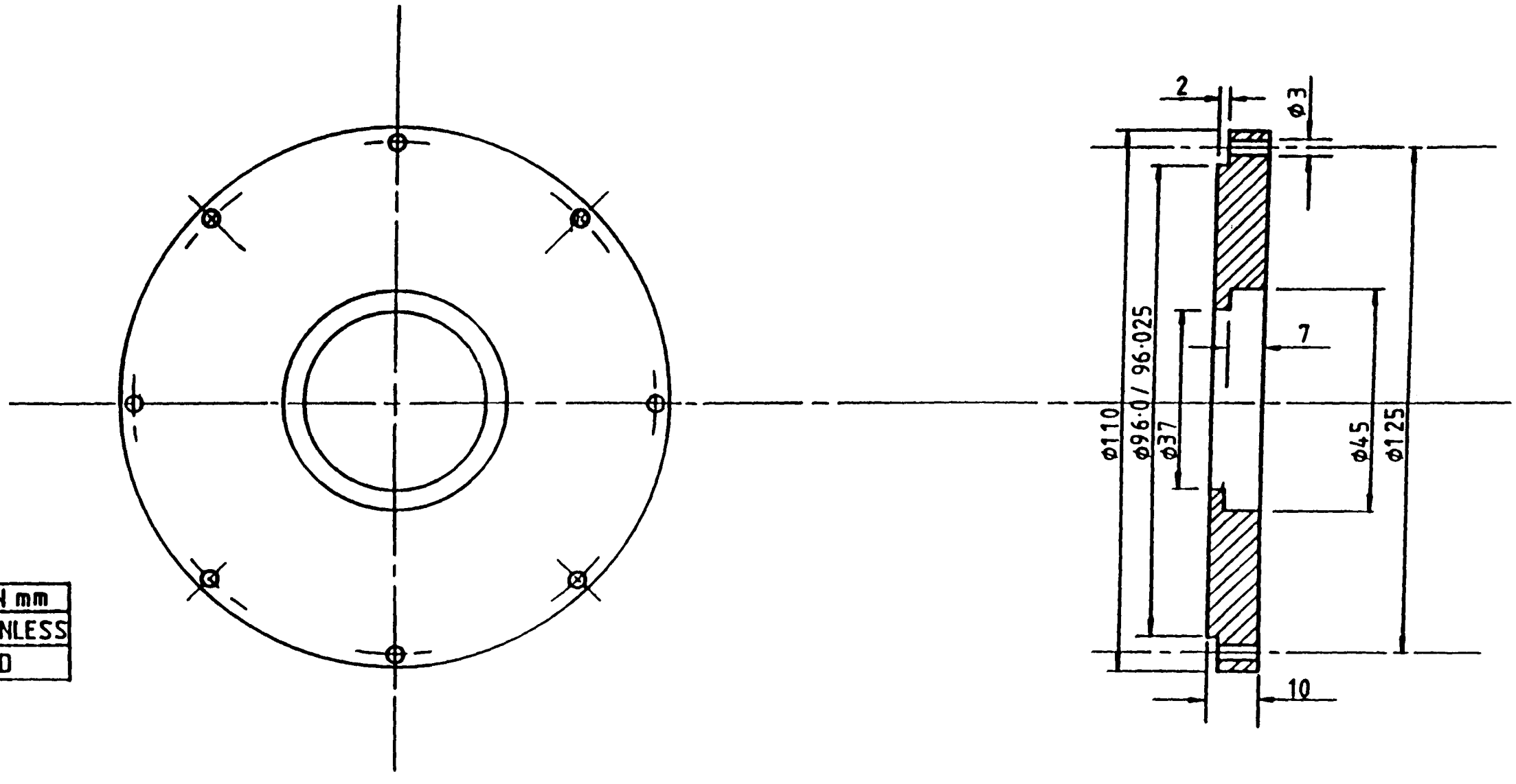

ALL DIMENSIONS IN mm
GEN· TOL :-± 0·1 UNLESS
OTHERWISE STATED

Fig 5.0.7 Oil chamber housing

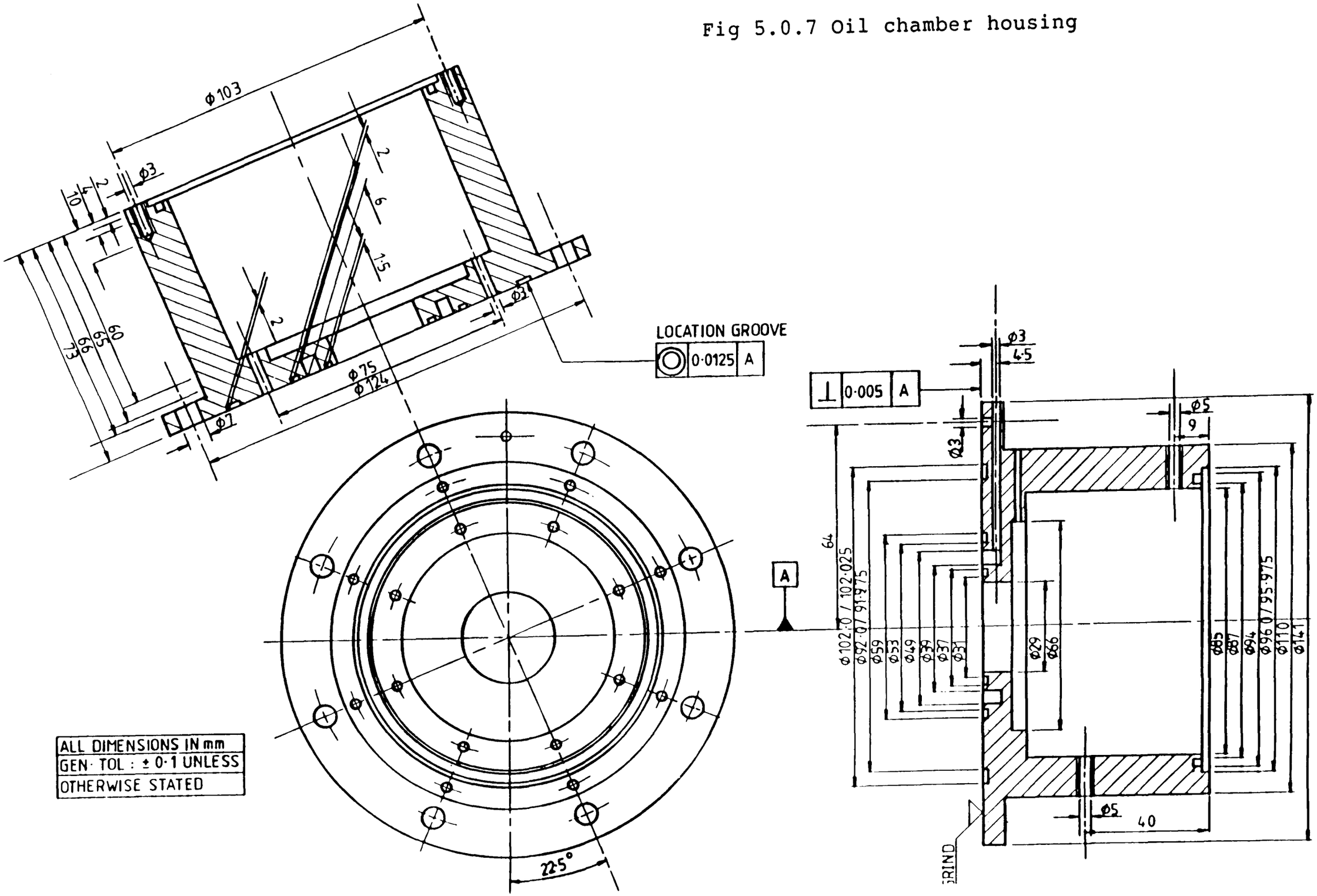

Fig 5.0.8 Oil chamber seal housing

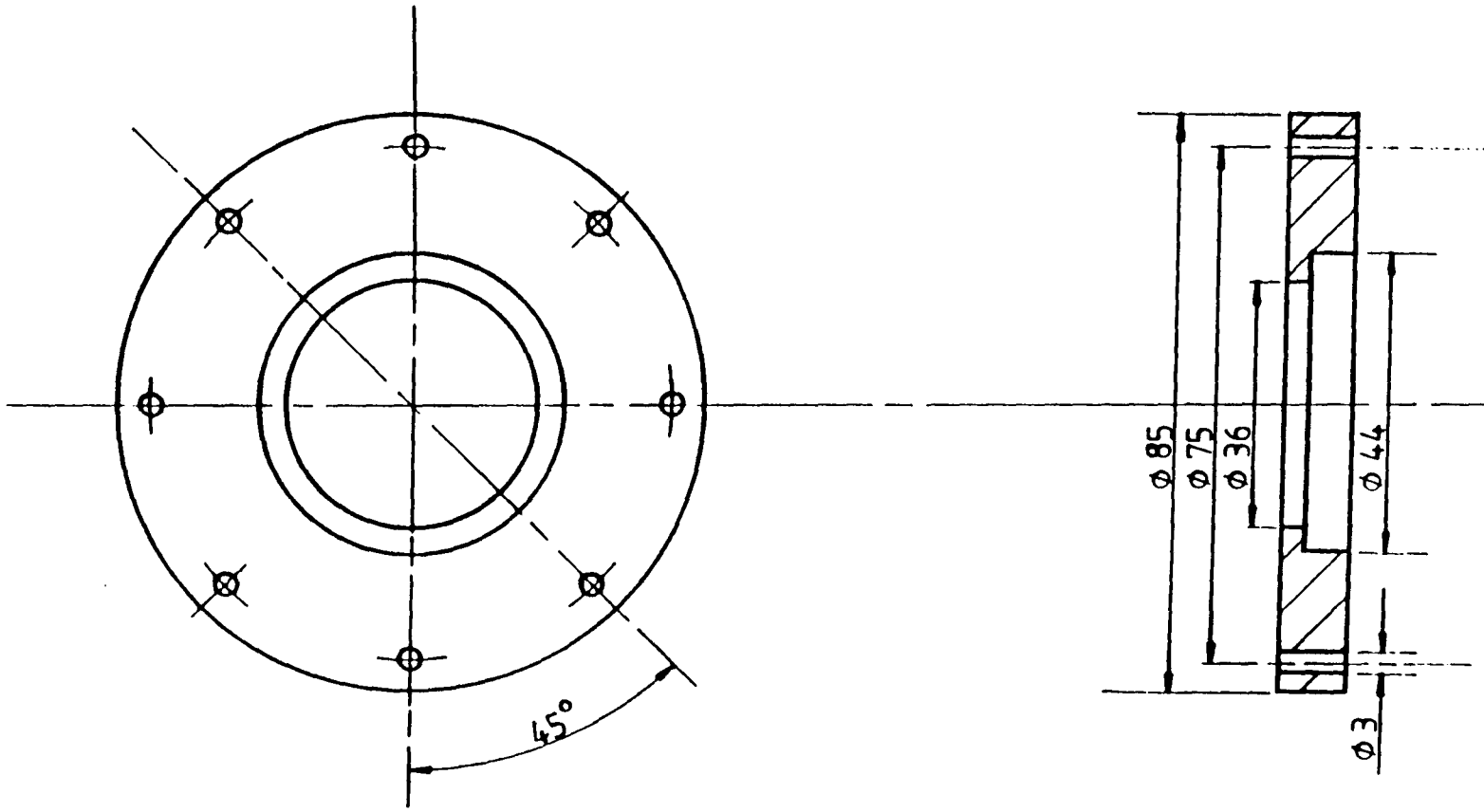

ALL DIMENSIONS IN mm
GEN· TOL : ± 0·1 UNLESS
OTHERWISE STATED

Fig 5.0.9 Bottom thrust plate

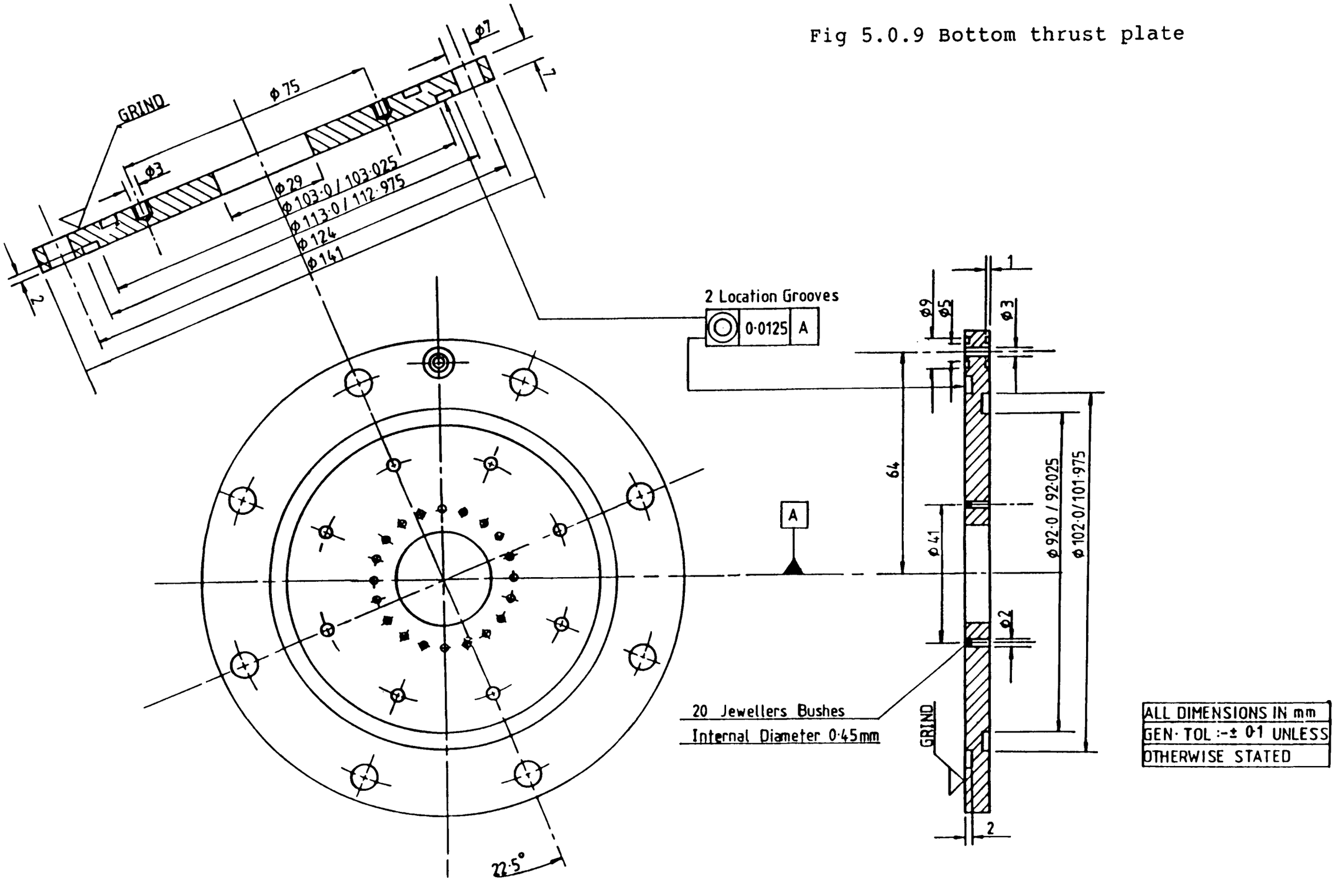

Fig 5.1.0 Spacing ring

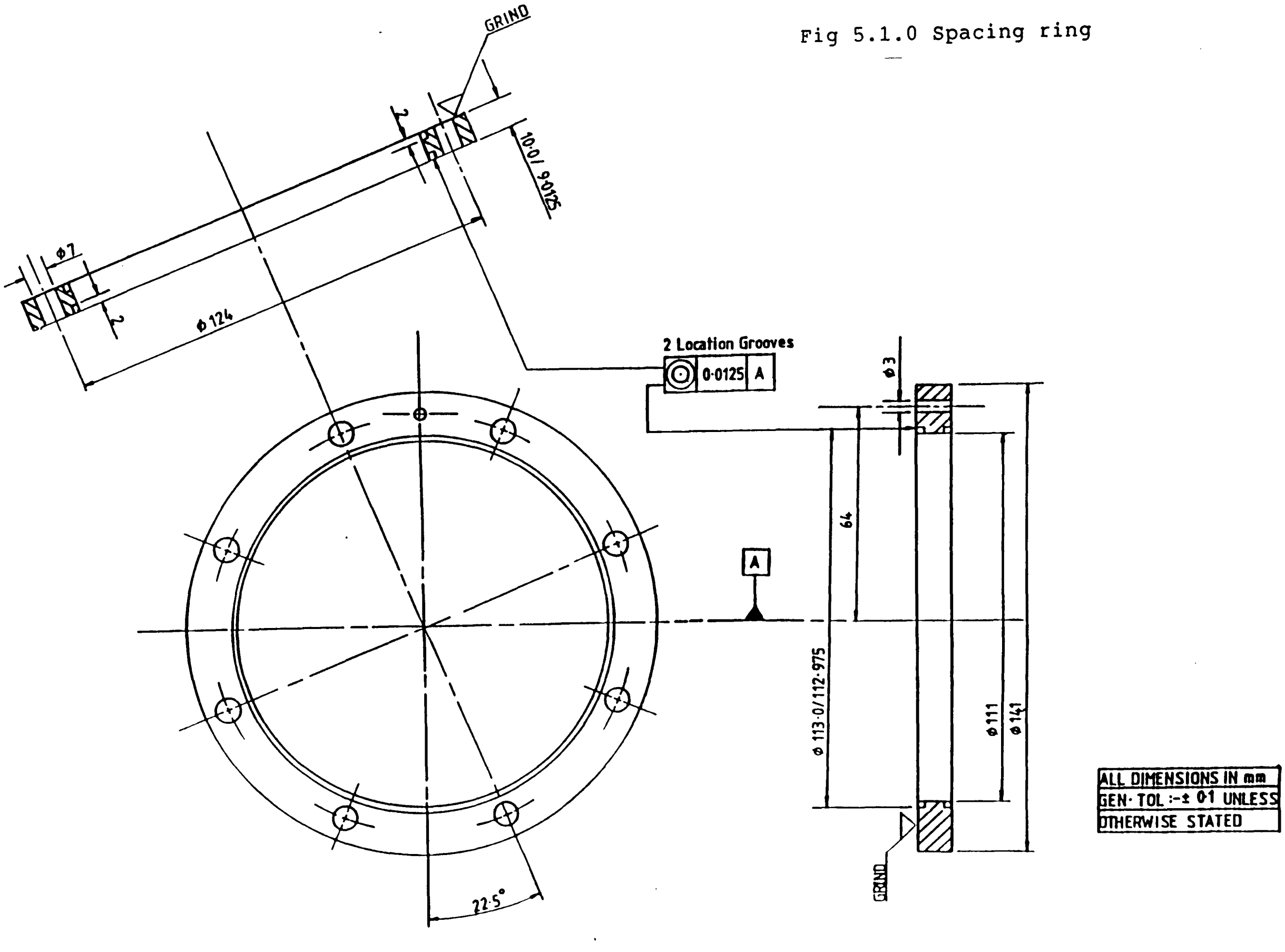

ALL DIMENSIONS IN mm
GEN· TOL :-± 01 UNLESS
OTHERWISE STATED

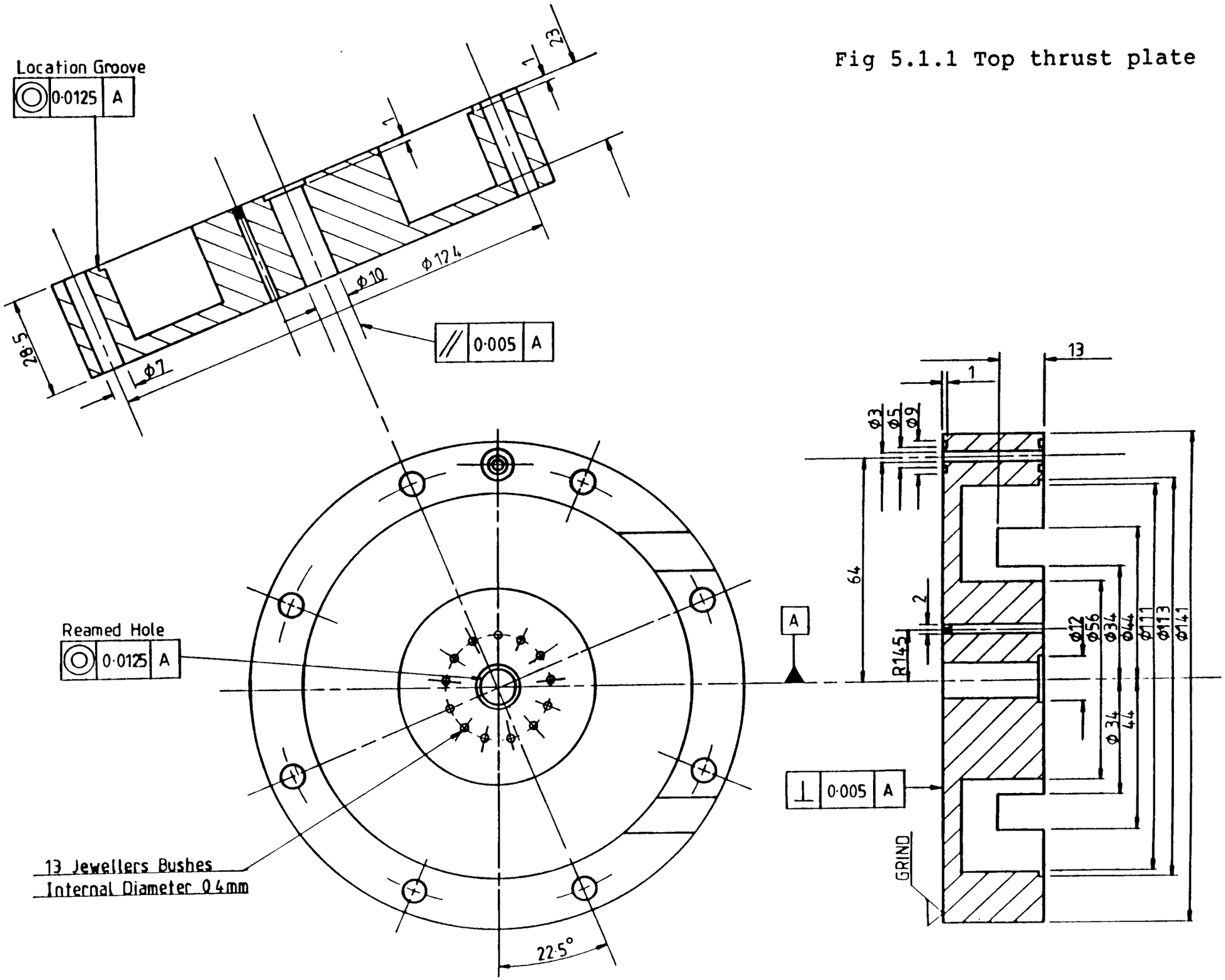

Fig 5.1.1 Top thrust plate

Fig 5.1.2 Rotary shaft seal rig assembley

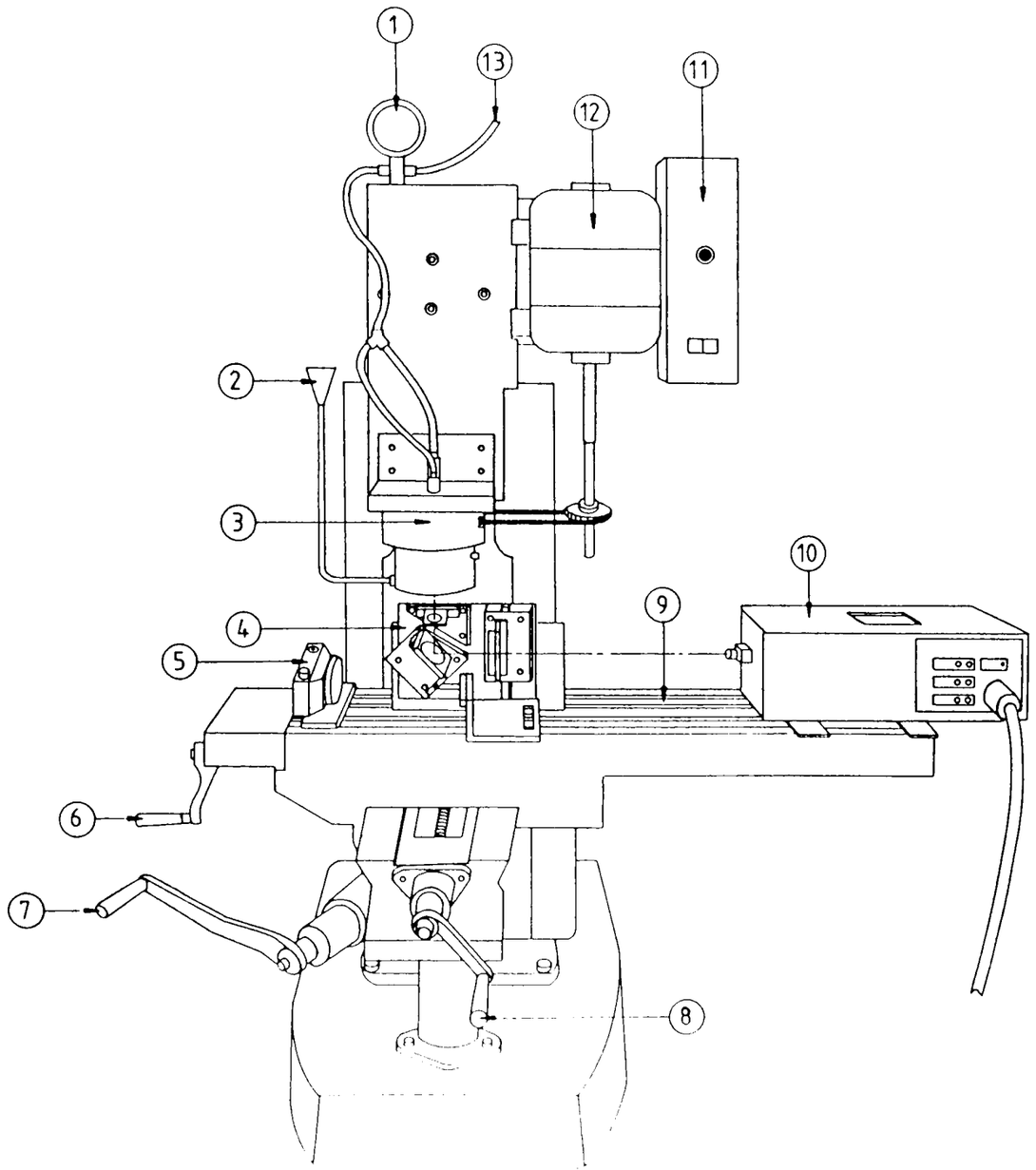

NUMBER	DRAWING DETAIL	FIGURE NUMBER
1	PRESSURE GAUGE	
2	OIL CHAMBER FILLING FUNNEL	
3	SHAFT BEARINGS & DRIVE MECHANISM	5.0.0
4	OPTICAL ASSEMBLEY	4.0.9
5	CAMERA	
6	X-DIRECTIONAL AJUSTMENT	
7	Z-DIRECTIONAL AJUSTMENT	
8	Y-DIRECTIONAL AJUSTMENT	
9	T-SLOT BED PLATE	
10	ARGON ION MULTILINE LASER	
11	ELECTRIC MOTOR VARIABLE SPEED CONTROLLER	
12	ELECTRIC MOTOR	
13	AIR PRESSURE INLET	

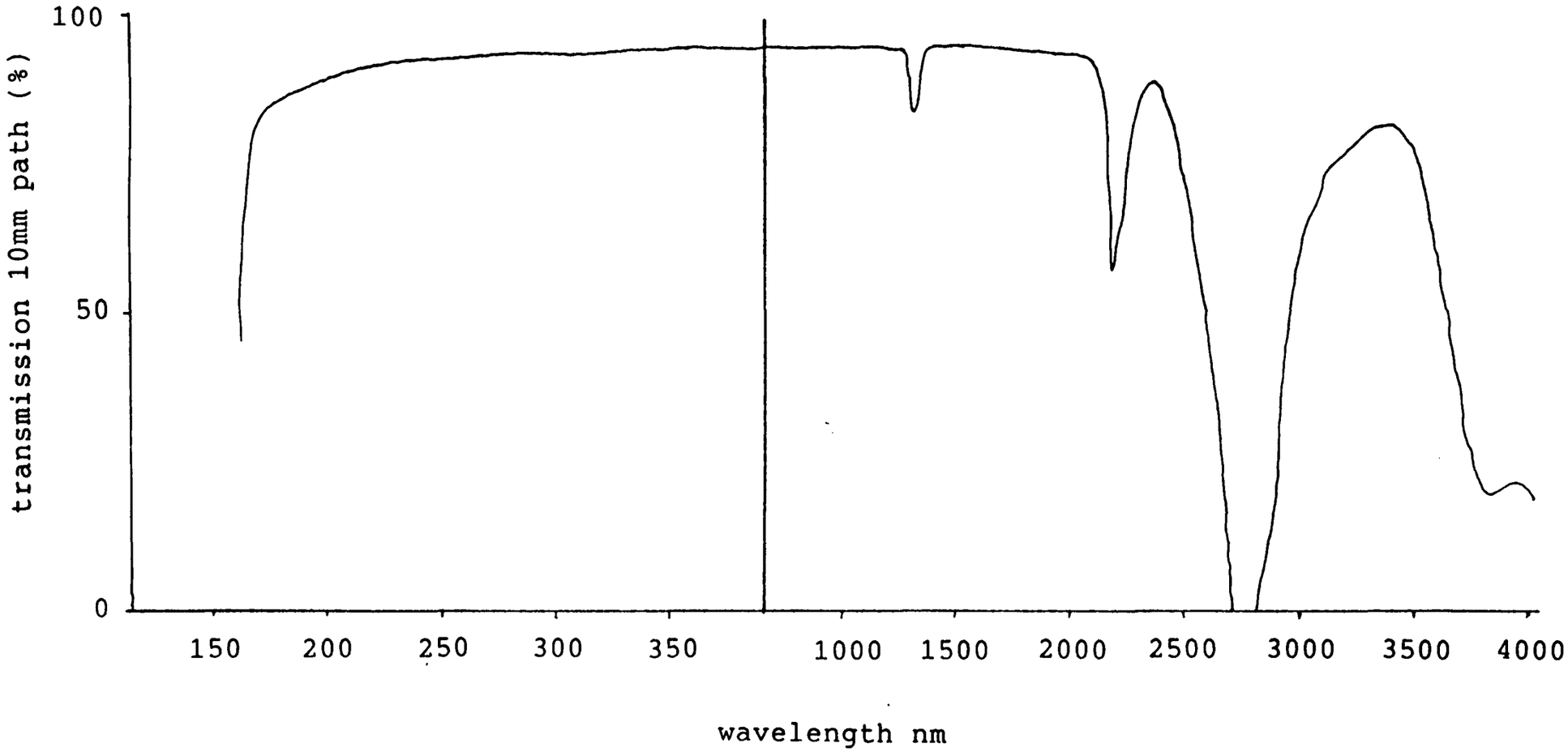

Fig 5.1.3 Spectral transmission of quartz

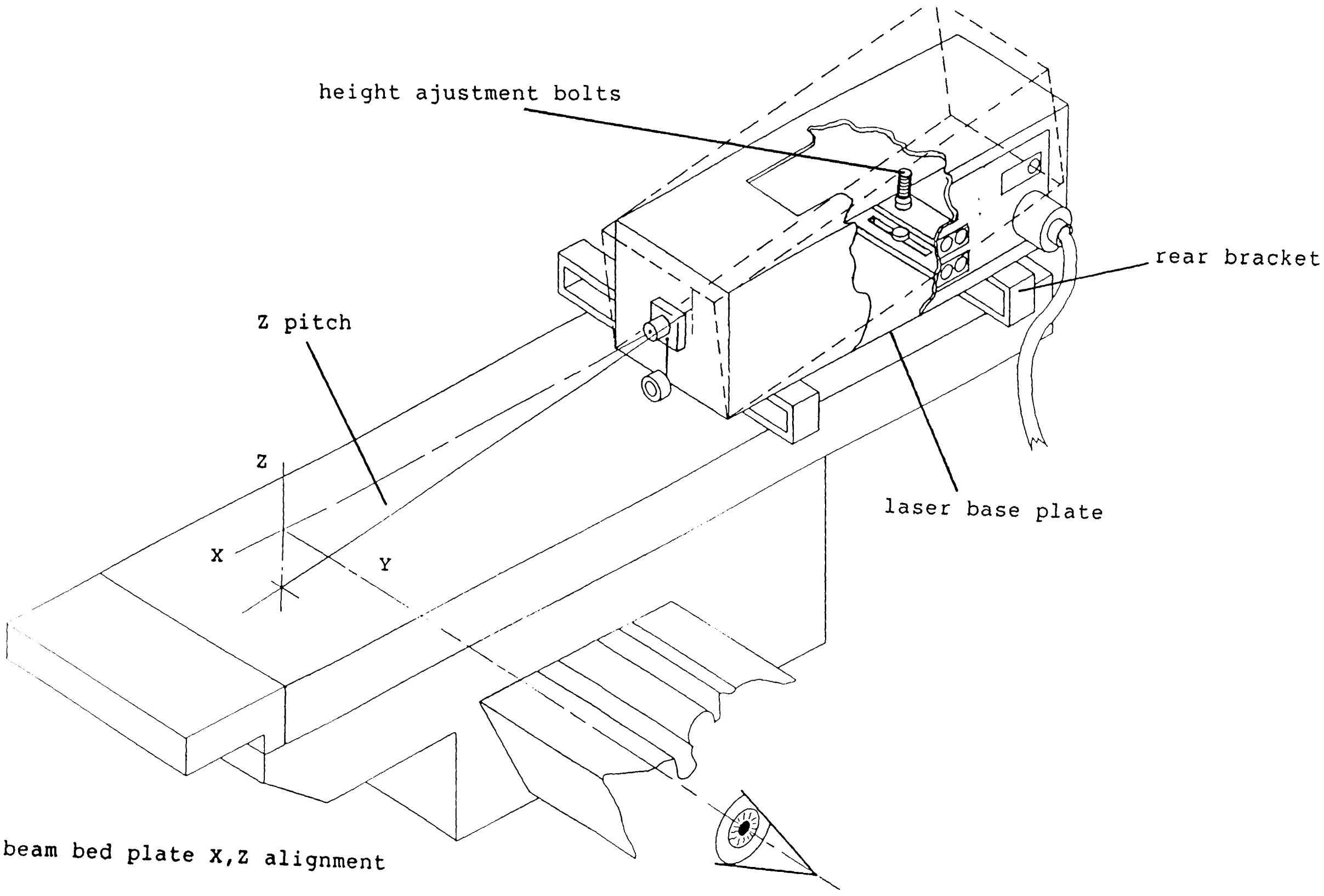

Fig 6.0.0 Laser beam bed plate X,Z alignment

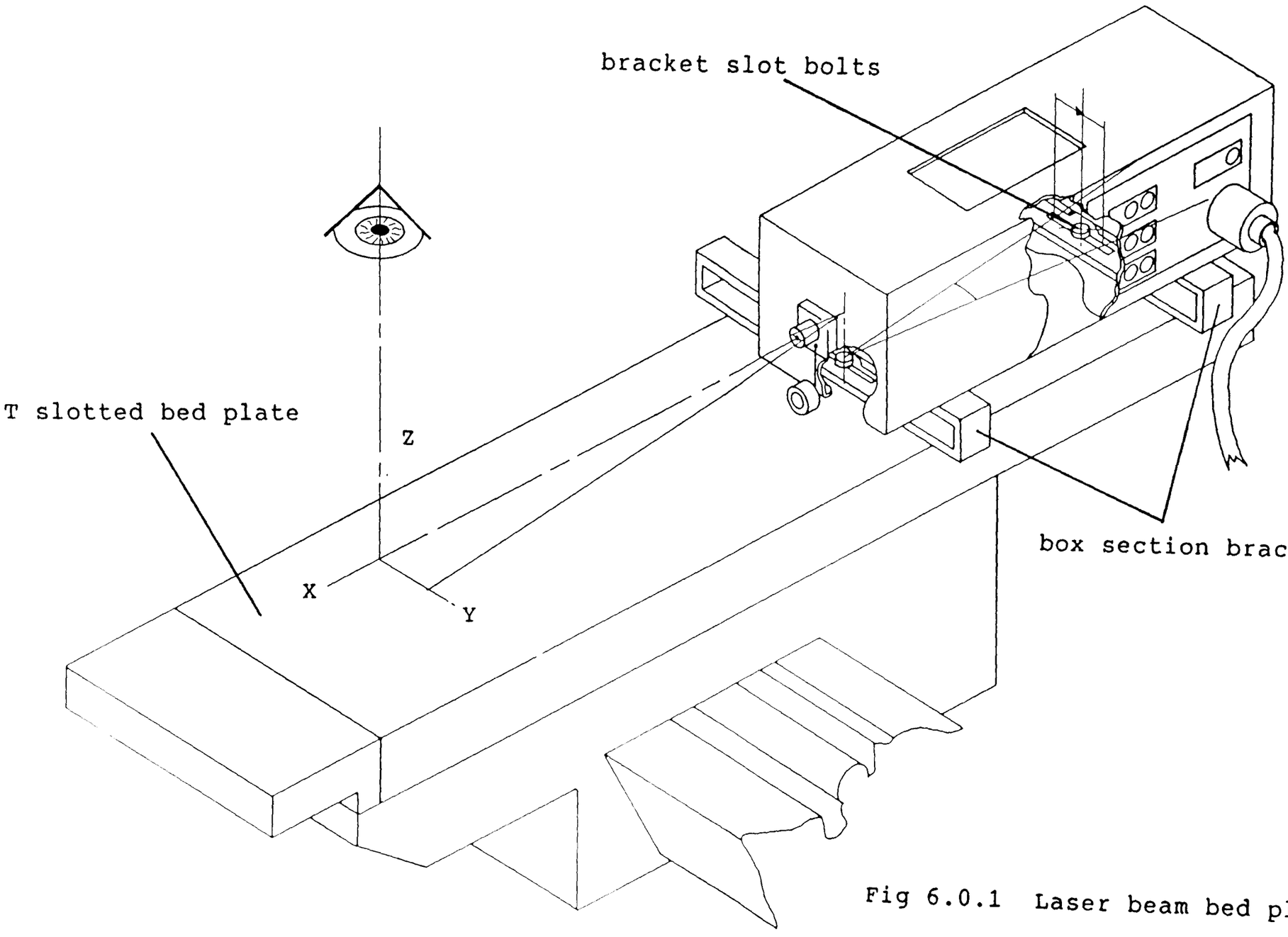

Fig 6.0.1 Laser beam bed plate X,Y alignment

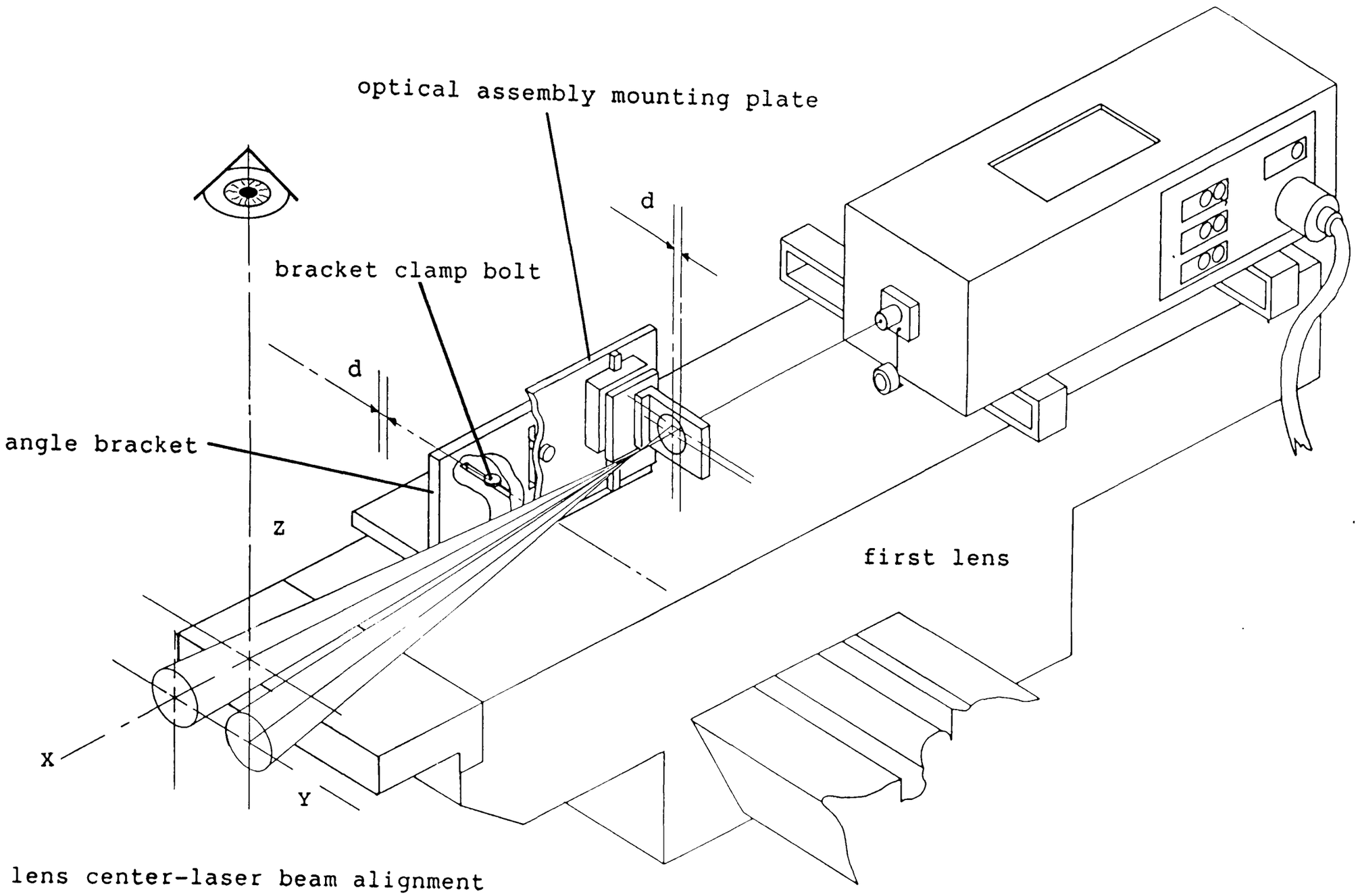

Fig 6.0.2 First lens center-laser beam alignment

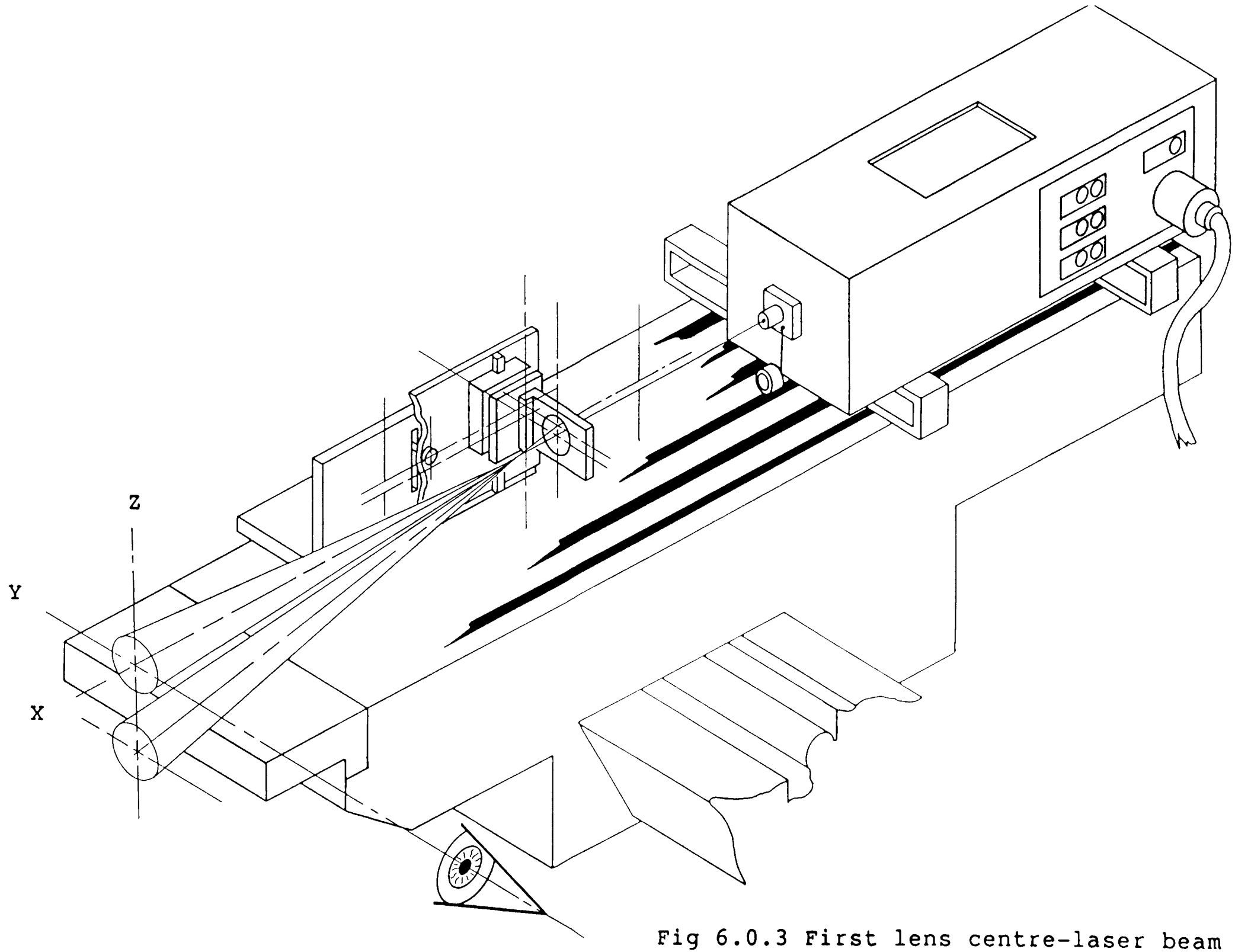

Fig 6.0.3 First lens centre-laser beam alignment

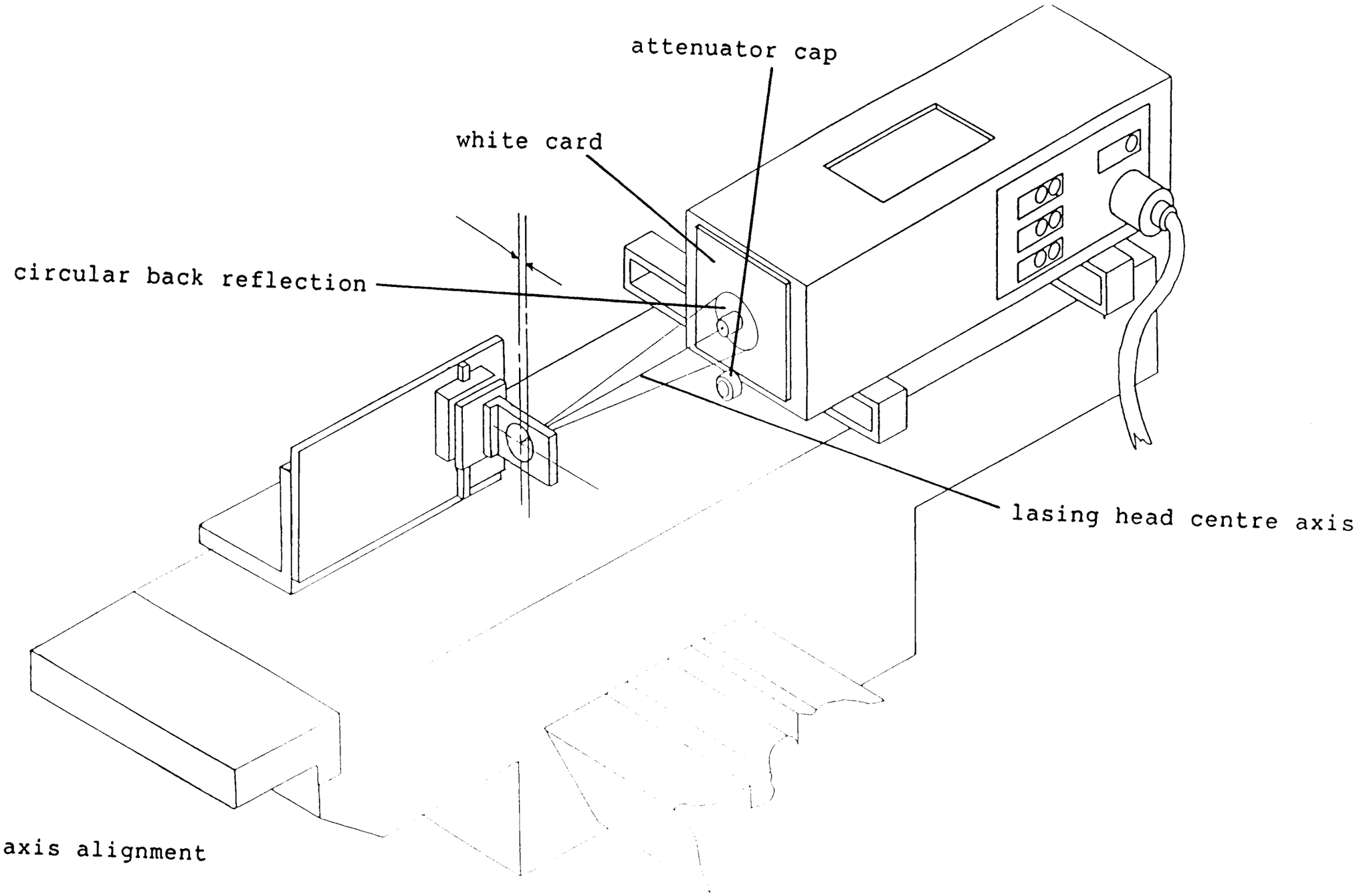

Fig 6.0.4 First lens axis alignment

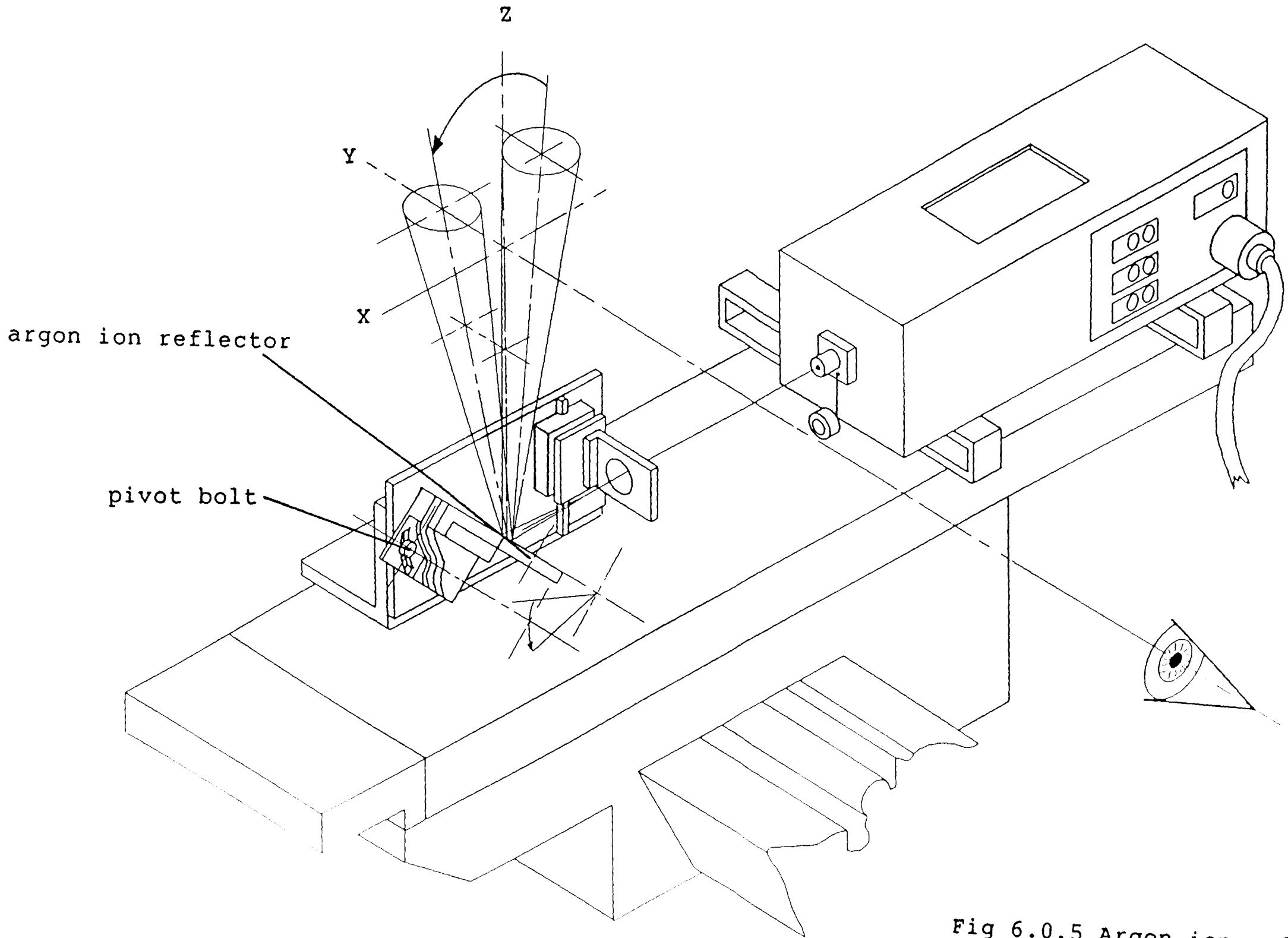

Fig 6.0.5 Argon ion reflector alignment

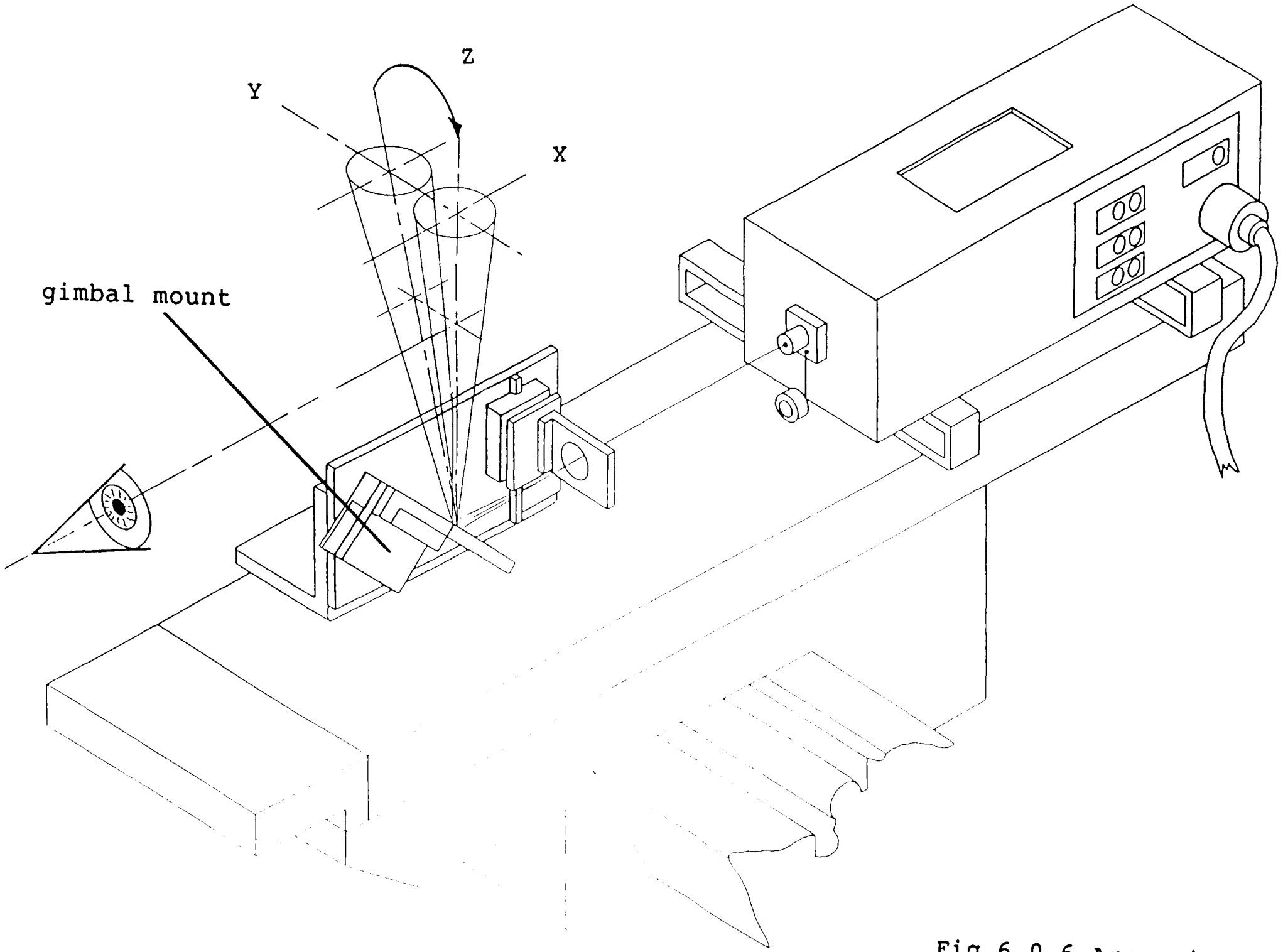

Fig 6.0.6 Argon ion reflector alignment

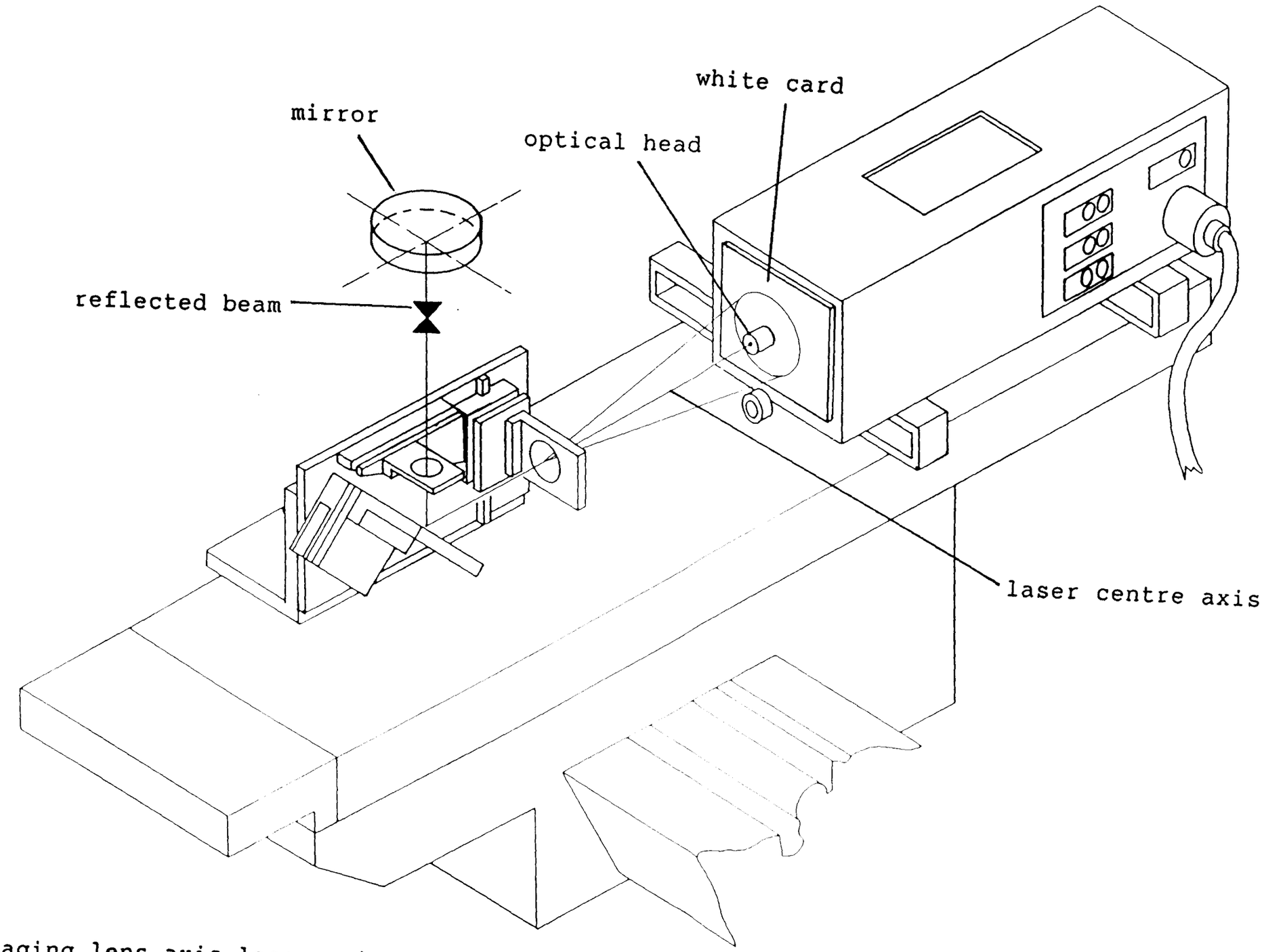

Fig 6.0.7 Second imaging lens axis-laser axis alignment

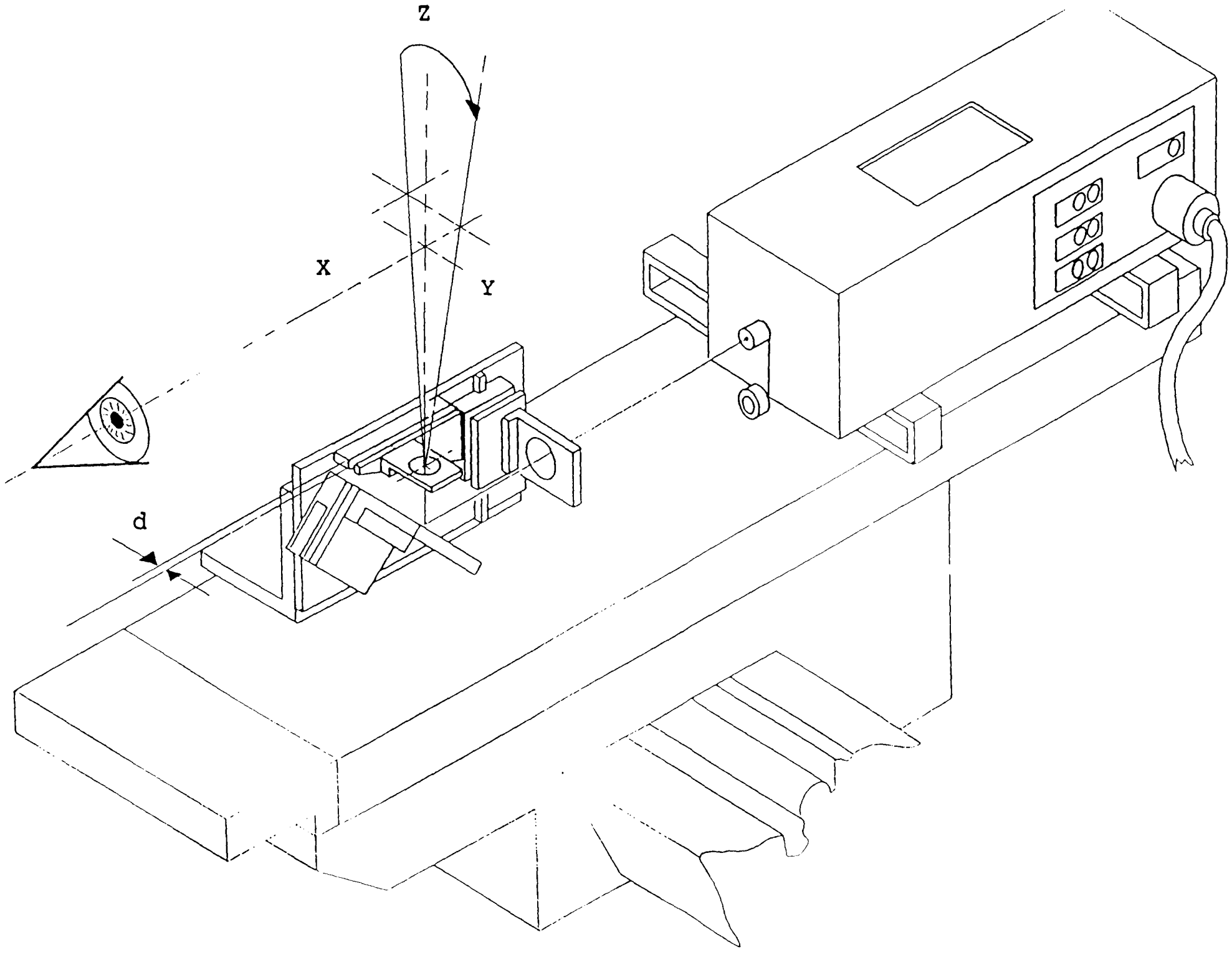

Fig 6.0.8 Second imaging lens centre-laser axis alignment

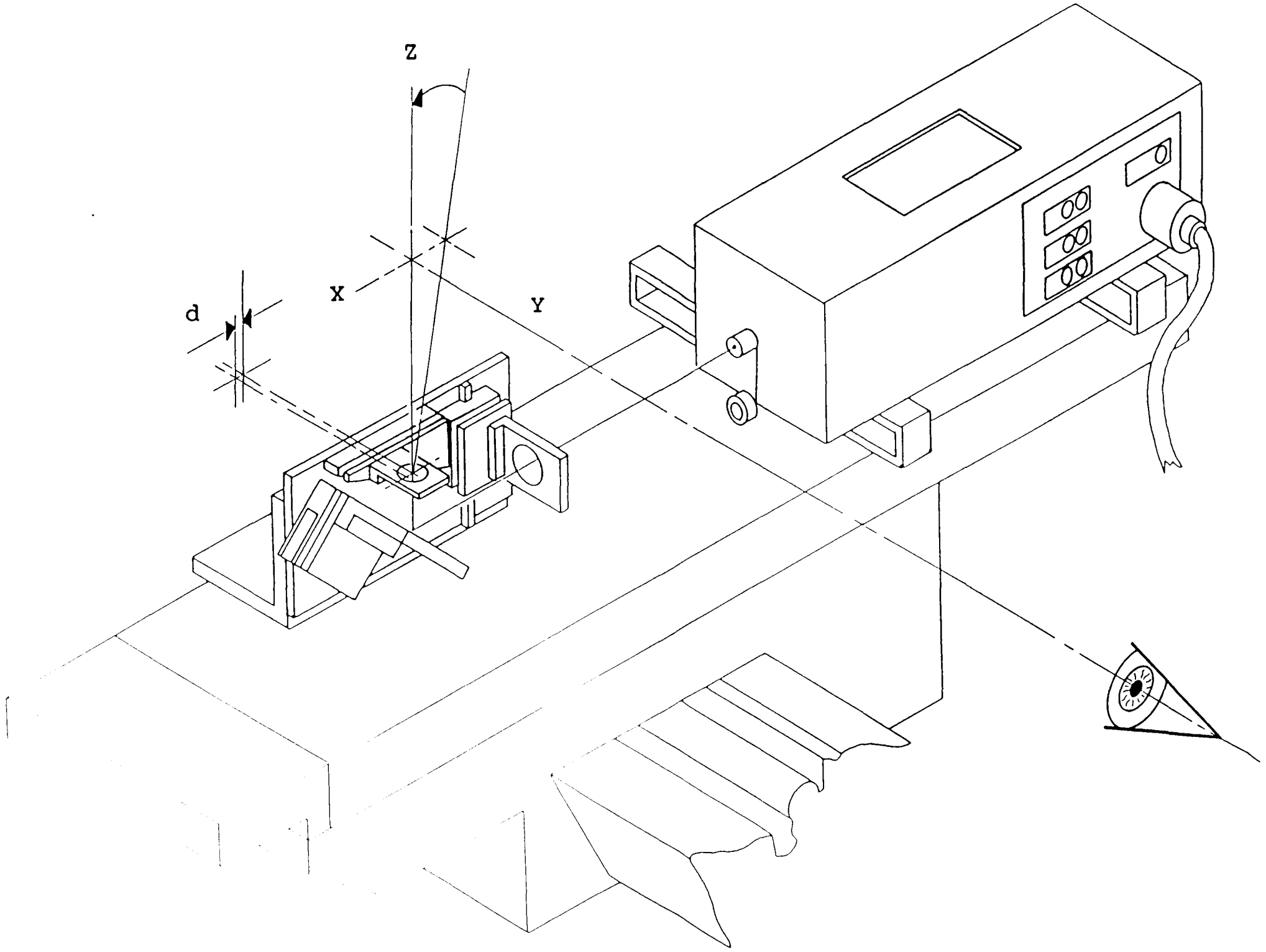

Fig 6.0.9 Second imaging lens centre-laser axis alignment

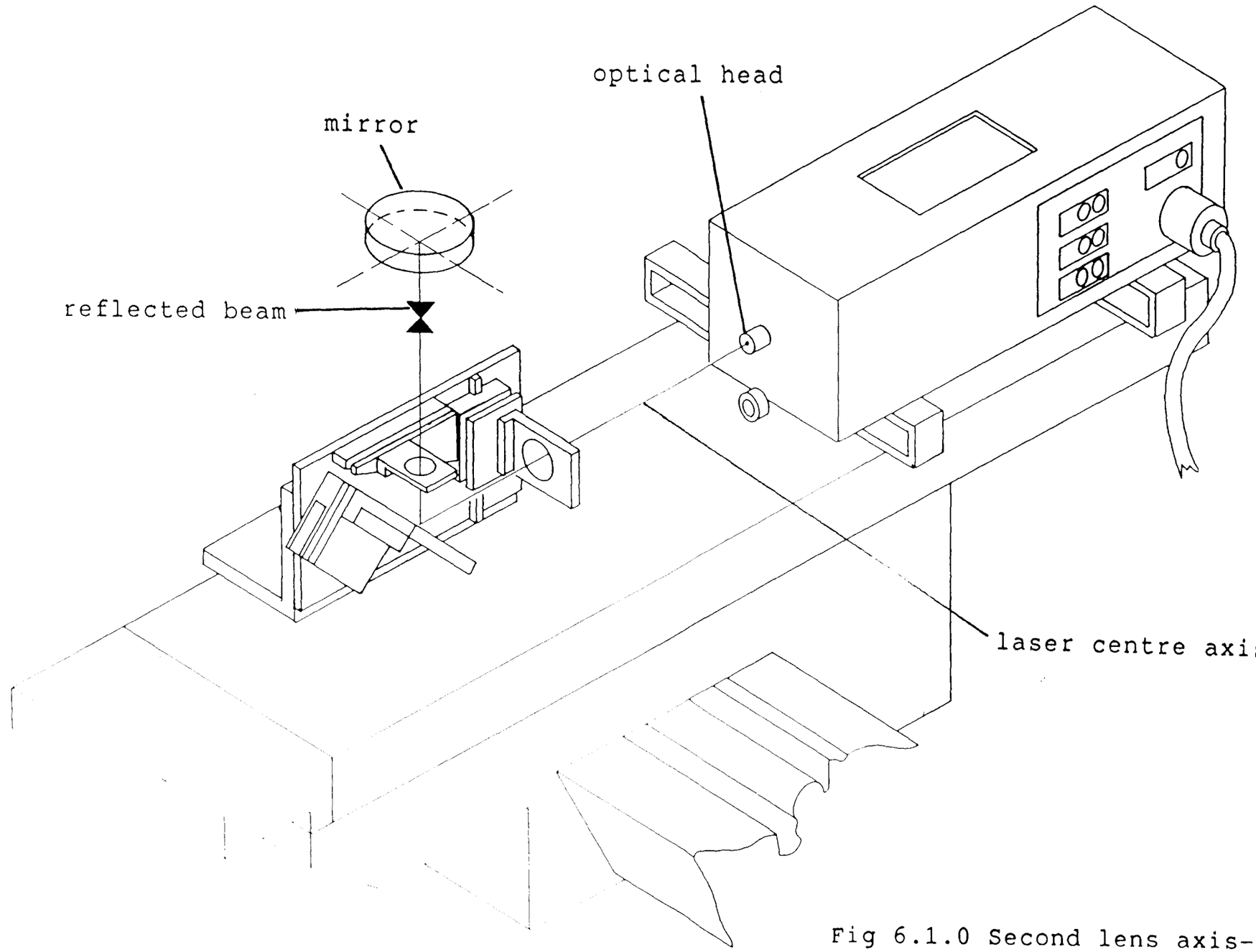

Fig 6.1.0 Second lens axis-laser axis alignment

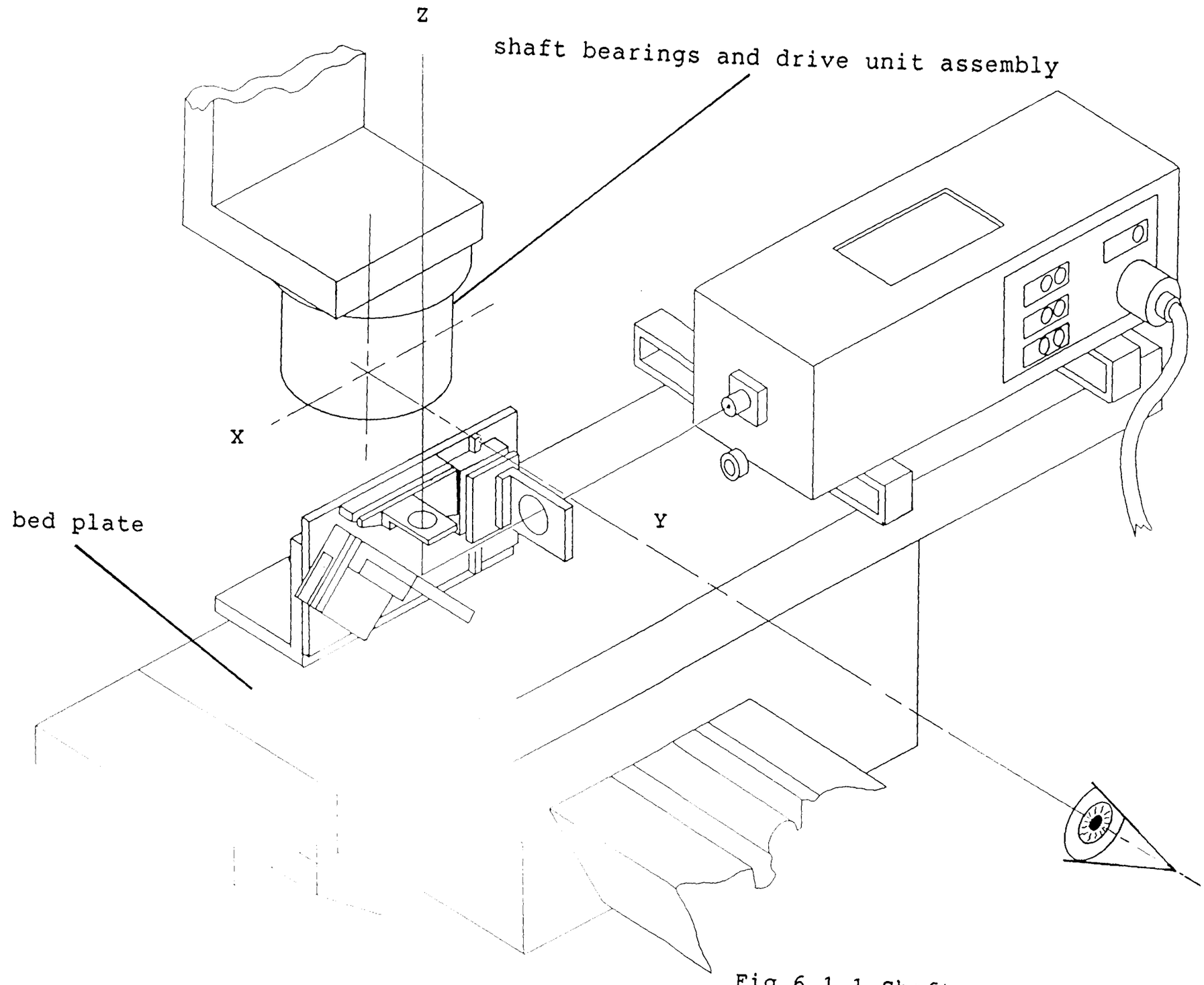

Fig 6.1.1 Shaft axis-laser beam axis alignment

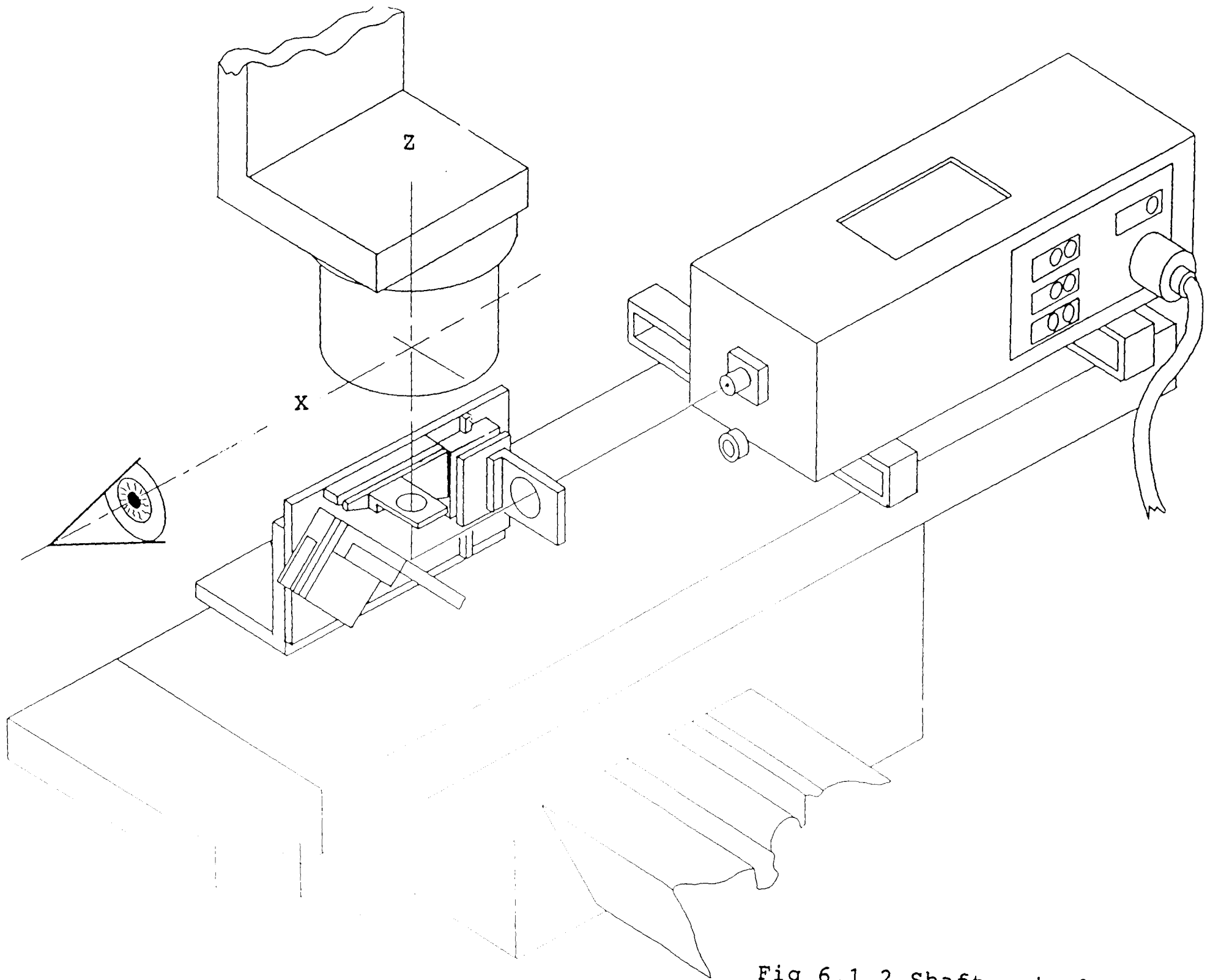

Fig 6.1.2 Shaft axis-laser beam axis alignment

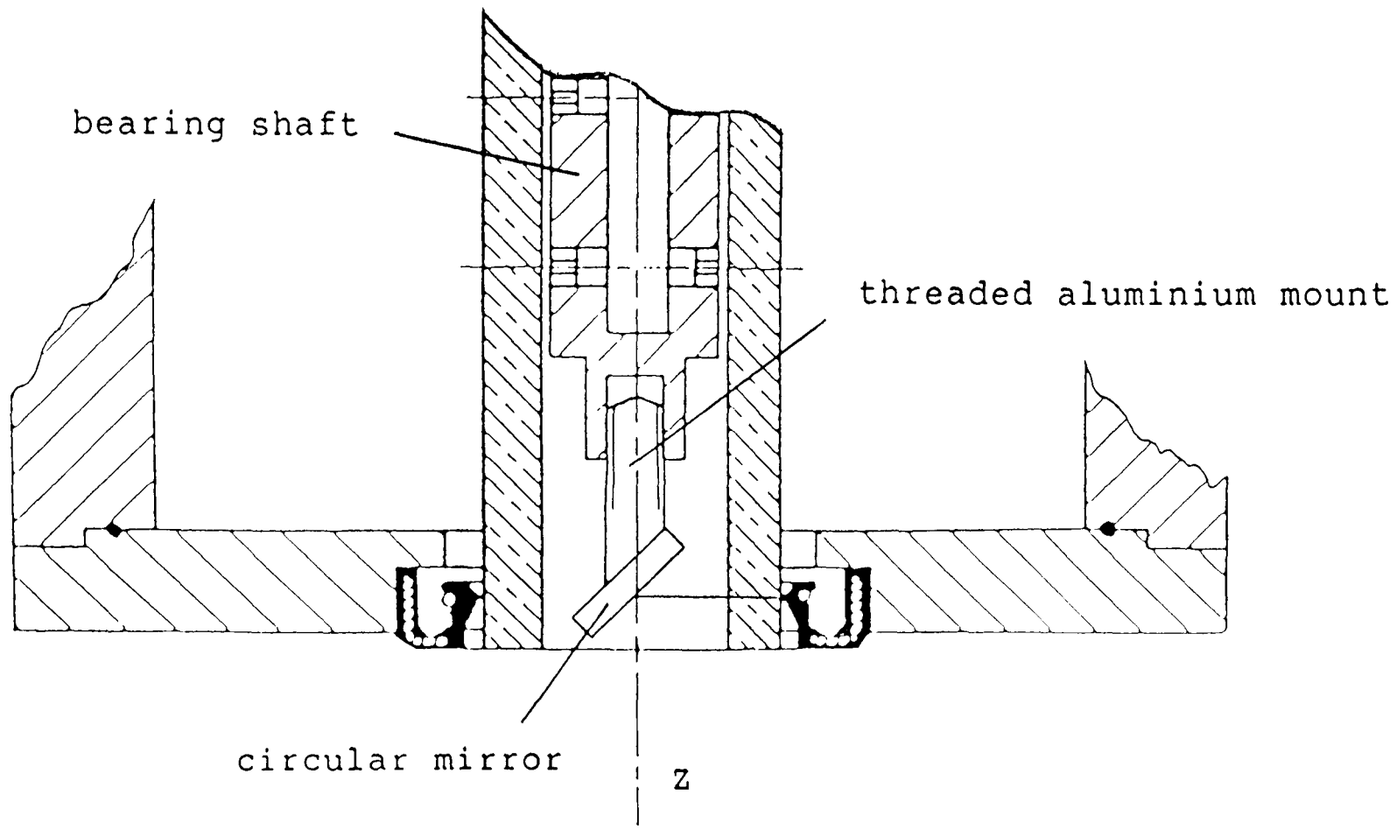

Fig 7.0.0 Laser beam localised contact alignment

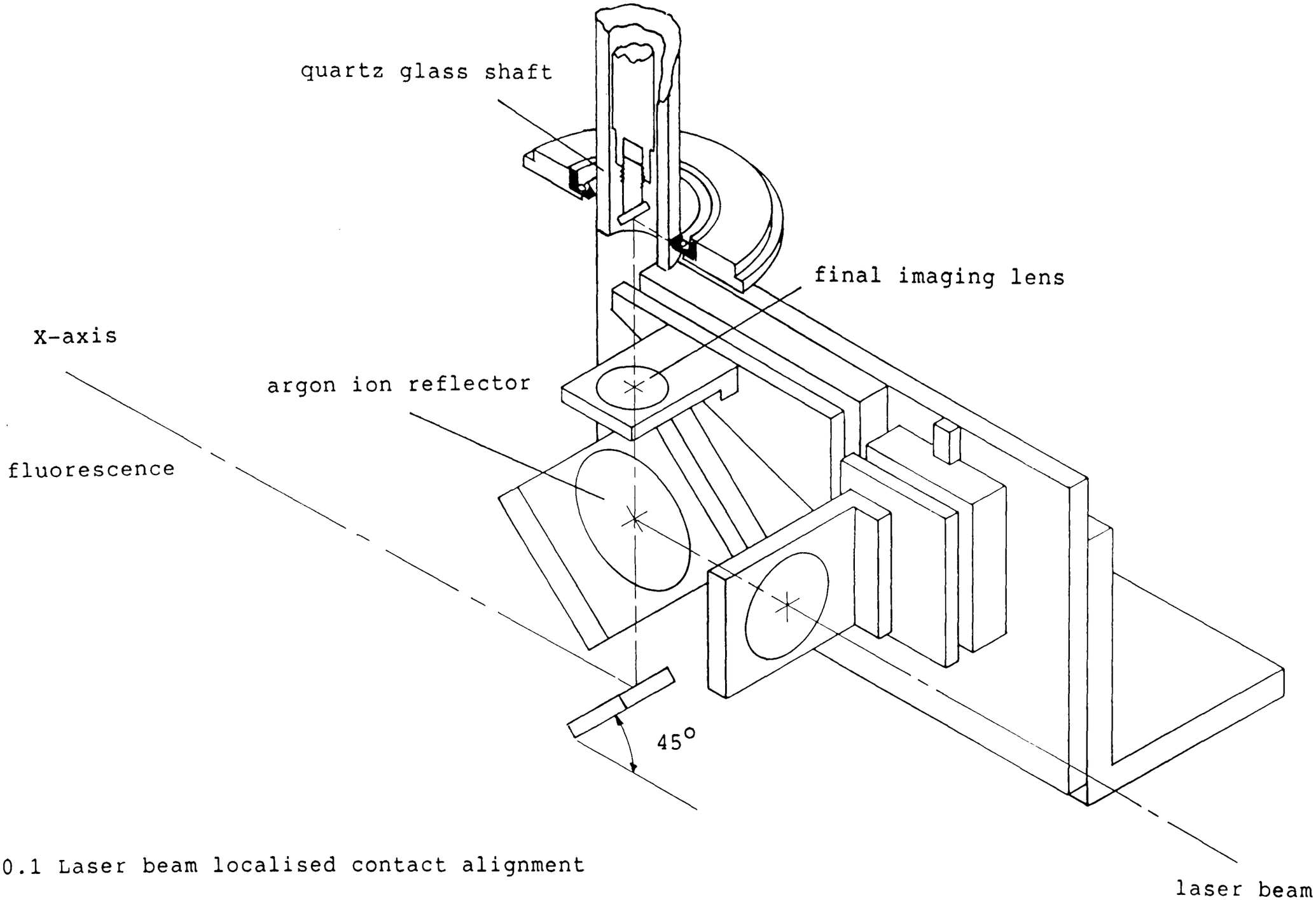

Fig 7.0.1 Laser beam localised contact alignment

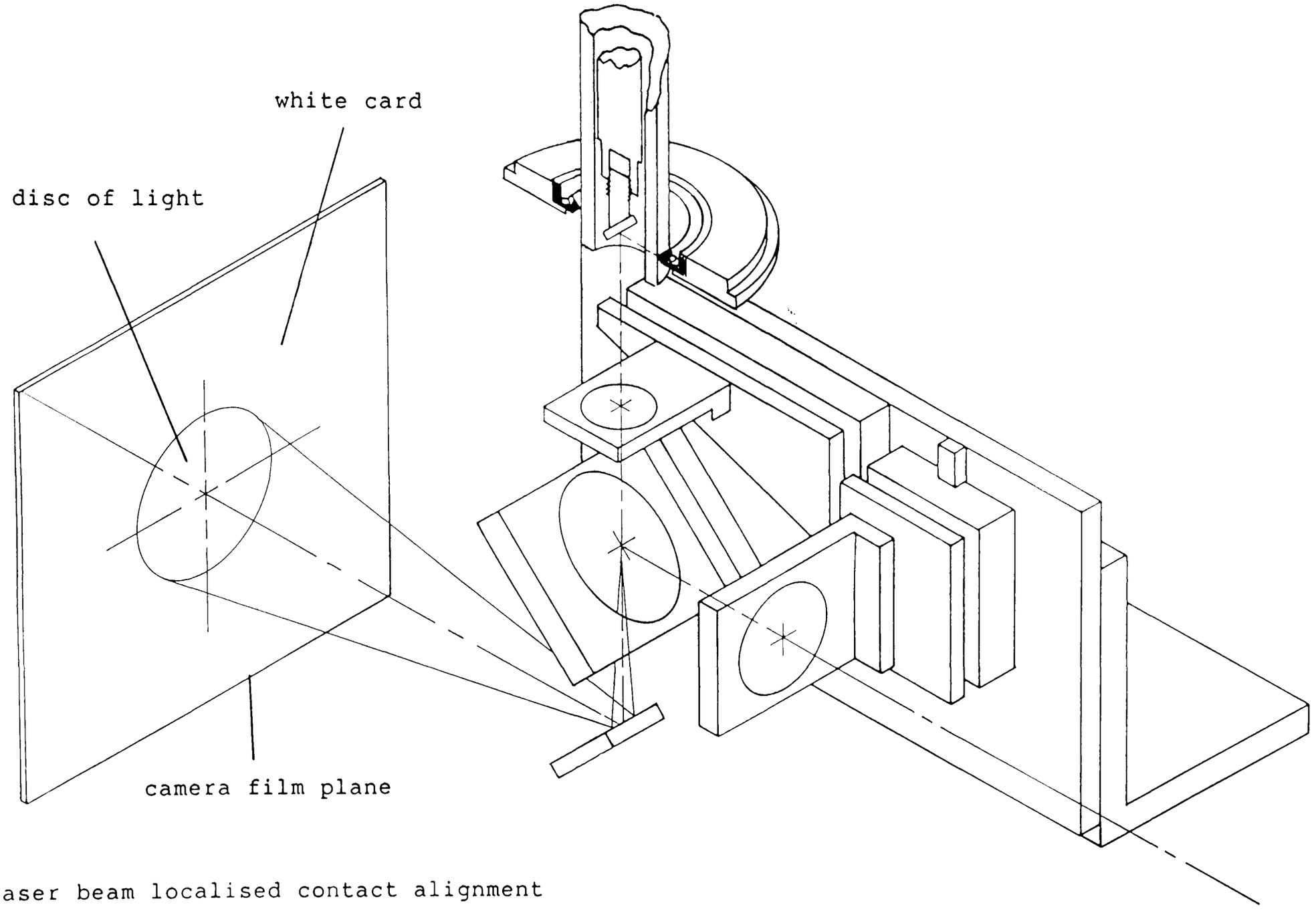

Fig 7.0.2 Laser beam localised contact alignment

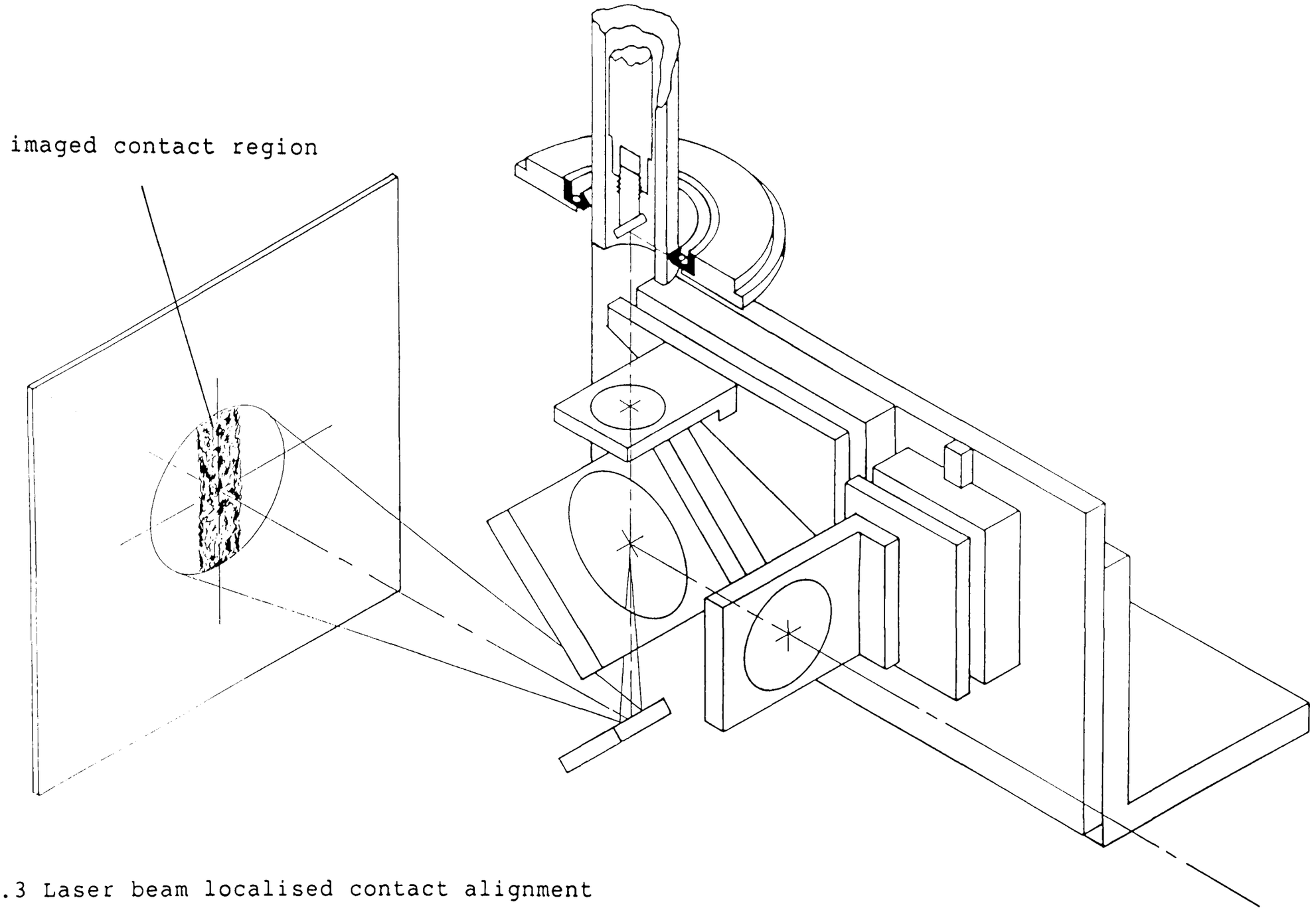

Fig 7.0.3 Laser beam localised contact alignment

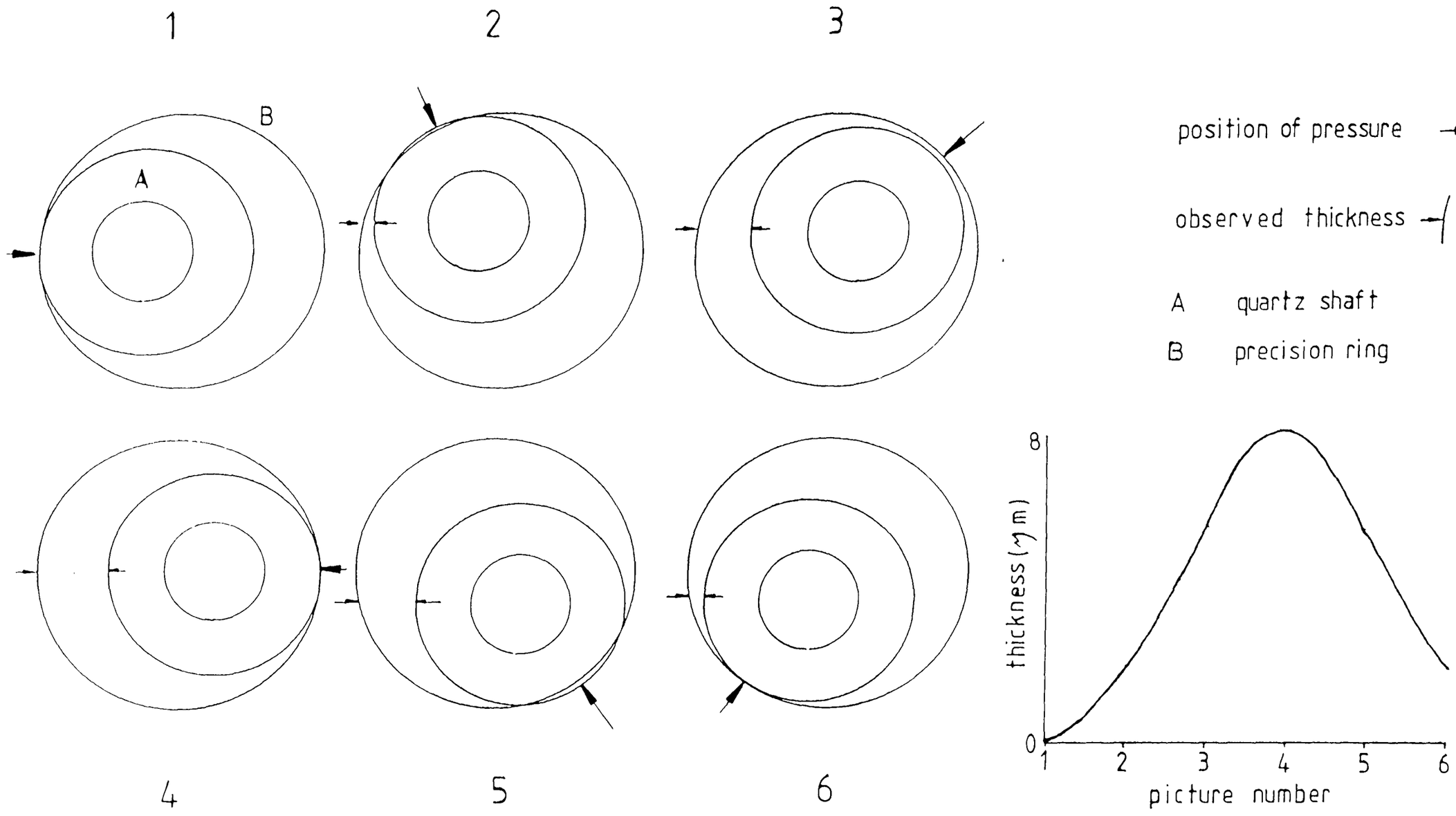

Fig 7.0.5 localised contact calibration procedure

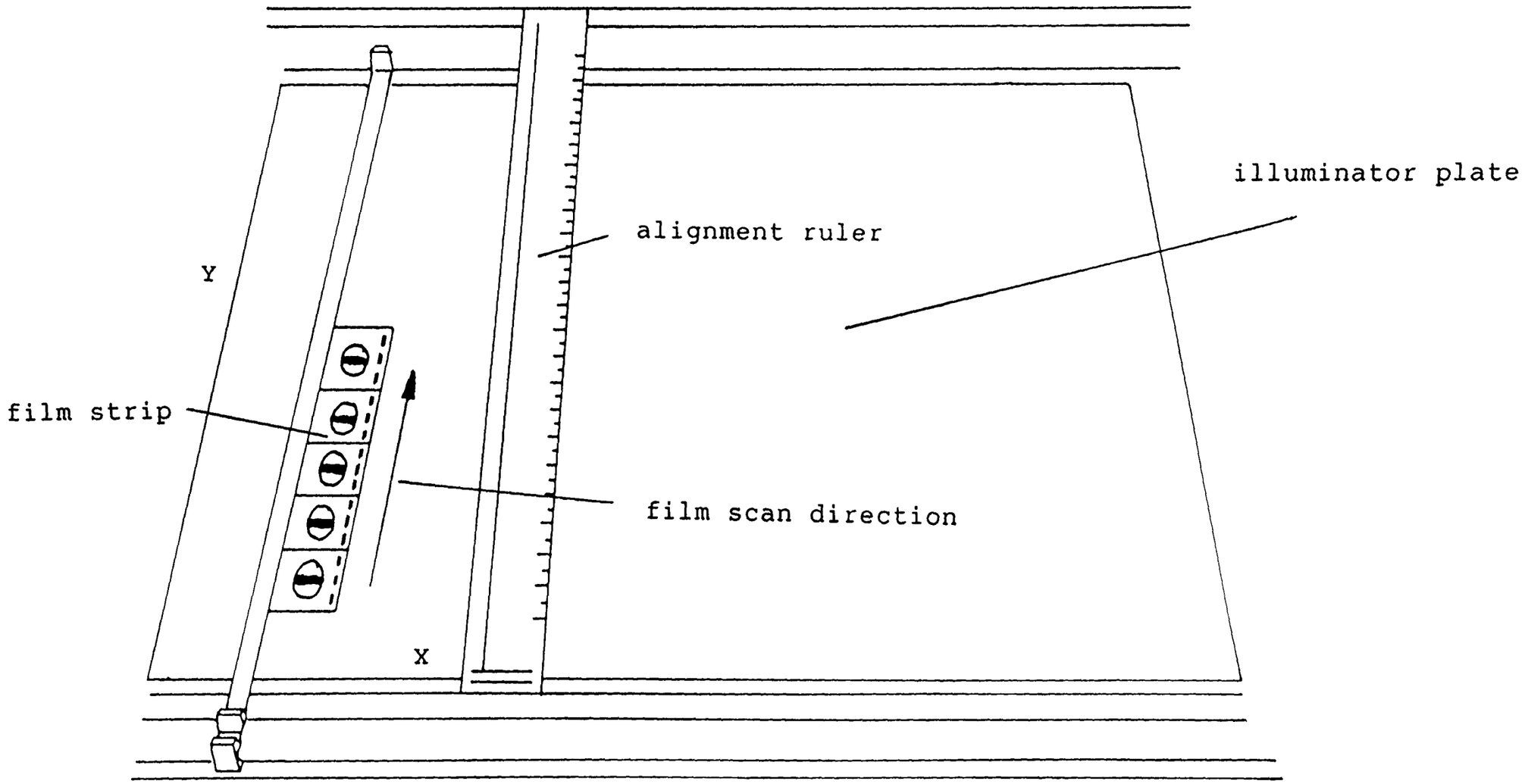

Fig 7.0.6 Localised film analysis

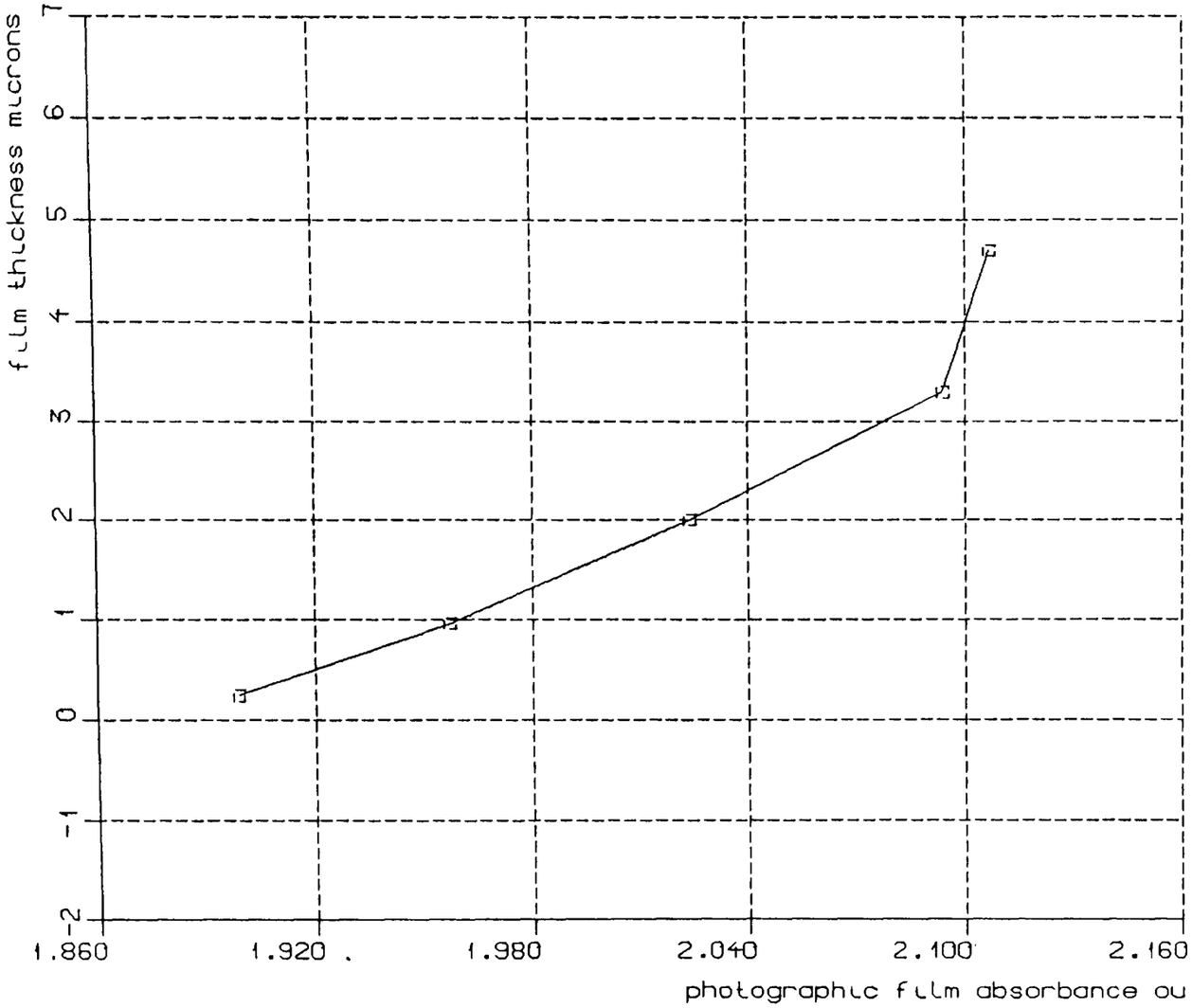

Fig 7.0.7 Calibration curve, film thickness v's optical absorbance

Fig 7.0.8 film thickness

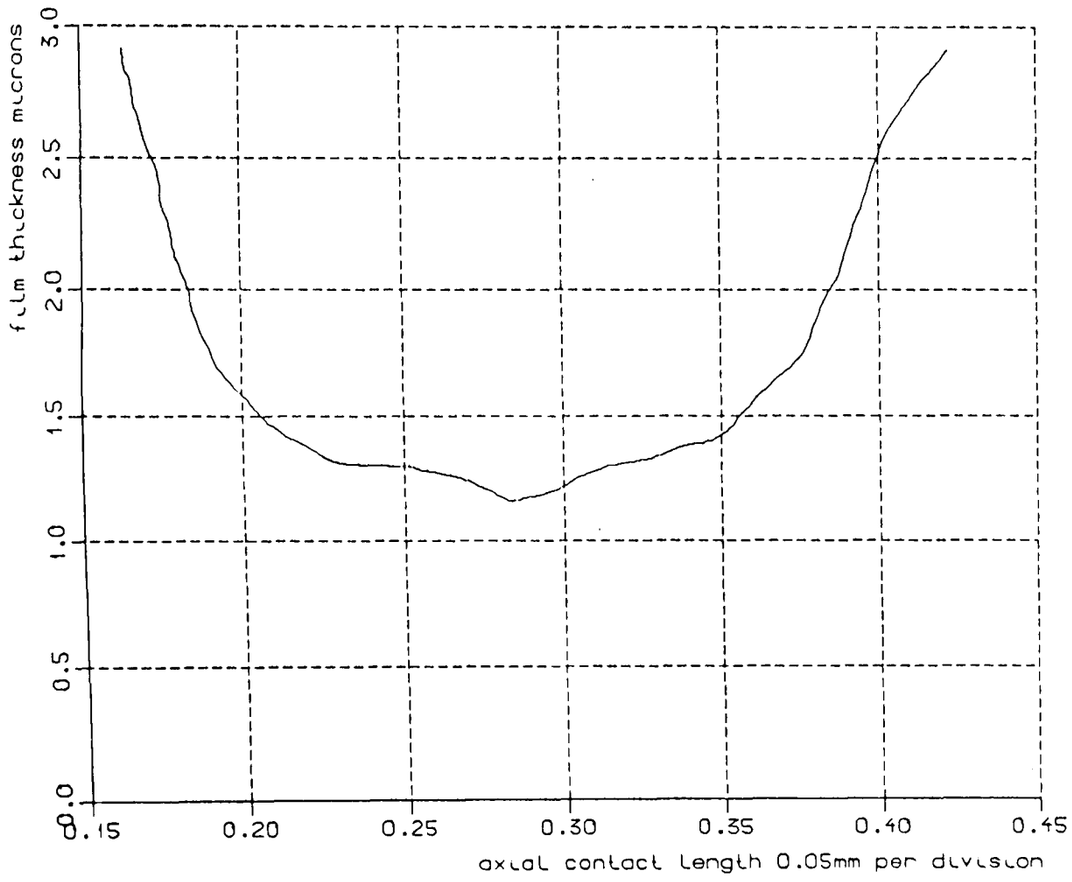

106rpm

Fig 7.0.9 film thickness

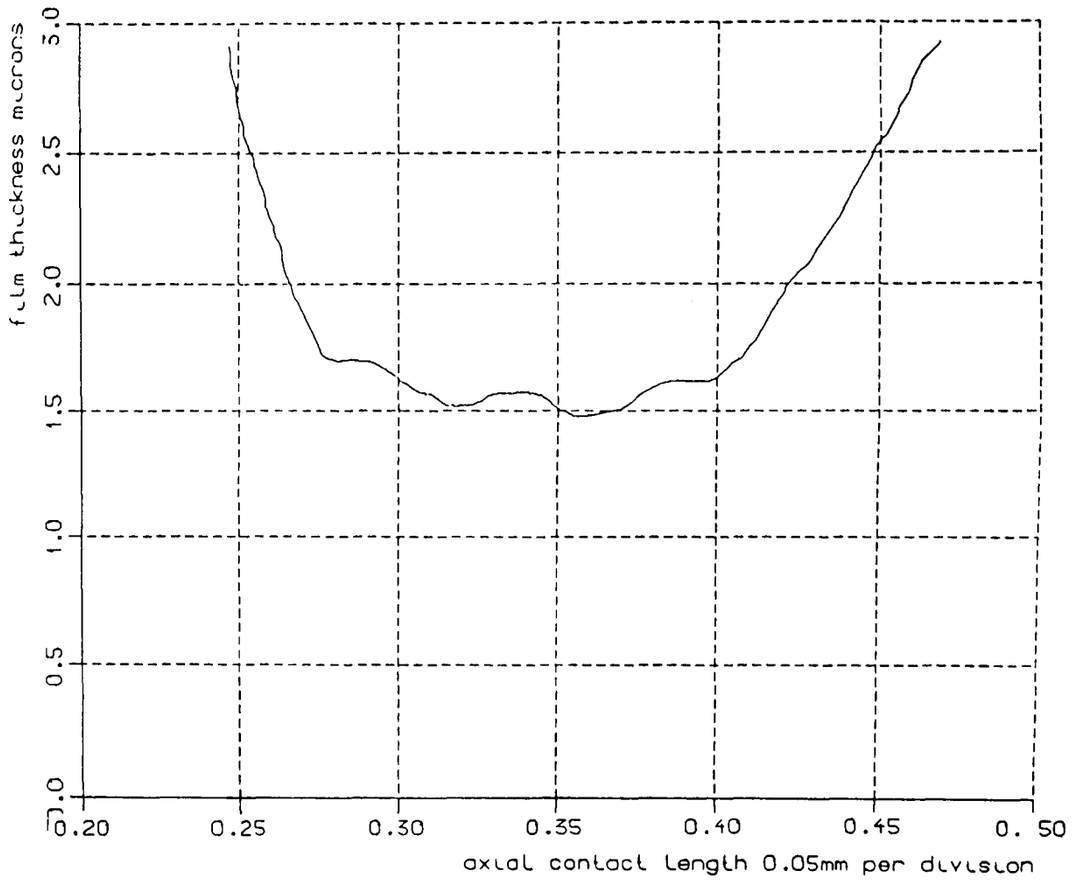

106rpm

Fig 7.1.0 film thickness

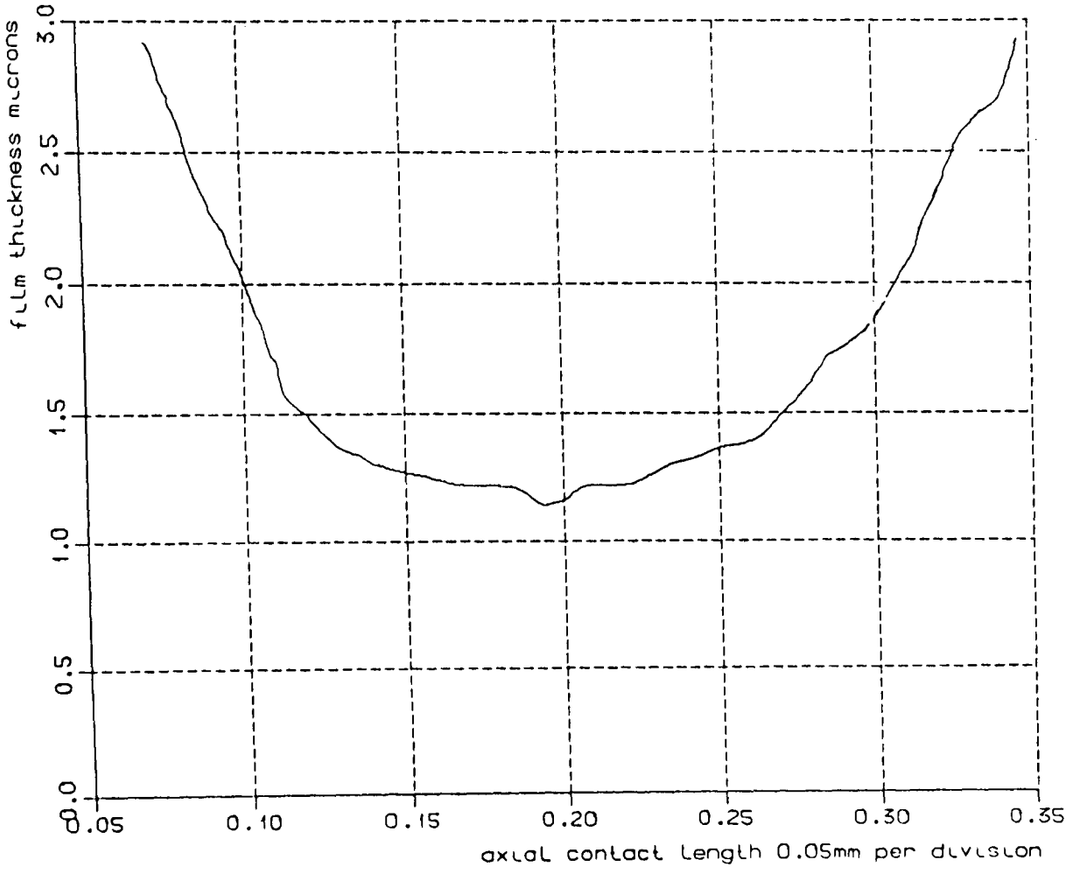

106rpm

Fig 7.1.1 film thickness

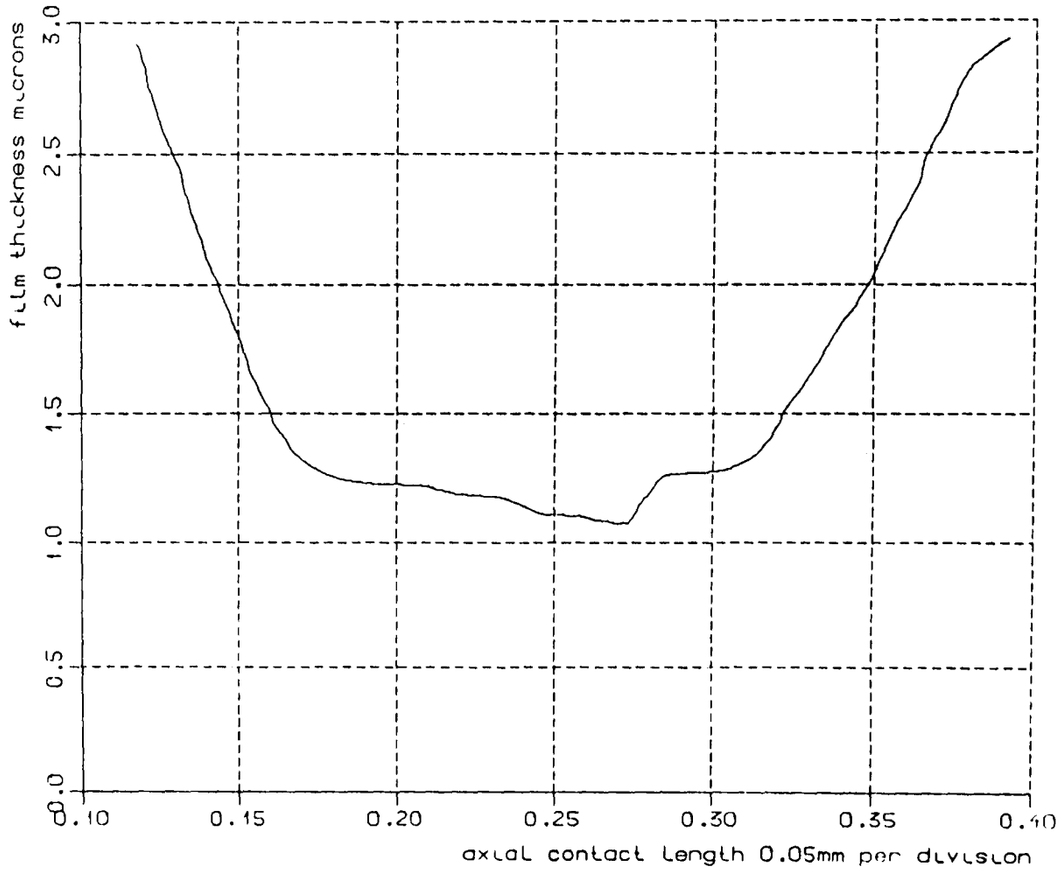

106rpm

Fig 7.1.2 film thickness

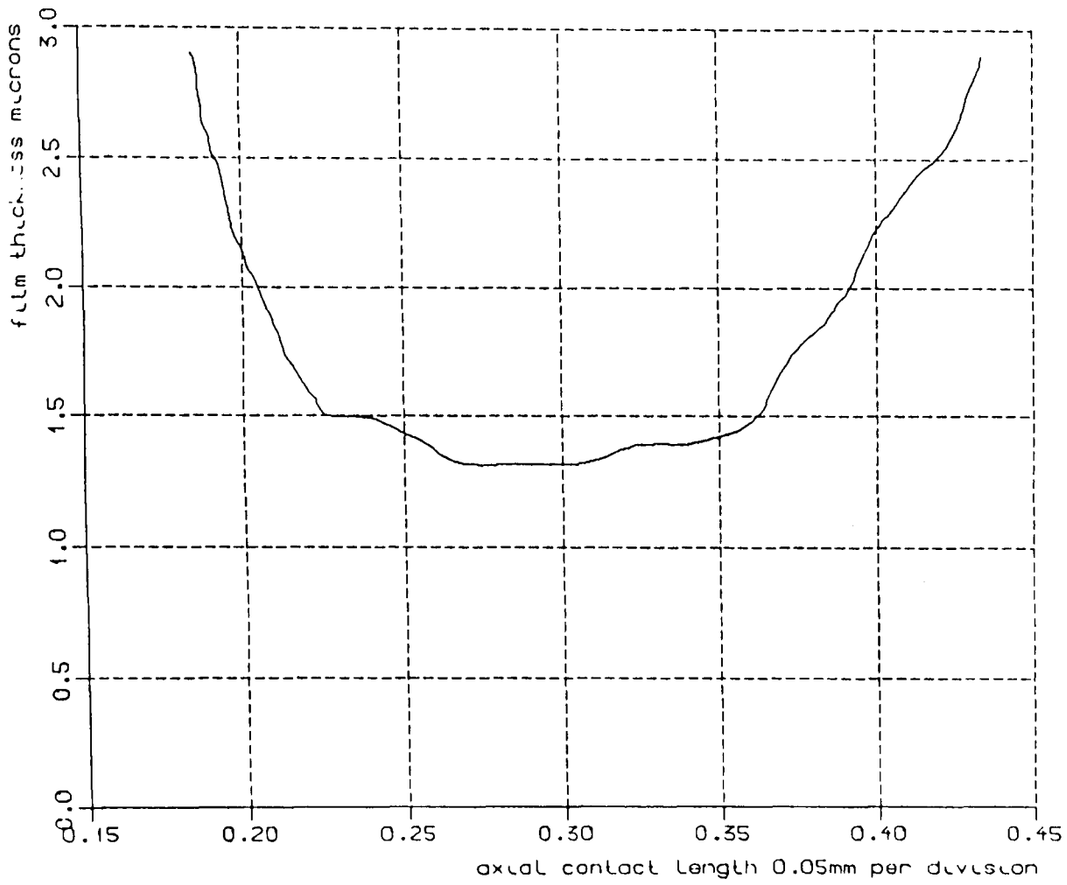

106rpm

Fig 7.1.3 film thickness

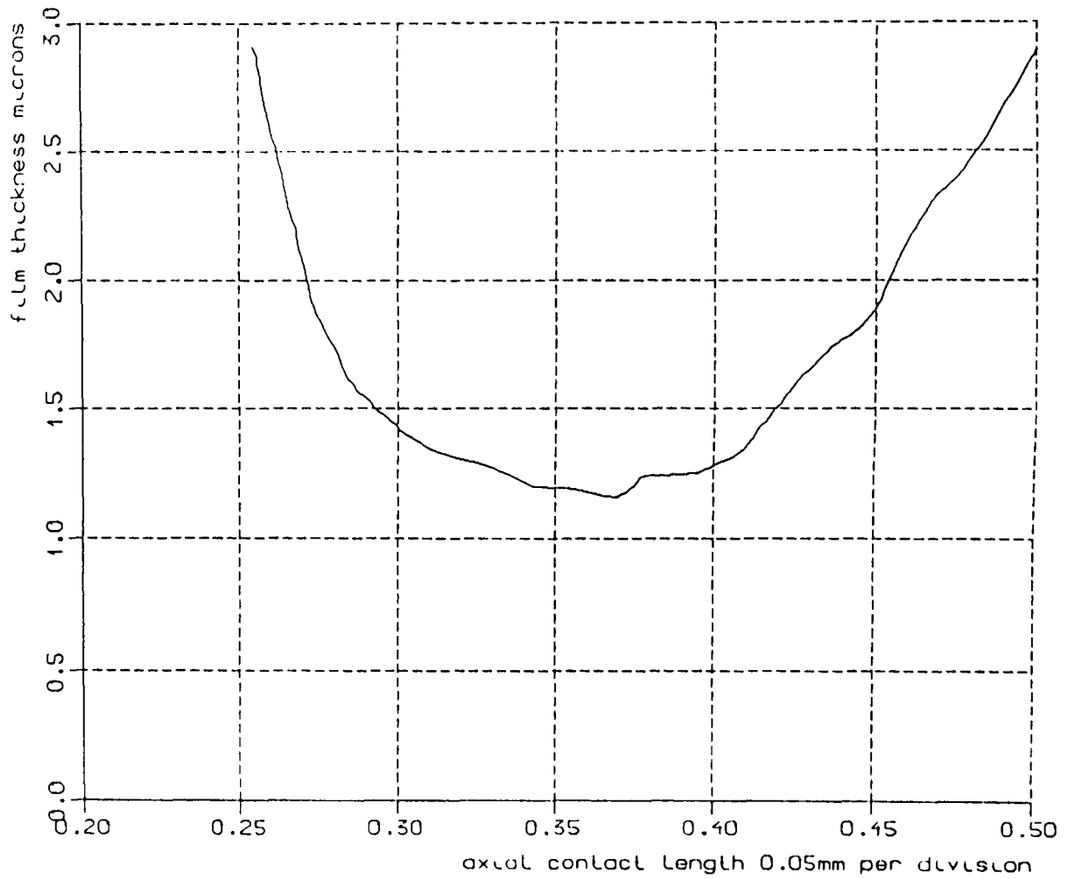

106rpm

Fig 7.1.4 film thickness

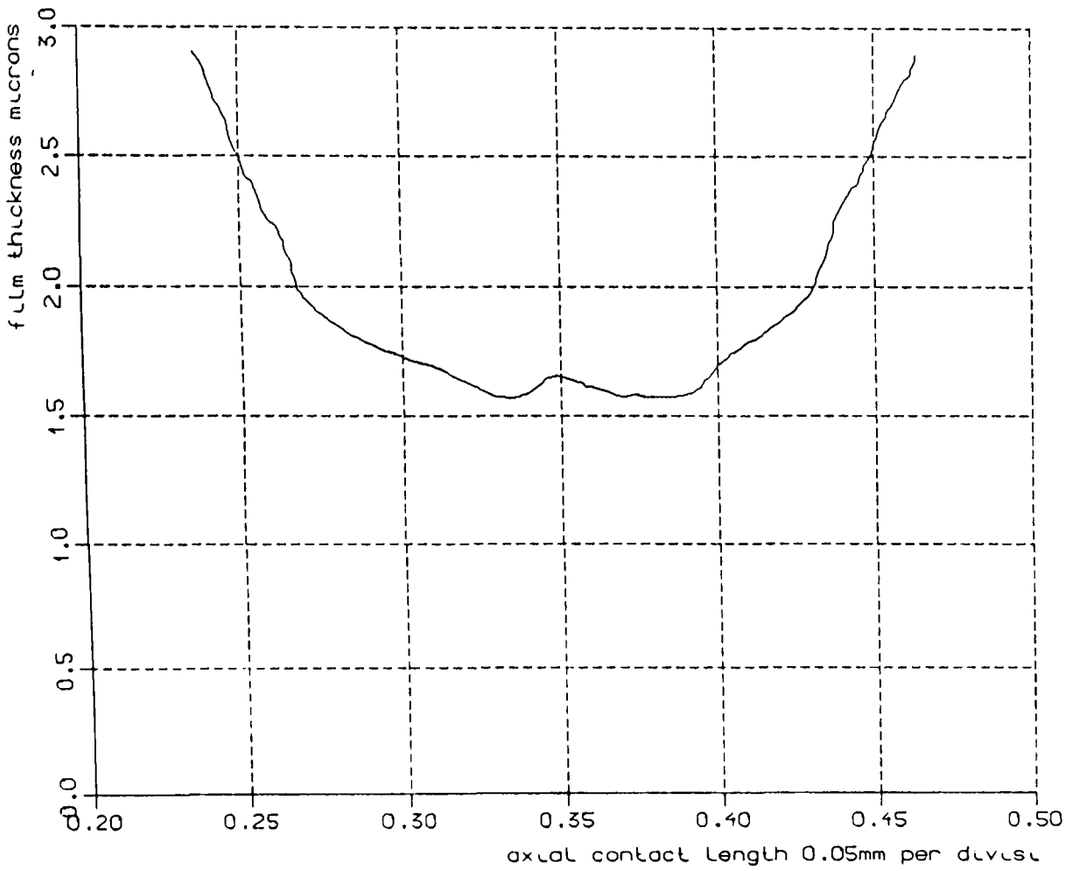

106rpm

Fig 7.1.5 film thickness

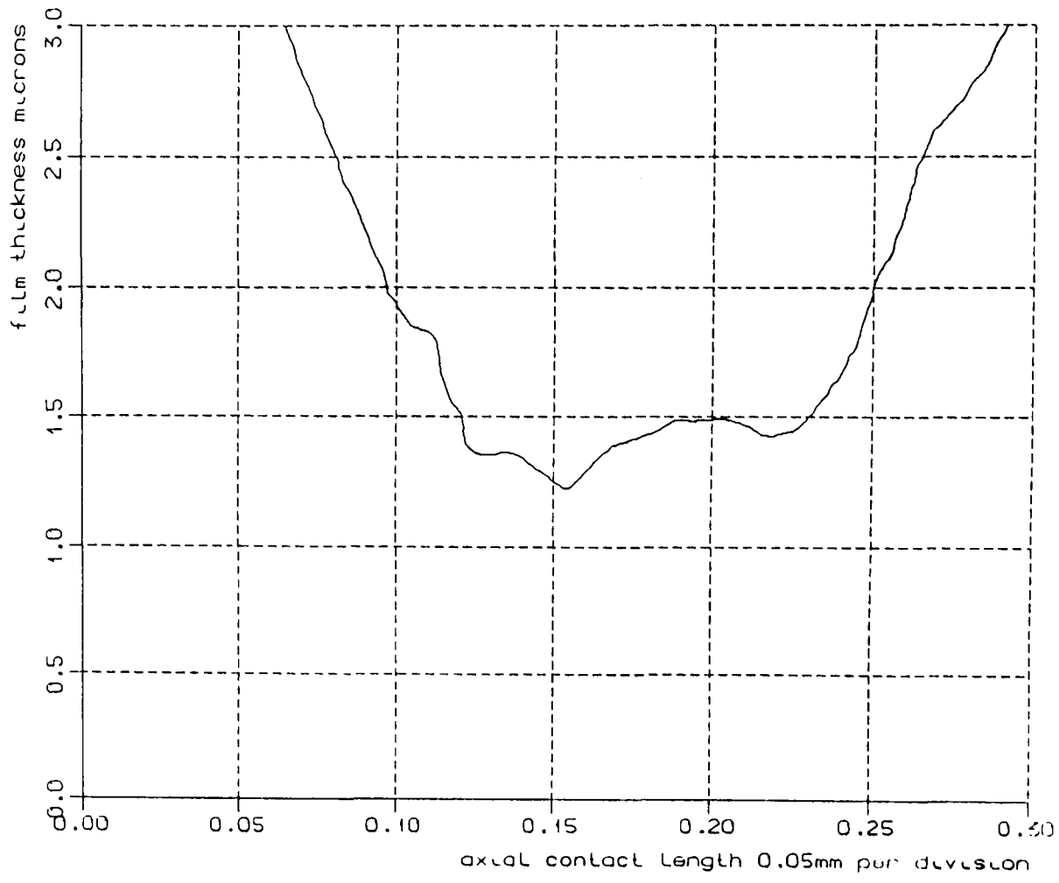

Fig 7.1.6 film thickness

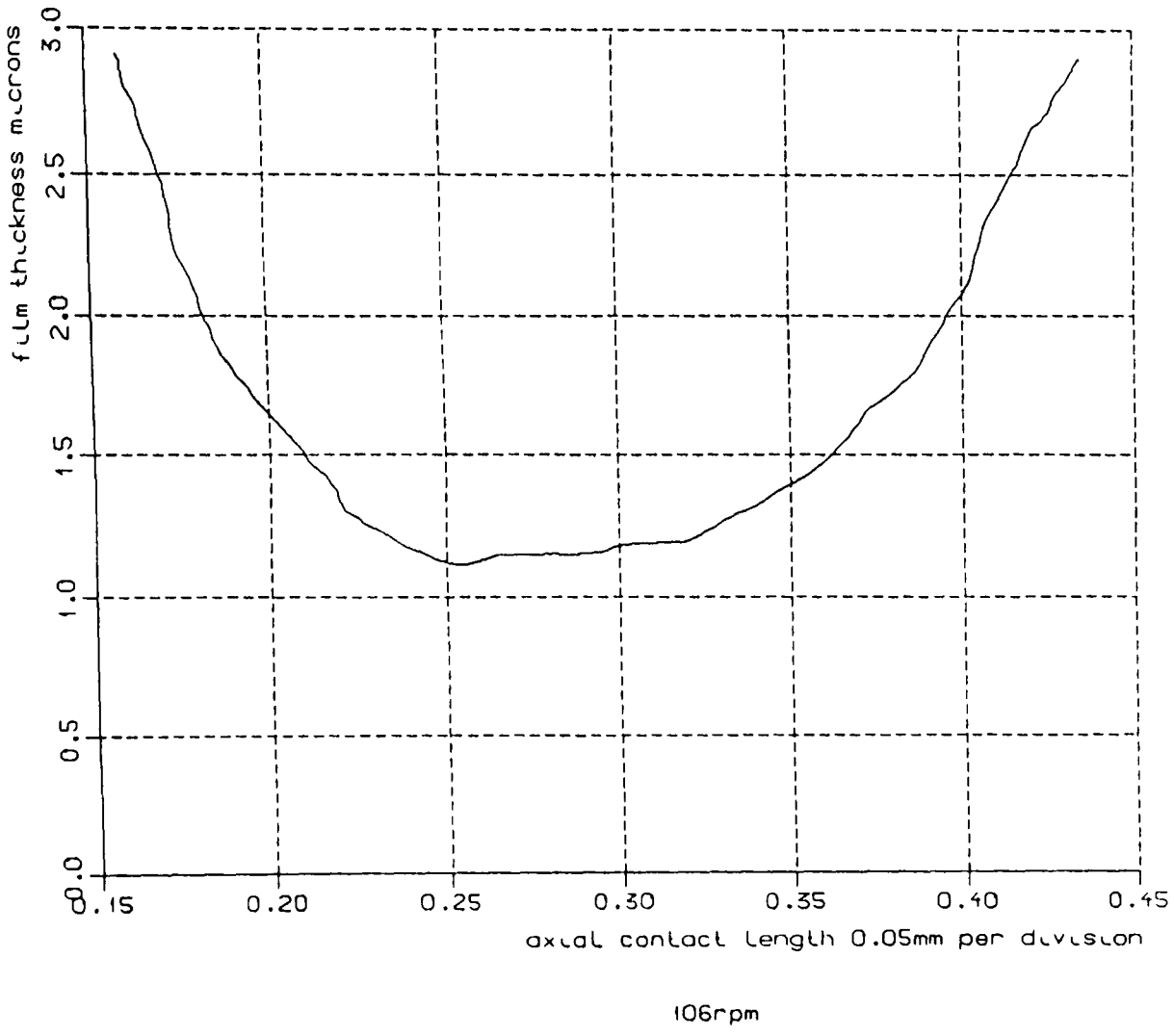

106rpm

Fig 7.1.7 film thickness

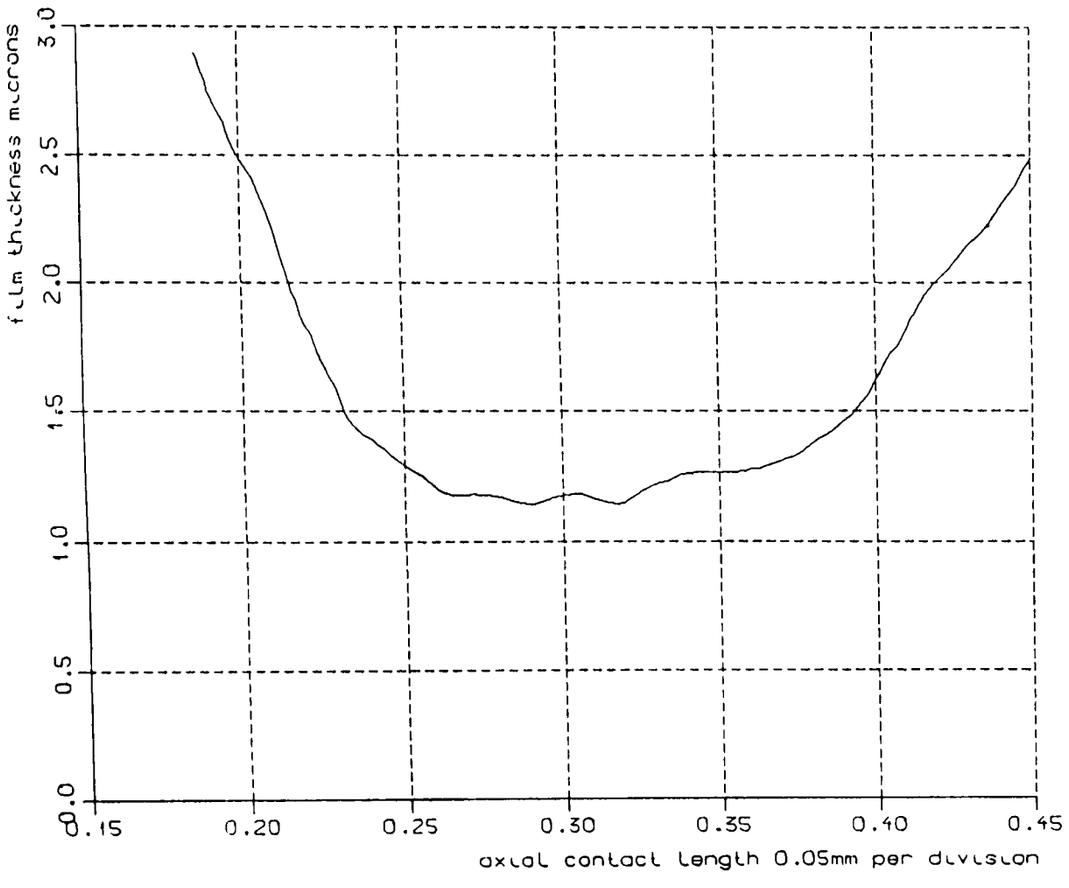

205rpm

Fig 7.1.8 film thickness

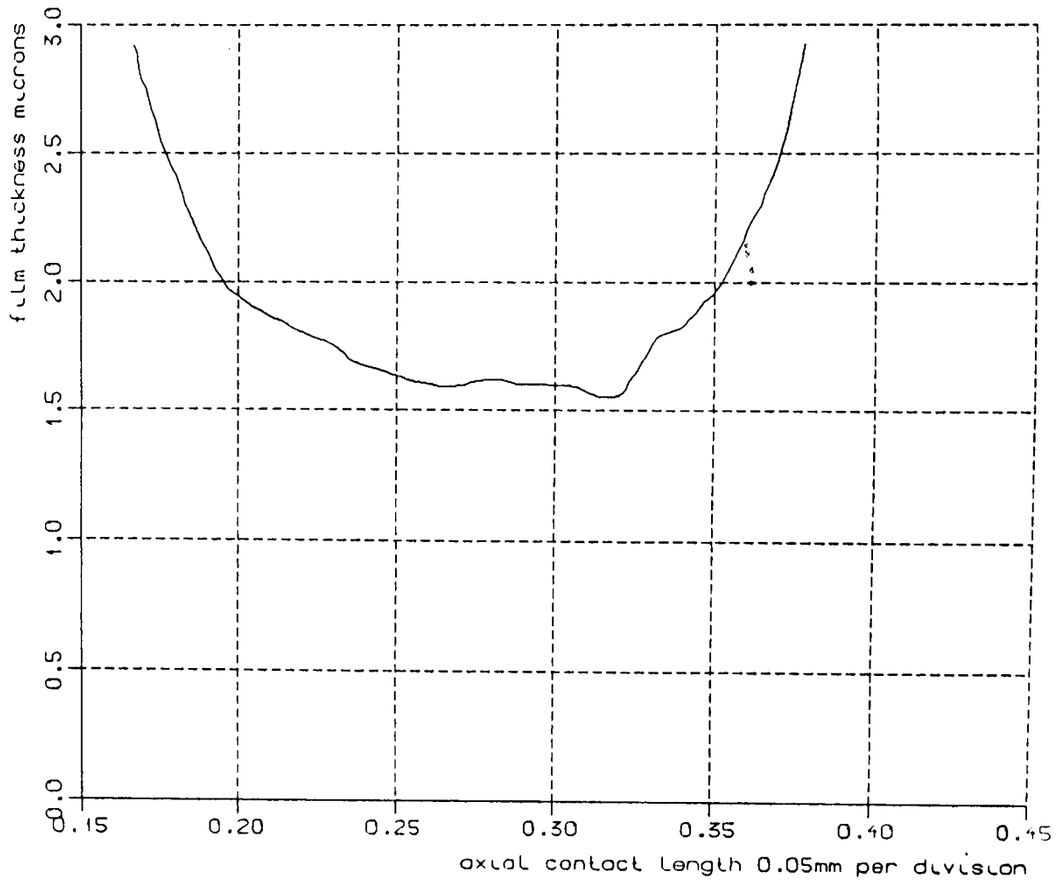

205rpm

Fig 7.1.9 film thickness

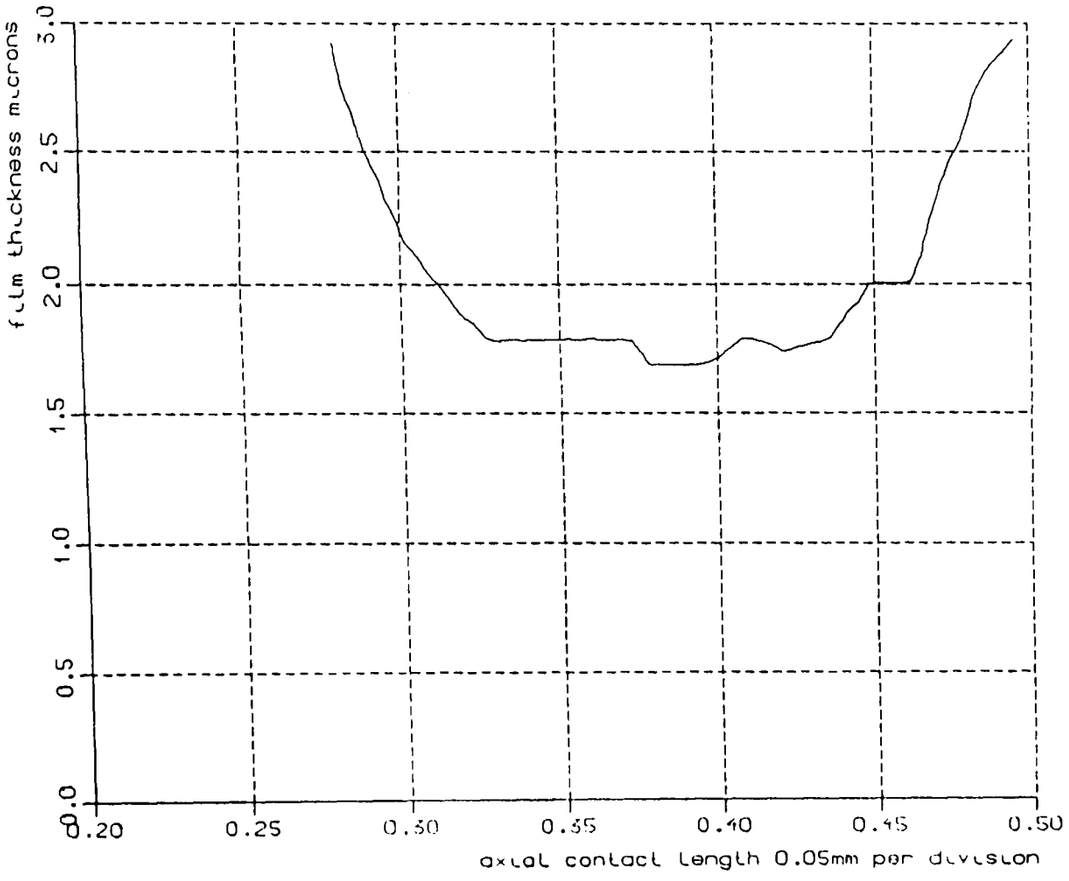

205rpm

Fig 7.2.0 film thickness

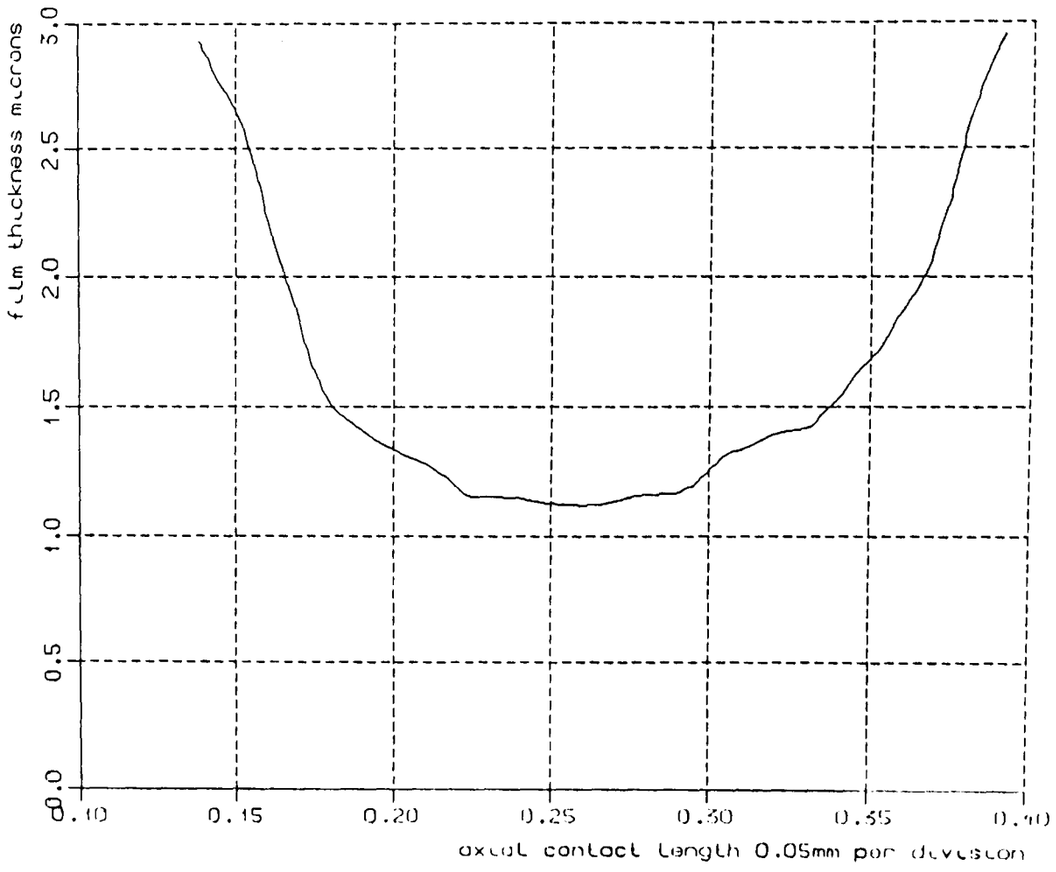

205rpm

Fig 7.2.1 film thickness

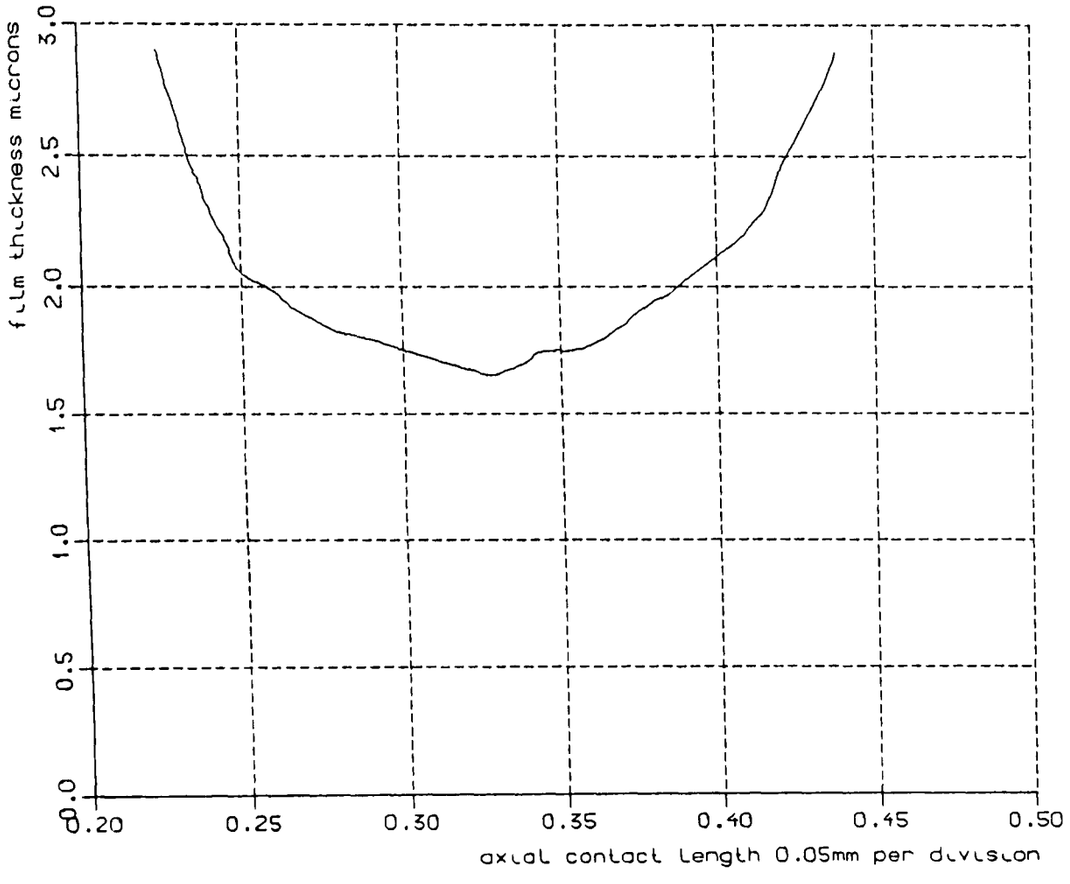

205rpm

Fig 7.2.2 film thickness

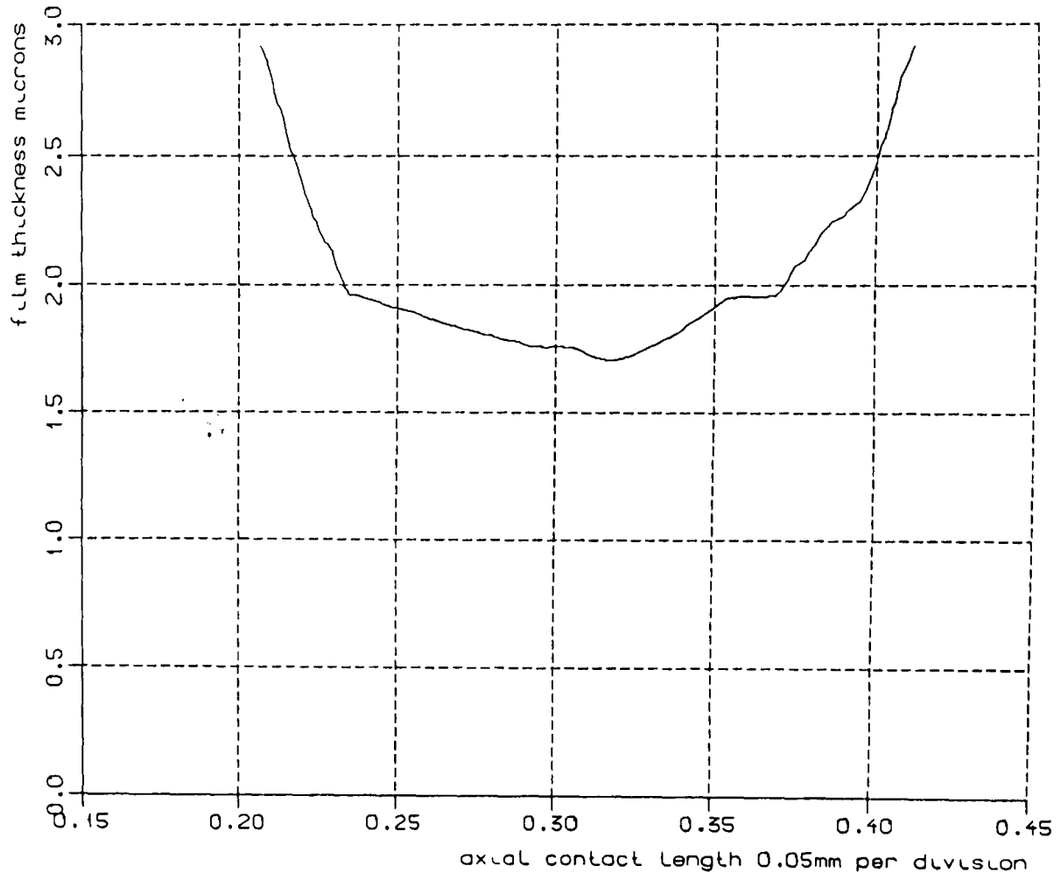

205rpm

Fig 7.2.3 film thickness

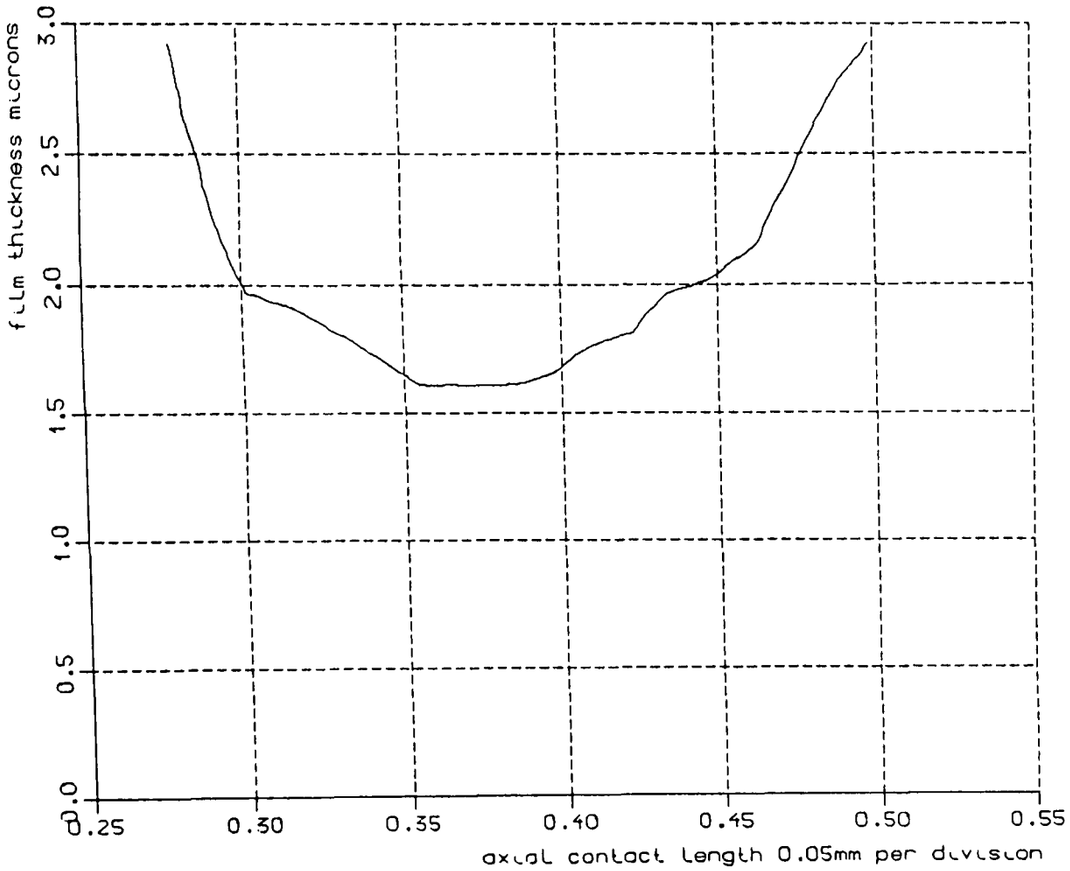

205rpm

Fig 7.2.4 film thickness

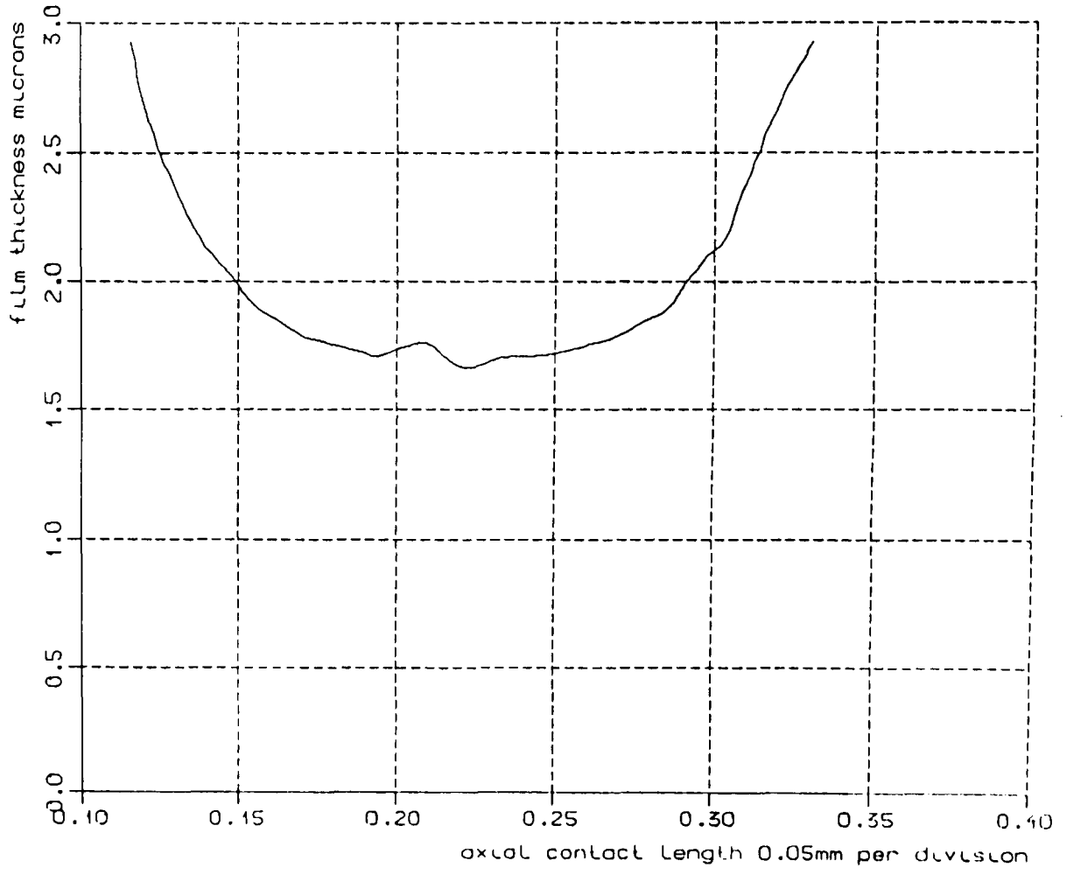

205rpm

Fig 7.2.5 film thickness

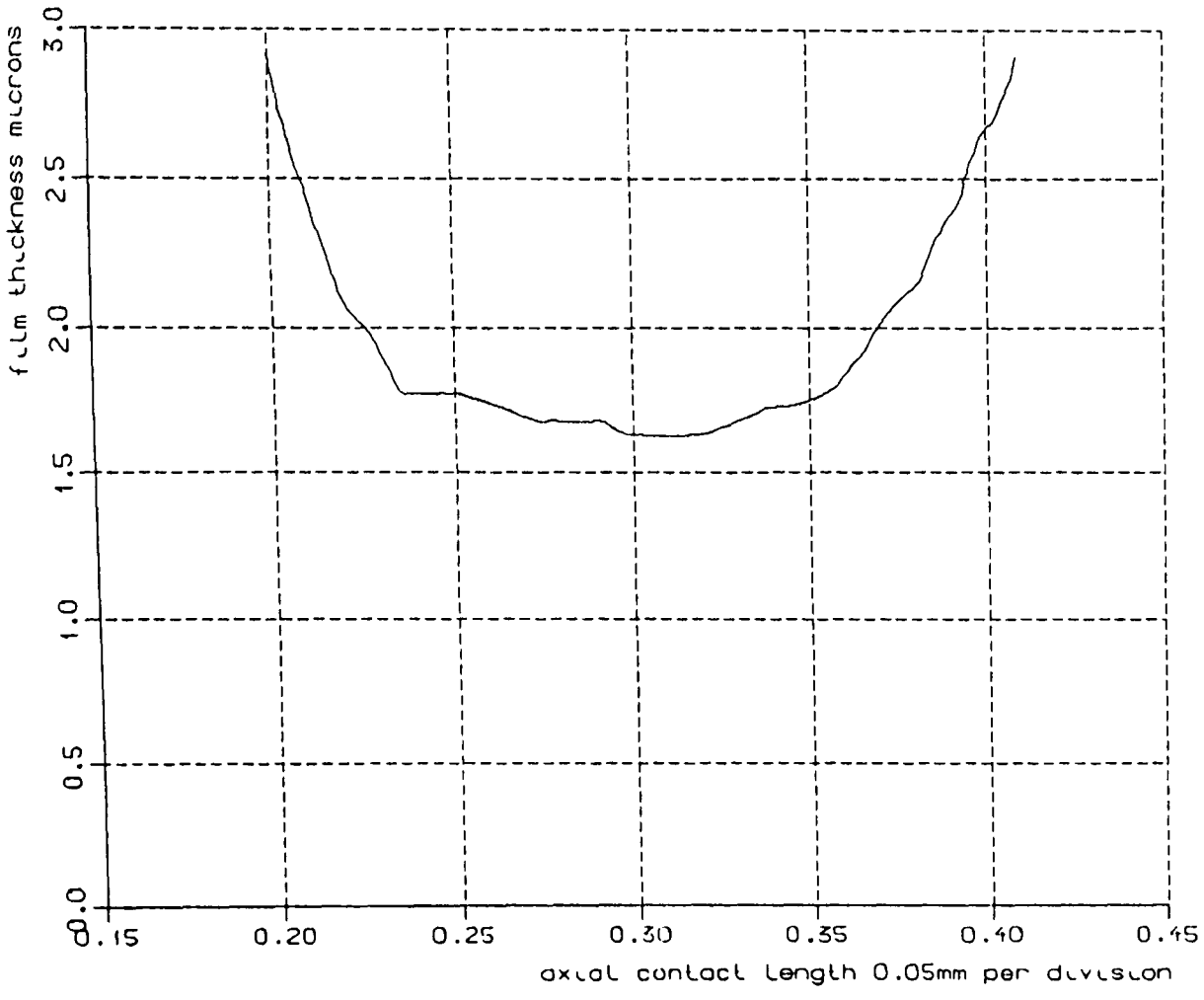

205rpm

Fig 7.2.6 film thickness

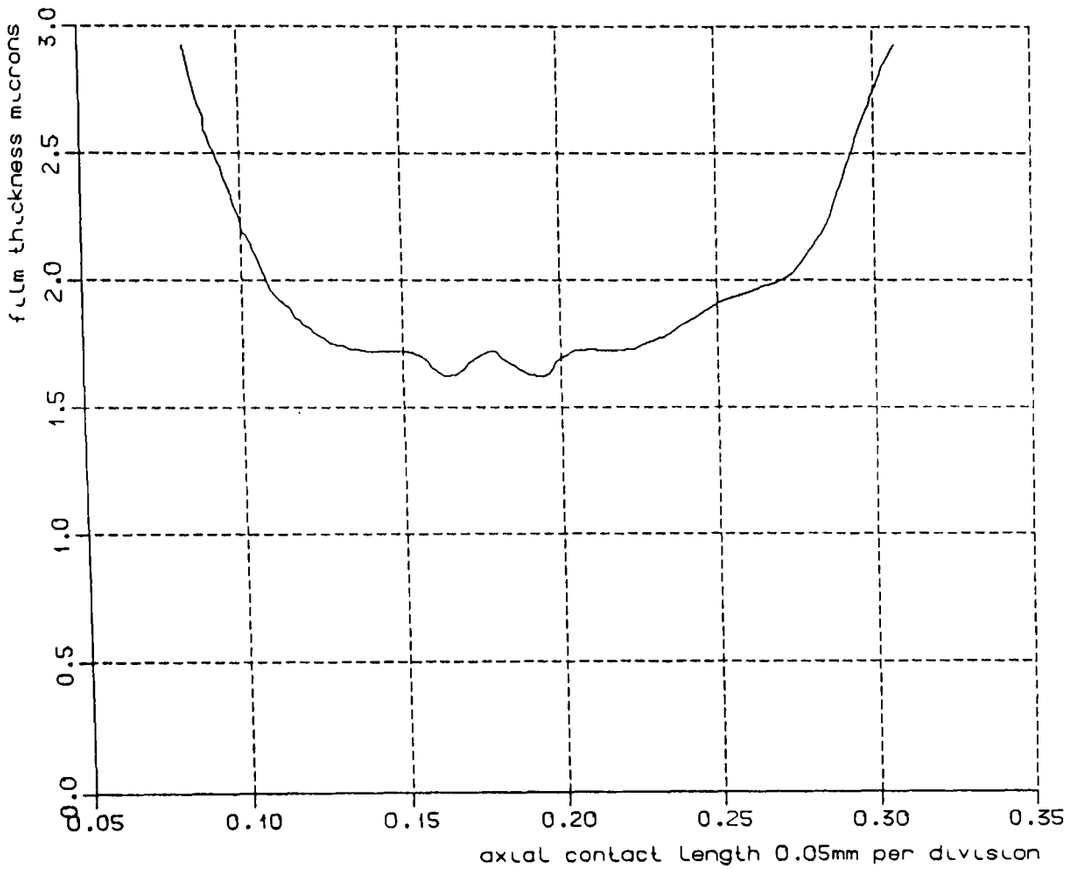

505rpm

Fig 7.2.7 film thickness

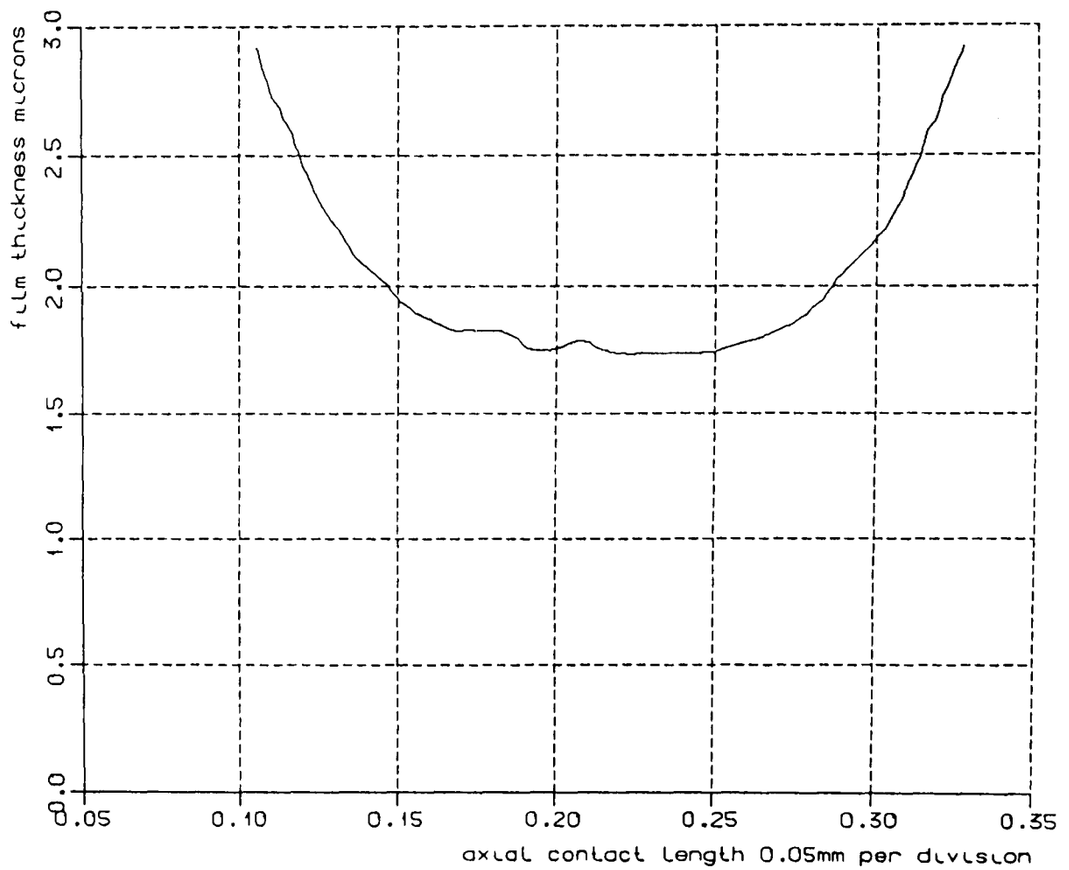

505rpm

Fig 7.2.8 film thickness

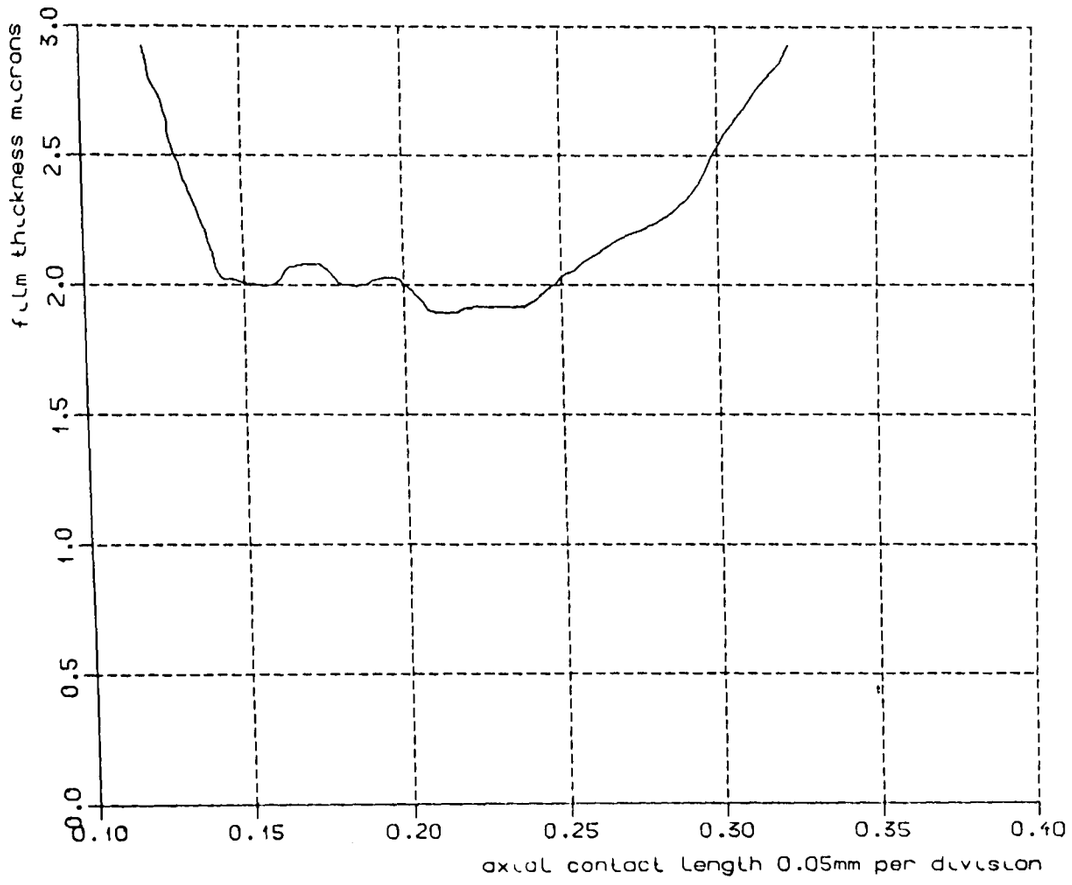

505rpm

Fig 7.2.9 film thickness

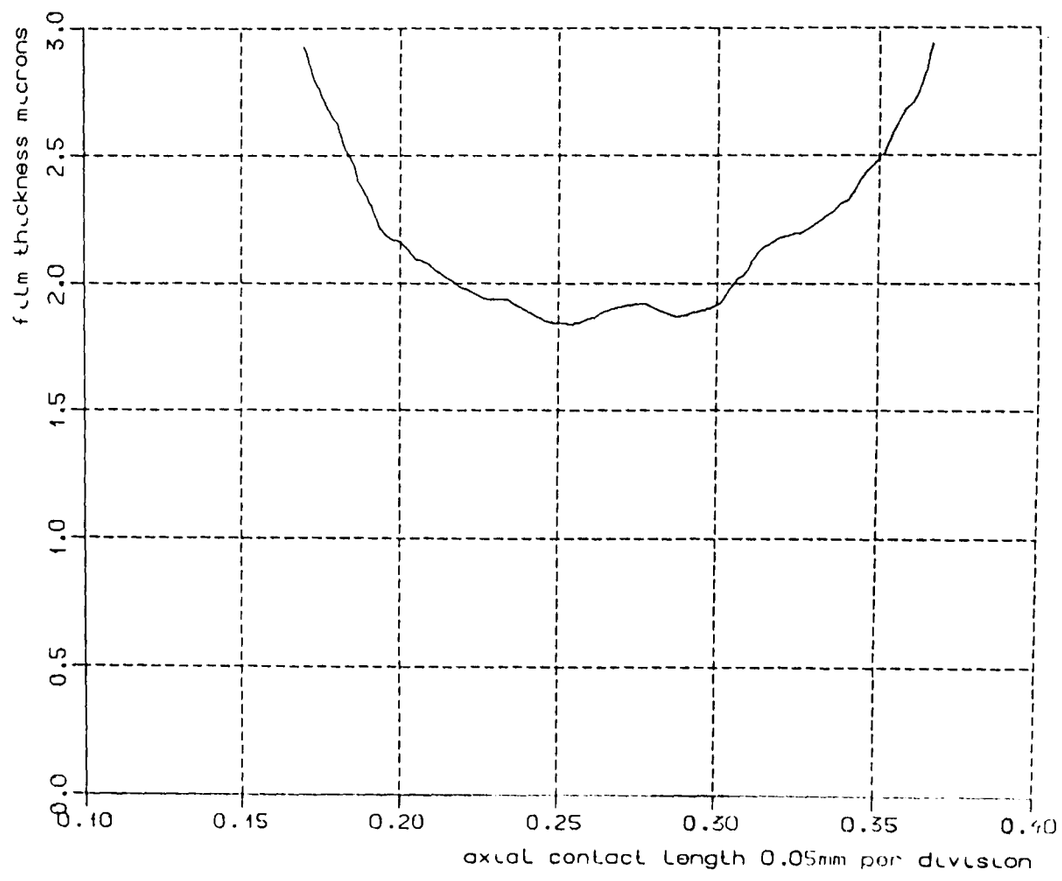

505rpm

Fig 7.3.0 film thickness

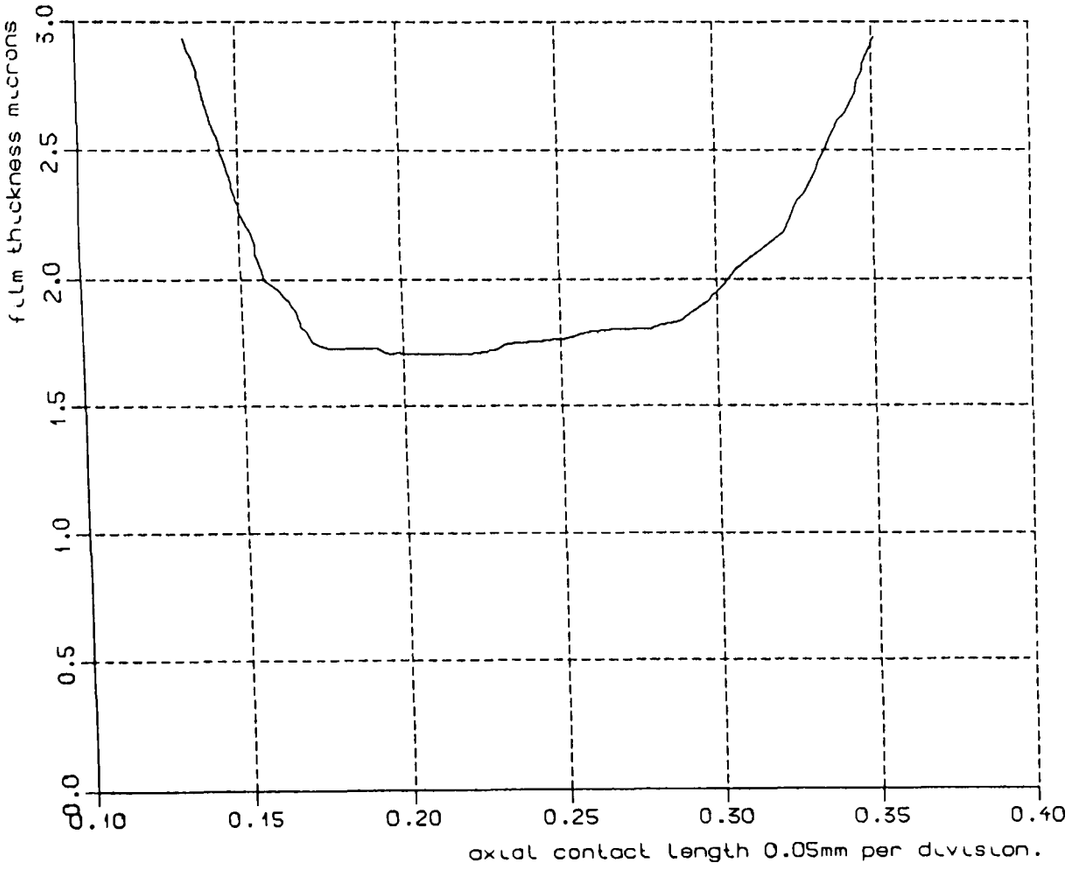

505rpm

Fig 7.3.1 film thickness

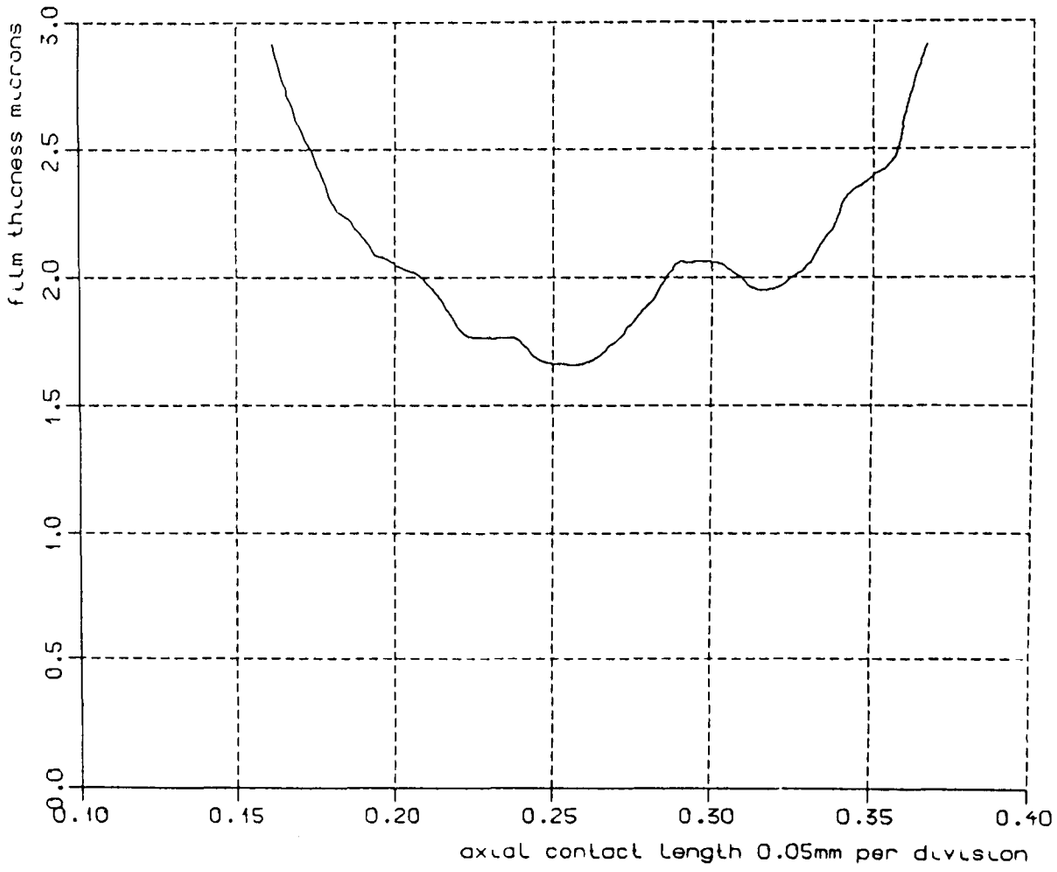

505rpm

Fig 7.3.2 film thickness

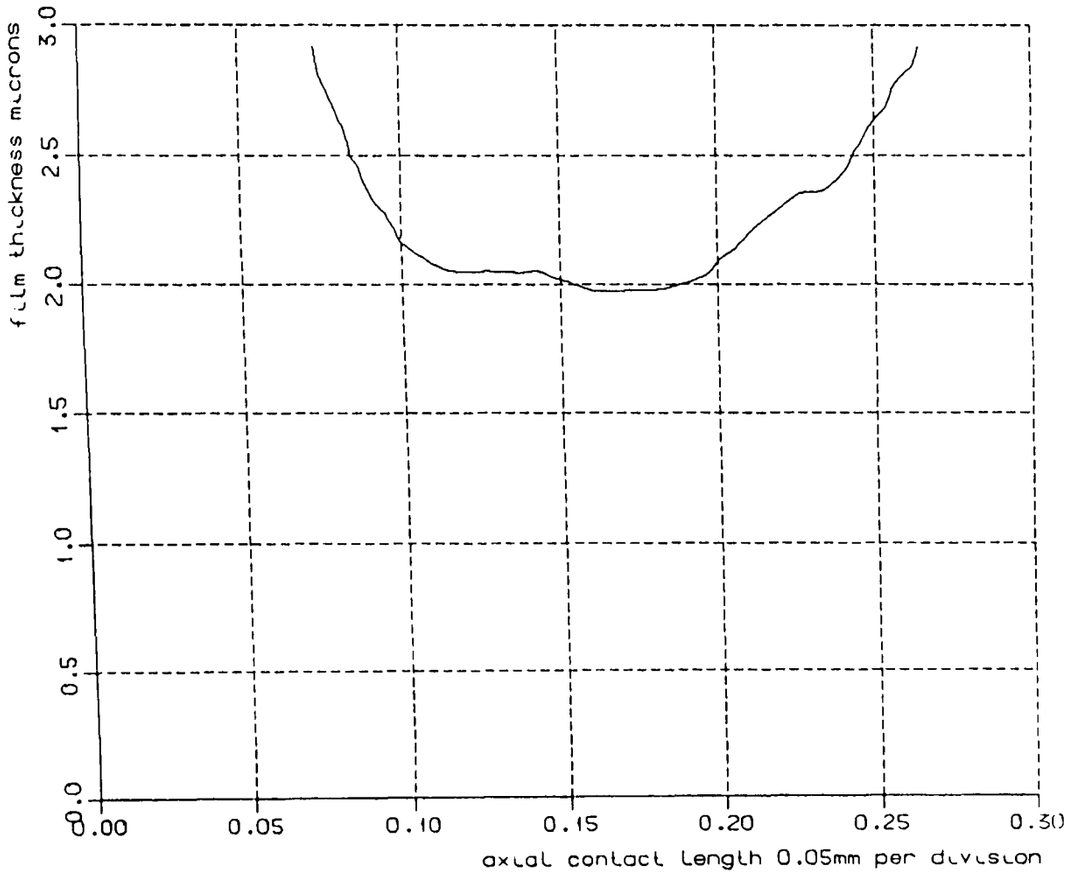

505rpm

Fig 7.3.3 film thickness

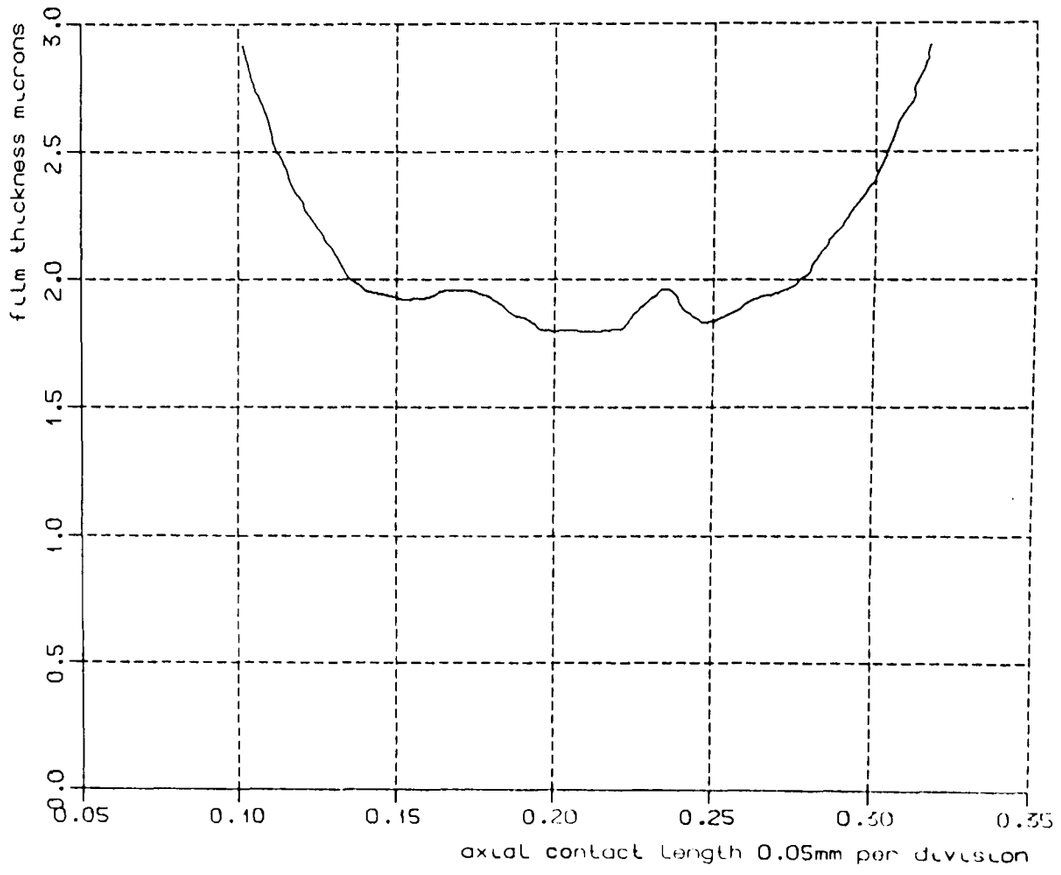

505rpm

Fig 7.3.4 film thickness

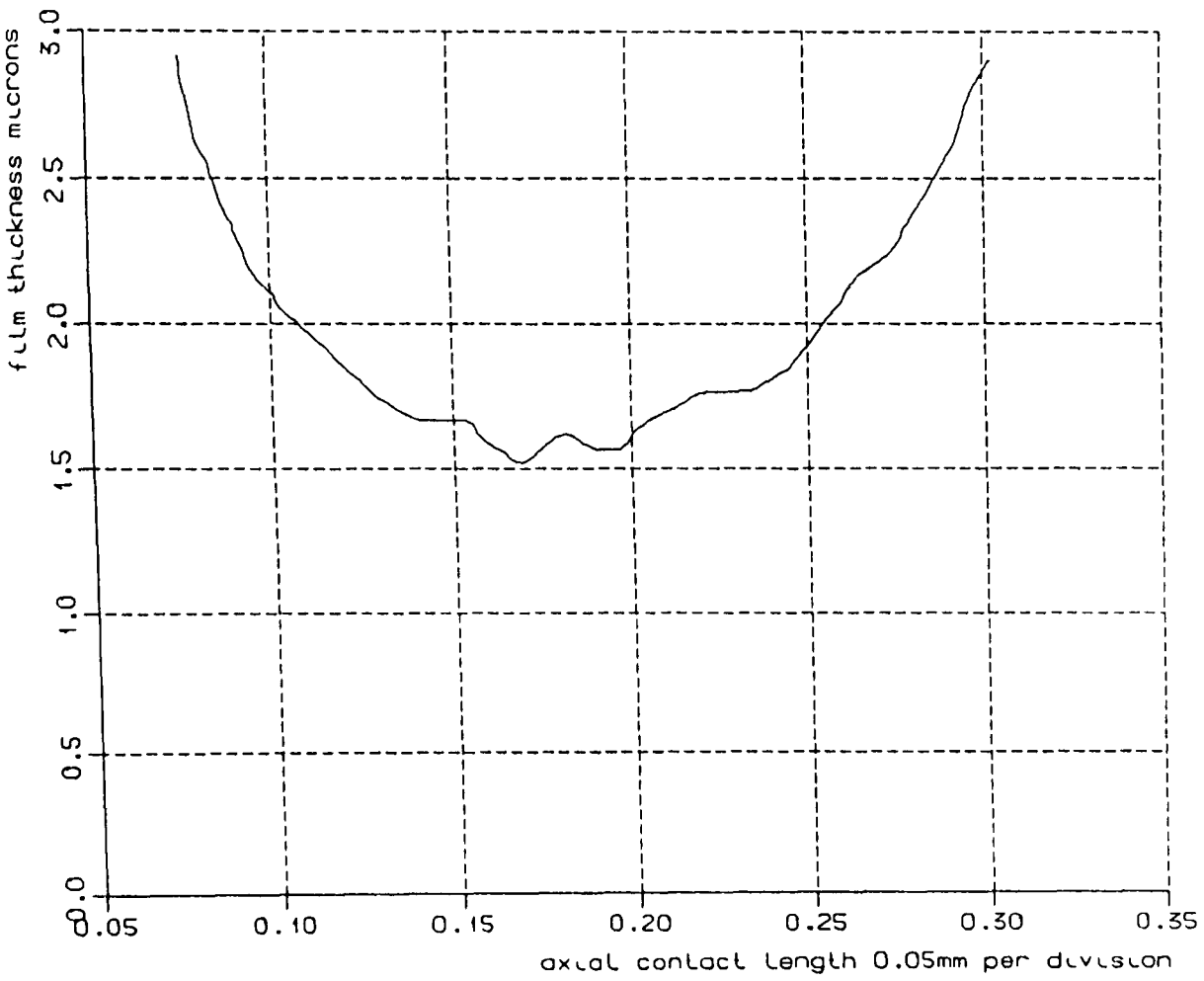

Fig 7.3.5 film thickness

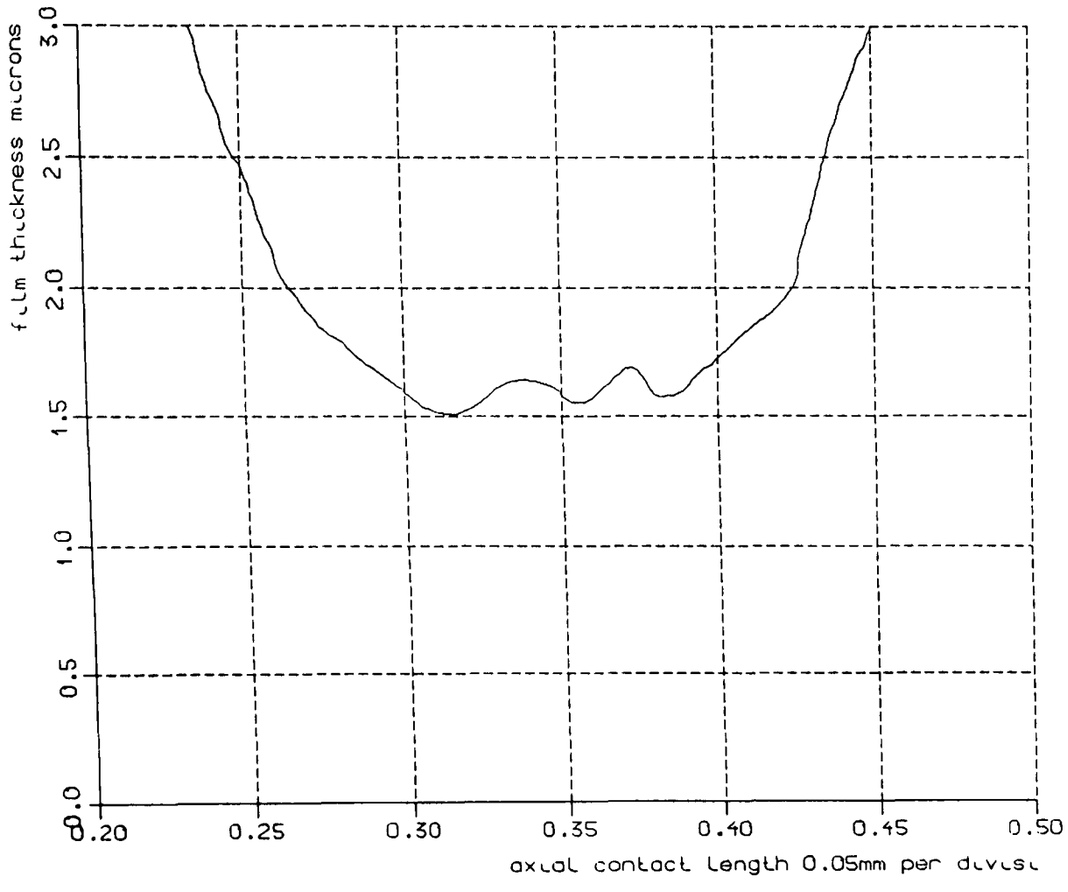

1016rpm

Fig 7.3.6 film thickness

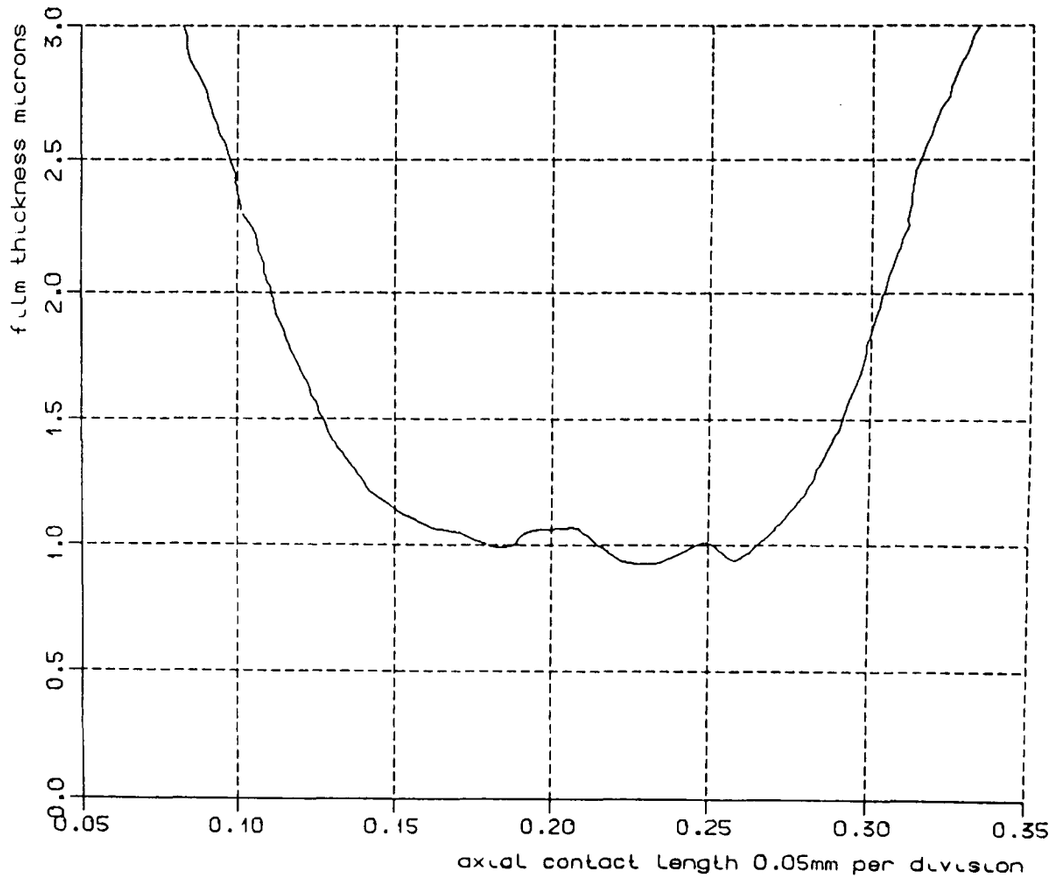

1016rpm

Fig 7.3.7 film thickness

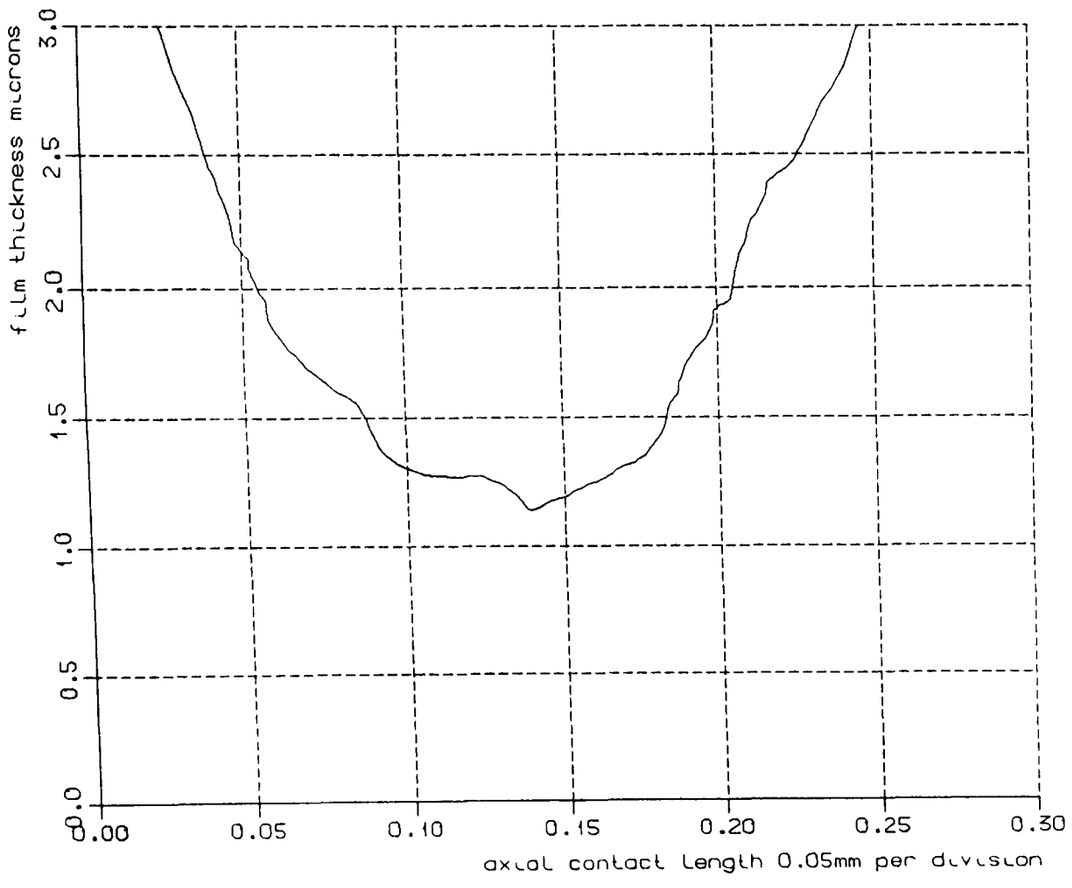

1016rpm

Fig 7.3.8 film thickness

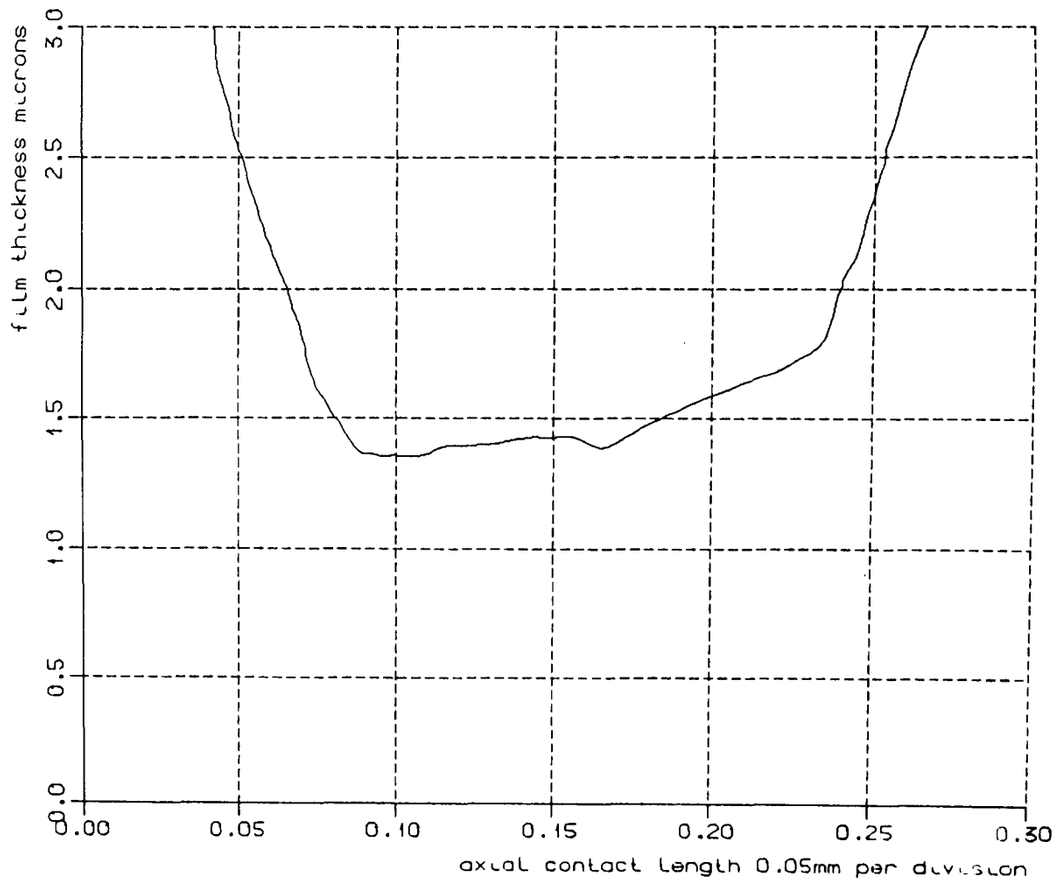

1016rpm

Fig 7.3.9 film thickness

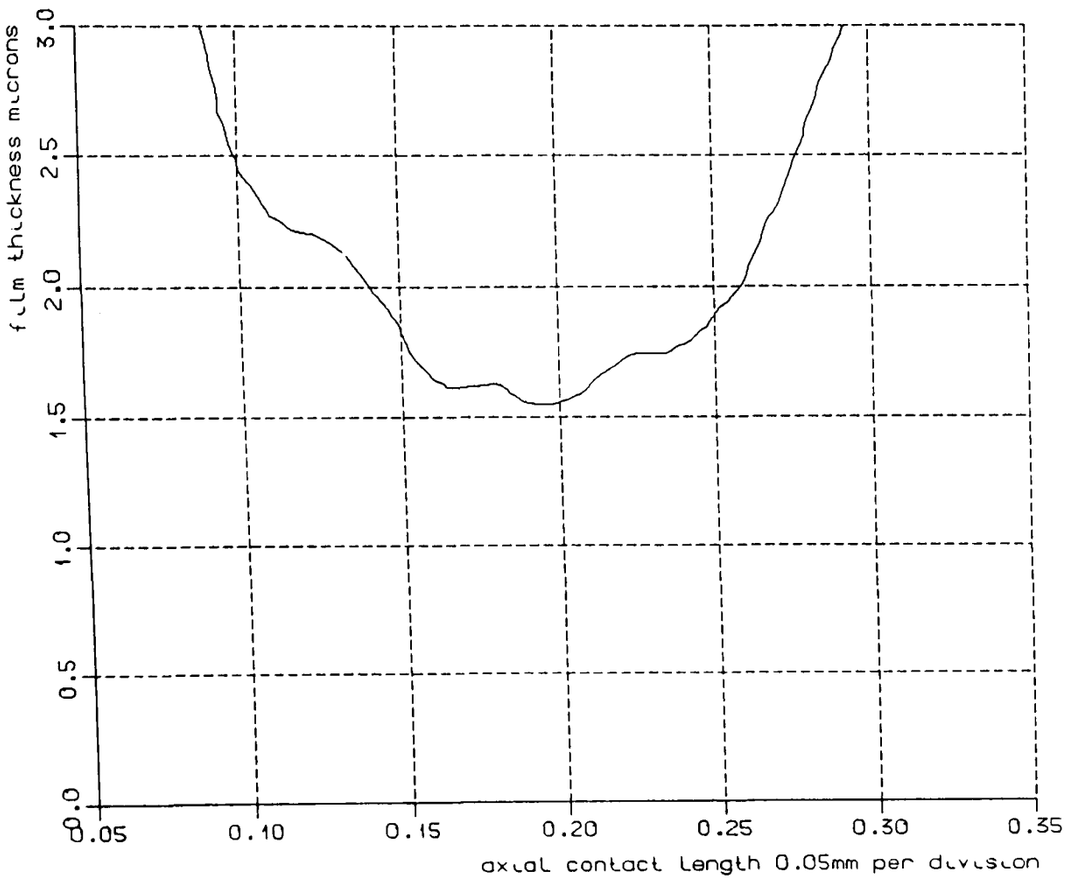

1016rpm

Fig 7.4.0 film thickness

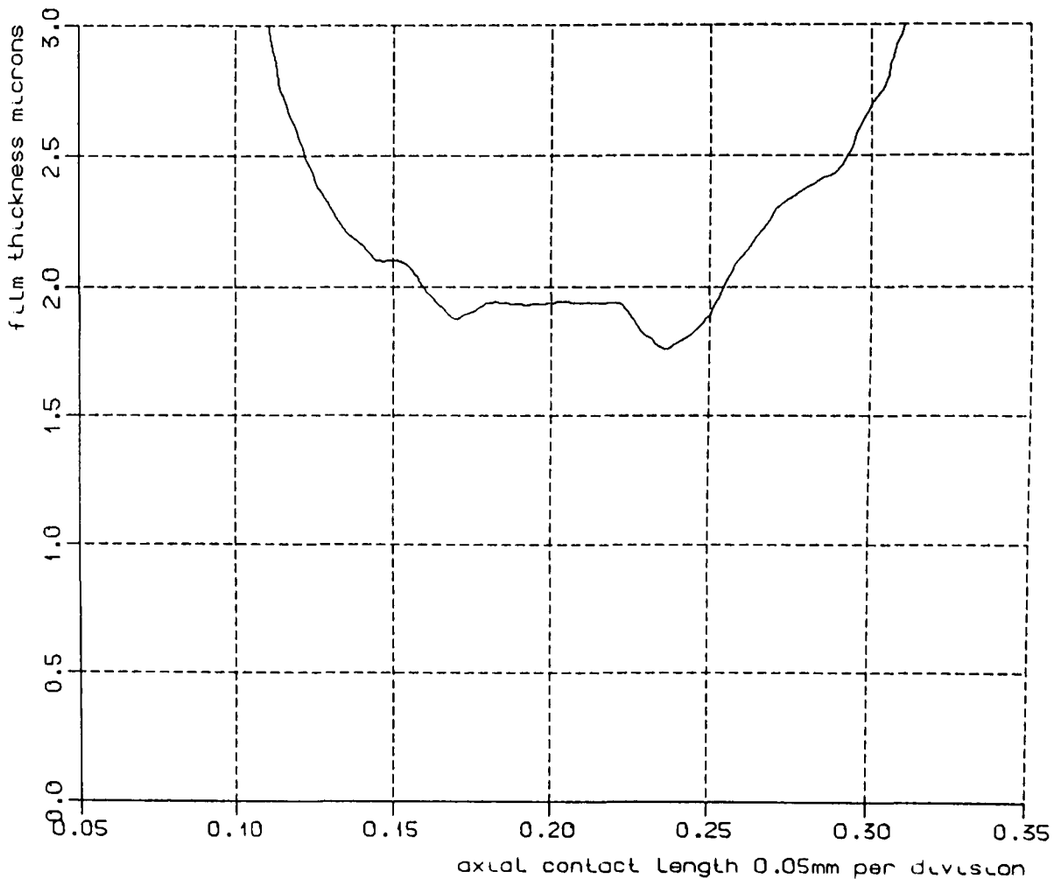

1016rpm

Fig 7.4.1 film thickness

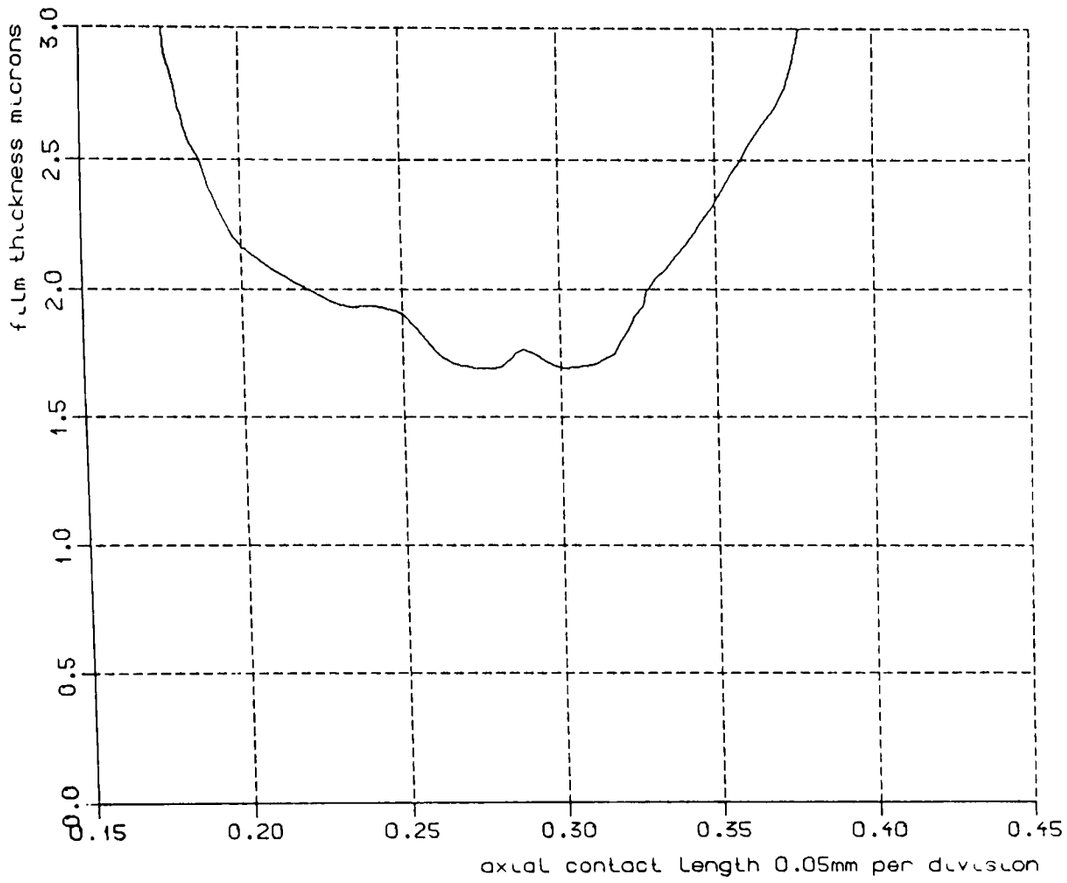

1016rpm

Fig 7.4.2 film thickness

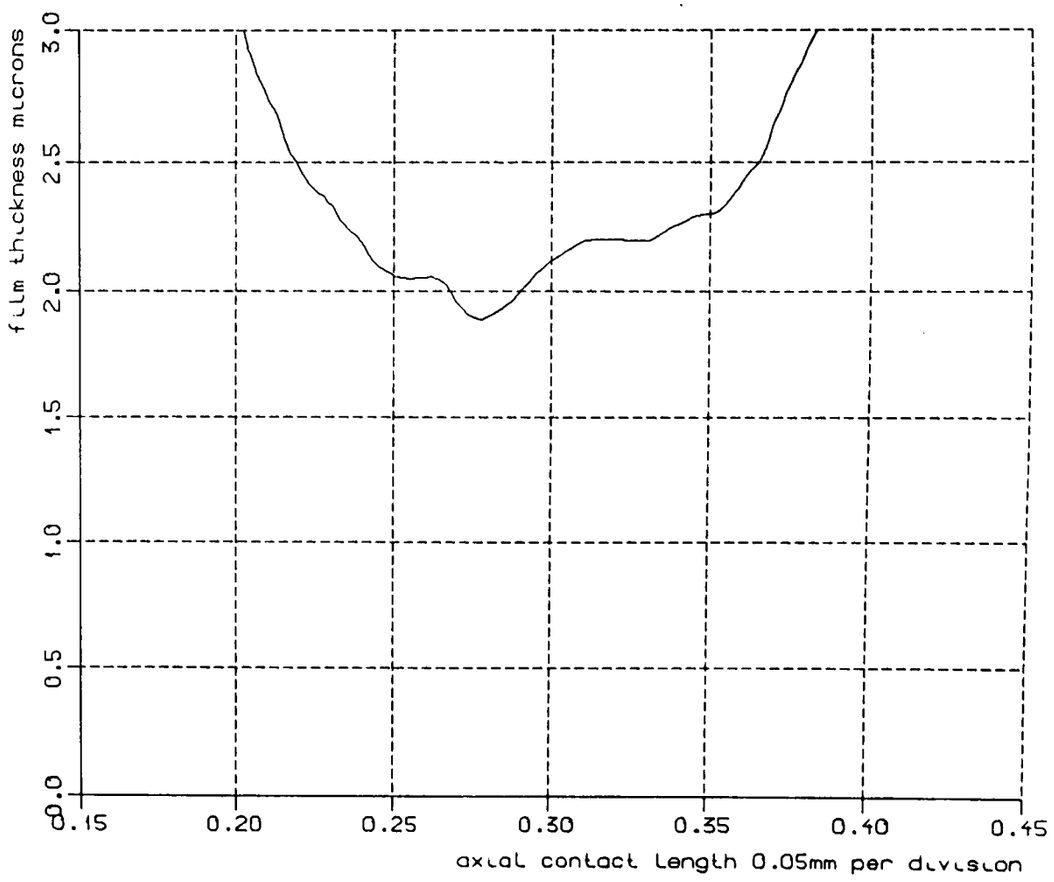

1016rpm

Fig 7.4.3 film thickness

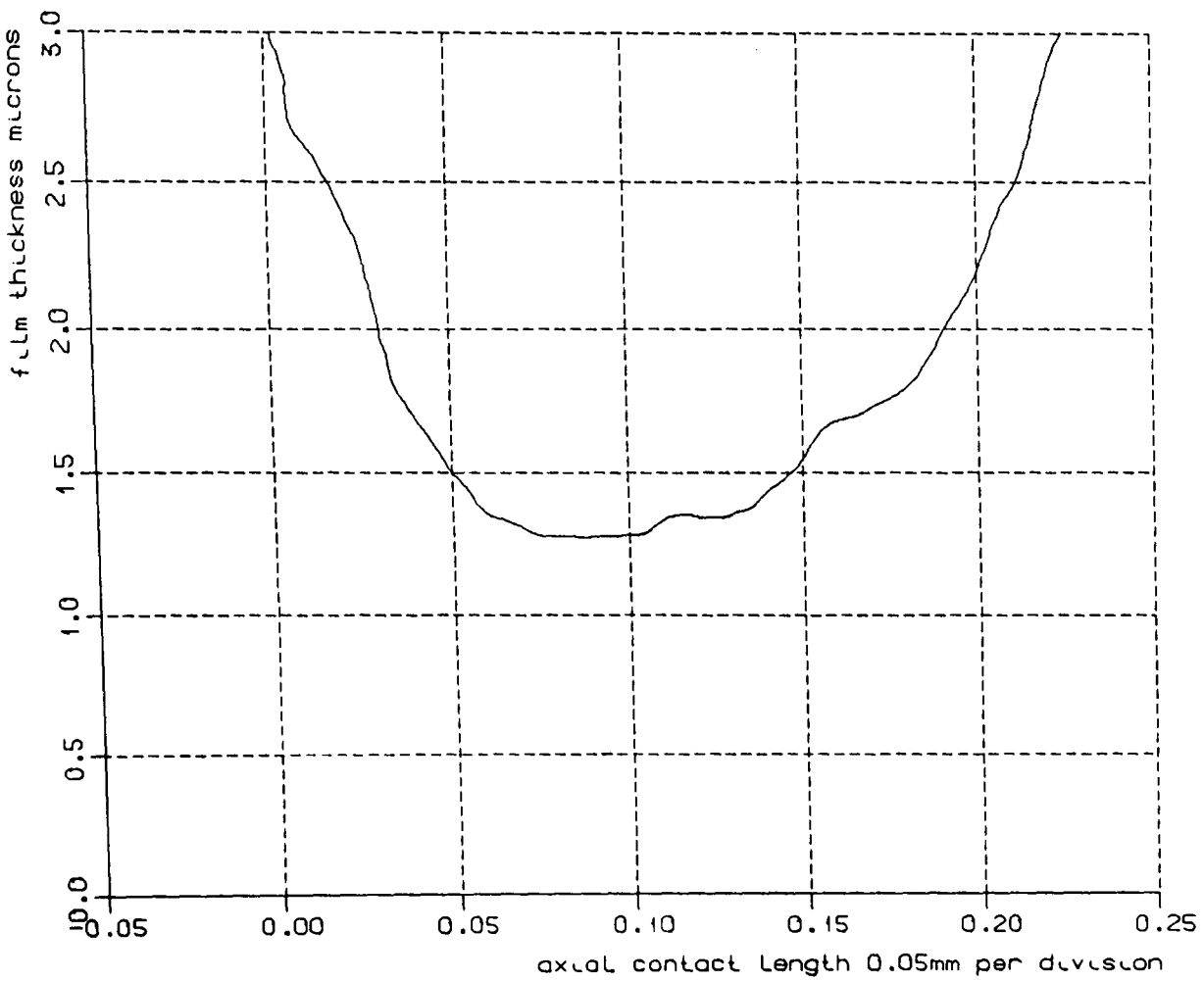

1016rpm

Fig 7.4.4 film thickness

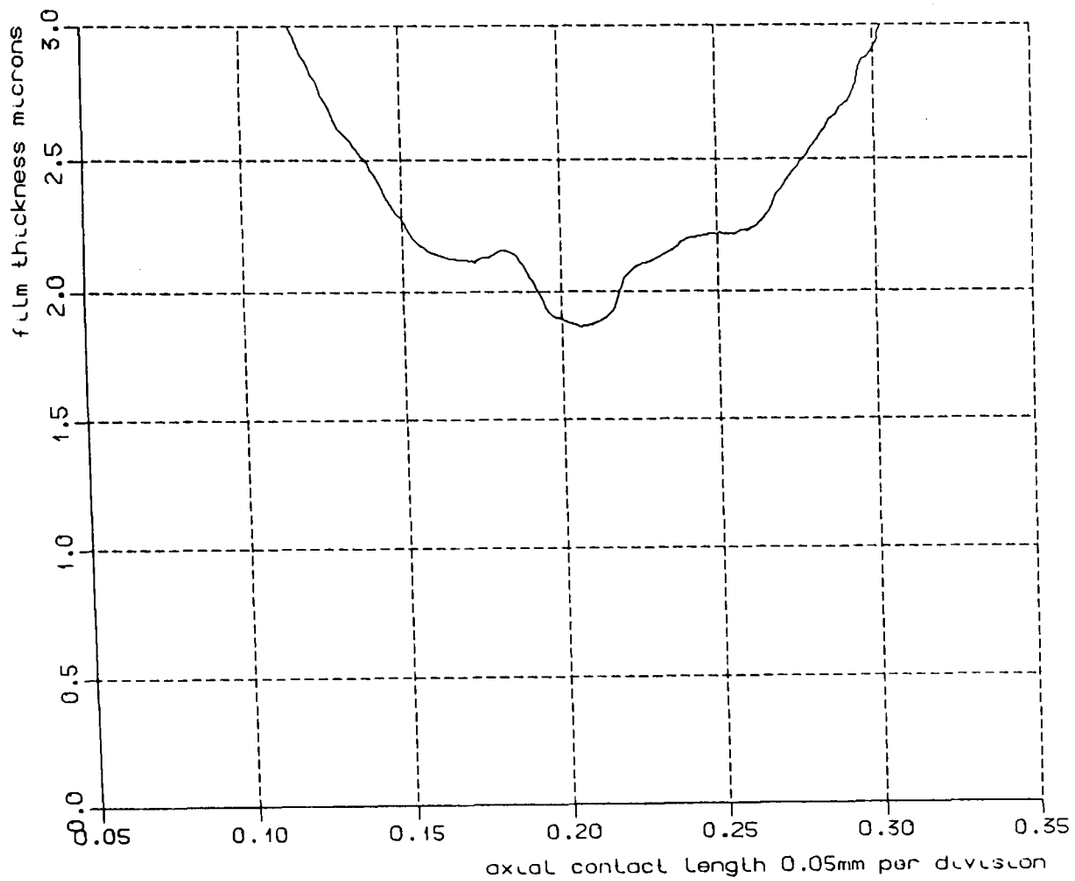

1512rpm

Fig 7.4.5 film thickness

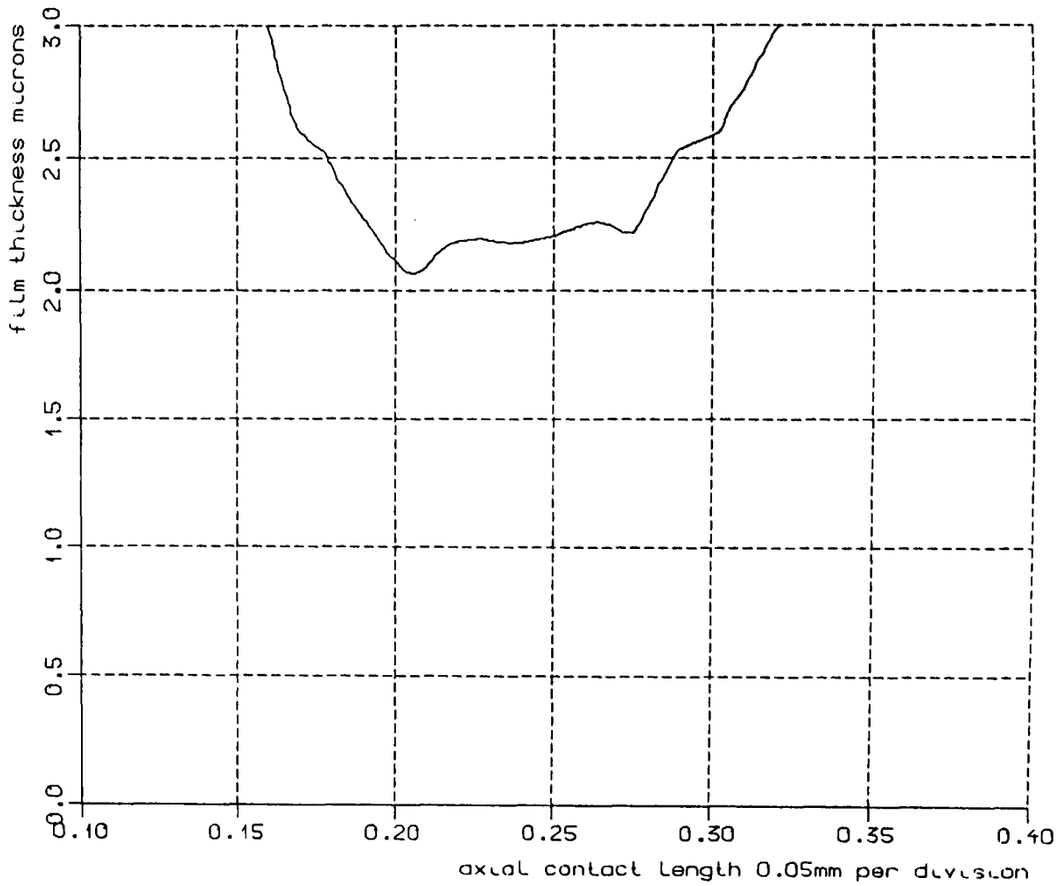

1512rpm

Fig 7.4.6 film thickness

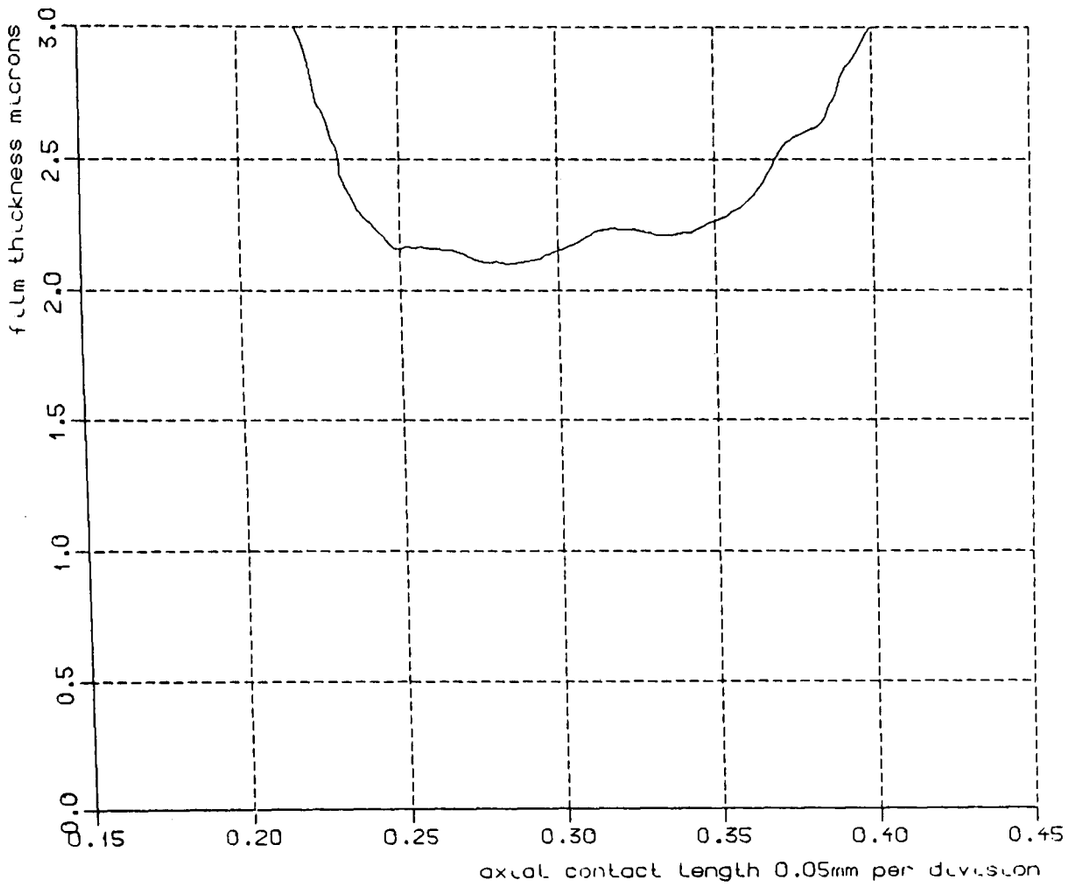

1512rpm

Fig 7.4.7 film thickness

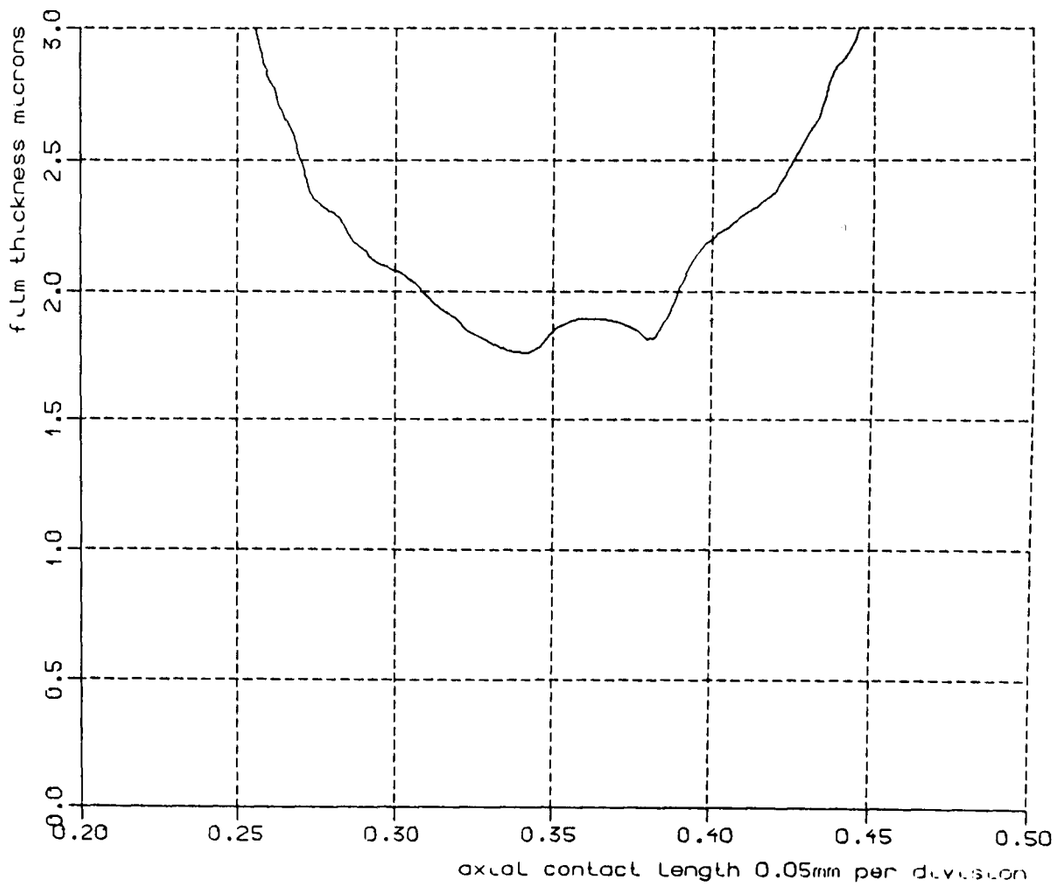

1512rpm

Fig 7.4.8 film thickness

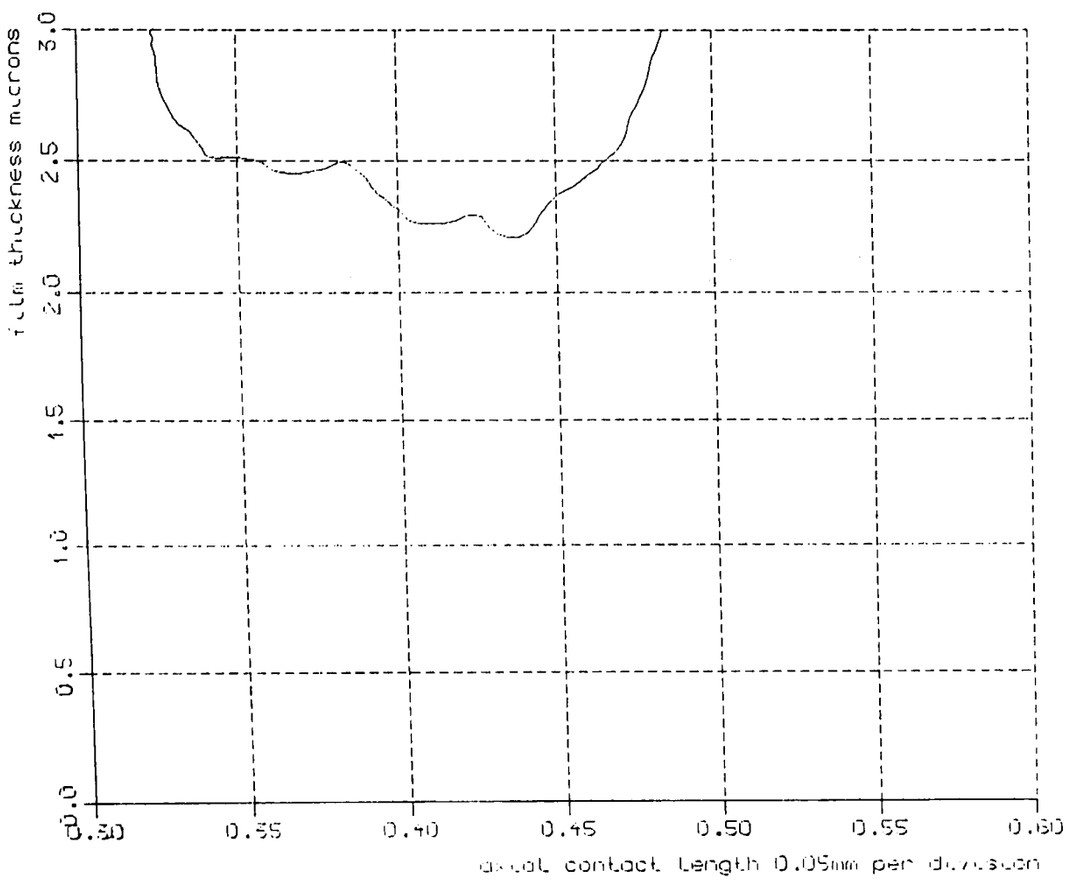

1512rpm

Fig 7.4.9 film thickness

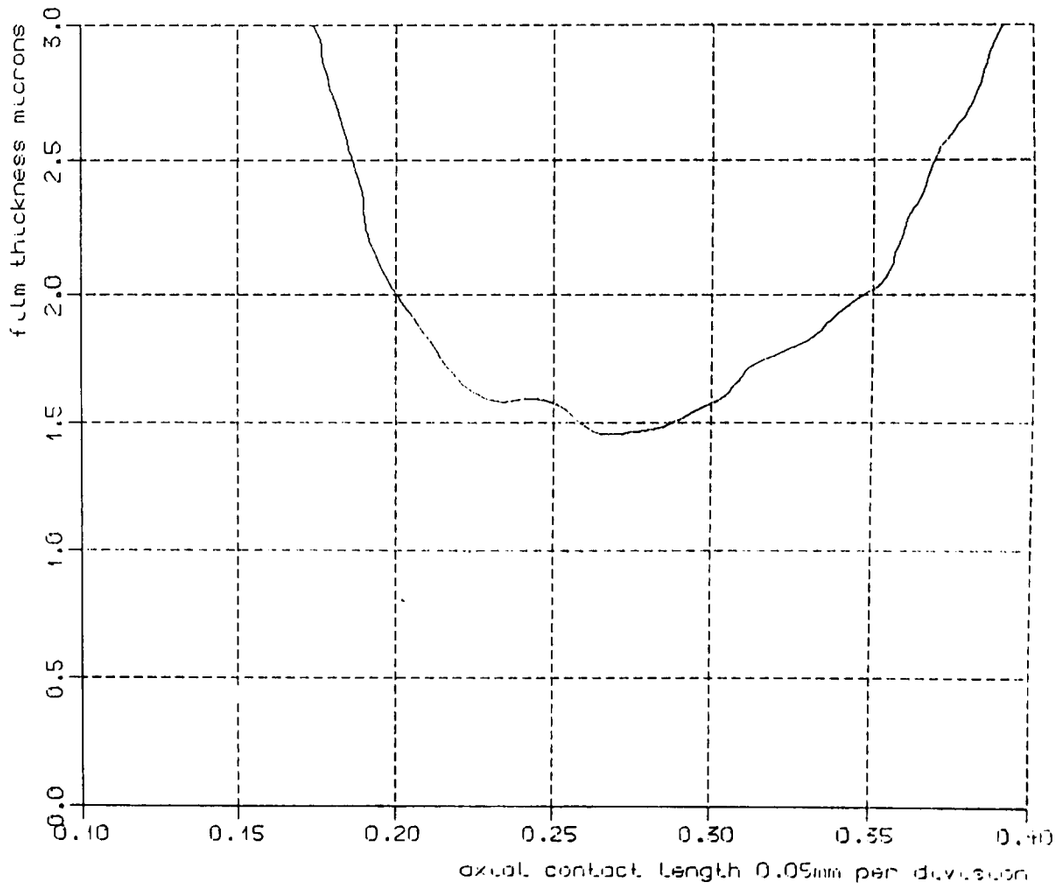

1512rpm

Fig 7.5.0 film thickness

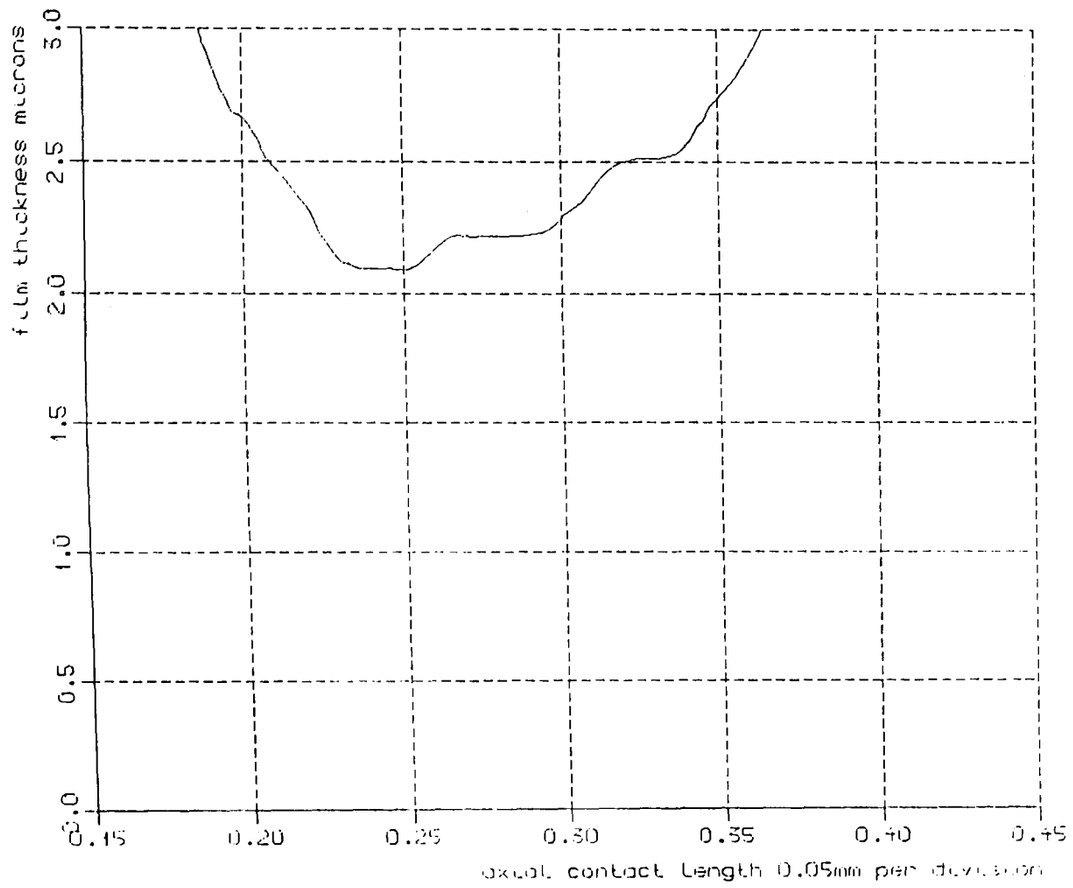

1512rpm

Fig 7.5.1 film thickness

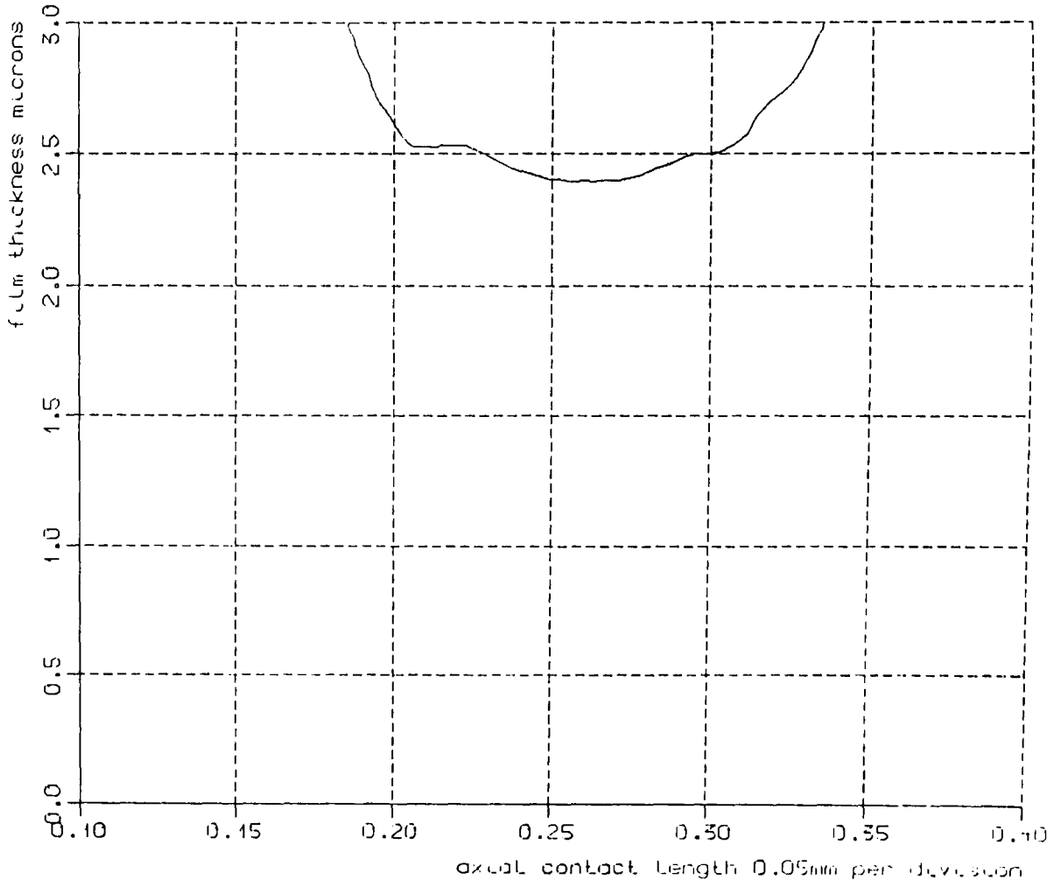

1512rpm

Fig 7.5.2 film thickness

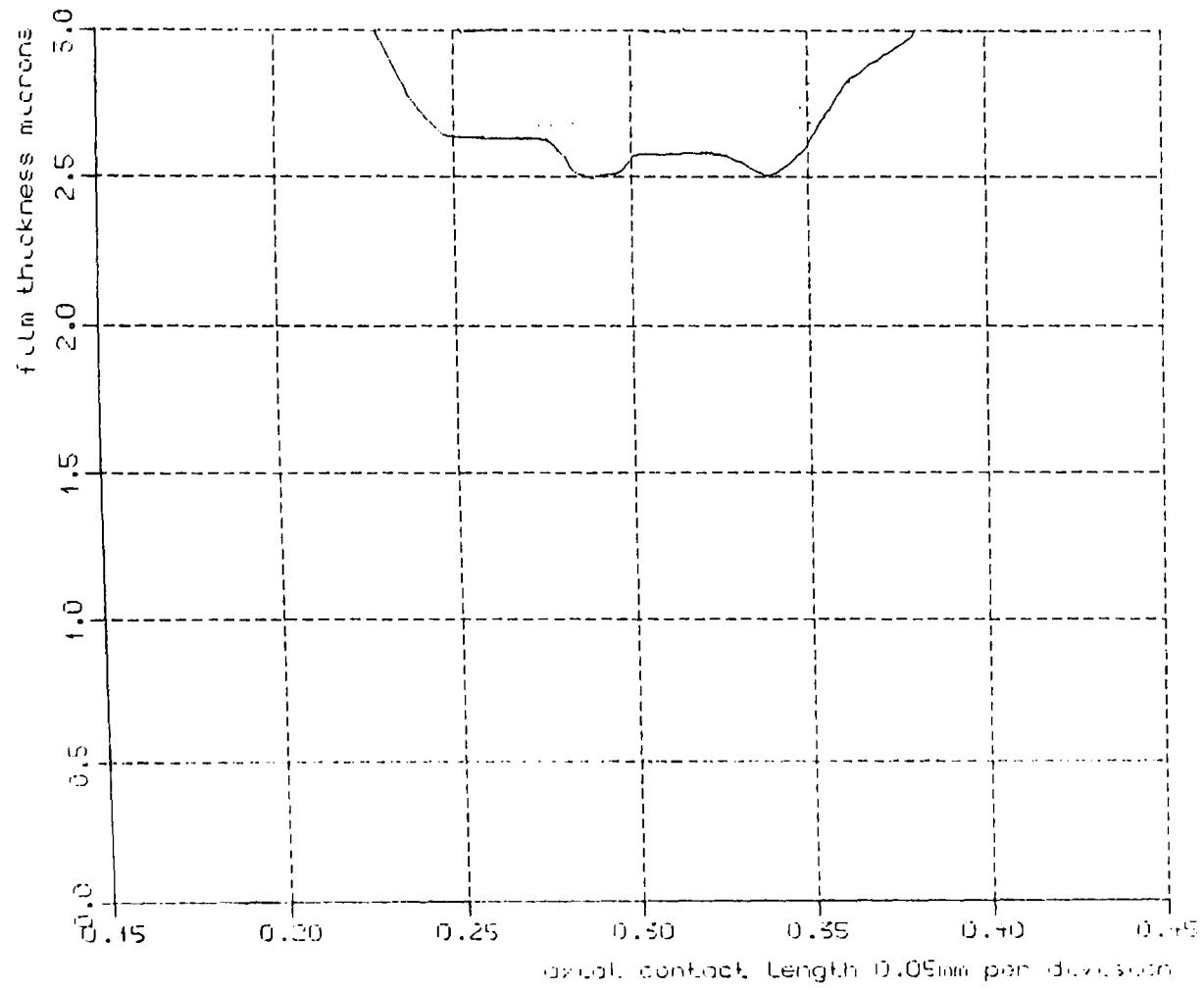

Fig 7.5.3 film thickness

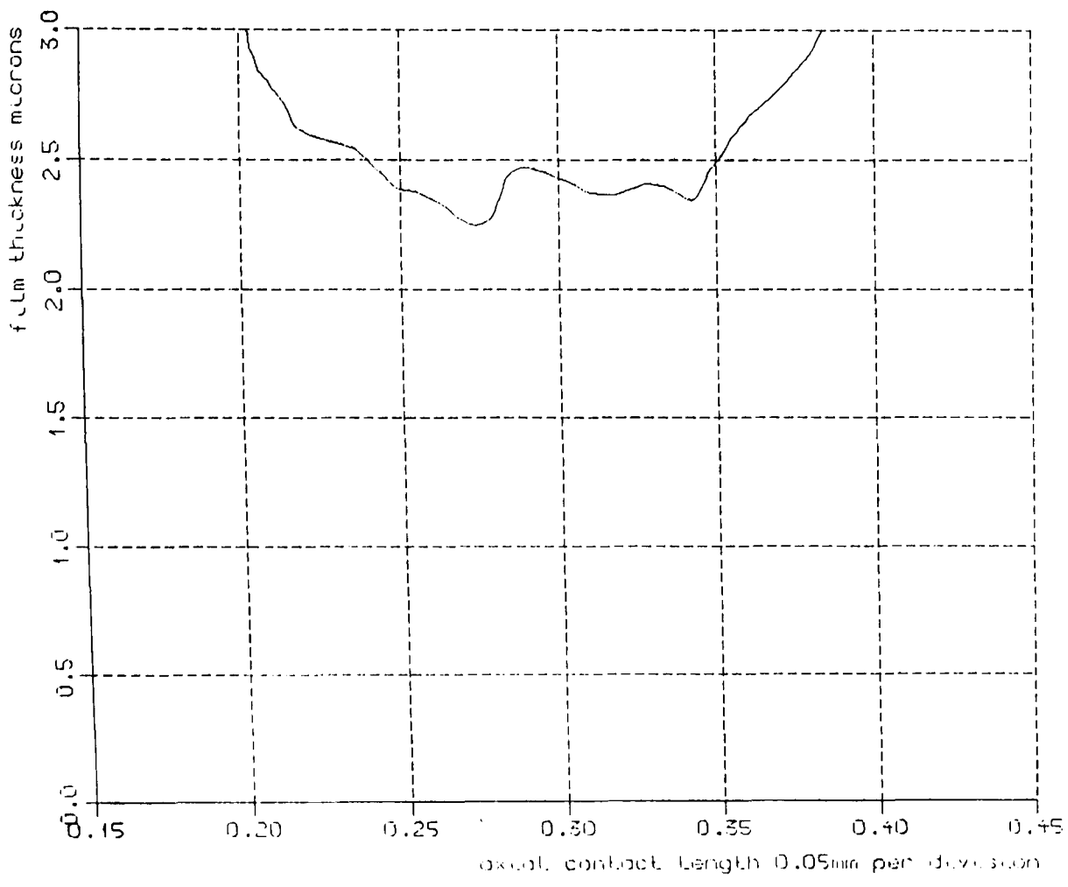

2008rpm

Fig 7.5.4 film thickness

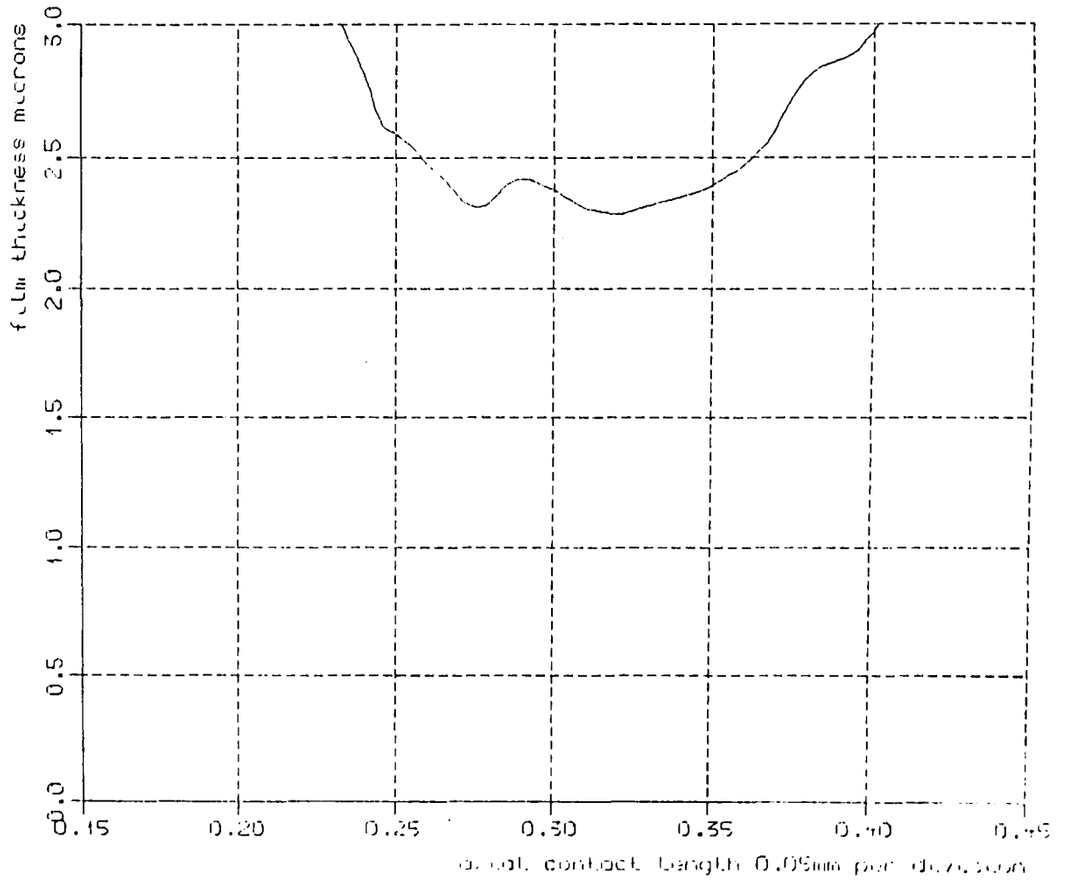

2008rpm

Fig 7.5.5 film thickness

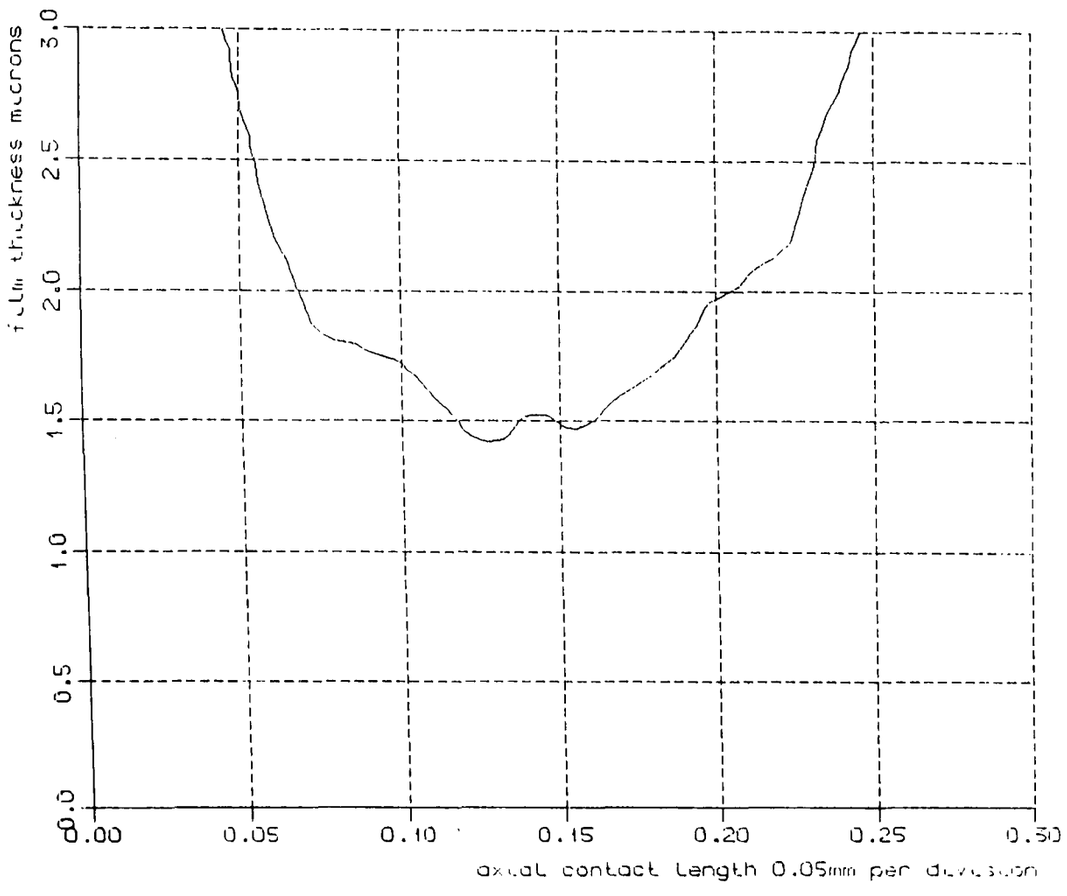

2008rpm

Fig 7.5.6 film thickness

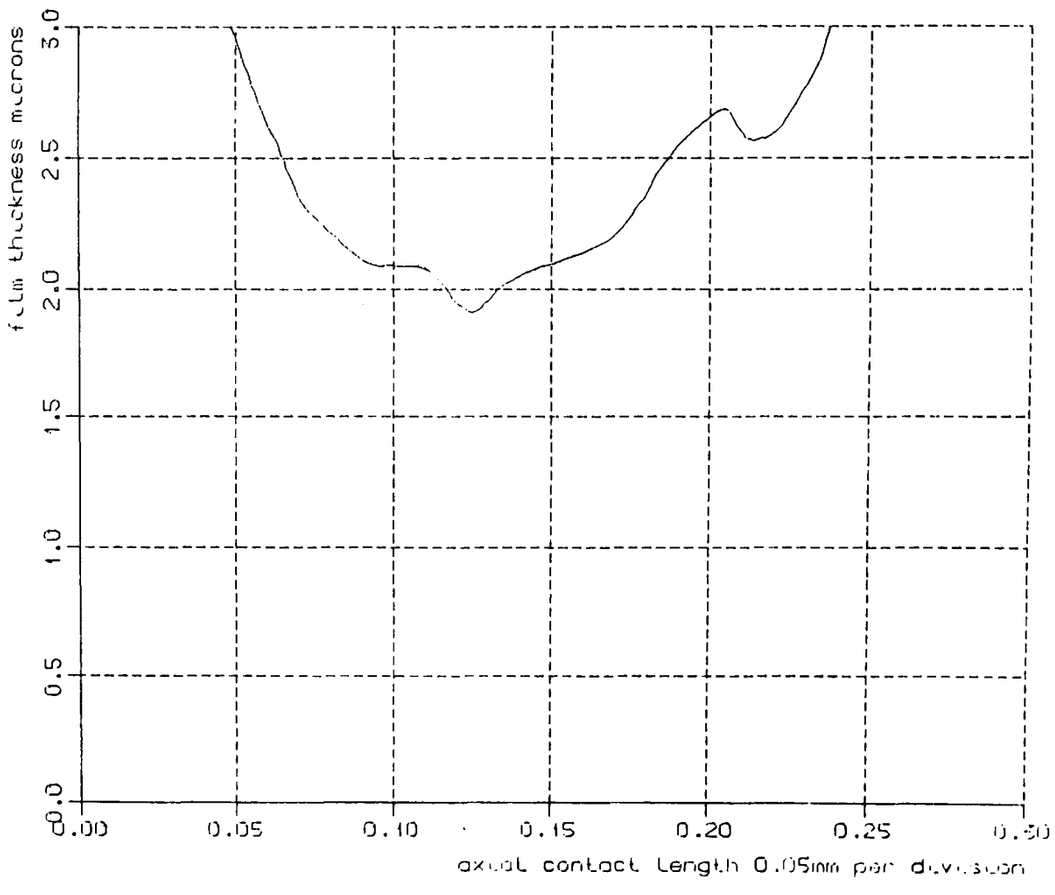

2008rpm

Fig 7.5.7 film thickness

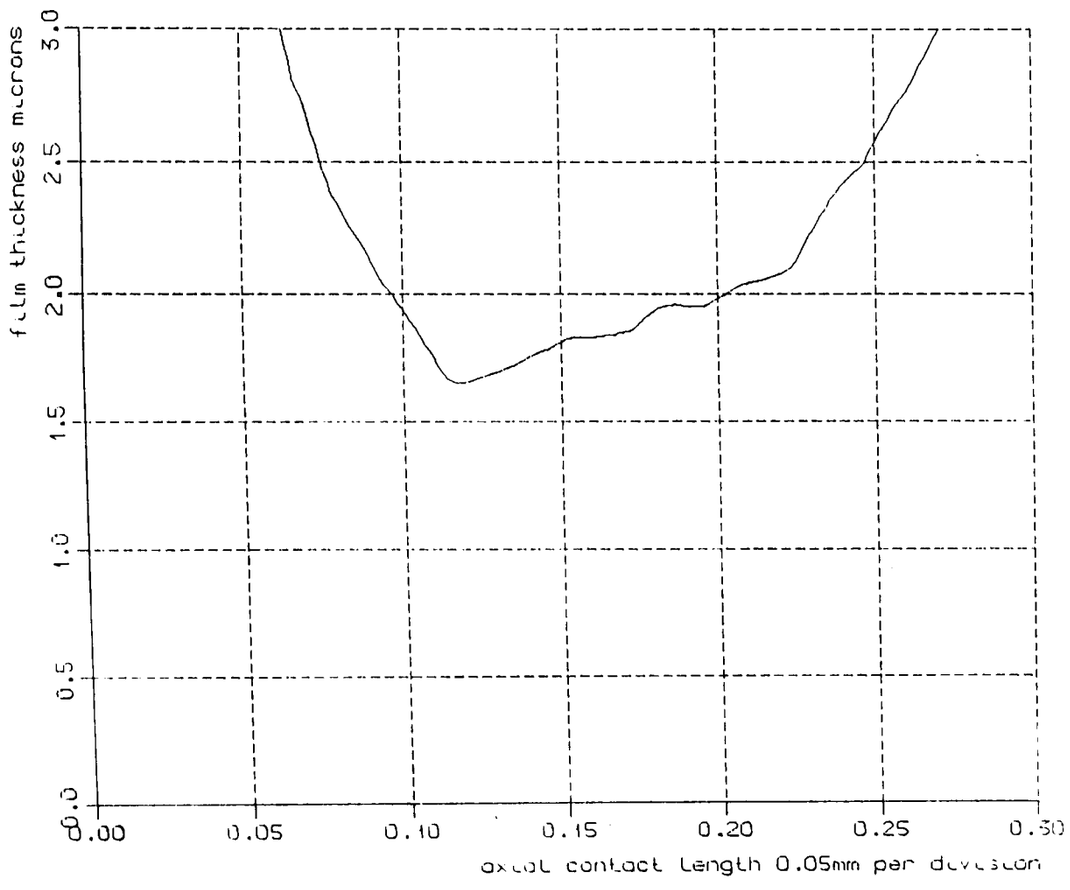

2008rpm

Fig 7.5.8 film thickness

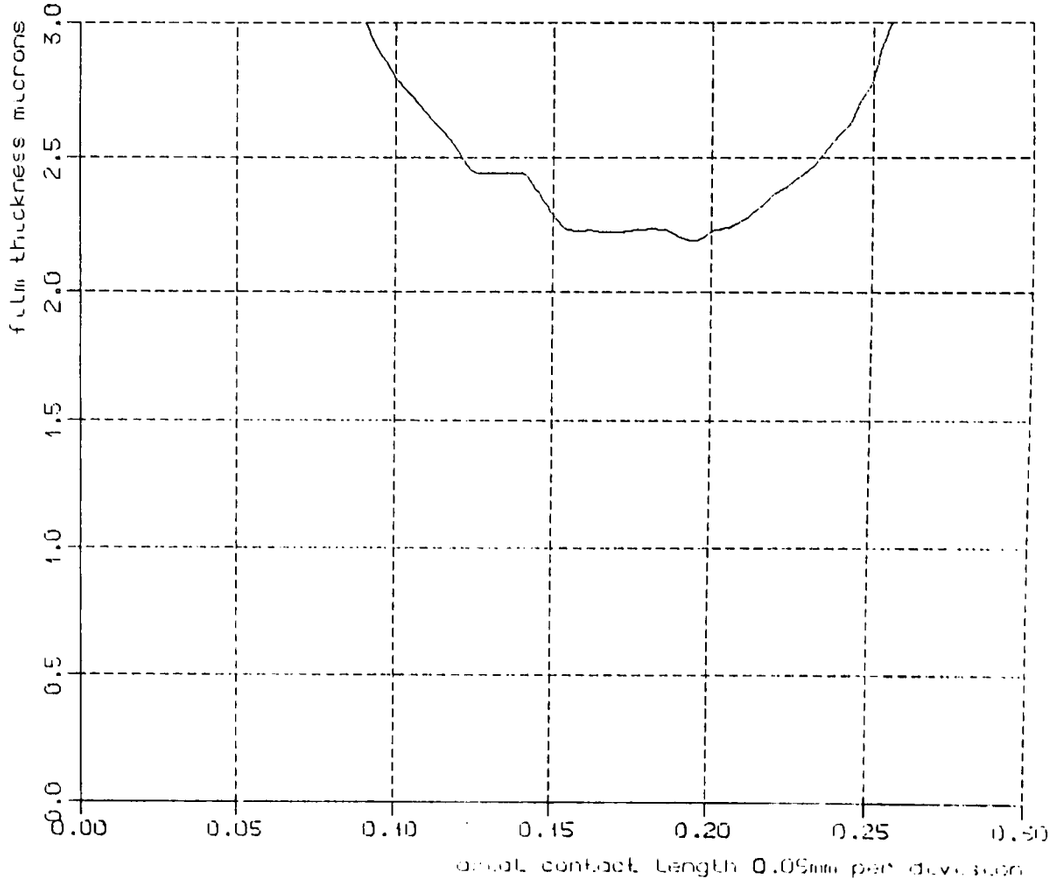

2008rpm

Fig 7.5.9 film thickness

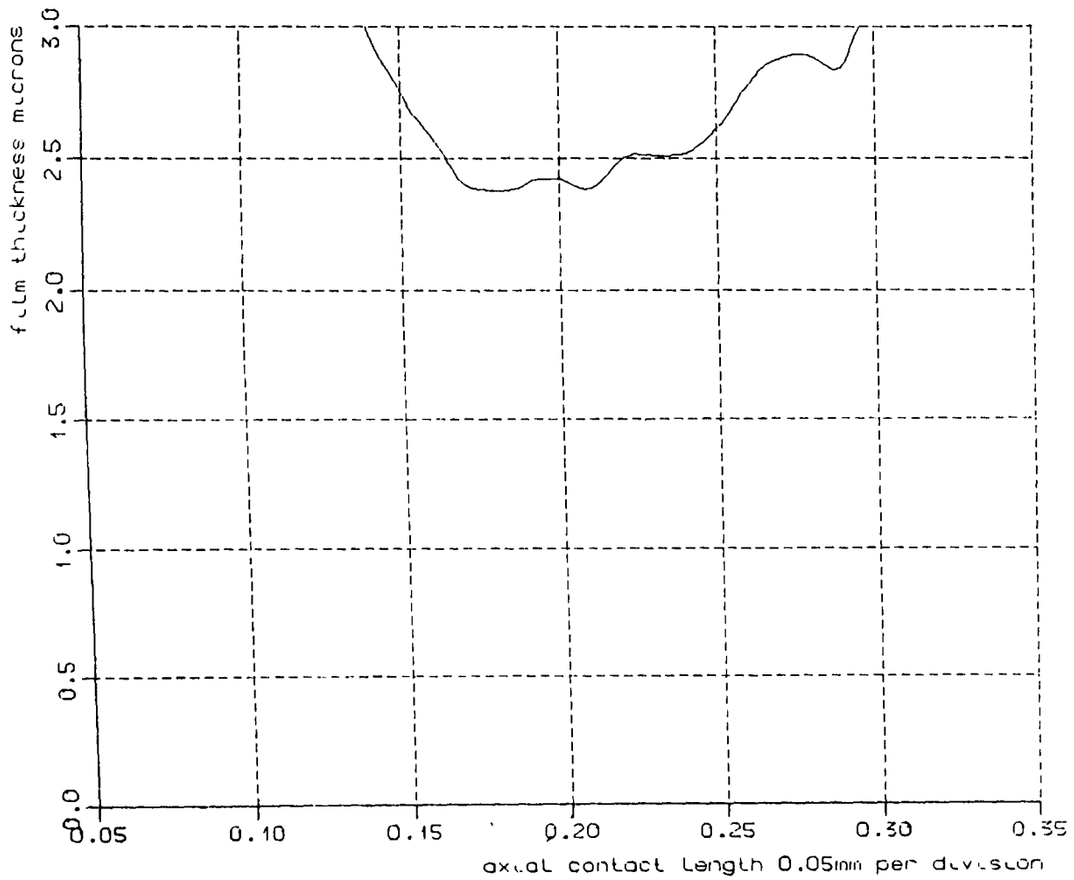

2008rpm

Fig 7.6.0 film thickness

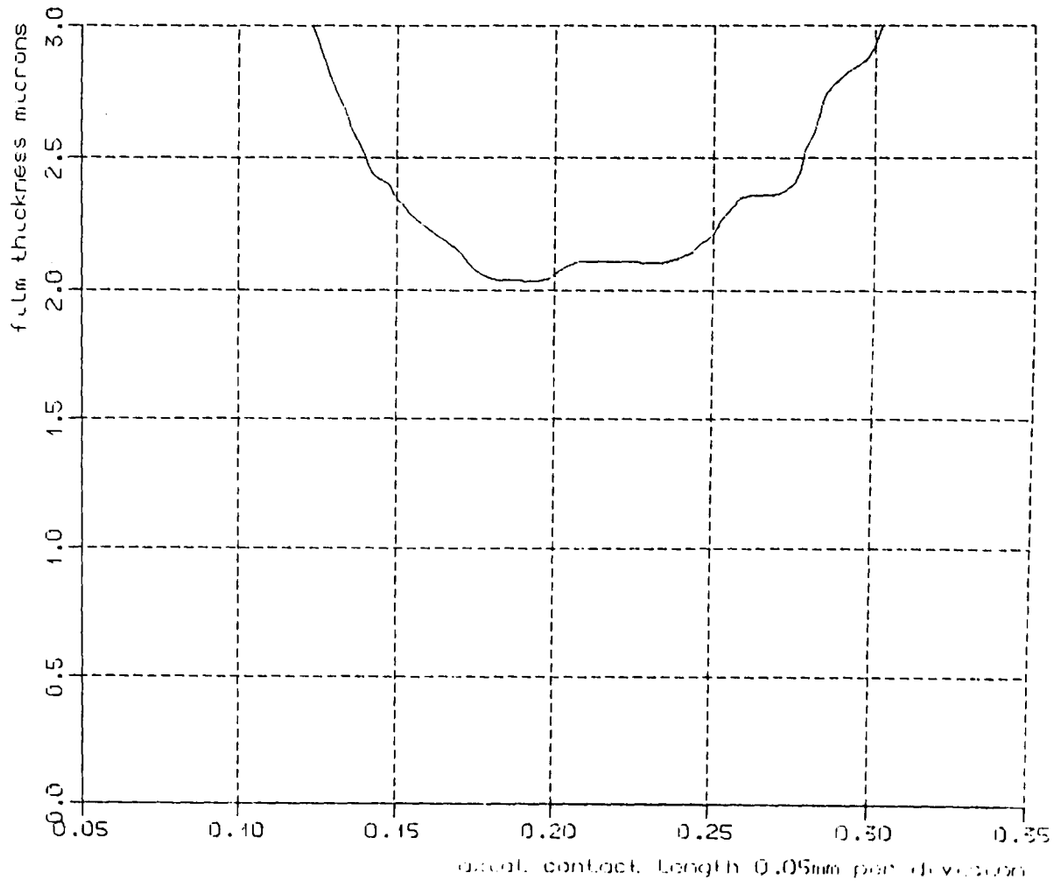

2008rpm

Fig 7.6.1 film thickness

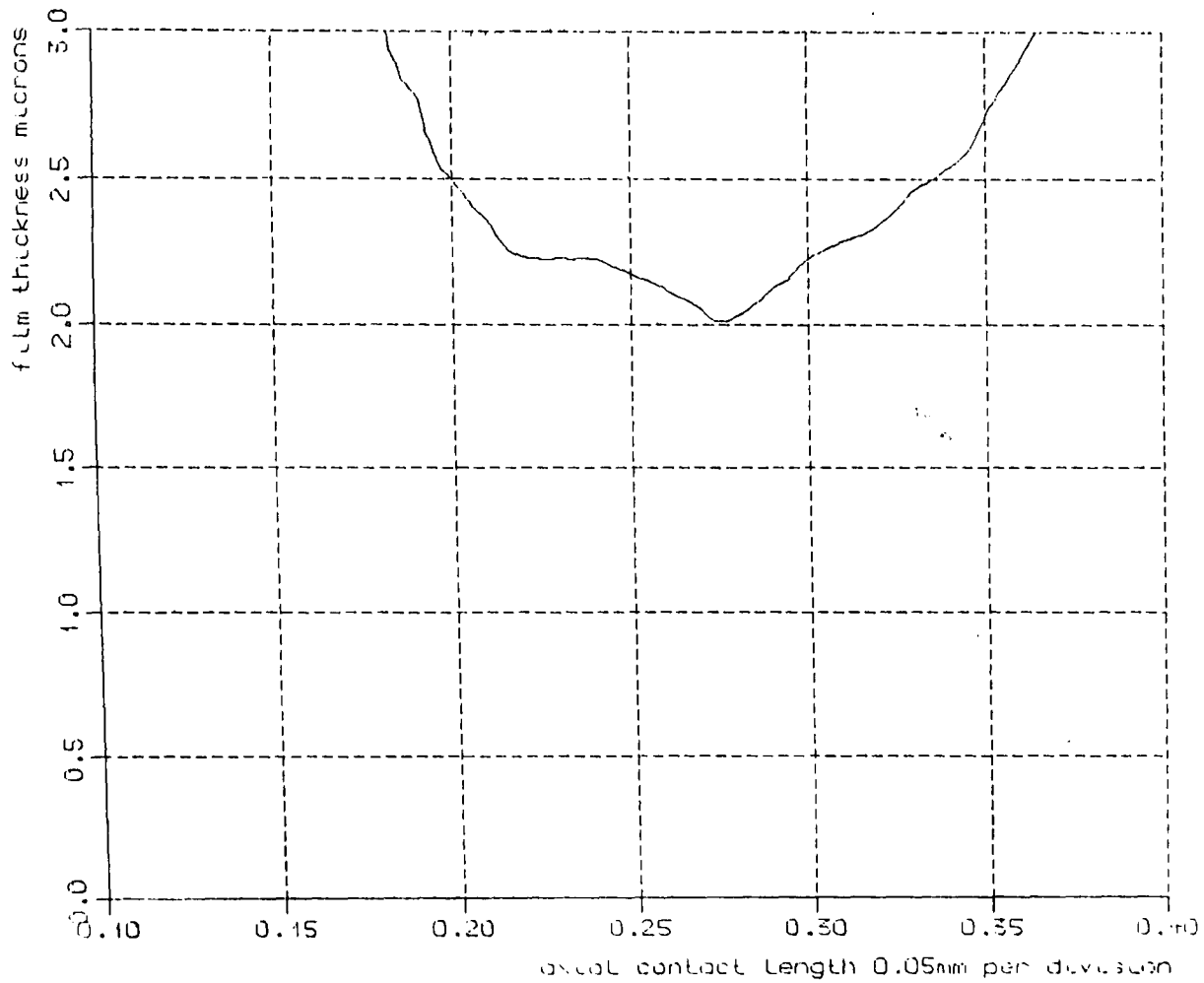

2008rpm

Fig 7.6.2 Film thickness at zero speed

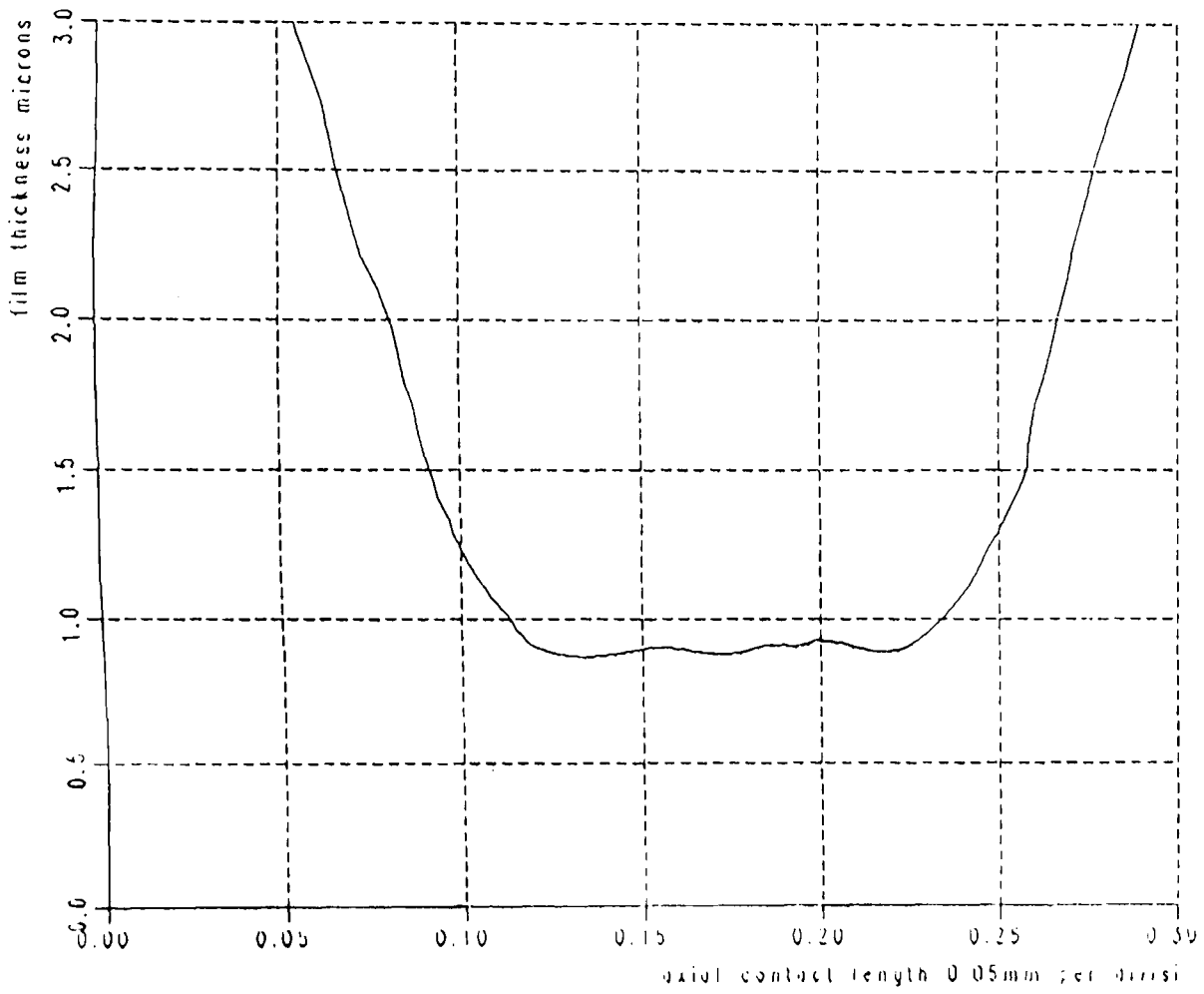

zero speed

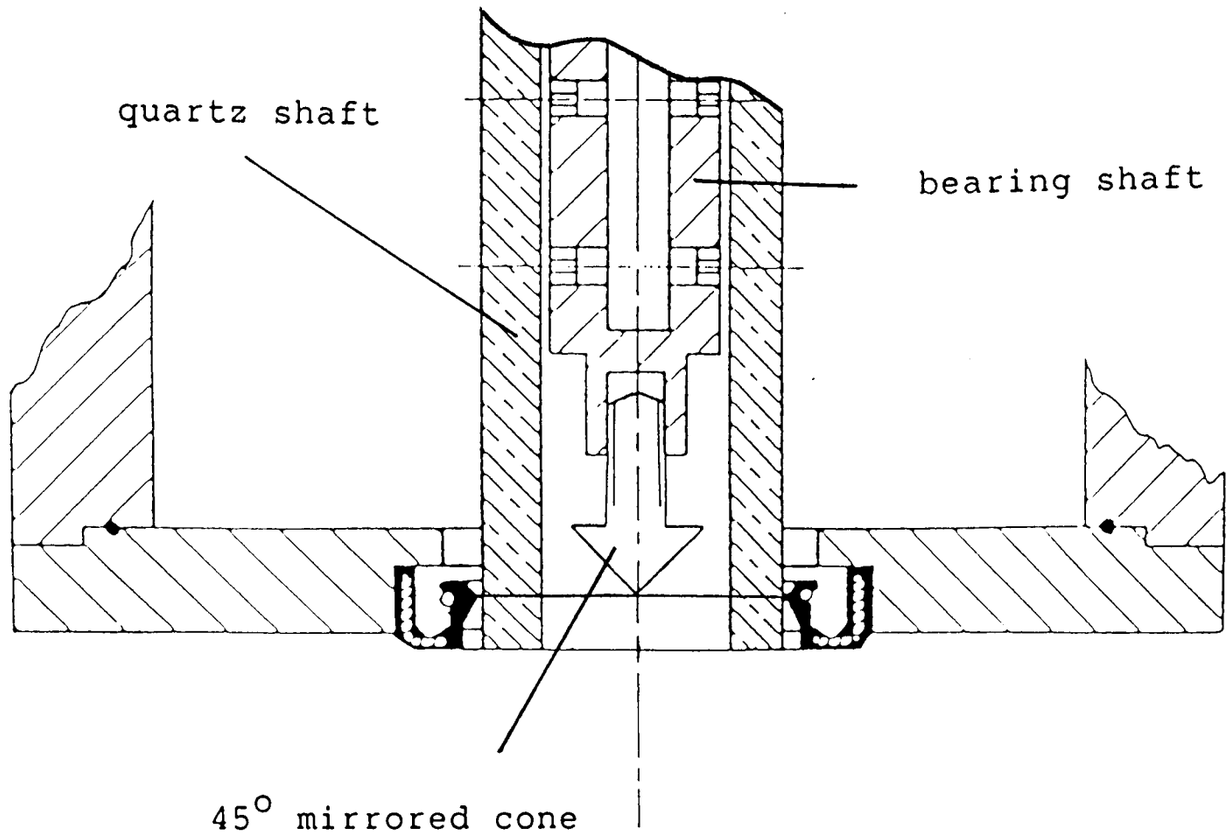

Fig 7.7.0 Laser beam-entire contact alignment

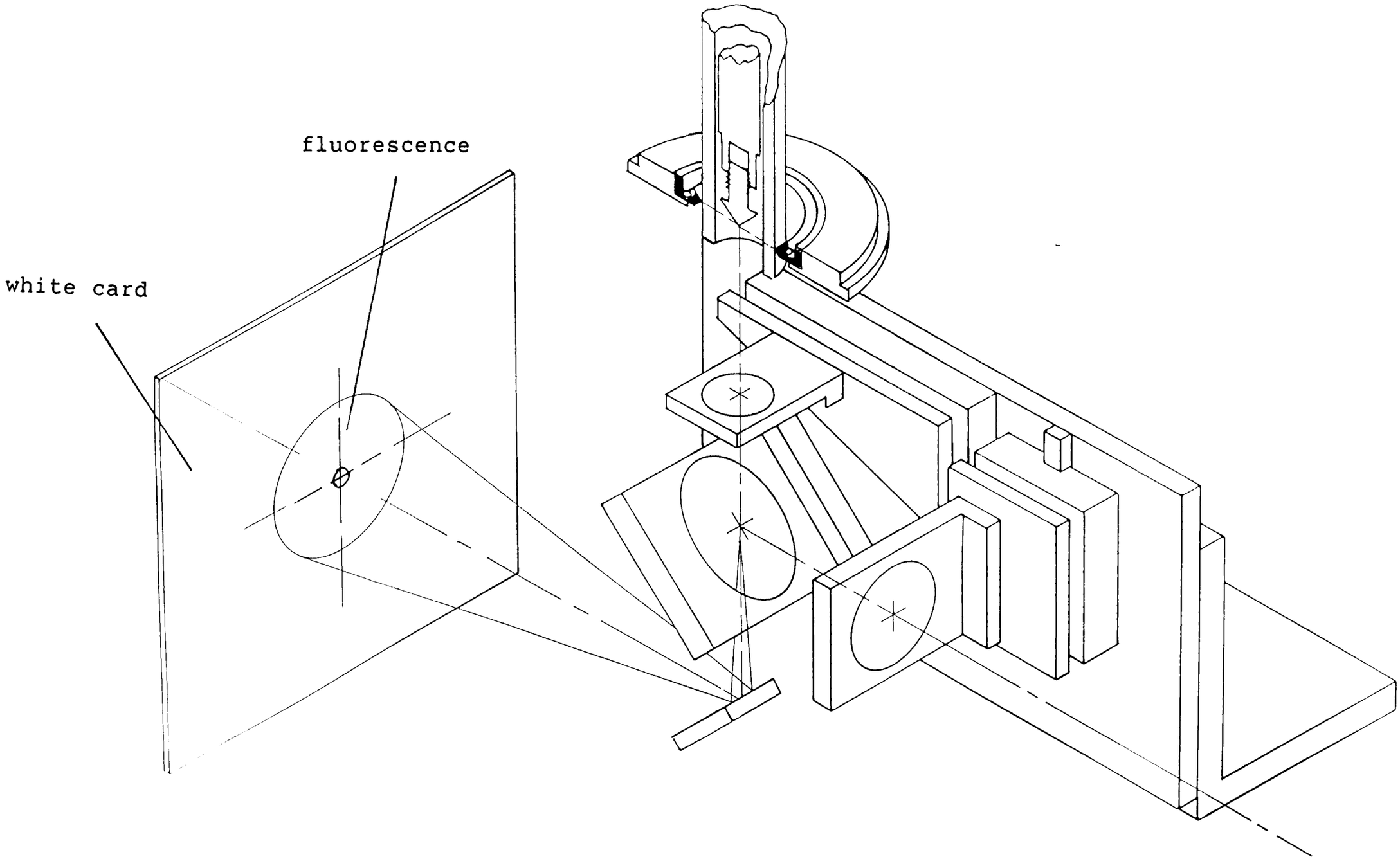

Fig 7.7.1 Laser beam-entire contact alignment

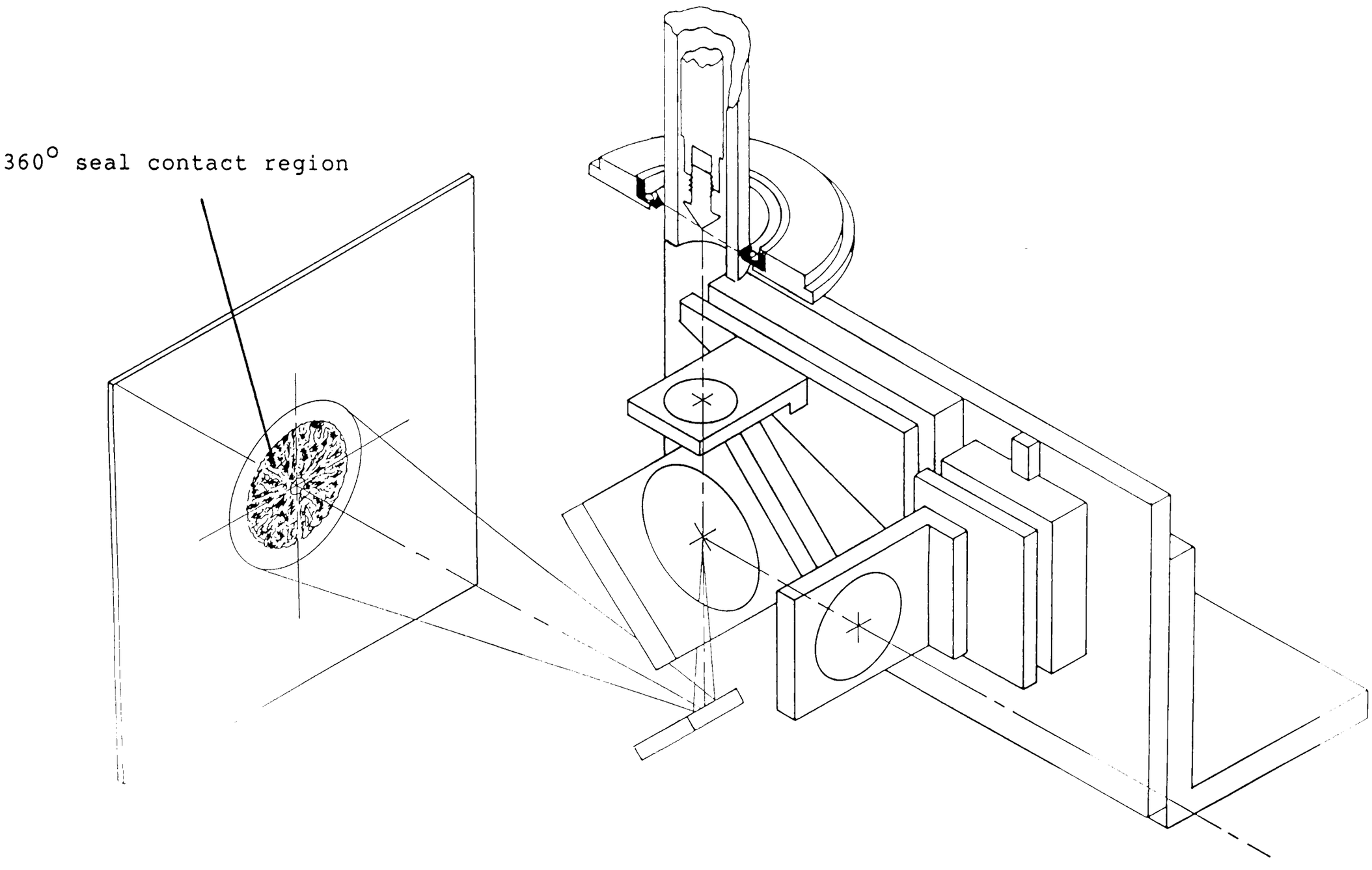

Fig 7.7.2 Laser beam-entire contact alignment

F1 - Analysis
F2 - Graph
F3 - Dump
F4 - Expand
F5 - Exclude
F6 - Z_Range

Mode	Cut Off	Filter	Reference	Ignore
ROUGHNESS	0.80 mm	ISO	STRAIGHT	0 %

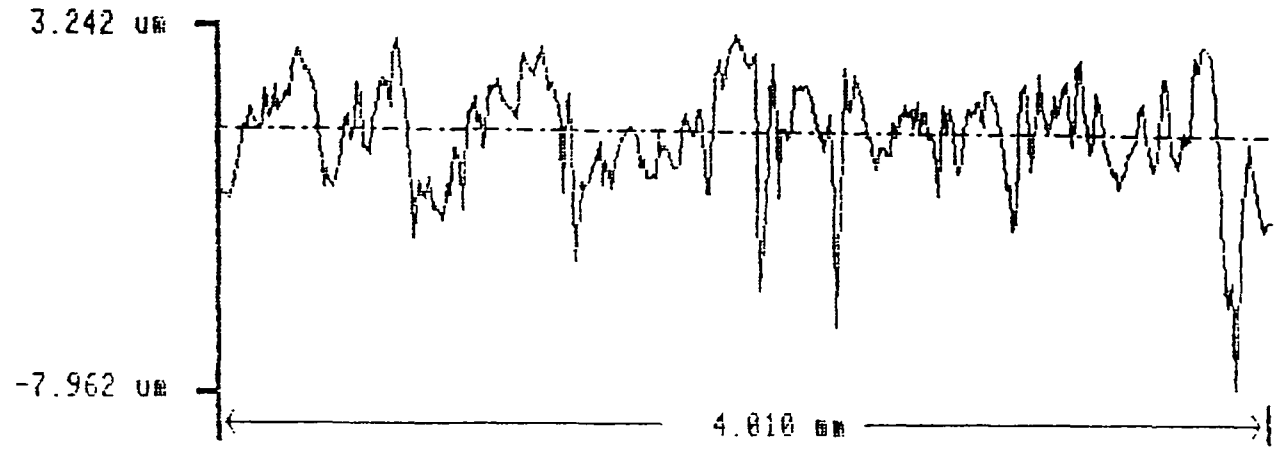

Peak To Valley = 11.204 um

Taylor-Hobson

F1 - Analysis

Mode	Cut Off	Filter	Reference	Ignore
ROUGHNESS	0.80 mm	ISO	STRAIGHT	0 %

Rtm	=	8.255 um	Lo	=	4.010 mm	Ra	=	1.245 um
Rpm	=	2.785 um	Rp	=	3.242 um	Rq	=	1.628 um
Ry	=	10.850 um	Rv	=	7.962 um	Rsk	=	-1.0
Rt1	=	6.918 um	Rt	=	11.204 um	Rku	=	5.1
Rt2	=	6.600 um				Delq	=	6.34 Deg
Rt3	=	9.967 um	SLOPE	=	-.63 Deg	Lamq	=	92.012 um
Rt4	=	6.939 um				S	=	35.920 um
Rt5	=	10.850 um				Sm	=	122.604 um
						R3z	=	4.726 um
						R3y	=	5.559 um

Taylor-Hobson

Fig 7.7.3 The roughness of the test seal contact

Table 8.0.2 Heights of the roughness peaks from the mean line

Peak number	Height of peak from mean line hx10-3 [mm]
1	0.63
2	1.25
3	1.34
4	2.42
5	0.54
6	1.43
7	1.61
8	2.78
9	-1.43
10	-1.43
11	1.08
12	1.88
13	2.33
14	2.69
15	1.17
16	-0.36
17	0.18
18	-0.36
19	0.54
20	0.72
21	2.24
22	2.96
23	2.42
24	2.06
25	2.24

$\overline{X} = 1.26 \times 10^{-3}$ mm

$X\sigma n = 1.22 \times 10^{-3}$ mm

Table 8.0.3 Estimating the peak summit curvature K_s

Peak number	Height of peak from base line $h \times 10^{-3}$ [mm]	Width of peak at base line $w \times 10^{-3}$ [mm]	K_s $[mm]^{-1}$
1	0.63	55.2	1.65
2	0.81	33.1	5.89
3	0.17	38.7	3.83
4	1.79	132.6	0.81
5	0.72	44.2	2.94
6	1.61	55.2	4.23
7	0.99	55.2	2.62
8	2.06	55.2	5.41
9	1.34	88.4	1.37
10	1.88	88.4	1.93
11	1.35	55.2	3.54
12	1.26	77.3	1.69
13	0.90	44.2	3.67
14	1.17	88.4	1.20
15	2.87	44.2	11.86
16	1.08	99.4	0.88
17	0.63	77.3	0.84
18	0.72	66.3	1.30
19	0.63	44.2	2.57
20	0.81	33.1	5.89
21	0.90	33.1	6.54
22	1.17	77.3	1.57
23	0.54	33.1	3.93
24	3.85	55.2	10.11
25	2.78	132.6	1.27

$\overline{K}_s = 3.501 \text{ mm}^{-1}$

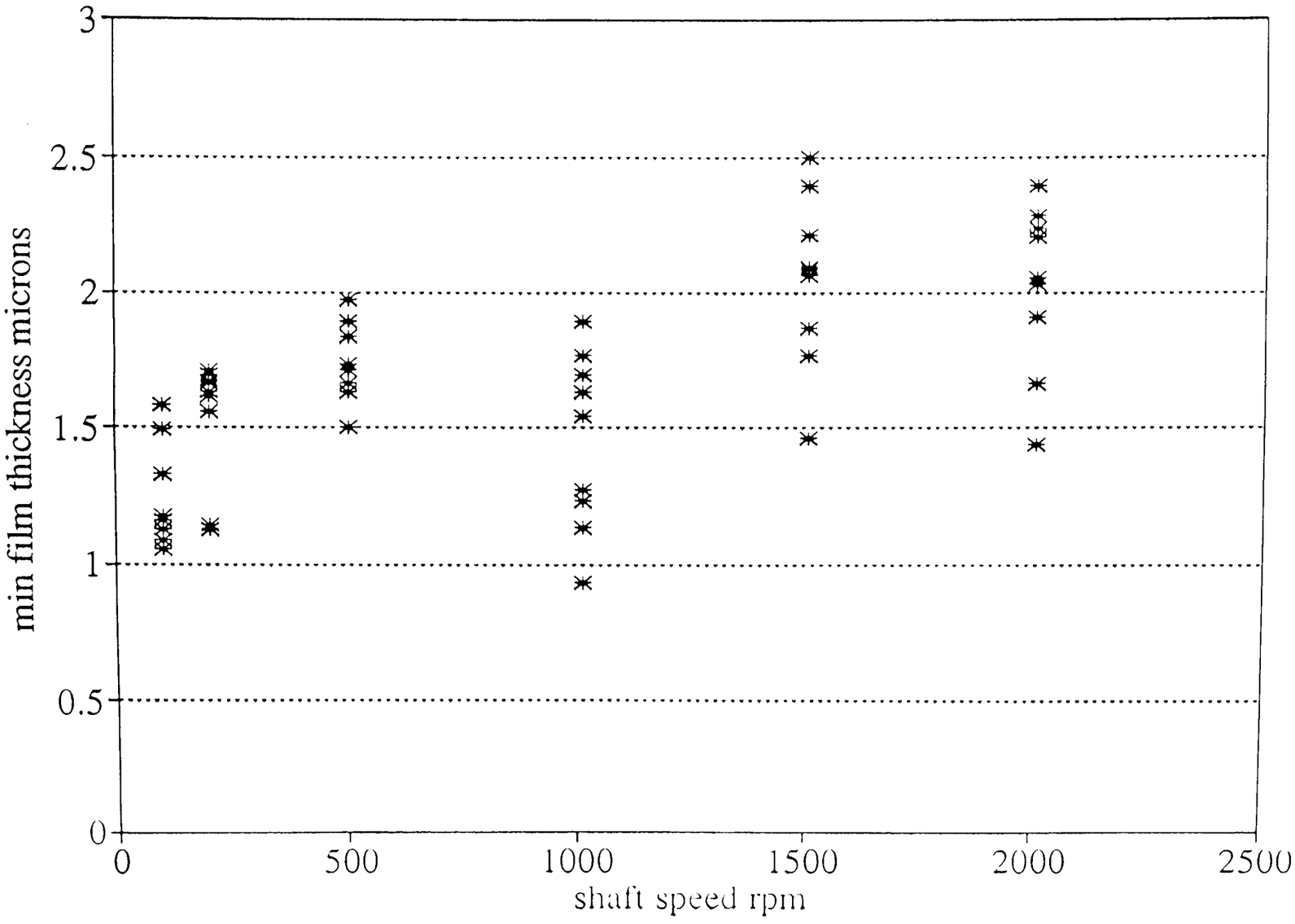

Fig 8.0.0 Variation in measured minimum film thickness at each speed

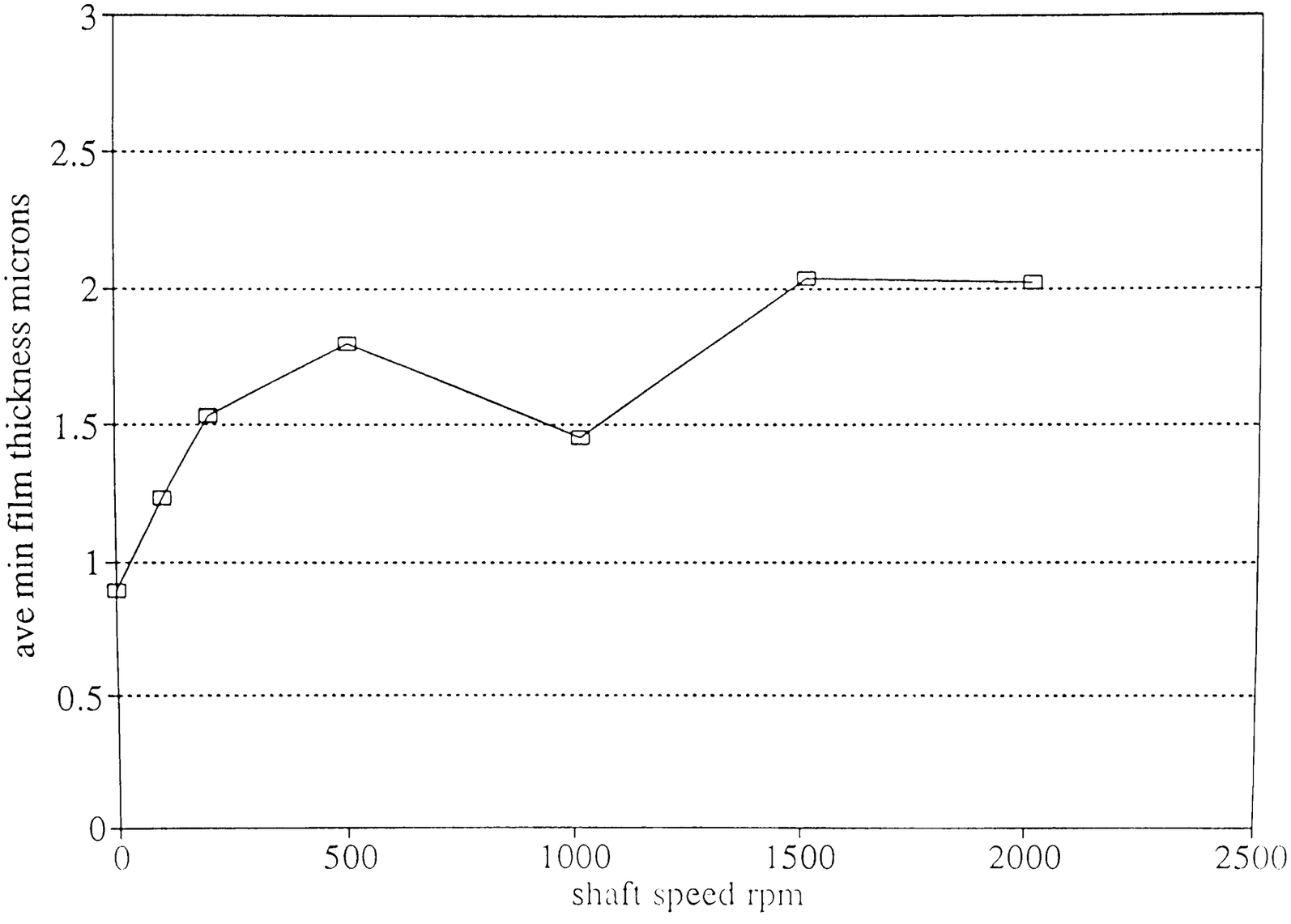

Fig 8.0.1 **Average minimum film thickness at each speed**

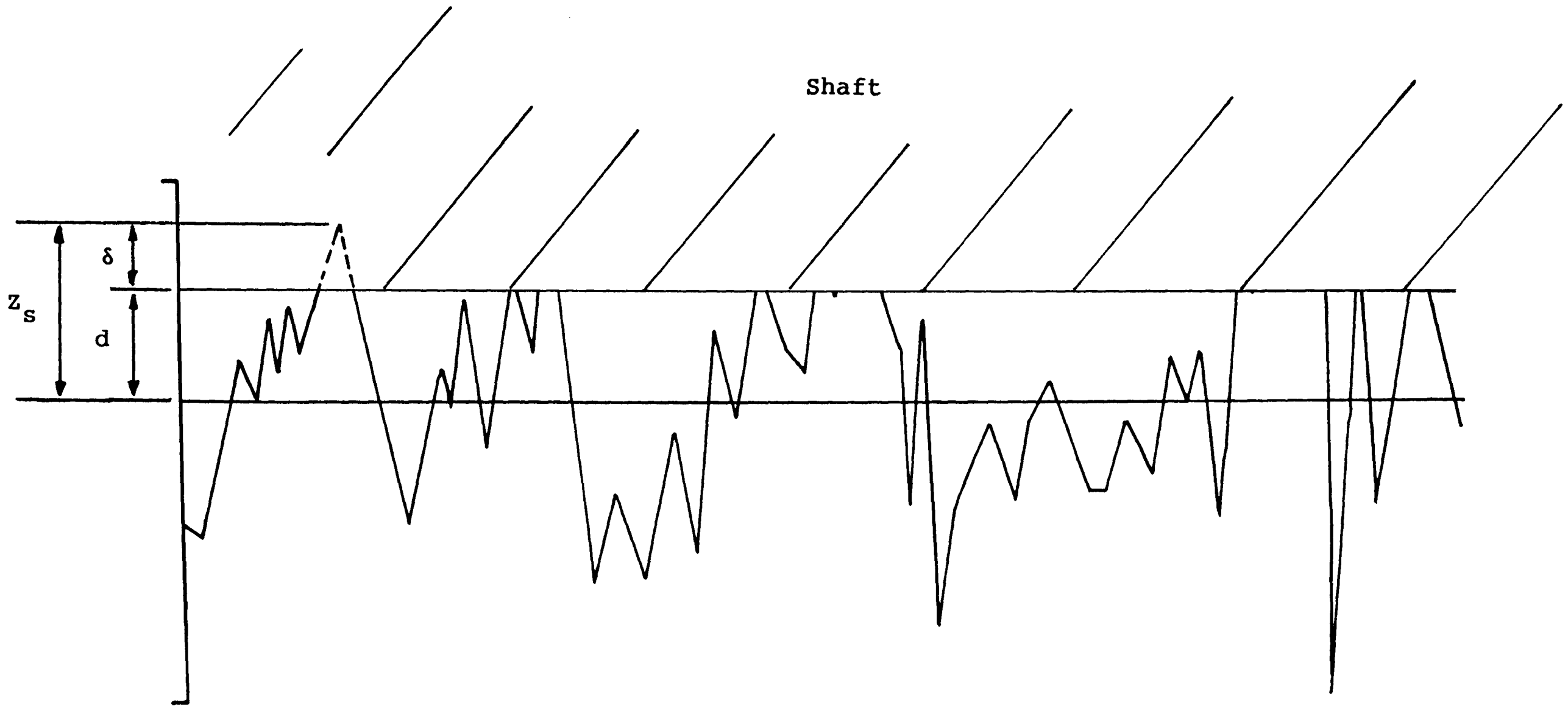

Fig 8.0.3 Seal contacting the shaft

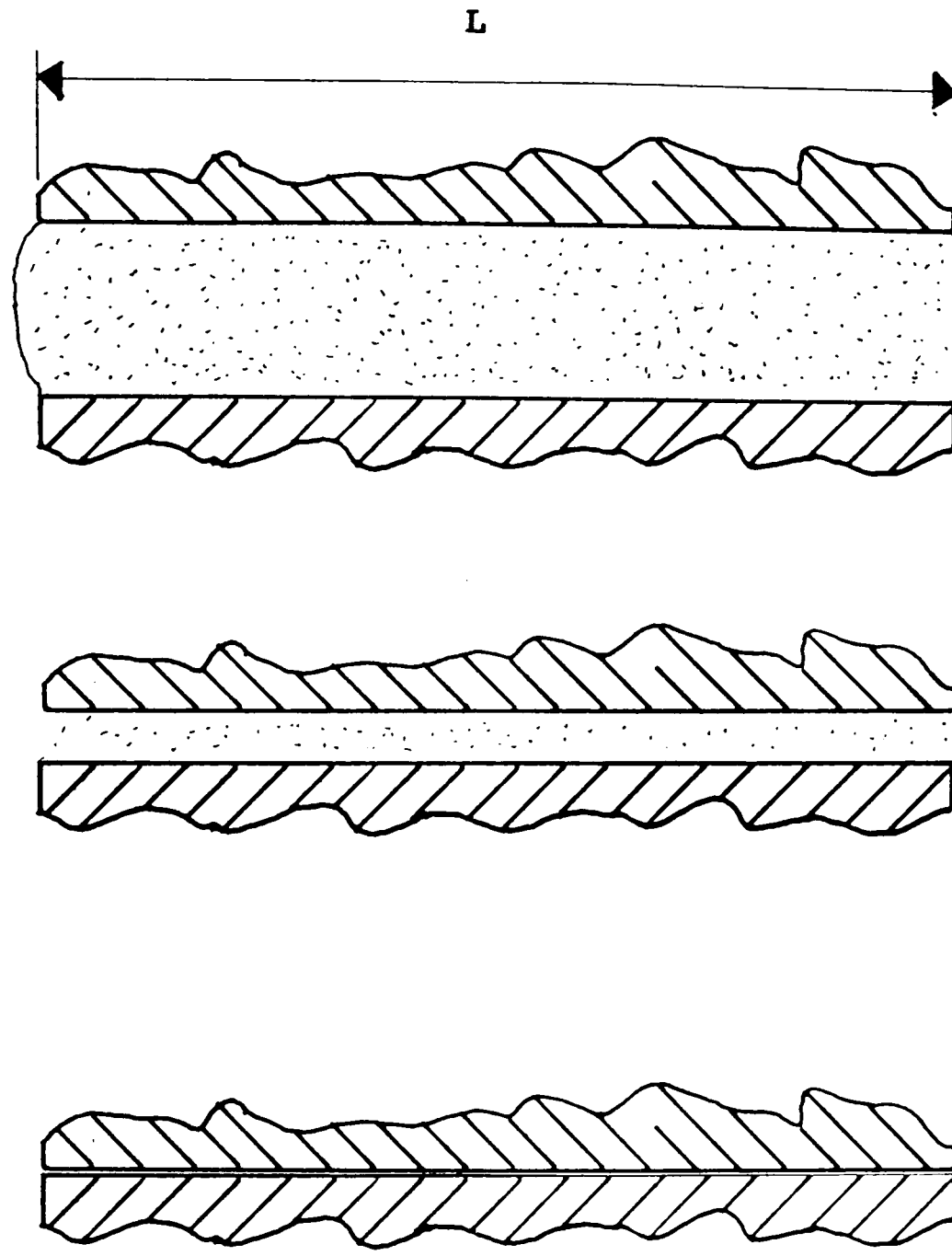

Fig 8.0.4 Two flat bodies approaching

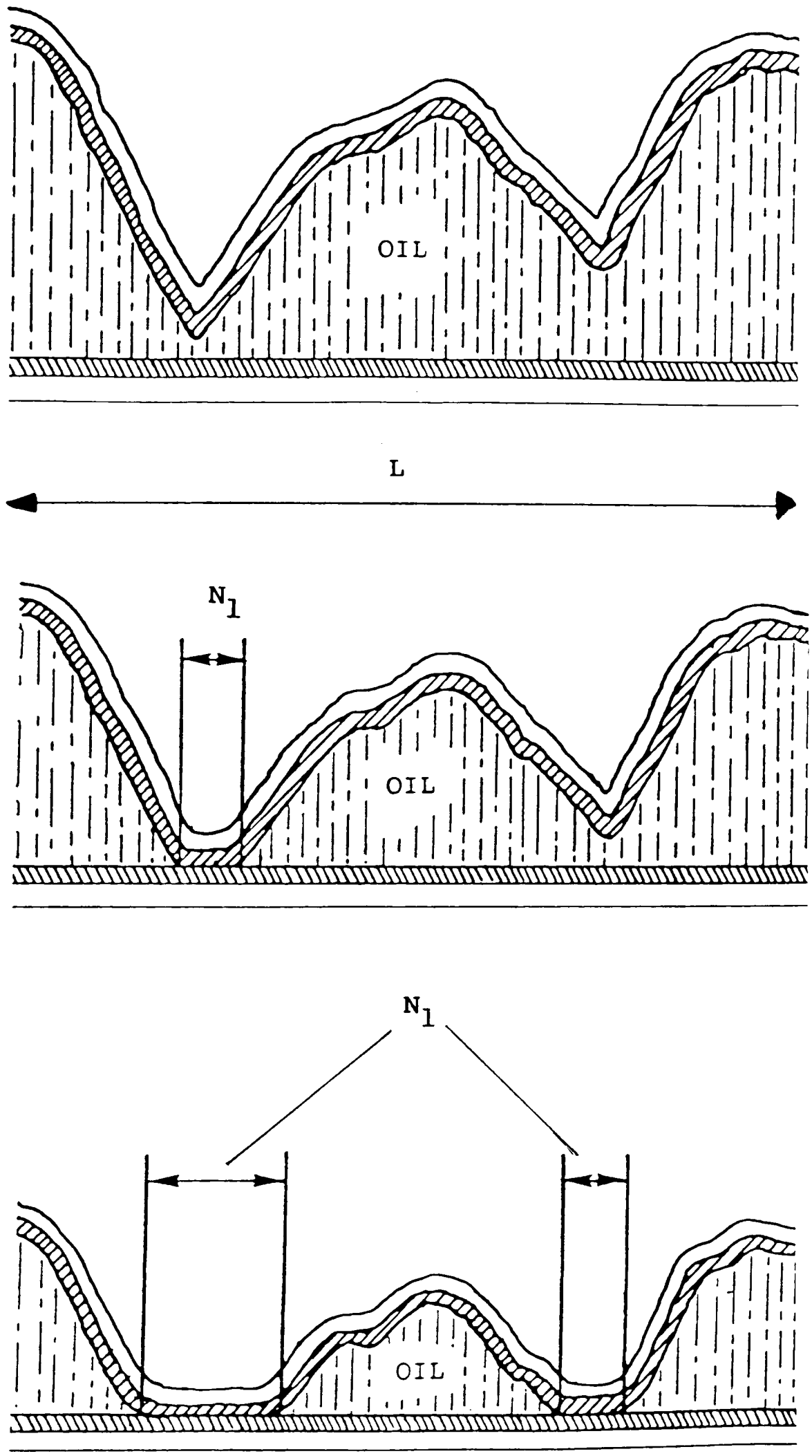

Fig 8.0.5 Two bodies approaching; One has two dimensional roughness

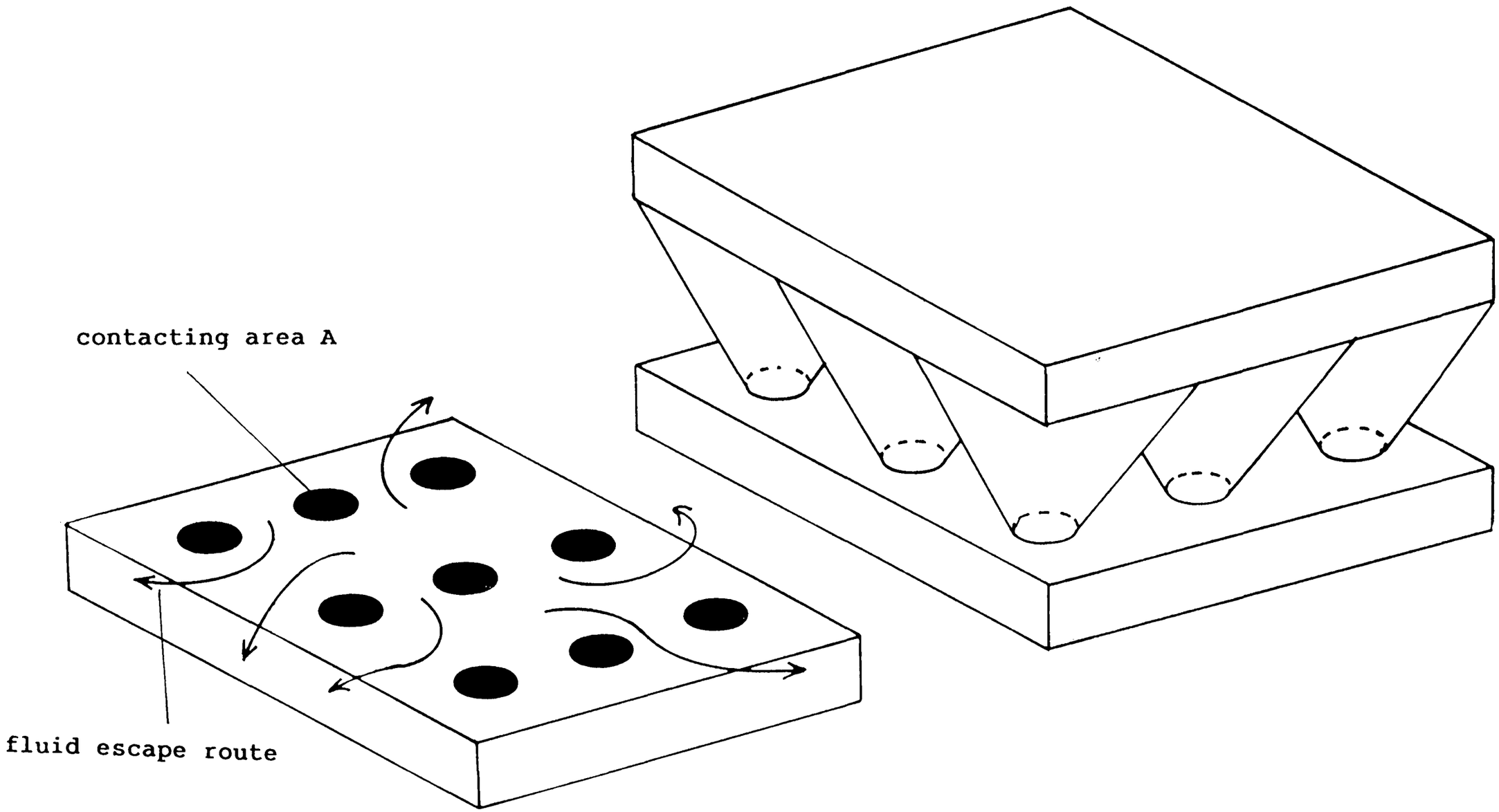

Fig 8.0.6 Two bodies approaching; One has three dimensional roughness

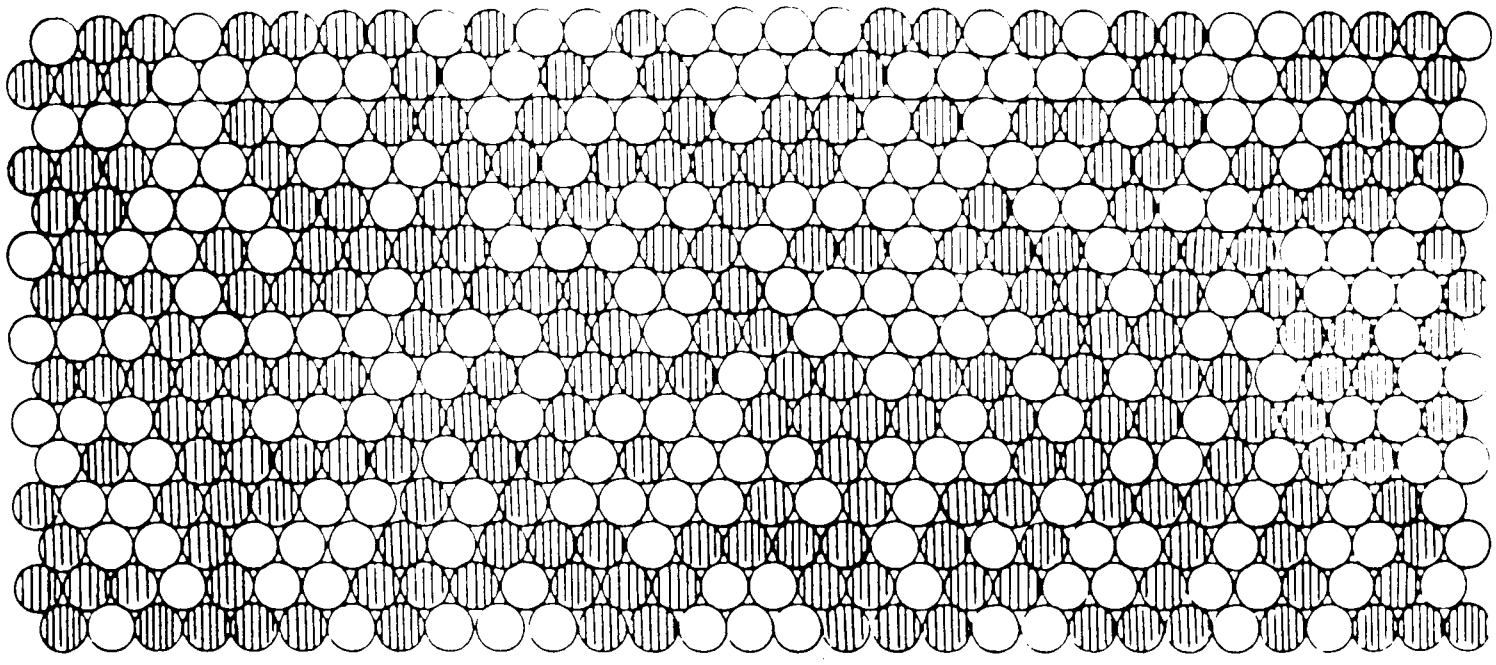

(a)

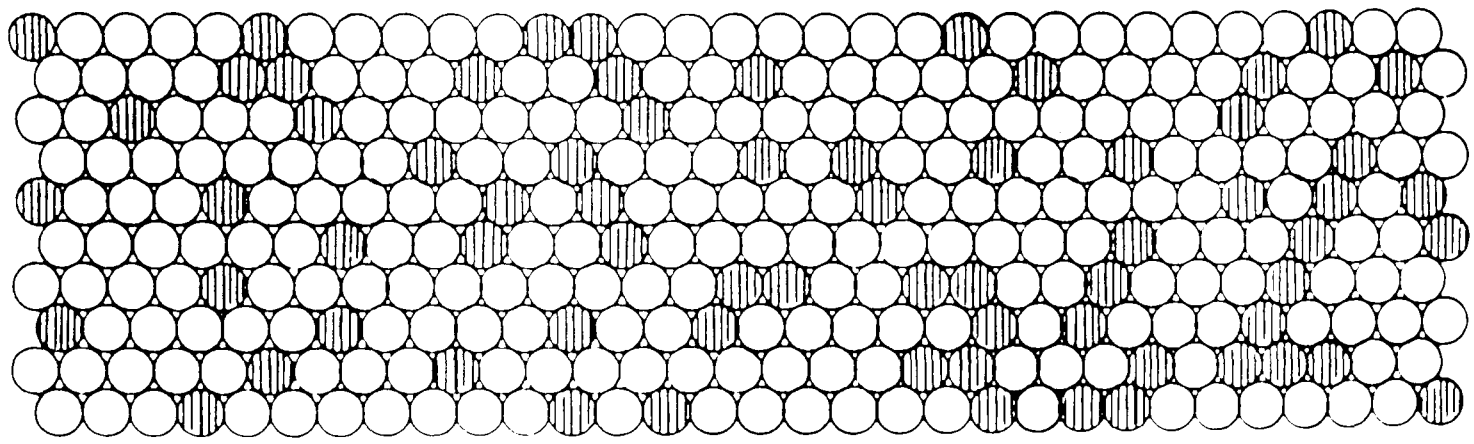

(b)

Fig 8.0.7 Percolation model (a) Percolation density of forty-six percent network nearly closed. (b) density eighteen percent network remains open.

reproduced from ref [56]

Fig 8.0.8 Increase in film thickness is proportional to speed